

**NUMERICAL EVALUATION OF SQUARE REINFORCED CONCRETE
SLABS INCORPORATING HIGH VOLUMES OF RECYCLED
MATERIALS**

IKPOTOKIN OSALUMHENSE PEACE

A THESIS SUBMITTED TO THE FACULTY OF GRADUATE STUDIES IN
PARTIAL FULFILLMENT OF THE REQUIREMENTS FOR THE DEGREE OF
MASTER OF APPLIED SCIENCE

GRADUATE PROGRAM IN CIVIL ENGINEERING
YORK UNIVERSITY
TORONTO, ONTARIO
CANADA

JANUARY 2024

ABSTRACT

Concrete remains the most widely used building material in the world, due to its locally available constituent materials, versatility of form and shape, functionality, and durability. However, due to the processes involved in the manufacturing of cement, the sustainability of concrete both globally and in local communities, is often called into question. Cement production accounts for approximately 7 percent of CO₂ emissions globally and, as the resources required for concrete production (e.g., aggregates, sand, potable water, etc.) continue to diminish, this poses a series problem for the long-term viability for the concrete construction industry. A three-pronged solution to this problem is therefore required which focuses on reducing, reusing, and recycling our concrete infrastructure. As urban populations are only expected to increase in the coming decades, concrete structures will continue to be constructed. This research is aimed at investigating the flexural response of two-way slabs produced using low-carbon concrete (LCC) containing recycled and secondary materials. Given that concrete floor slabs account for the largest portion of concrete in a typical building, the use of LCC in slabs has the potential to have a significant reduction in the structure's overall CO₂ footprint. The primary objective of this research is to examine the effects of replacing portland cement with high volumes of slag, fine and coarse recycled concrete aggregates (RCAs). To address the main research objective, a three-phase experimental program was completed. The first phase involved the material characterization of the various constituent materials including cement, slag, natural sand, natural coarse limestone aggregates, and fine and coarse RCAs. The second phase focused on concrete mixture design development. An experimental matrix included the batching and testing of several low carbon concrete mixtures consisting of one target strength class (30 MPa) and combinations of up to 100% replacement of natural limestone and sand with fine and coarse RCAs and up to 50% replacement of portland cement with ground granulated blast furnace slag. The next phase of experimental testing program was then completed to help better understand the individual and combined effects of the various constituent materials on fresh (e.g., slump, density, air content) and hardened concrete properties (e.g., compressive and splitting tensile strength) of low carbon concrete. Based on the top performing concrete mixtures, the third phase incorporated their measured material properties into a finite element model. Four two-way slabs (one control slab and three slabs containing different LCC mixtures) were then analyzed to evaluate and compare the maximum flexural capacity, deformational characteristics, and crack patterns. The obtained flexural and

deformation response of the slabs were then compared with results obtained from the yield line analysis, Response 2000 sectional analysis which is based off the moment capacity and results were compared to CSA empirical code equations. Findings showed that firstly, the predicted pattern of failure from the finite element analysis was in concordance with that of the yield line analysis, secondly an inverse relationship between density LCC and the replacement ratio of recycled/secondary materials was obtained, and thirdly, that 50% of the numerical deflection values were in alignment with ACI crossing beam method. In terms of flexural capacity, relatively low decreases in load of 4.6%, 8.7%, and 9.8%, were computed for LC-C, LC-CF, LC-CFS, respectively. These results are promising for demonstrating the feasibility of utilizing LCC incorporating high volumes of recycled and secondary materials in two-way slab systems.

Key words: *Two-way slabs, Sustainability, Low-Carbon Concrete(LCC), Finite Element Modelling, Yield Line Analysis, Sectional Analysis*

ACKNOWLEDGEMENTS

Firstly, I would like to thank York University for this opportunity to study at one of Canada's leading universities and for their financial support. My sincere gratitude goes to Prof. Liam J. Butler, who guided me throughout these 3 years of my master's degree studies and was supportive every step along the way. I am also thankful for his financial assistance during my program. To my supervisory committee-Prof. Stavroula Pantazopoulou, I am indeed indebted to her for her guidance, technical insights, and kindness during this research work. Thanks also to Lafarge and Ash Grove.

I would also like to thank the Graduate Program Assistant, Sindy Mahal of the Department of Civil Engineering for her kindness, help, and support from the start to finish of this program. My profound appreciation goes to my friend and senior colleague Farah Dameh, who provided support knowledge on the use of ATENA for the modelling aspect of this research project and also to Thirumakal Panchalingam for their friendship these years. To the Lassonde IT Personnel, Robert Reynolds, for his availability in always helping remotely on technical issues encountered during the Finite Element Analysis aspect and other software's I used for my study and research. To my friends who also contributed their time during the laboratory work, such as Ismail Mohammed, Amer Shaik, Adrein Sparling, Alessandro Paglia, and others too numerous to mention. I am grateful for their support. To other friends and co-researchers such as Zoi Ralli, Jordan Santorsola, Sarp Olcun, Arefeh Shamshany, Sara Guavera, Saad Saad, Roberto Salazar, Osama Baraka, & Dr. Iman Babiyezi. To my undergraduate professors, and senior colleagues such as: Prof. J. O. Afolayan, Prof. A O. Owolabi, and to Ereyi Winifred, Jonah Ikhuoria. To my other kind-hearted friends within and outside of Canada such as: Nosa Idahagbon, David Owolabi, Olajide David, Seyed Hadi Moosavian, Feyi Adebayo, and Dr. Tomori Damilola for always checking up on me and other colleagues in the graduate office. I also use this opportunity to appreciate the technicians in the department of civil engineering: for their time, insights, and support during the experimental phase of this project, especially Kujan Rupakheti for his encouragements. Also, to the facilities team at Lassonde, I am grateful for their timely response always.

My special gratitude goes to the members of my family, my parents-Mr & Mrs A. A Ikpotokin, my siblings and beloved ones, who believed in me and provided emotional support from afar during this period.

TABLE OF CONTENT

ABSTRACT.....	ii
ACKNOWLEDGEMENTS	iv
TABLE OF CONTENT.....	v
LIST OF FIGURES	xi
LIST OF TABLES	xvi
1. CHAPTER ONE: INTRODUCTION AND BACKGROUND	1
1.1. Background	1
1.2. Recycled Concrete.....	2
1.3. Objectives of the Thesis	3
1.4. The Thesis Organisation	4
2. CHAPTER TWO: LITERATURE REVIEW.....	6
2.1. Low Carbon Concrete	6
2.1.1. The Production Process of Recycled Concrete.....	6
2.1.2. Low-Carbon Concrete	7
2.1.3. Mechanical Properties of Low-Carbon Concrete	8
2.1.4. Mechanism, Grading and Absorption of Recycled Aggregates.....	12
2.1.5. Moisture Content Evaluation of Recycled Concrete Aggregates	15
2.1.6. Advantages of Recycled Concrete	16
2.1.7. Disadvantages of Recycled Concrete.....	17
2.1.8. Limitations to the Adoption of Recycled Concrete in Practice.....	17
2.1.9. Structural Use of Low-Carbon Concrete.....	18
2.1.10. Behaviour of Reinforced Low-Carbon Concrete Slabs	19
2.2. Flexural Behaviour and Design of Reinforced Concrete Slabs	20
2.2.1. One-Way Slabs	21
2.2.2. Two-Way Slabs.....	23
2.2.3. Differences between One-way and Two-way Slabs.....	26
2.2.4. Analytical Methods for Computing Design Moments of Two-Way Reinforced Concrete Slabs	27
2.2.5. Flexural Behaviour of Slabs	29
2.2.6. Code Provisions for Flexural Design of Two-Way Slab Systems	31
2.3. Fibre Optic Sensing.....	32

2.3.1. Background & History	33
2.3.2. Fiber Optic Sensors.....	34
2.3.3. Distributed Fibre Optic Sensing.....	35
2.3.4. Advantages of Distributed Fiber Optic Sensing vs Traditional Instrumentation Techniques	38
2.3.5. Applications of DFOS Reinforced Concrete.....	39
2.3.6. Identification of Gaps/Summary	39
2.4. Yield Line Analysis	40
2.4.1. Principles of Yield Line Analysis.....	40
2.4.2. Procedure for Yield Line.....	41
2.4.3. Identification of Yield Line Patterns.....	41
2.4.4. Collapse Yield Moment and Slab Capacity Determination	41
2.4.5. Advantages of Yield Line over Linear Elastic Analysis	42
2.4.6. Disadvantages of the Yield Line	42
2.5. Finite Element Analysis.....	42
2.5.1. Different Constitutive Models.....	42
2.6. Studies that have Investigated the Modelling of Different Slabs.....	46
3. CHAPTER THREE: METHODOLOGY & EXPERIMENTAL PROGRAM	47
3.1. Methodology Overview and Background	47
3.2. Experimental Program Overview	47
3.2.1. Aggregates Properties Testing	48
3.3. Concrete Mixture Design Development and Fresh and Hardened Properties Testing	49
4. CHAPTER FOUR: FRESH & HARDENED PROPERTIES TESTS & DISCUSSIONS	50
4.1. Concrete Mix Design & Process	50
4.1.1. Mix Design by Absolute Volume Method	50
4.1.2. Concrete Mixing Process.....	51
4.2. Aggregate Characterization.....	52
4.2.1. Mixing Constituents.....	52
4.2.2. Moisture Content Test.....	53
4.2.3. Absorption Test.....	57
4.2.4. Relative Density.....	60
4.2.5. Sieve Analysis & Particle Size Distribution.....	64

4.3. Tensile Tests on Reinforcing Steel.....	67
4.4. Mechanical & Fresh Properties of Concrete	72
4.4.1. Compressive Strength Results	72
4.4.2. The Splitting Tensile Tests	78
4.4.3. Workability (Slump).....	83
4.4.4. Modulus of Elasticity	84
4.4.5. Poisson's Ratio	85
5. CHAPTER FIVE: THE REINFORCED CONCRETE SLABS DESIGN METHODOLOGY	89
5.1. The Design of the Slabs According to CSA A23.3-04	89
5.1.1. Selection of Slab Thickness & Effective Depth	90
5.1.2. Reinforcement Spacing.....	91
5.1.3. Detailing of the Reinforcement & Slabs.....	91
5.1.4. Provision of Corner Reinforcement to Slabs.....	92
5.1.5. Provision of Cover to the Reinforcement.....	92
5.1.6. Check for Shear Requirements.....	93
5.1.7. Factored Moment Computation	93
5.1.8. Permissible Deflections	95
5.2. Yield Line Analysis of the Two-Way Slab	96
5.2.1. Evaluation of the Slab Capacity based on the Moment of Resistance	97
5.2.2. ACI Crossing Method for Deflection	98
6. CHAPTER SIX: FINITE ELEMENT MODELLING OF TWO-WAY LOW-CARBON CONCRETE SLABS	100
6.1. Scope & Motivation for Finite Element Modelling.....	100
6.2. ATENAGid Constitutive Model	101
6.2.1. Reinforcement Stress Strain Laws	101
6.2.2. Bond Strength of Concrete.....	102
6.2.3. The Yield Mechanism of ATENA.....	102
6.3. The Slab Geometry	102
6.3.1. The Use of Symmetry Condition	103
6.4. The Material Properties	103
6.4.1. The Actual Elastic Modulus of Concrete & Recycled Concrete.....	104
6.4.2. Fracture Energy of Conventional and Low-Carbon Concrete.....	104

6.4.3. Tensile Strength of the Concrete	105
6.4.4. Compressive Strength of Concrete.....	106
6.5. Reinforcing Steel Properties	106
6.6. Application of Boundary Conditions	107
6.7. The Model Generation.....	107
6.8. Meshing Parameters	108
6.9. Slab NC	109
6.9.1. Load vs Displacement Curve	109
6.9.2. Stresses	109
6.9.3. Strains	110
6.9.4. Tensile Strength	110
6.9.5. Crack Patterns & Failure Mode.....	111
6.10. Slab LC-C	112
6.10.1. Load vs Displacement Curve	113
6.10.2. Stresses	113
6.10.3. Strains	114
6.10.4. Tensile Strength	114
6.10.5. Crack Pattern & Modes of Failure.....	115
6.11. Slab LC-CF.....	116
6.11.1. Load vs Displacement Curve	116
6.11.2. Stresses	117
6.11.3. Strains	118
6.11.4. Tensile Strength	118
6.11.5. Crack Patterns & Modes of Failure	119
6.12. Slab LC-CFS.....	121
6.12.1. Load vs Displacement Curve	121
6.12.2. Stresses	122
6.12.3. Strains	122
6.12.4. Tensile Strength	123
6.12.5. Crack Patterns & Modes of Failure	124
6.13. Summary of the FE Results	125
6.13.1. Maximum Load.....	125

6.13.2. Peak Displacement of the Slabs	126
6.13.3. Crack Width of the Slabs	126
6.13.4. Percentage Decrease of the Slab Capacity	126
7. CHAPTER SEVEN: SECTIONAL ANALYSIS AND CODE COMPARISON	128
7.1. Section Analysis with the Use of Response-2000-Background	128
7.1.1. Material Properties, Full Member Properties, Material Reduction Factors	129
7.1.2. Analysis of the Slab Section NC.....	129
7.1.3. Slab Capacity.....	136
7.1.4. Slab Deflection.....	137
7.1.5. Mohr Circles.....	138
7.1.6. Analysis of the Slab Section LC-C.....	138
7.1.7. Slab Capacity.....	145
7.1.8. Response-2000 Slab Capacity	146
7.1.9. Slab Deflection.....	146
7.1.10. Mohr Circles.....	147
7.1.11. Analysis of the Slab Section LC-CF	148
7.1.12. Slab Capacity.....	155
7.1.13. Response-2000 Slab Capacity	155
7.1.14. Slab Deflection.....	155
7.1.15. Mohr Circles.....	156
7.1.16. Analysis of the Slab Section LC-CFS.....	156
7.1.17. Slab Capacity.....	163
7.1.18. Slab Deflection.....	164
7.1.19. Mohr Circles.....	165
7.1.20. Comparison of the Maximum Crack Widths.....	165
7.1.21. Collapse Load Summary	166
7.1.22. Deflection Comparison	166
7.1.23. Summary-Percentage Difference of FE Deflection & Response-2000	166
7.1.24. Summary-Percentage Difference of ACI Crossing Beam Analogy Deflection Result & Response-2000	167
8. CHAPTER EIGHT: CONCLUSIONS & RECOMMENDATIONS	168
8.1. Conclusions.....	168

8.1.1. Materials Characterization	168
8.1.2. Yield Line Analysis	168
8.1.3. Finite Element Analysis.....	168
8.1.4. Sectional Analysis.....	169
8.1.5. Deflections Using the Crossing Beam Analogy Method	169
8.2. Limitations and Shortcomings of this Research Study	169
8.3. Application of the Research Findings	170
8.4. Recommendations for Future Research	170
REFERENCES.....	171
Appendix A: Calculation Sheets	189
A1 Slab Design.....	189
A2 Yield Line Calculations	191
A3 Response-2000 Calculations	192
Appendix B: Experimental Testing of Two-Way LCC Slab-Completed Works	193
B1 Fabrication of the Formwork.....	193
B2 The Reinforcement Work.....	196
B2.1 Cutting of the Reinforcement, Anchorage & Bending of the Reinforcement.....	196
B2.2 Placement of the Reinforcement & Spacing	197
B3 Concrete Testing Standards	199
B3.1 Strain Guage FOS & Instrumentation Design	200
B3.2 Strain Guage Instrumentation Design.....	200
B3.3 Strain Gauge Application	201
B3.4 DFOS Instrumentation & Concreting.....	205
Appendix C: Experimental Testing of Two-Way LCC Slabs-Future Work.....	216
C1 The Set-Up &, DFOS Acquisition & Slab Flexural Response	216
C2 Testing Methodology of the Two-Way Slabs.....	216
C2.1 Slab Testing Set-up & Design	216
Appendix D: Material Certificates	218

LIST OF FIGURES

Figure 2.1-Production Process of RCA(Source: Adapted from Xiao, 2018)[31]	7
Figure 2.2-Relative Flexural strength Trend (Source: Adapted from Zhou & Chen 2017)[51]	10
Figure 2.3-Relationship between Modulus of Elasticity & Water/Cement ratio (Source: Adapted from Frondistou-Yannas, 1977) & (Nixon, 1978)[40][53]	11
Figure 2.4-Shape of Deflection of One-Way Slab Loaded Uniformly (Source: Adapted from Darwin & Charles, 2021)[84]	22
Figure 2.5-Illustration of a Unit Strip as a Basis for Design in Flexure(Source: Adapted from Darwin & Charles, 2021)[84]	22
Figure 2.6-Typical One-Way Slab (Source: Adapted from Darwin & Charles, 2021)[84]..	23
Figure 2.7-Center Strips Bending (Source: Darwin & Charles, 2021) [84].....	24
Figure 2.8-Grid of Slab Model (Source: Darwin & Charles, 2021)[84]	24
Figure 2.9-Minimum Reinforcement Extension for Slabs without Beams(Source: Adapted Darwin & Charles, 2021) [84]	25
Figure 2.10-Equivalent Frame Definition (Source: Adapted form ACI 318-11)[87].....	28
Figure 2.11-Fiber Optic Layers (Adapted from Soga & Luo, 2018)[98]	32
Figure 2.12-Glued Strain Gauges on Reinforcing Bars b) Fibre Optical Sensors on a Reinforcing bar by the use of Fibre Bragg Grating (Source: Adapted from Lemcherreq, 2022)[99].....	33
Figure 2.13-The Working Principle of DFOS Using Rayleigh Backscattering (Adapted from Berrocal et. al 2021)[110]	36
Figure 2.14-Spot Gauges Differences in Comparison to DFOS Sensors for a Slab (Adapted from Buda-Ozog et. al., 2022)[113].....	37
Figure 2.15-Some Possible Patterns (Adapted from Alasam, 2006)[126]	41
Figure 2.16-Menetrey-Willam Surface (Source: Adapted from Dmitriev et. al. 2020)[128]	44
Figure 2.17-Linear Softening using the Drucker-Prager Modelling for Materials	45
Figure 3.1-Experimental Program Phases.....	48
Figure 4.1-The Mixing of the Concrete Constituent Materials	52
Figure 4.2-Preparation to Pour the Mixed Concrete.....	52
Figure 4.3- Determining the Moisture Content of the Recycled Fine Aggregate.....	56
Figure 4.4-Determining the Moisture Content of the Recycled Coarse Aggregate	56
Figure 4.5-Determining the Moisture Content of the Normal Coarse Aggregate	57
Figure 4.6-Initial Sample for Absorption of Fine & Coarse Aggregates	59
Figure 4.7-Relationship between Density & Compressive Strength for 0.015m ³ of Concrete	62
Figure 4.8-Relationship between Density & Replacement Percentage	63
Figure 4.9-Sieve Set.....	66
Figure 4.10-Lab Sifter	66
Figure 4.11-The Sifter Undergoing the Mechanical Shaking of the Sieve Set	66
Figure 4.12-Sieve Analysis Chart for the Normal Coarse Aggregate and the Recycled Coarse Aggregate	67

Figure 4.13-Extensometer and Reinforcing Steel Arrangement for the Test.....	69
Figure 4.14-Stress/Strain Curve for Specimen 1.....	70
Figure 4.15-Stress/Strain Curve for Specimen 2.....	70
Figure 4.16-Stress/Strain Curve for Specimen 3.....	71
Figure 4.17-Typical Fracture Patterns by ASTM 39/C 39M-01[136].....	73
Figure 4.18-Compressive Strength Test on Concrete.....	73
Figure 4.19-Failure Specimen for the Normal Concrete.....	74
Figure 4.20-Failure Specimens for the Low-Carbon Concrete LC-C.....	74
Figure 4.21-Compressive Strength Development Profile for Normal Concrete up to 28 days	74
Figure 4.22-Compressive Strength Development Profile for LC-C Concrete up to 28 days	75
Figure 4.23-Compressive Strength Development Profile for LC-CF Concrete up to 28 days	75
Figure 4.24-Compressive Strength Development Profile for LC-CFS Concrete up to 28 days	76
Figure 4.25-Linear Relationship between Water/Cement Ratio & Replacement Percentage	77
Figure 4.26-Experimental Set-Up of Splitting Tensile Test	79
Figure 4.27-Split Specimen	80
Figure 4.28-Summary Splitting Tensile Strength for Normal Concrete, and Low-Carbon Concretes vs Percentage Replacement.....	80
Figure 4.29-Splitting Tensile Strength versus Cylinder Strength using Linear Regression	81
Figure 4.30-Splitting Tensile Strength versus Water/Cement Ratio using Linear Regression	82
Figure 4.31-Splitting Tensile Strength vs Normalized Cylinder Strength	83
Figure 4.32-Slump Test Illustration	84
Figure 4.33-Measurement of the Concrete Slump	84
Figure 4.34-Elastic Modulus vs Percentage Replacement.....	87
Figure 4.35-Compressometer	88
Figure 4.36-Cylinder Positioning inside the Compressometer	88
Figure 4.37-Alignment of the Specimen and the Compressometer	88
Figure 4.38-Elastic Modulus & Poisson's Ratio Test-Set-Up	88
Figure 5.1-Slab Layout	89
Figure 5.2-Reinforcing Bar Details	92
Figure 5.3-Factored Moment Diagram for the Two-Way Slab	95
Figure 5.4-The Slab Assumed Yield Line Pattern	97
Figure 6.1-Stress-Strain Law for Reinforcement.....	101
Figure 6.2-The Slab Model.....	102
Figure 6.3-Discret Model of the Reinforcement	103
Figure 6.4-Input Material Properties of the Natural Concrete	107
Figure 6.5-The Reinforced Concrete Slab Model	108
Figure 6.6-Mesh Generation for the Models	108
Figure 6.7-Load vs Displacement Curve for NC Slab	109

Figure 6.8-Stresses for Concrete for Slab NC	109
Figure 6.9-Stresses in Steel for Slab NC	109
Figure 6.10-Concrete Strain & Failure Pattern for NC at 30 Days	110
Figure 6.11-Reinforcement Strains & Failure for NC at 30 Days	110
Figure 6.12-Tensile Strength of the Concrete.....	110
Figure 6.13-First Level Cracks	111
Figure 6.14-Second Level Cracks	111
Figure 6.15-First Level Cracks	112
Figure 6.16-Load vs Displacement for the LC-C Concrete.....	113
Figure 6.17-Stresses in Concrete Type Slab	113
Figure 6.18-Stresses in the Steel	113
Figure 6.19-Strains in the Concrete	114
Figure 6.20-Strains in the Steel.....	114
Figure 6.21-The Tensile Strength of the Reinforced Concrete Slab LC-CF	114
Figure 6.22-Level 1 Cracks	115
Figure 6.23-Level 2 Cracks	115
Figure 6.24-Level 3 Cracks	116
Figure 6.25-Load vs Displacement Curve for LC-CF	117
Figure 6.26 - Stresses for Concrete for Slab LC-CF.....	117
Figure 6.27-Stresses for Concrete for Slab LC--CF	117
Figure 6.28-Strains in the Concrete	118
Figure 6.29-Strains in the Steel.....	118
Figure 6.30-The Tensile Strength of the Reinforced Concrete Slab LC-CFS.....	119
Figure 6.31-Level 1 Cracks	119
Figure 6.32- Level 2 Cracks	120
Figure 6.33-Level 3 Cracks	120
Figure 6.34-Load vs Displacement Curve.....	121
Figure 6.35-The Stresses in the Concrete	122
Figure 6.36-The Stresses in the Steel.....	122
Figure 6.37-Stains in the Concrete	123
Figure 6.38-Strains in the Steel.....	123
Figure 6.39-The Tensile Strength of the Concrete.....	123
Figure 6.40-Level 1 Cracks	124
Figure 6.41-Level 2 Cracks	124
Figure 6.42-Level 3 Cracks	125
Figure 7.1-Section Geometric Properties.....	128
Figure 7.2-Full Member Properties.....	129
Figure 7.3-Cross-Section Properties.....	129
Figure 7.4-Slab Crack Pattern.....	129
Figure 7.5-Reinforcing Steel Results	130
Figure 7.6-Member Crack Data, Max=5.56mm.....	130
Figure 7.7-Bottom Reinforcing Details	131
Figure 7.8-Concrete & Steel Stresses	131

Figure 7.9-The Displacement of the Section, Max=6.37mm	132
Figure 7.10-Moment vs Curvature, Max=19.09kNm & 521.36mrad/m	132
Figure 7.11-Moment vs Maximum Cracking Width, Max=6.58mm	133
Figure 7.12-Moment vs Reinforcement Strain, Max=42mm/m.....	133
Figure 7.13-Moment vs Longitudinal Strain, Max=23.76mm/m.....	134
Figure 7.14-CSA 2014 M-V Interaction.....	134
Figure 7.15-AASHTO-2000 M-V Interaction.....	135
Figure 7.16-Moment & Shear Diagrams	135
Figure 7.17-Stiffness & Axial Diagrams	136
Figure 7.18-Mohr Circle.....	138
Figure 7.19-Section Properties.....	138
Figure 7.20-Slab Cracking Pattern	139
Figure 7.21-Compression & Tensile Results	139
Figure 7.22-Member Crack Data, Max 5.60mm.....	140
Figure 7.23-Bottom Reinforcing Details	140
Figure 7.24-Concrete & Steel Stresses	141
Figure 7.25-The Displacement of the Section, Max=6.32mm	141
Figure 7.26-Moment vs Curvature, Max= 19.25kNm & 514.06mrad/m	142
Figure 7.27-Moment vs Maximum Crack Width, Max=6.53mm.....	142
Figure 7.28-Moment vs Reinforcement Strain, Max=41.74mm/m.....	143
Figure 7.29-Moment vs Longitudinal Strain, Max=23.75mm/m.....	143
Figure 7.30- CSA 2014 M-V Interaction.....	144
Figure 7.31-AASHTO-2000 M-V Interaction.....	144
Figure 7.32-Moment & Shear Diagrams	145
Figure 7.33-Stiffness & Axial Diagrams	145
Figure 7.34-Mohr Circles	147
Figure 7.35-Slab Crack Pattern.....	148
Figure 7.36-Compressive & Tensile Stresses.....	148
Figure 7.37-Member Crack Data, Max= 5.62	149
Figure 7.38-Bottom Reinforcing Details	149
Figure 7.39-No Shear Plot	150
Figure 7.40-The Displacement of the Section, Max=6.31mm	150
Figure 7.41-Moment vs Curvature, Max=19.22kNm & 515.34mrad/m	151
Figure 7.42-Moment vs Maximum Crack Width, Max=6.58mm.....	151
Figure 7.43-Moment vs Reinforcement Strain, Max=42.11mm/m.....	152
Figure 7.44-Moment vs Longitudinal Strain	152
Figure 7.45-CSA 2014 M-V Interaction.....	153
Figure 7.46-AASHTO-2000 M-V Interaction.....	153
Figure 7.47-Moment & Shear Diagrams	154
Figure 7.48-Stiffness & Axial Diagrams	154
Figure 7.49-Mohr Circles	156
Figure 7.50-Slab Crack Pattern.....	156
Figure 7.51-Compressive & Tensile Stresses.....	157

Figure 7.52-Member Crack Data	158
Figure 7.53-Bottom Reinforcing Details	158
Figure 7.54-Concrete & Steel Stresses	159
Figure 7.55- The Displacement of the Section, Max=6.01mm	159
Figure 7.56-Moment vs Curvature, Max= 19.22kNm & 515.34	160
Figure 7.57-Moment vs Maximum Crack Width, Max=6.57mm	160
Figure 7.58-Moment vs Reinforcement Strains, Max=42.08mm/m	161
Figure 7.59-Moment vs Longitudinal strain, Max=24.04mm/m	161
Figure 7.60-CSA 2014 M-V Interaction.....	162
Figure 7.61-Moment & Shear Diagrams	162
Figure 7.62-Axial & Stiffness Diagram.....	163
Figure 7.63-Mohr Circles	165

LIST OF TABLES

Table 2.1-Comparative Concrete Strength with Tensile Strength (Source: Xiao, 2018)[31]	9
Table 2.2-Requiremenets for Testing Recycled Coarse Aggregates(Source: Xiao, 2018) [31]	13
Table 2.3-Grading of Crusher Products(Source: ACI 555R-01)[60]	14
Table 2.4-Findings on RCA Water Absorption Capacity (Source: ACI 555R-01)[60]	15
Table 2.5-Summary of Concrete Investigating the Structural use of Low-Carbon Concrete	18
Table 2.6: Minimum Thickness for Slabs without Interior Beams (Source: Darwin & Charles, 2021), ACI 318 Code)[84][87]	26
Table 2.7: Differences Between One-Way & Two-Way Slab	26
Table 4.1- Low Carbon Concrete Mix Designs(kg/m3)	50
Table 4.2-Fresh & Hardened Properties of the Low-Carbon Concretes	50
Table 4.3-Aggregate Sample Size for Test Based on C 566-97 (2000)[132]	54
Table 4.4-Percentage Moisture Content	55
Table 4.5-Values for Percentage Water Absorption Content of NFA	59
Table 4.6-Values for Percentage Water Absorption Content of NCA	59
Table 4.7-Values for Percentage Water Absorption Content of RFA	60
Table 4.8-Values for Percentage Water Absorption Content RCA	60
Table 4.9-Cylinder Density per m ³ of the Concrete Mixes	61
Table 4.10-Total Mass of Materials (Aggregates + Supplementary Materials) in kg & Density per 0.1728m ³ for the Slab	62
Table 4.11-Test Samples for Conformity	65
Table 4.12-Material Specification for Steel	69
Table 4.13-Specimen Dimensions	69
Table 4.14-Tensile Test Result Summary	71
Table 4.15-Table of Replacement Percentage Cylinder Strength and Water Content	76
Table 4.16-Splitting Tensile Test Results for LC-C	78
Table 4.17-Splitting Tensile Test Results for LC-C	78
Table 4.18-Splitting Tensile Test Results for LC-CF	79
Table 4.19-Splitting Tensile Test Results for LC-CFS	79
Table 4.20-Results of the Sump Test for the Different Mix ID's	84
Table 4.21-Elastic Modulus Data Set for NC	85
Table 4.22-Elastic Modulus Data Set for LC-C	86
Table 4.23-Elastic Modulus Data Set for LC-CF	86
Table 4.24-Elastic Modulus Data Set for LC-CFS	86
Table 5.1-Spacing Requirements for Slabs	91
Table 5.2-Cast-in-Place Non-prestressed Concrete Members Specified Concrete Cover (Source ACI 318-19)	93
Table 5.3-Negative & Positive Factored Moment	94
Table 5.4-Distributed Factors using Total Factored Static Moment	94
Table 5.5-The Factored Moments Obtained	95

Table 5.6-Maximum Permissible Deflection Requirements.....	96
Table 5.7-Summary of the Deflection of the Natural Concrete Slab & Low-Carbon Concrete	99
Table 5.8-Deflection Comparison for FEA with Limiting Value	99
Table 5.9-Deflection Comparison for FEA with Limiting Value	99
Table 6.1-Fracture Energy Properties of the Concrete Mixes.....	104
Table 6.2-Tensile Strength of Hardened Concrete Cylinders at 30 Days	105
Table 6.3-The Reinforcement Properties.....	106
Table 6.4-Maximum Load Obtained.....	125
Table 6.5-Peak Displacements	126
Table 6.6-FE Maximum Crack Width.....	126
Table 6.7-Percentage Decrease of the Slab Capacity.....	127
Table 7.1-FEA vs Yield Line Comparison.....	136
Table 7.2-FEA vs Response 2000 Comparison.....	137
Table 7.3-FEA vs Response-2000 Comparison	137
Table 7.4-FEA vs Response-2000 Comparison	137
Table 7.5-FEA vs Yield Line Comparison.....	146
Table 7.6-FEA vs Yield Line Comparison.....	146
Table 7.7-FEA vs ACI Code.....	146
Table 7.8-FEA vs Response-2000.....	147
Table 7.9-FEA vs Yield Line Comparison.....	155
Table 7.10-FEA vs Response-2000 Comparison	155
Table 7.11-FEA vs Crossing Beam Method.....	155
Table 7.12-FEA vs Response-2000 Comparison	156
Table 7.13-FEA vs Yield Line Comparison.....	163
Table 7.14-FEA vs Yield Line Comparison.....	164
Table 7.15-FEA vs Response-2000 Comparison	164
Table 7.16-FEA vs Response-2000 Comparison	164
Table 7.17- Maximum Crack Widths Comparison of FE & Response-2000	165
Table 7.18-Load Comparison	166
Table 7.19-Deflection Comparison	166
Table 7.20-Summary: Percentage Comparison of FE Results & Response-2000.....	166
Table 7.21- Summary: Percentage Comparison of FE Results & Response-2000.....	167

1. CHAPTER ONE: INTRODUCTION AND BACKGROUND

1.1. Background

Concrete stands as the most widely employed construction material worldwide, and the production of cement, a key ingredient in concrete, contributes to approximately 7% of the total global CO₂ emissions, with Canada accounting for around 1.5% of this figure. Through a concerted effort and close collaboration with the Canadian government and stakeholders throughout the construction supply chain, Canada's cement and concrete sector is primed to realize an ambitious objective. This partnership aims to collectively eliminate over 15 million tonnes of greenhouse gas emissions by 2030. Furthermore, it envisions continuous annual reductions of more than 4 million tonnes in the emissions resulting from cement and concrete production within Canada (Government of Canada, 2022)[1]. Research studies by Ortiz et al. (2010) [2] suggest that up to 80% of construction and demolition waste could be recycled and reused. Other studies by Berndt (2009), Ferreira et al. (2011), Fonseca et al. (2011), Kou & Poon (2012), and Pedro et al. (2014), have explored the properties and durability of recycled concrete aggregates (RCA), showing positive findings regarding their use[3][4][5][6].

Recent investigations by Li (2008)[7], Pacheco et al. (2015)[8][9], and Xiao et al. (2012)[10] have demonstrated the economic viability and structural performance of RCA concrete, indicating its potential for use in civil engineering structures. However, the long-term structural performance of RCA concrete is still not fully understood, particularly in reinforced concrete slabs. This study aims to contribute to the existing knowledge by evaluating the material characteristics and structural performance of two-way slabs made using both conventional concrete and RCA concrete, incorporating fine and coarse RCA as well as supplementary cementitious materials like granulated blast furnace slag.

While numerous research studies (Santorsola 2021, Wimpenny 2009, Pedro et al., 2014, Malesev et al., 2010, Gomes & Brito 2009, Xiao & Ding 2013, and Hoffman et. al., 2012) have explored the behavior of structural concrete elements with low carbon content [11][12][13][14][15][16][17], few studies have investigated using low carbon concrete in reinforced floor slabs embedded with fiber optic sensors. Despite the Canadian government's target of reducing embodied carbon in structural materials by up to 30%, the use of cement is still projected to reach 55 million tons in

the next five years;[18] hence this has also necessitated this study. This proposed study aims to address the gap in understanding the distributed strain behavior of two-way slabs when using RCAs and cementitious materials.

Previous studies by Nuno et al. (2015)[19], Bruno et al. (2021)[20], and Flavio et al. (2017)[21] have provided insights into the behavior of slabs incorporating RCA, such as punching behavior, mechanical properties, deterioration at elevated temperatures, and cracking performance. The use of fiber optic sensors for detecting moisture ingress through cracks has also been explored by Bremer et. al. (2016)[22]. These studies form the foundation for the proposed research.

This study aims to investigate the behaviour and performance of two-way slabs produced using low-carbon concrete containing recycled and secondary materials as compared to slabs produced using conventional concrete. The effects of replacing conventional concrete constituents with high volumes of slag, fine and coarse RCAs will be examined. A finite element model was developed for the normal concrete and the low-carbon concretes, and a sectional analysis also performed with the results compared to the ACI codes. The data and the results obtained will help to understand the impact of these materials. This information will enable researchers, construction professionals, and consultants to make informed decisions based on the collected data, which will be made publicly available.

1.2. Recycled Concrete

Aside from water, concrete remains the most frequently used material globally in terms of mass, with an average yearly consumption of 30 billion tonnes with its use still increasing (Monteiro, et al. 2017)[23]. While developing nations seem to be seriously spent in the new infrastructures, developed countries find it difficult trying to replace historic and already existing structures (Monteiro, et al. 2017)[23].

The amount of waste generated in the construction industry from concrete construction has greatly increased over time (Etxeberria et al., 2007)[24]. The impact posed by the use of both natural resources and the demolition waste from construction has necessitated recycling and reuse of concrete in particular (Etxeberria et al., 2007)[24].

Numerous research conducted earlier on recycled concrete was done outside the United States, which limits the adoption of the outcome of these research domestically, which is attributed to the materials and quality control variation (Knaack & Kurama, 2013)[25]. In order to promote the use of recycled concrete in reinforced concrete structures, it becomes necessary to design a mix in a way that would be consistent enough to provide good quality and durable concrete (Knaack & Kurama, 2013)[25]. Thus, also able to determine the mechanical properties of the specified concrete (Knaack & Kurama, 2013)[25].

The term recycled concrete is becoming synonymous with low carbon concrete. For the purpose of this research, the term low-carbon concrete will be used as it encompasses the use of materials beyond just those which are derived for recycling.

In this thesis, the characteristics of the aggregates that make up the low carbon concrete will be evaluated as well as the different properties of the fresh and hardened concrete. The flexural performance of the two-way slabs (i.e., moment capacity and load-deflection profile) will be compared against current CSA code predictions.

1.3. Objectives of the Thesis

Due to the ongoing investigations of low carbon concrete and demolished concrete materials, it is pertinent to further research into the structural applications in two-ways slabs and to bridge some of the existing gaps, which is what this thesis partly answers. In view of the forementioned, the research objectives of this thesis are as follows:

- i. To investigate the flexural behaviour of two-way slabs produced using low-carbon concrete containing recycled and secondary materials as compared to slabs produced using conventional concrete.
- ii. To evaluate the effects of replacing typical concrete constituents with high volumes of slag, fine and coarse RCA on the resulting fresh and hardened concrete properties. This objective aims to address how the level of replacement affect the structural behaviour and the deflection of the four slabs in consideration.
- iii. To predict the capacity of the reinforced concrete slabs using yield-line analysis and to compare the result with the result from sectional analysis, using Response-2000.

- iv. To develop a finite element model of the two-way slabs tested in flexure (simply supported on all sides) and compare the model predictions to the experimental results.
- v. To evaluate whether current CSA code predictive equations for estimating flexural capacity of two-way slabs can be applied when using LCC.
- vi. To obtain the distributed strain behaviour of the slabs using special data acquisition systems, which is a work in progress.

1.4. The Thesis Organisation

This thesis includes a total of seven chapters. A summary of each chapter is outline below:

Chapter 1 – *Introduction*: This chapter discusses the recycled concrete as a term itself and provides a generic knowledge on the reason for this study, the research objectives, the justification as well as the scope covered in this research.

Chapter 2 – *Literature Review*: The findings of the previous research in low-carbon concrete that have investigated fine and coarse recycled concrete aggregates individually as well as in combined form are reviewed extensively. In addition, the production, properties, grading, applications in reinforced and two-way slabs as well as Fibre optic sensing are extensively covered in this chapter of this thesis.

Chapter 3 – *Experimental Program Overview*: The detailed experimental program which was crucial to this research and aided the modelling and the collation of the results is discussed in this chapter.

Chapter 4 – *Two-Way Slab Design Methodology*: The design of two-way slab, as well as relevant data obtained from the laboratory material evaluation, and the yield line analysis are grouped under this chapter of the thesis.

Chapter 5 – *Material Testing & Mix Development*: This section contains the various material testing and the evolvement of the mix designs alongside with the fresh and the hardened properties of the concretes.

Chapter 6 – *Finite Element Modelling of the Two-Way Slabs*: As a benchmark for comparison of the actual laboratory results and the modelling results in conjunction with analytical results, the

actual FEA of the slab was carried out using ATENAgid and 3D for the modelling, and the results obtained are discussed under this section.

Chapter 7 – *Sectional Analysis & Code Comparison:* This will present the use of Response-2000 for the purpose of obtaining the moment capacity of the section and to be able to compare the result obtained with the results of FEA and CSA Code.

Chapter 8 – *Conclusions & Recommendations:* The conclusion chapter presents the major findings from this study. The conclusions are summarized for each major phase of the research program.

Recommendations informed by this study and proposal of future areas of research are also detailed in this chapter.

2. CHAPTER TWO: LITERATURE REVIEW

2.1. Low Carbon Concrete

Apart from water, concrete remains the most widely utilized material globally in terms of mass, with an annual consumption averaging 30 billion tonnes and still on the rise (Monteiro, et al., 2017)[23]. While developing nations exhibit a significant investment in new infrastructures, developed countries encounter challenges in replacing historical and existing structures (Monteiro, et al., 2017)[23].

Concurrently, the quantity of waste generated in the construction industry has markedly increased over time (Etxeberria et al., 2007)[24]. The environmental impact stemming from the utilization of natural resources and demolition waste has underscored the urgency of recycling and reusing concrete in particular (Etxeberria et al., 2007)[24].

Prior research on low carbon concrete as a more sustainable concrete, has predominantly been conducted beyond the confines of the United States, limiting the local applicability of these findings due to variations in materials and quality control (Knaack & Kurama, 2013)[25]. To facilitate the integration of recycled concrete into reinforced structures, it becomes imperative to devise consistent mix designs that ensure high-quality and durable concrete (Knaack & Kurama, 2013)[25]. This approach is also instrumental in determining the mechanical properties of the specified concrete (Knaack & Kurama, 2013)[25].

2.1.1. The Production Process of Recycled Concrete

There are different materials that can be recycled and used to produce recycled concrete. Some of these materials can replace normal aggregate used for construction purposes. These materials include concrete bricks, (Kabir et.al., 2012)[26]; ceramics,(Hanifi, 2007)[27]; glass, (Karen, 1997)[28], and rubber (Ali & Ayhan, 2012)[29]; etc.

Recycled concrete aggregates (RCA) can be obtained by crushing already existing concrete with the intention of its usage in a new concrete mix (Verian et. al., 2018)[30]. Usually, the process to produce RCA is designed to both optimize the quantity, as well as the quality (Verian et. al., 2018)[30].

Figure 2.1 presents an illustration by Xiao (2018)][31] on the production process of RCA.

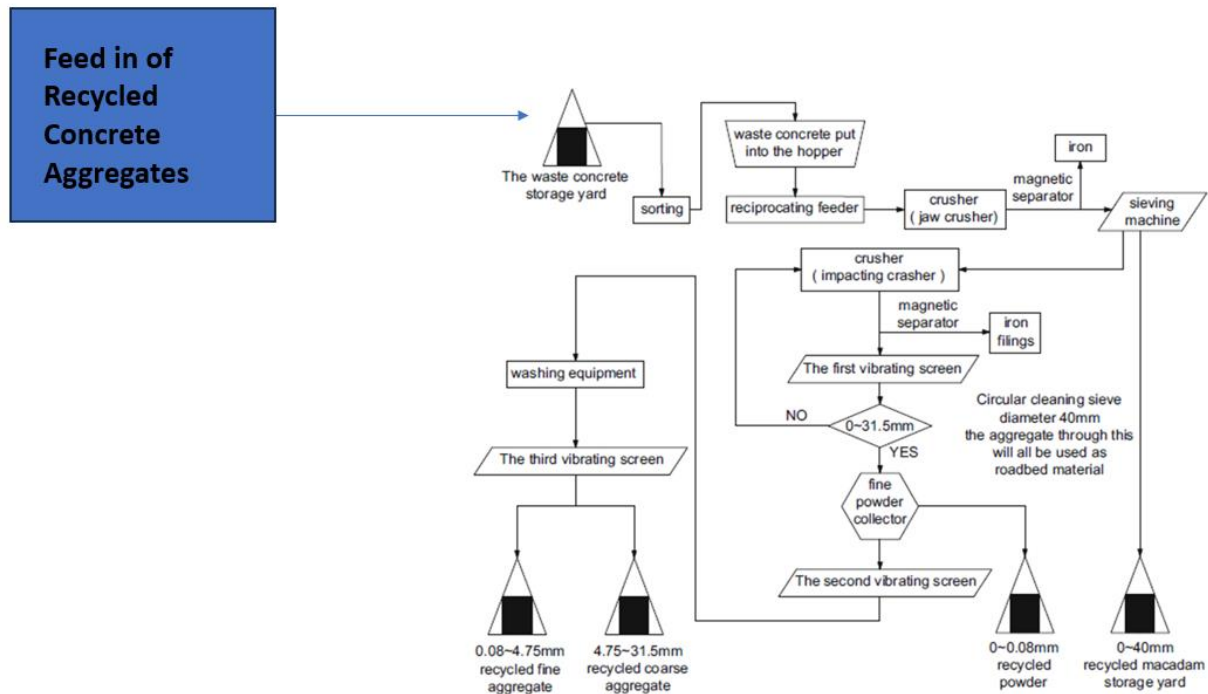


Figure 2.1-Production Process of RCA(Source: Adapted from Xiao, 2018)[31]

2.1.2. Low-Carbon Concrete

Approximately about 82 to 87% of the total global emissions of green house gases are from building materials; while 6 to 8% is from the movement of the building material (Yan et. al., 2010)[32]. The amount of CO₂ generated from each tonne of cement is up to 1 tonne(Wimpenny 2009)[33]. While up to 42% is obtained from the fuel that is used in the process, up to 58% is the by-product of limestone de-carbonization which occurs in the kiln(Dhir et al., 2015)[34].

Purnell and Black, 2012 states that emissions of eCO₂ (equivalent CO₂) from concrete are based on how the cementitious materials replaced are used and also on the design strength of the concrete[35].

In a research study conducted by Flower and Sanjayan in 2007, it was discovered that the emissions of eCO₂ both of normal cement concrete and blended, falls between values of 0.225 and 0.322kg/m³, which is quite high.[36].

2.1.3. Mechanical Properties of Low-Carbon Concrete

Currently, there are no dedicated methods of testing the mechanical properties of recycled concrete or low-carbon concrete in the laboratory. It is important to note that for many years, many researchers and institutions have continued to adopt the same process for measuring the mechanical properties of normal concrete.

This implies it is ideally okay to test the mechanical properties of LCC by using the same standards of measurement as conventional concrete. In subsequent sections of this thesis the different properties of low concrete are presented.

2.1.3.1. Compressive Strength

After conducting a comprehensive analysis of the results, Nixon (1978) observed a reduction in the compressive strength of recycled aggregate concrete (RAC) by 20% compared to natural aggregate concrete (NAC)[37]. Wesche and Schulz (1984)[38] compared the early-stage test results of Buck (1976)[39], and Frondistou-Yannas (1977), and discovered an approximate 10% decrease in the compressive strength of RAC when compared to NAC[40]. In the research conducted by Sri and Tam (1985), it was observed that the compressive strength of RAC exhibited a reduction ranging from 8% to 24% in comparison to NAC[41].

2.1.3.2. Tensile Strength

Another very important property of concrete is the tensile strength. In 2007, Ahmad et al. found that the splitting tensile strength of RAC is nearly identical to that of NAC[42]. On the other hand, Kasai et al., (2023) discovered that RAC's tensile strength is 6% lower than NAC's[43]. Hansen in 1986[44] determined that the splitting tensile strength of RAC is 10% less than NAC's.

In 2015, Ravindrarajah et al., demonstrated a similar 10% reduction in RAC's tensile strength compared to NAC's[45].

In 2001, Sagoe-Crentsil et al., revealed that the ratio of compressive and tensile strength in RAC is higher than that in NAC[46]. Also in 1996, Salem's test suggested that the calculation formulae specified by the American Concrete Institute (ACI) regulations for estimating NAC's tensile and compressive strengths can also be applied to estimate the corresponding strengths of RAC[47].

To further investigate the tensile strength of RAC, Xiao in 2018 conducted a test using 30 prism specimens of RAC with varying replacement percentages of RCA denoted as "r," including 0%, 30%, 50%, 70%, and 100%. The results of this test can be found in Table 2.1 below[31]:

Table 2.1-Comparative Concrete Strength with Tensile Strength (Source: Xiao, 2018)[31]

RCA % Replacement	Compressive Strength (MPa)	Tensile Strength (MPa)	Peak tensile strain (10⁻⁶)	Original Tangent Modulus (MPa)
0	43	2.97	98	35
30	45	2.76	103	33
50	42	2.67	105	31
70	40	2.36	101	28
100	38	2.06	102	25

The conclusions from the study showed that the tensile strength parameters decreased with increasing replacement of the RCA .When RCA was replaced in higher ratios up to 100 %, there was a decrease of the tensile strength by 31%[31] .

2.1.3.3. Flexural Strength

When the actual application for concrete is for use in pavement, or on ground level as in the case of slabs, then the flexural properties and the modulus of rupture becomes an important hardened property to quantify (ACI CRC 18.517) [48].

Abou-Zeid et al., (2005) discovered that the flexural strength of concrete systems using RCA was comparable to or slightly lower than systems using natural aggregates[49]. This similarity or slight reduction in strength was attributed to the enhanced interfacial bond between the coarse RCA and the cement binder, which resulted from the rough surface and angularity of the coarse RCA. It is presumed that this improved bond may be a result of a reaction occurring between the RCA and the surrounding cement paste[49].

Salem (1996) discovered that when using ACI regulations, the relationship between compressive strength and tensile strength for normal aggregate concrete(NAC) is overly conservative when applied to RCA[50].

In a study by Xiao in 2018, flexural strength test on 30 prism specimens with varying percentages of RCA replacement, ranging from 0% to 100% were conducted. Figure 2.3 illustrates the progression of RAC's flexural strength with different replacement percentages. From the Figure 2.3, it is evident that RAC's flexural strength is relatively lower compared to NAC.[31]

In another flexural strength study by Zhou & Chen in 2017 investigating roller compacted recycled concrete (RCRC), they noted an upward trend in flexural strength as the replacement percentage increase, attributed to the decrease in the actual water-cement ratio. However, it should be noted that roller compacted concrete (RCP) did not exhibit a significantly higher relative strength than the RCRC. This suggested that, under flexure, the interface between the new cement and RCA may no longer be the weakest interface [51].

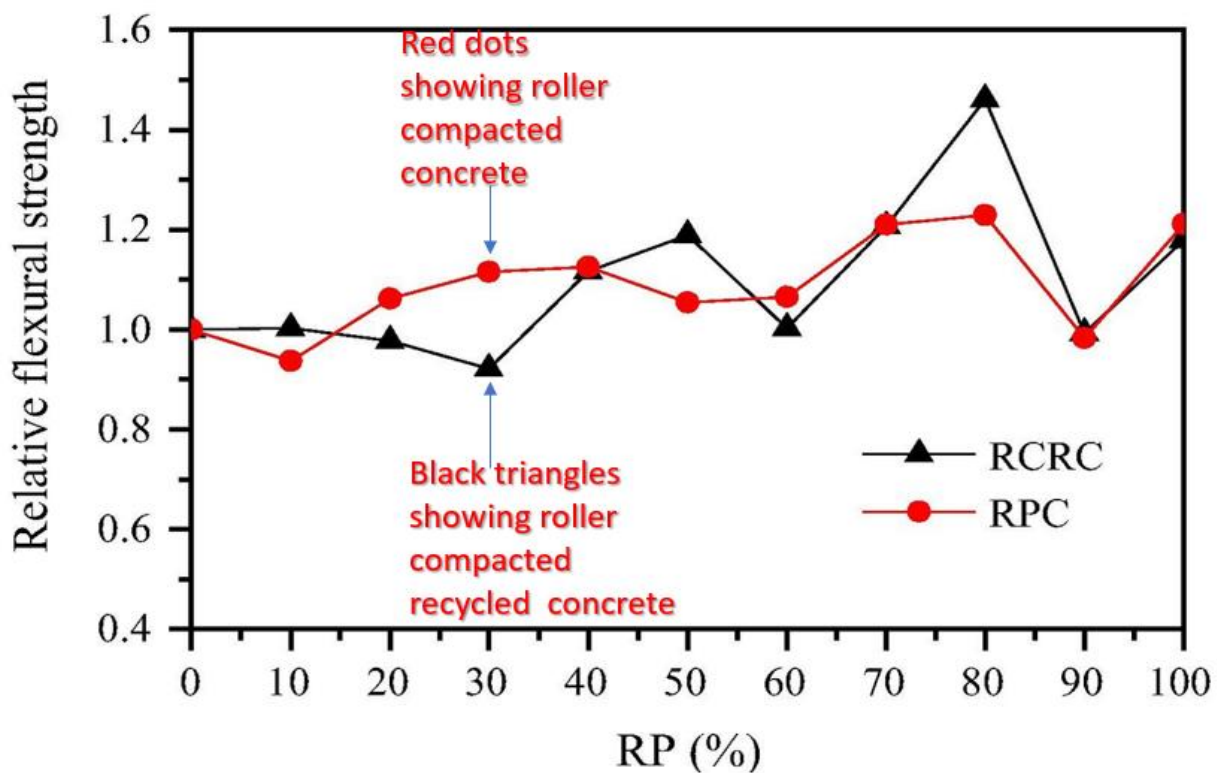


Figure 2.2-Relative Flexural strength Trend (Source: Adapted from Zhou & Chen 2017)[51]

2.1.3.4. Modulus of Elasticity

Tests on modulus of elasticity using different concrete showed that for concrete where fine aggregates were replaced with 30% of recycled content, there was a reduction in the modulus of

elasticity. In the case where the replacement was up to 100%, there was a significant reduction in the modulus of elasticity (Evangelista & De Brito, 2007)[52].

Some related findings for the modulus of elasticity for recycled concrete are visually represented in Figure 2.3, as shown below.

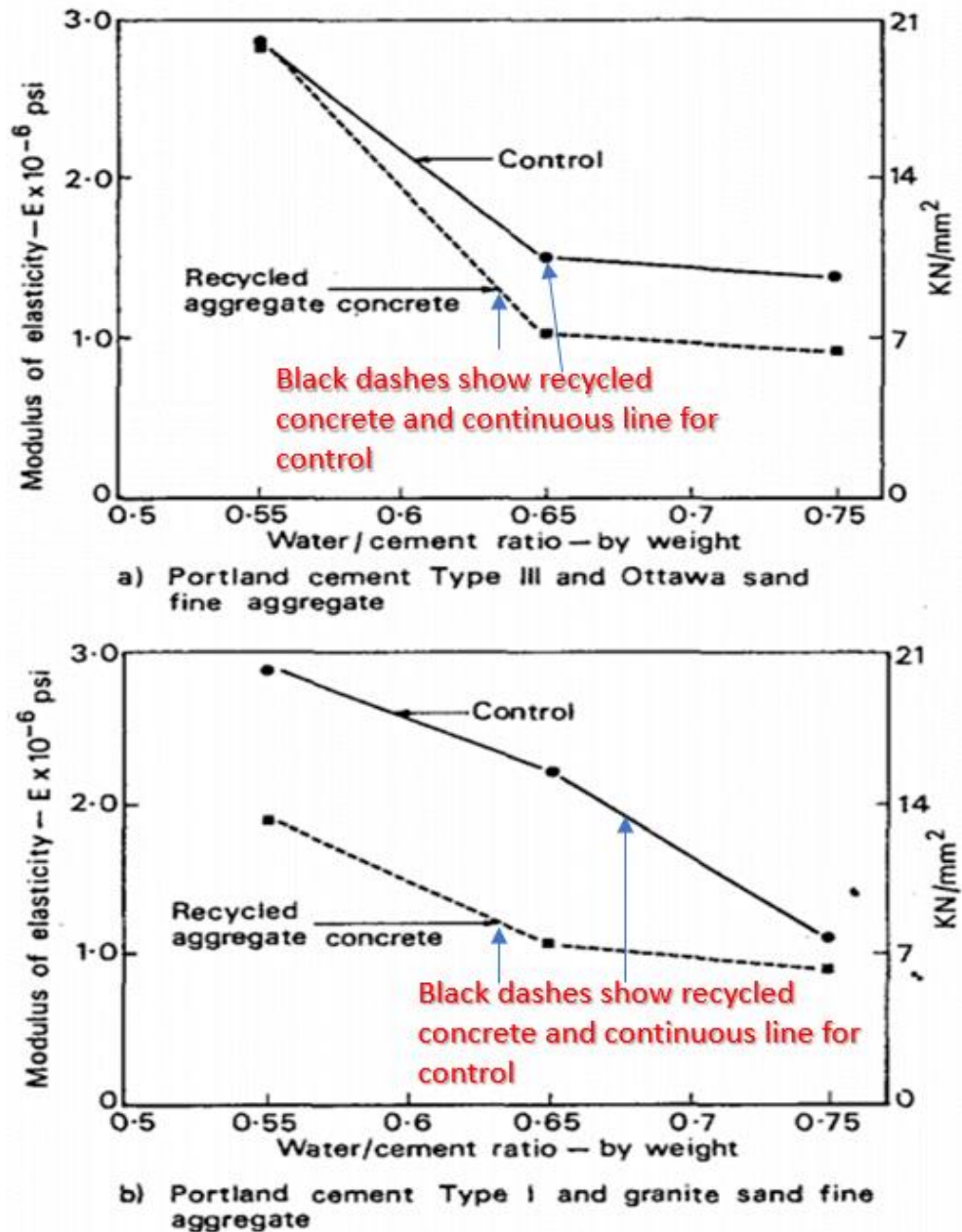


Figure 2.3-Relationship between Modulus of Elasticity & Water/Cement ratio (Source: Adapted from Frondistou-Yannas, 1977) & (Nixon, 1978)[40][53]

The elastic modulus of RAC has generally been measured to be lower compared to NAC, primarily due to the presence of adhered mortar, which is a weak and porous material phase[48]. Furthermore, reducing the maximum aggregate size leads to a further decrease in the elastic modulus. This reduction is attributed to the combined effects of increased surface area of the cement mortar paste in the concrete and the increased content of adhered mortar in the system[53]. Overall, it has been observed that the elastic modulus of RAC is typically 5% to 20% lower than that of concrete made with natural aggregates[53][54][55][56].

2.1.3.5. Poisson's Ratio

The Poisson's ratio for conventional concrete ranges between 0.15 and 0.22, this is because this value is highly dependent on the properties of the aggregate that constitute the mixture (Neville, 1997)[57]. In general, there are very few studies that have measured Poisson's for RAC. Therefore, this constitutes a gap to which further research can provide answers to.

2.1.4. Mechanism, Grading and Absorption of Recycled Aggregates

The mechanism for the grading and the absorption of the aggregates for recycled concrete is synonymous with that of recycled concrete. While there are a few codes which specify how to approach recycled materials in terms of assessment, there is not yet a distinct one that specifies the grading and absorption of aggregates to be different from that of recycled concrete.

ACI CRC 18.517 suggest the use of ASTM C136 and other similar methods for determining the gradation of the aggregates.[48][58]

According to Xiao (2018), recycled concrete have specialize machinery and equipment used for crushing, ranging from jaw crushers to impact crushers[31]. Hansen (1986) & Chen et. al., (2003) discovered that by using a crusher, it was possible to obtain a gradation that was similar to that of normal aggregates[59][60]. Although they can be readily packed and transported from and to different sites. However, the means of conveyance should meet certain requirements listed below:

1. The different sizes of the coarse and fine aggregates should be packed separately
2. Care should be taken to avoid the RCA mixing with normal aggregates
3. Avoidance of clay materials which can adjust the properties of the aggregate or its final product

4. The data of the materials crushing and grading should be correctly logged and kept readily accessible

Table 2.2 shows the testing requirements for recycle coarse aggregate, while table 2.3 shows the sieve sizes for gradation of crusher products as given by ACI 555R-01[60] .

Table 2.2-Requiremenets for Testing Recycled Coarse Aggregates(Source: Xiao, 2018) [31]

No	Test
1	Sieve Analysis
2	Apparent Density
3	Moisture Content & Water Absorption
4	Porosity
5	Clay Amount
6	Clay Lumps Amount
7	Elongated and Flaky Particles Content
8	Organic Material Content
9	Robustness
10	Crush Value
11	Sulphides & Sulphates
12	Alkali Activity Test
13	Chloride Ion Content

Table 2.3-Grading of Crusher Products(Source: ACI 555R-01)[60]

Sieve Sizes in (mm)	Mass(%)
>1.5 (37.5)	97
1.5 (37.5)	68
1.0 (25.0)	53
0.75 (19.0)	34
0.50 (12.5)	26
0.38 (9.5)	13
0.19 (4.75)	0

Another very important property of recycled concrete is its water-absorbing properties. It is generally known that recycled aggregates are more porous than normal aggregate. To buttress this point, ACI 555R-01 describes the absorption property of recycled concrete as a unique distinguished feature from normal aggregate[60]. Based on findings, Hansen (1986) discovered that due to the adherence of the old cement mortar, it had contributed to the high absorption of the coarse recycled aggregates. Therefore, ACI CRC 18.5 recommends that the free water in recycled concrete is ideally about 5% above that of normal concrete made with conventional materials in cases when superplasticizers are not used. Therefore making a hypothesis that this rate of absorption can influence the fresh concrete properties, and in that case may affect the shrinkage capabilities due to the exchange of water that occurs between the period of its drying shrinkage to the period of hydration[48].

A few studies have also provided a range for the absorption capacities which is shown in table 2.4 below:

Table 2.4-Findings on RCA Water Absorption Capacity (Source: ACI 555R-01)[60]

References	RCA Sources	Water Absorption Capacity (%)
Rahal [61]	1	3.47
Etxeberria et al. [62]	1	4.45
Movassaghi [63]	2	5.2-11.6
Gokce et. al. [64]	2	3.19-5.58
Hansel and Narud [65]	3	5.7-6.0
Xio and Falkner [66]	1	9.25
Tam and Tam [67]	10	0.57-8.74

2.1.5. Moisture Content Evaluation of Recycled Concrete Aggregates

The moisture content for a given sample of recycled aggregate can be determined by simply following the ASTM C 566-97 Standards for determination of Moisture Content for normal aggregates by simply drying[68]. It further gives the formula for calculating the moisture content for a given aggregate after sampling.

$$p = 100(W - D)/D \quad 2.1$$

Where:

P = total moisture content of the sample expressed in percentage

W= original mass of the sample in grams

D = mass of oven dry sample in grams

Sun et. al., (2022) studied the effect of moisture content on the performance and durability of concrete produced using recycled aggregate. They discovered that the moisture content which was

in the range of 50-65% enhanced the pore structure and products of hydration with an internal mechanism of curing[69]. While Poon et. al., (2004) have related slump values to the moisture states of the aggregates used in the recycled concrete[70].

2.1.6. Advantages of Recycled Concrete

With continued research in low-carbon concrete, many researchers have begun to consider the effects of replacing normal aggregates with recycled concrete aggregate but still preserving the durability and strength properties of the concrete. Some of these studies have emphasized some of the applications and advantages of using recycled concrete which are detailed below:

1. According to Limbachiya (2004), high-quality recycled aggregates can be obtained from demolished buildings[71]
2. Limbachiya (2004) suggests that demolition debris can serve as recycled aggregate for new concrete production[71]
3. The study conducted by Limbachiya (2004) revealed promising results, indicating that using 100% recycled aggregate (RCA) in concrete does not negatively impact its strength[71]
4. To effectively manage the influence of recycled aggregate, it is advisable to control the water-cement ratio of the concrete mix, as proposed by Limbachiya (2004). As noted by Limbachiya (2004), adjusting the water/cement ratio in the specified recycled concrete mix allows for achieving equivalent strength between normal aggregate and recycled aggregate (RCA) concrete[71]
5. It is economical compared to conventional concrete and has a good ability to resist heat and acid respectively (Baikerikar, 2014)[72]
6. There is a reduction in the use of cement and also the pollutants emitted during the production is reduced (Baikerikar, 2014)[72]
7. In certain materials, it exhibit better compressive and the splitting tensile strength when compared to normal concrete (Baikerikar, 2014)[72]

2.1.7. Disadvantages of Recycled Concrete

1. The time taken to sort the aggregates and to separate them into the right sizes is a key factor in determining if the recycled concrete is sustainable. Paranhos et. al., 2016 proposed a sorting platform to eliminate this difficulty since sensor based sorting has been considered a great idea[73]
2. Another disadvantage is the transportation costs involved in the movement of the aggregates. Paranhos et. al., (2016) found out that cost is reduced exponentially with the rate of substitution of the recycled materials, which is evidence when there is improved quality[73]
3. Compressive strengths are less compared to normal concrete (Baikerikar, 2014)[72]
4. Shrinkage and creep are higher compared to normal concrete (Baikerikar, 2014)[72]
5. Flexural strength is less in green concrete (Baikerikar, 2014)[72]
6. Lifespan of structures made from green concrete is less (Baikerikar, 2014)[72]

2.1.8. Limitations to the Adoption of Recycled Concrete in Practice

Since sustainability is a concept that is being continuously explored when recycled aggregates are used for the production of concrete, there are still drawbacks that tend to pose limitations to the use of RCA in construction works and in research. Some of these drawbacks have been highlighted below.

1. As mentioned in the disadvantages, a second thought is usually given when considering the time taken for the materials to be sorted, transported and the cost of handling were applicable.
2. Another thing is since material sources and properties are bound to change, investigating the aggregates may be at an additional cost which users may ponder upon. This implies that additional cost is incurred during the testing and validating of the RCA. This is unlike natural aggregates that don't need much testing since they already have their specifications and standards.

3. The legal was for the acquisition of landed property to be used for recycled operations (Khan, 2005)[74]
4. The process involved in removing contaminants. While the recycled aggregates obtained from demolished builds tend to be usable. There is need to remove other unwanted materials that may act as contaminants if immediately used for the production of concrete. Therefore, it becomes an issue of cost. (Khan, 2005)[74]
5. Constant power supply required for the process (Khan, 2005)[74]. If a mechanised means will be adopted to separate the aggregates based on their sizes, then an uninterrupted power supply would be required to achieve it.
6. Applicable taxes, fees, permits, and depreciation costs (Khan, 2005)[74]

2.1.9. Structural Use of Low-Carbon Concrete

The variability of the materials used in producing recycled concrete has therefore been in question over the years. Although researchers have continued to explore the effect of using recycled concrete in different structural members. These studies have generally included beams, slabs, walls, and a very few foundations. Therefore, some of these structural uses are listed in the table below.

Table 2.5-Summary of Concrete Investigating the Structural use of Low-Carbon Concrete

No.	Structural Application	Note
1.	High Strength Concrete	Limbachiya et. al., (2000) tested the use of recycled aggregates in high strength concrete when replacement of the coarse aggregate was up to 30 % and there was no effect on the strength properties, after which an increase in the recycled aggregates led to a decreased strength[75].
2.	Composite Members	Zhang et. al., (2023) have shown the application of recycled concrete when concrete-steel hollow beams are tested. The result showed that FRP

		Concrete-Steel hollow beams were ductile. Which is a typical example of its application in composite members[76].
3.	Flexural Members	It has also been used for multi-generation concrete beams made from recycled aggregate in a study by Visintin et. al., (2022), findings showed that there were no negative effects when multi-generation recycled concrete was used. However the cracks and tension stiffening were affected the serviceability limit.[77]
4.	Compression Members-Columns and Geopolymer Concrete Columns	Research into the compressive behavior of columns has been carried out and the strengths were in line with standards (Choi & Yun et. al., 2012)[78]. Also, Raza et. al., (2021) used recycled concrete for geopolymer concrete columns and they discovered that by decreasing the space of the GFRP spirals, the ductility and lateral confinement was increased[79].

2.1.10. Behaviour of Reinforced Low-Carbon Concrete Slabs

There have been numerous of studies and still ongoing studies on how the material properties of recycled aggregate can affect the performance of slabs. A summary of these findings and research work is detailed below:

An investigation into the punching shear behaviour of slabs when RCA was used showed that there was a decrease in the stiffness and that the cracking load also decreases. With the use of numerical model, the experimental response of the slabs were decoded and the effect of the fracture energy was also noted (Reis, 2015)[19].

Another study on the punching shear evaluation of slabs made from recycled concrete revealed that the mechanical performance reduced with increasing ratios of the recycled aggregates and highlighted the importance of the reinforcement role in the analysis (Francesconi et. al., 2016)[80]. A study by Stochino et. al., (2017) on the “Cracking of Reinforced Recycled Concrete Slabs” also showed decreasing performance by increasing recycled aggregates ratio[21]. This also confirmed results presented in a study by (Francesconi et. al., 2016)[80].

Lima et al., (2018) investigated the use of short sisal fiber reinforced recycled concrete block for use in one-way precast concrete slabs”. They found that slabs containing SSFRC had a higher stiffness when it was compared with other blocks. There was no linked effect of cracking or the maximum flexural stress by the recycled aggregates[81].

Michaud et al., (2016) evaluated the shear performance of slabs when recycled concrete aggregate were used to cast them. They applied the use of fibre optic sensing also known as FOS; in their investigation, it discovered that the shear capacity and shear force was exceeded that of the control specimens, and consequently recommended special design consideration for specimens in the range of 20% replacement by volume[82].

The mechanical and environmental assessment of steel-bars truss slab when recycled concrete reinforced with steel fiber was used revealed that the addition of steel fibres had a chance to improve the crack patterns, while increasing the thickness of the slab can greatly improve the flexural capacity of a steel-bar truss slab (Yuan et. al., 2023)[83].

2.2. Flexural Behaviour and Design of Reinforced Concrete Slabs

To support the slabs, structural members such as beams or even walls and columns may be used, and it is constructed in such a way that they are connected monolithically (Darwin & Charles, 2021)[84].

The slab may be supported on two sides, which is referred to as a one-way slab. In another instance the slab may be supported on all four sides, and referred to as two-way slab, Beams may or may not be provided on both sides or intermediary, depending on the design and the loading conditions (Darwin & Charles, 2021)[84].

While slabs resist gravity loading through flexure, punching shear is a typical failure pattern that is peculiar to slabs with two-way action. There have been numerous experimental research studies

focused on incorporating sustainable and recycled materials in reinforced concrete slabs whose review, will form the basis of this thesis work.

In the sub-section of this section 2.2, details on the different slabs and how they act and carry loads will be discussed, and finding on the different types of slabs and their evaluation based on the different available and applicable codes locally will be discussed in the context.

2.2.1. One-Way Slabs

One-way slabs are generally referred to as slab that span in one way direction. As generally know, their main reinforcement is usually in the one-way direction to be able to resist the stress it is subjected to along the plane. This stress is termed the bending stress.

In the case of analysis, one-way slabs could be restrained at the support to any degree or might also be unrestrained depending on the conditions that are applicable (Hoffman et. al. 1998)[85].

In cases where the ACI Code mandates stirrup but excludes footing and slab from such requirement, this may refer to one-way slab, depending on code definitions. One way slab could be ribbed, hollow or even solid. In cases where ribbed slabs exceed the minimum limits, they are otherwise designed as a beam or slab (Hoffman et. al. 1998)[85].

While one-way slabs may not be of same depth, they could be possibly hunched; and in such cases, its effect on the moment, stiffness, flexural properties, as well as shear strength and deflective parameters will be considered.

Lots of researchers have paid critical detail to how one-way slabs behave. For example, an experimental investigation into a reinforced pre-cast one-way slab revealed that the presence of steel truss could possibly avert the brittle failure that developed and give rise to a ductile failure, and that the spacing as well as the length of the lapping of the rebars can influence the load capacity of the slab (Liu et. al., 2021)[86].

Figures 2.4, 2.5, and 2.6 illustrate the behaviour of a one-way slab.

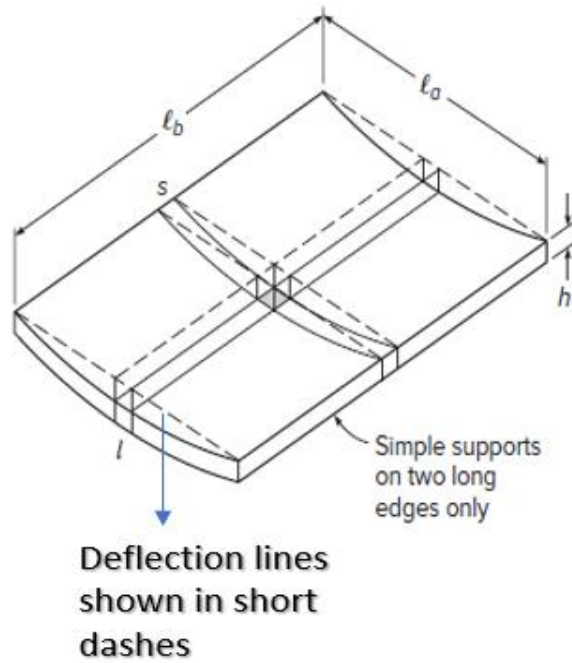


Figure 2.4-Shape of Deflection of One-Way Slab Loaded Uniformly (Source: Adapted from Darwin & Charles, 2021)[84]

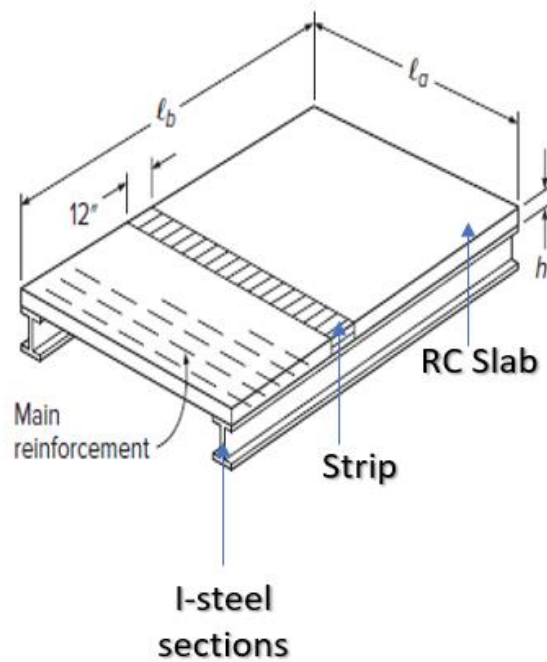


Figure 2.5-Illustration of a Unit Strip as a Basis for Design in Flexure (Source: Adapted from Darwin & Charles, 2021)[84]

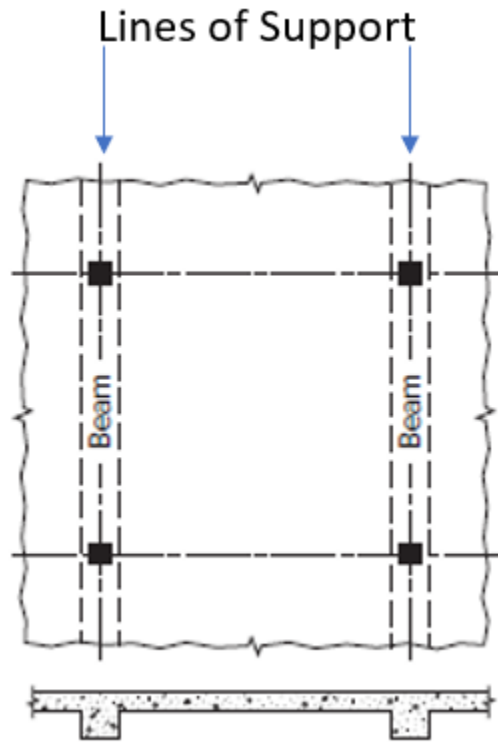


Figure 2.6-Typical One-Way Slab (Source: Adapted from Darwin & Charles, 2021)[84]

2.2.2. Two-Way Slabs

When a two-way slab supports gravity loads, it is expected to be curved in its both directions, and this is because of the existence of moments in both directions. Therefore, reinforcement is typically provided in both directions to resist the occurrence of these moments [84].

Typical characteristics of a two-way slab include it is supported by walls or beams on the four sides and therefore subjected to two-way action. In its simplest form, it could also be supported by very stiff, deep, or monolithically connected beam, in some cases by walls or even steel girders. Another point to note is that the support offered in both directions must be sufficiently stiff to prevent yielding or significant deflection. A more convenient illustration is given below in figure 2.7 and 2.8 respectively. [84]

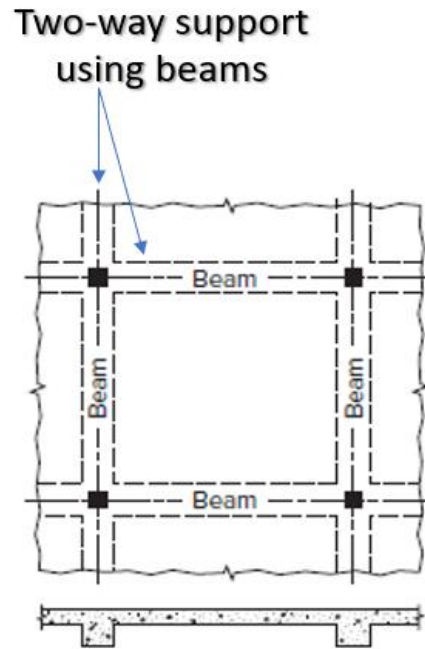


Figure 2.7-Center Strips Bending (Source: Darwin & Charles, 2021) [84]

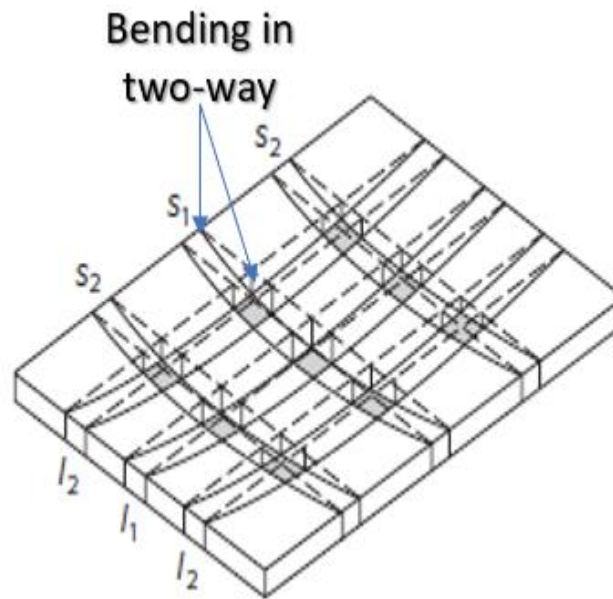


Figure 2.8-Grid of Slab Model (Source: Darwin & Charles, 2021)[84]

To compute the midspan deflection of the two-way slab, the following formula may be used.

$$\delta = 5wl^4/384EI \quad 2.2$$

Where

W = the uniform loading acting (kN/m)

E = modulus of elasticity (MPa)

L = length (m)

I = the moment of inertia (m^4)

Then the value obtained is compared to that for the limiting deflection given as:

$$\delta = L/250 \quad 2.3$$

To account for the cracks, a better approach will be to use a Finite Element Model or special coefficients. Since this thesis work is focus on two-way slabs, the deflection approach of the ACI crossing beam method will be studied and how the design parameters govern the properties of the slab in detailed sub-sections below. Figure 2.9 shows describes this better.

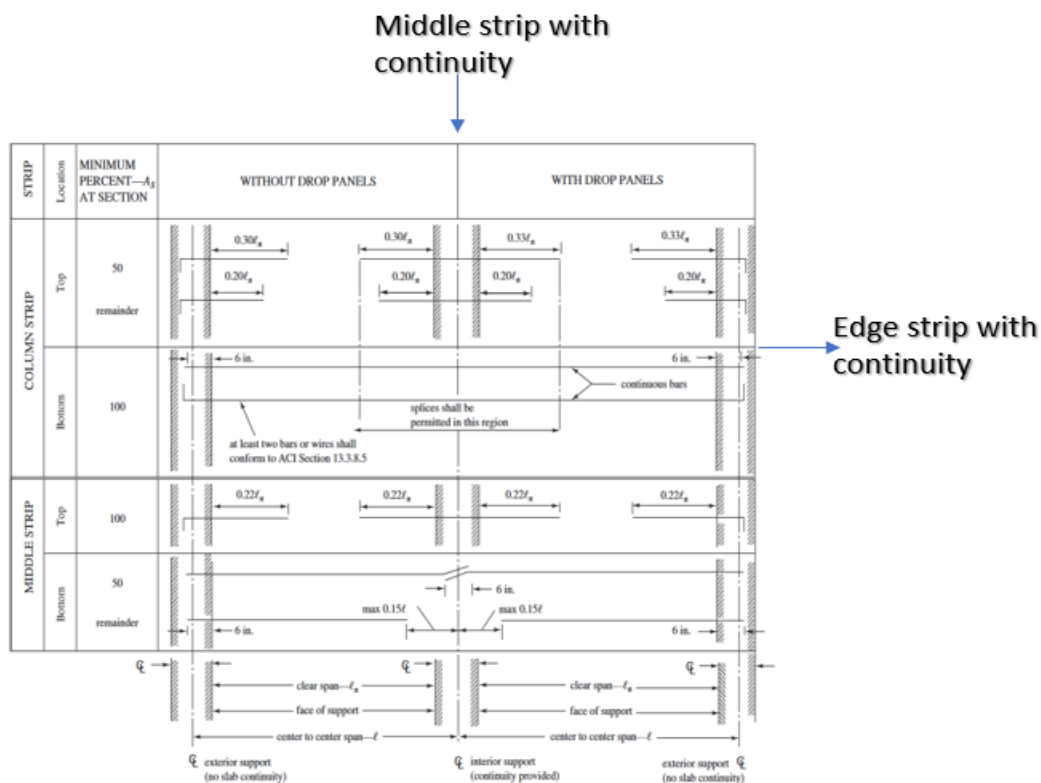


Figure 2.9-Minimum Reinforcement Extension for Slabs without Beams(Source: Adapted Darwin & Charles, 2021) [84]

Figure 2.9 above gives the minimum slab reinforcement when there are no beams in consideration. Furthermore, the table below shows the requirement for the minimum thickness and how it affects interior beams.

Table 2.6: Minimum Thickness for Slabs without Interior Beams (Source: Darwin & Charles, 2021), ACI 318 Code)[84][87]

Yield Stress f_y , psi	Without Drop Panels			With Drop Panels		
	Exterior Panels		Interior Panels	Exterior Panels		Interior Panels
	Without Edge Beams	With Edge Beams ^a		Without Edge Beams	With Edge Beams ^a	
40,000	$\ell_n/33$	$\ell_n/36$	$\ell_n/36$	$\ell_n/36$	$\ell_n/40$	$\ell_n/40$
60,000	$\ell_n/30$	$\ell_n/33$	$\ell_n/33$	$\ell_n/33$	$\ell_n/36$	$\ell_n/36$
80,000	$\ell_n/27$	$\ell_n/30$	$\ell_n/30$	$\ell_n/30$	$\ell_n/33$	$\ell_n/33$

^a Slabs with beams along exterior edges. The value of α_f for the edge beam shall not be less than 0.8.

2.2.3. Differences between One-way and Two-way Slabs

While one-ways and two-way slab system provides an excellent structure upon which components or loads are applied, they vary in their individual capacities and therefore it is important to distinguish them from one another based on their features, bending patterns and definitions. Table 2.7 offers some of the common differences known by engineers.

Table 2.7: Differences Between One-Way & Two-Way Slab

No.	One-Way Slab	Two-Way Slab
1.	The ratio of the long span to the short span is greater than or equal to 2	The ratio of the long span to the short span is usually less than 2
2.	Loads are primarily carried in one direction, therefore bending occurs in one direction only	Load is carried by two-way action in both direction and therefore bending occurs in two directions
3.	The supports are usually on both sides which could be beams and walls	The supports are on the four sides of the slabs which could either be beams or walls

4.	Economical in the sense that the steel quantity used is usually lesser.	This is more expensive as the larger area and 2 directions each require more quantities of steel
----	---	--

2.2.4. Analytical Methods for Computing Design Moments of Two-Way Reinforced Concrete Slabs

The behaviour of a slab is fundamentally dependent on the type of slab selected which is based on the design, safety, and cost effectiveness, which is usually selected by the design engineer. A combination of the above-mentioned factors will help to choose the most effective but suitable design for the building or the load to be distributed.

Several studies have approached design of slabs differently based on different applicable codes in the jurisdiction or locality and also based on proposed existing models and analytical models. Some of the different methods of slab design and analysis is discussed in the following sessions.

2.2.4.1. Strip Method

The Hillerborg's strip method for slab design and analysis is based on the theory of plasticity, which is similar to the yield line method of analysis. To begin with this method, a pattern of loading is assumed, and then average design moments are calculated in such a way that they are consistent with the load distribution that was assumed. To eliminate the difficult in treating column and walls, Hillerborg developed an advanced strip method which was based on the provision of a corner support element (Alexander 1999)[88].

2.2.4.2. Direct Design

The direct design method uses a semi empirical approach to solve for the moment and the shear in two-way slab. While this approach is quite restrictive in the sense that it requires a minimum of three continuous spans that are almost equal, and three could be variations in the column positions. Therefore, it cannot be used for footing designs and when prestressed concrete slabs are required (Darwin & Charles, 2021)[84].

Section R13.6 of ACI-318-11 named the provides the fundamental steps for the use of the direct design methods as follows[87]:

1. Solve for the total factored statical moment
2. Distribute the total factored statical moment

3. Distribute the moments that are negative and positive to the supports and middle strips and to beams were applicable

The total statical moment can be computed as follows:

$$M_o = q_u l_n^2 / 8 \quad 2.4$$

Where

M_o = total factored static moment in kNm

q_u = load in kN

l_n = the length of clear span considered in the direction of action of moments in meters

2.2.4.3. Equivalent Frame Method

According to (Darwin & Charles 2021), the equivalent frame method was proposed by Peabody in 1948 and was updated based on laboratory testing. This method assumes that analysis will be carried out using the moment distribution method and where applicable a computer program is used[87].

According to ACI 318-11, section R13.7, this method analyses a three-dimensional slab as a two-dimensional frame which is centred on a column or by using support lines[87]. Figure 2.10 further illustrates the equivalent frame method of analysis.

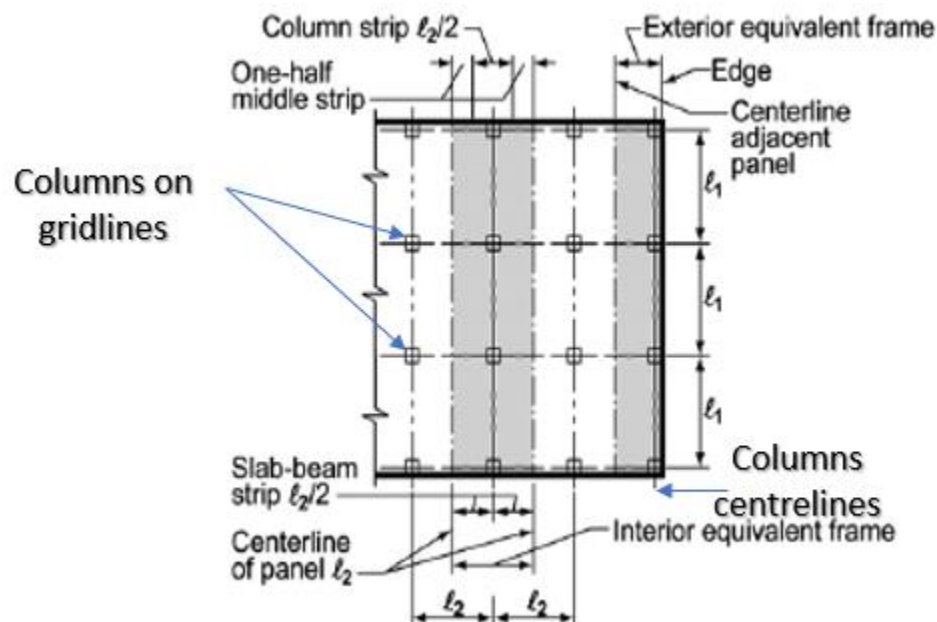


Figure 2.10-Equivalent Frame Definition (Source: Adapted form ACI 318-11)[87]

2.2.5. Flexural Behaviour of Slabs

Slabs are generally subjected to bending due to the loads acting on it and its direction will be based on the type of slab. As a structure is subjected to loads it become prone to flexure and deflections due to the internal stresses being developed as a result of the applied loads. Numerous investigations into the flexural behaviour of slabs have been ongoing for several years. A few of these studies will be reviewed in this section.

In 2003, Marzouk et. al, studied the flexural strengthening of two-way slabs by using fiber reinforced polymers; they successfully increased the stiffness of the flexural specimen; but this led to a ductile decrease in the specimens. Carbon FRP strips and glass FRP laminates can be effectively employed to enhance the flexural capacity of two-way slabs, resulting in an average increase of up to 36% when compared to the reference specimen, which remains unstrengthened, according to the authors. These strengthening measures also lead to an enhancement in the initial stiffness of the flexural specimens. However, it is worth noting that there is a noticeable reduction in overall ductility.

Their study also incorporated a finite element analysis of the two-way slabs that have been strengthened in flexure. The analysis utilized an incremental elastic-plastic concrete model, taking into account the concrete's behavior under compression. In this model, the concrete behaves elastically until it reaches a yield point, beyond which it exhibits irrecoverable plastic strain. The study considers both pre-cracking and post-cracking behaviors of concrete, with a specific focus on the influence of FRP materials on concrete's fracture energy and, consequently, its tension stiffening behavior.

It is assumed that there is a full bond between the concrete and the steel and FRP materials used for strengthening. The results obtained from the finite element analysis are then compared with the experimental findings, demonstrating a high level of agreement between the two sets of results. [89].

Chung et.al., (2018) studied “Two-Way Flexural Behaviour of Donut-Type Voided Slabs” while using the yield line method of analysis. The research examines the feasibility of implementing a two-way voided slab with a donut-type configuration. The investigation involved conducting a 12-point two-way bending test, primarily focused on assessing the global behaviors of this slab configuration. These behaviors encompassed various aspects such as load-bearing capacity,

flexural stiffness, ductility, deflection, and load distribution. Furthermore, the study delved into the design methodology for a donut-type two-way voided slab, utilizing the yield line method. The yield line method was applied to predict the load-bearing capacities of the donut-type voided slabs, demonstrating an impressive level of accuracy, with predictions aligning with actual capacities to approximately 95%.[90].

The test results yielded valuable insights. One of the donut-type two-way voided slabs exhibited behavior akin to that of a conventional two-way reinforced concrete slab, with an even distribution of load in multiple directions. However, a different donut-type two-way voided slab exhibited distinct characteristics, including uneven load distribution and different crack patterns.

Lee et al., (2018) studied the flexural behaviour of slabs both experimentally and analytically. The findings concerning the prediction of the flexural capacity of reinforced concrete (RC) slabs strengthened in flexure using a basalt fabric-reinforced cementitious matrix (FRCM). A total of 13 specimens were meticulously fabricated to comprehensively assess the flexural behavior of RC slabs that had been reinforced with a basalt FRCM composite. These specimens were subsequently subjected to rigorous testing under four-point loading conditions. Several experimental variables were considered in the study, including the type of fiber used, the ratio of tensile reinforcement, and the number of layers of fabric employed. The results revealed a notable increase in the maximum load-bearing capacity of the FRCM-strengthened specimens, ranging from an 11.2% to a remarkable 98.2% increase relative to the reference specimens. However, it was observed that the energy ratio and ductility of the FRCM-strengthened specimens tended to decrease with higher quantities of fabric and tensile reinforcement. Furthermore, the study successfully demonstrated that the effective stress level of the FRCM fabric could be accurately predicted by employing a bond strength model based on ACI 549 and Jung's model[91].

When the flexural behaviour of two-way slab was considered by Pawar et al., in 2022, they examine a total of five specimens, with one of these specimens being a solid slab and the remaining four being voided slabs. The voided slabs incorporate cube-shaped voids, with variations in the sizes and spacing between them, serving as void formers in the biaxial voided slabs. To assess the two-way flexural strength, they subjected each slab to sixteen-point loading, covering the entire slab area. Subsequently, they also obtained the load vs. deflection curves for each of the voided

slabs and compare them with those of the solid slab. The evaluation of flexural strength was conducted using the Rankine-Grashoff Theory, and the obtained results are compared with results generated by software simulations. The principal aim of this study is to investigate the elastic behavior of voided slabs and draw comparisons with solid slabs. The findings from the investigation substantiate that the flexural behavior of voided slabs employing dice-shaped void formers exhibits a strong correlation with that of solid slab systems[92].

One of the most recent studies on one-way slabs by Elgohary (2023), showed that new span to depth ratio could be used for slab limits not considered in the ACI-318 code. In his research, he conducted a parametric investigation on one-way slabs that provide support for non-structural elements. The primary objective was to assess how various design parameters influence the calculated thickness of these slabs. For the purpose of the analysis, he applied a deflection limit of ($L/480$). Based on the results of our parametric study and in alignment with the deflection limits outlined in the ACI-318 Code, he developed novel formulations for span-to-depth ratios. These formulas incorporate the impact of design variables on the structural characteristics of the slabs. Subsequently, he compared the outcomes obtained using our proposed formulas with the deflection limits specified in the code. Remarkably, the deflection values predicted by our formulations consistently fell below the code-prescribed limits in all the cases considered[93][94].

Finally, based on a research on the flexural behaviour of recycled concrete graded slab, it was revealed that the reinforcement ration, the percentage replacement of the aggregates as well as the grading can impact the flexural behaviour of slabs (Xiao et. al., 2014)[95].

It is therefore important to mention that the individual characteristics of the materials used will be studied and investigated independently and their interaction on the slab behaviour.

2.2.6. Code Provisions for Flexural Design of Two-Way Slab Systems

In the design procedure for flexure, slab system may be designed by the use of any procedure that does satisfy compatibility and equilibrium conditions, giving consideration to the supports. In this regards, it has to be evident that the factored resistance at each section must at minimum be equal to the factored loads and that the serviceability requirements and the deflection limits are also satisfied in accordance with the concrete design handbook, CSA A23.3-04[96].

2.3. Fibre Optic Sensing

Fibre optic sensing is the process of using fibre optic sensors to acquire data or information about the strain, temperature, humidity, or other parameters by using specialized interrogation techniques.

Distributed Fibre Optical Sensing permits the measurement of continuous strain while using a wide variety of gauge lengths and frequencies for the measurements (Galkovski et. al, 2021)[97].

Figure 2.11 below shows the fiber optic layers for use in the distributed fiber optic sensing's process as indicated by Soga & Luo, (2018)[98].

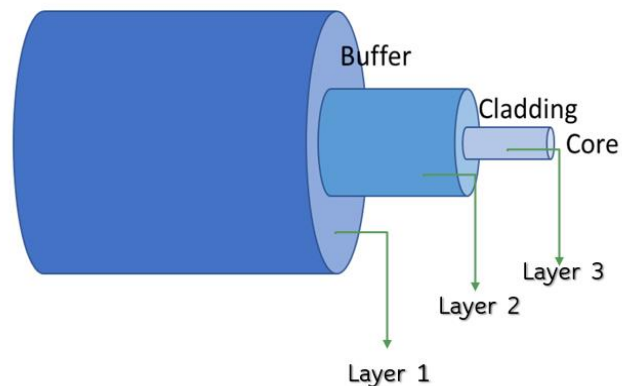


Figure 2.11-Fiber Optic Layers (Adapted from Soga & Luo, 2018)[98]

The response of reinforced concrete members is ideally governed by how the reinforcement and the concrete interact with each other. There have also been difficulties in investigating the transfer of stresses between the concrete and the reinforcing steel, which is due to certain limitations in the technology used for the measurements. Therefore efforts are still ongoing to unravel the variations in the steel used for structural concrete (Lemcherreq, 2022) [99].

Figure 2.12 below shows the differences in the strain gauge applied method when compared to the fibre optic sensors for strain measurement acquisition, and the principle of Rayleigh backscattering.

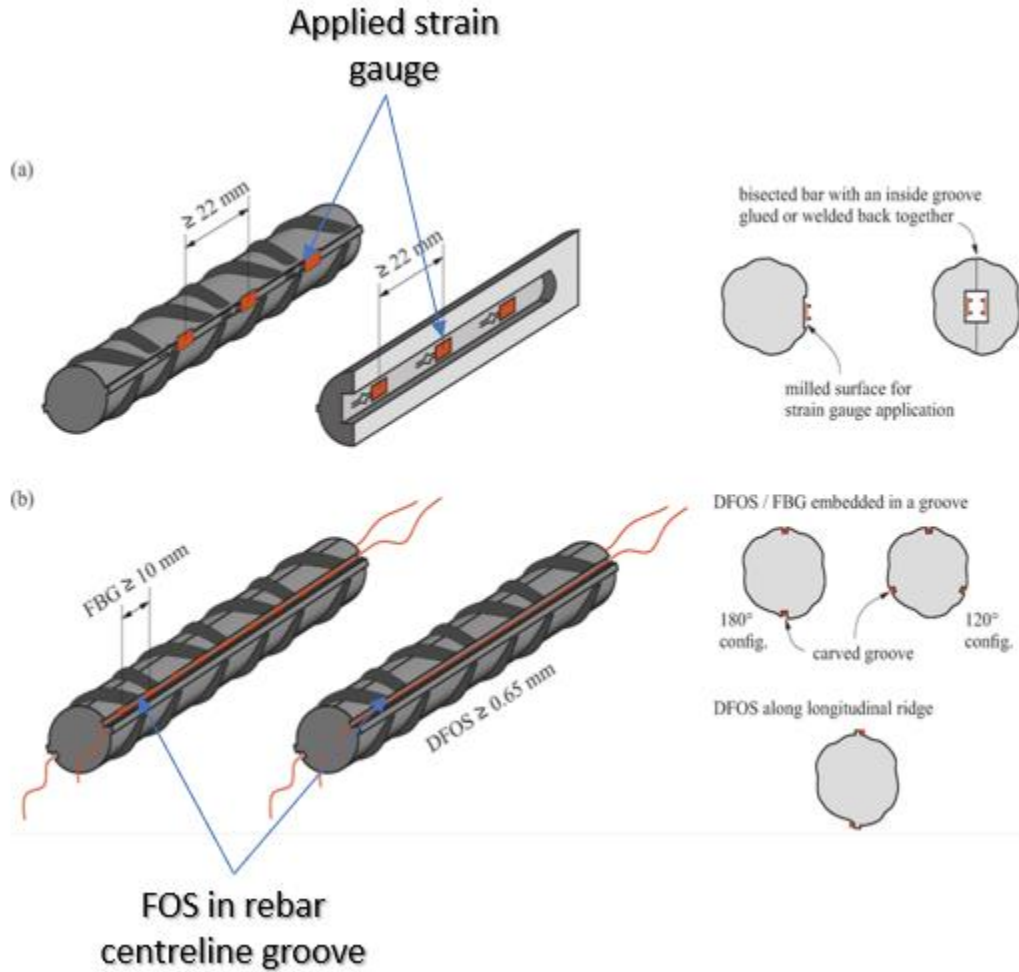


Figure 2.12-Glued Strain Gauges on Reinforcing Bars b) Fibre Optical Sensors on a Reinforcing bar by the use of Fibre Bragg Grating (Source: Adapted from Lemcherreq, 2022)[99].

2.3.1. Background & History

The fundamental essence of structural health monitoring (SHM) has been eloquently delineated by Housner et al. (1997)[100]. SHM was defined as the ongoing or periodic measurement and analysis of critical structural and environmental parameters during operational conditions. The primary objective is to detect unusual states or potential accidents at an early stage Housner et al. (1997)[100].

The application of fiber optic sensors for structural health monitoring was introduced approximately three decades ago. Over this span of time, the technique has undergone significant refinement, now yielding measurements of comparable accuracy to standard strain gages and extensometers. The contemporary landscape features three distinct types of fiber optic sensors for

structural health monitoring: localized fiber optic sensors (interferometric FOSs local sensors), quasi-distributed sensors (Fiber Bragg grating (FBG) sensors), and distributed fiber optic sensors, such as optical time domain reflectometry (OTDR) or Brillouin scattering (Sergi & Casas, 2013)[101].

Leung (2001) furnishes a comprehensive assessment of the potential utility of fiber optic sensors in monitoring concrete structures. Furthermore, innovative distributed fiber optic sensing approaches for concrete structures, encompassing flexural crack detection and delamination identification, are expounded[102].

Li et al., (2004) present an overarching overview of ongoing research and advancements in the realm of structural health monitoring with applications in civil engineering[103]. More recently, Majumder et al. (2008) have encapsulated research and development undertakings in SHM utilizing FBG. Their work provides a holistic state-of-the-art panorama, critically appraising FBG usage while pinpointing areas necessitating further exploration[104].

Distributed sensors hinge on the modulation of light intensity within the optical fiber. The two principal methodologies for DFOS are optical time domain reflectometry (OTDR) and Brillouin scattering. OTDR harnesses Rayleigh and Fresnel scatterings for perceiving structural perturbations. Conversely, Brillouin scattering detects light frequency Doppler shifts linked to measurements (Sergi & Casas, 2013)[101].

The principle of distributed sensing involves in transmitting a narrow light pulse through the optical fiber and capturing the backscattered light signal. The acquired signal furnishes intricate insights into local loss distribution or reflections along the fiber due to various attenuation mechanisms or fiber non-homogeneities. The defect's location can be determined through 'time of flight' calculations. Although resolution is on the order of meters, the operating range can extend several kilometers, rendering this technique highly effective for pinpointing fiber breaks (Sergi & Casas, 2013)[101].

2.3.2. Fiber Optic Sensors

The initial mention of fiber optic sensors can be traced back to the development of flexible endoscopes during the first half of the twentieth century, ushering in a revolutionary era in the medical field that persists to this day (Udd & Spillman, 2011)[105]. However, the true

commencement of the modern era of optical fiber sensors was in 1977, primarily for long-distance telecommunications, and over the past four decades, it has witnessed a remarkable exponential advancement. Sensing applications emerged as a derivative of this technology, capitalizing on advancements in optoelectronic components and principles (Barrias & Casas, 2016)[106]. By 1982, a diverse range of fiber optic sensors had already been devised and were under research, encompassing magnetic, acoustic, pressure, temperature, acceleration, gyro, displacement, fluid level, torque, photoacoustic, current, and strain sensors (Gialllorenzi et. al., 1982)[107]. This progressive phase of fiber optic sensor development was made possible through the creation of optical fibers with exceedingly low-loss characteristics, a feat achieved in the late 1970s(Udd & Spillman, 2011)[105].

The domain of fiber optic communications has indubitably transformed the telecommunications sector by delivering enhanced performance and reliability in communication links, all while reducing bandwidth costs. As the prices of components have plummeted and quality enhancements have been introduced, the potential of fiber optic sensors to replace conventional electric sensors has become increasingly viable (Yin et. al., 1963)[108].

A multitude of inherent advantages underscore the applicability of fiber optic sensors. Notable among these advantages are their resistance to electromagnetic interference, lightweight nature, compact size, heightened sensitivity, capability to withstand high temperatures, immunity to corrosion, and wide bandwidth capabilities.

2.3.3. Distributed Fibre Optic Sensing

Distributed Optical Fiber Sensors (DOFS) utilize the alteration in return light caused by the backscattering along the fiber due to various phenomena. This obviates the need for modifying the fiber core, as each fiber segment operates as a sensor. Consequently, DOFS offers a remarkable enhancement in spatial resolution compared to FBG systems. Simultaneously, three distinct scattering phenomena occur, providing the means to gauge fluctuations in temperature and/or strain along the fiber: Raman, Brillouin, and Rayleigh scattering (Soga & Luo, 2018)[98].

The analysis of Rayleigh scattering relies on the utilization of Optical Frequency Domain Reflectometry (OFDR). In this approach, the Rayleigh scattering pattern that occurs along the fiber is initially recorded and stored as a distinct fingerprint or signature of the fiber in its reference state. Subsequently, the Rayleigh scattering profile is re-measured when the fiber experiences

mechanical strain or temperature fluctuations. Both sets of data are divided into smaller segments, which are then transformed into the frequency domain through Fourier transformation. By conducting a cross-correlation process between the reference and perturbed states, a noticeable shift in the correlation peak's spectral position can be identified. This shift can then be calibrated to accurately represent variations in strain or temperature (Ding et al., 2018)[109]. The fundamental principle behind OFDR is to precisely discern alterations in the fiber's scattering behavior as influenced by external factors (Ding et. al., 2018)[109].

For this research project, the focus will be on the principle of using Rayleigh scattering method to obtain the distributed strain data, and which will also be the focus of this sub-section of the thesis.

Figure 2.13 below shows the working principle of DFOS using Rayleigh backscattering.

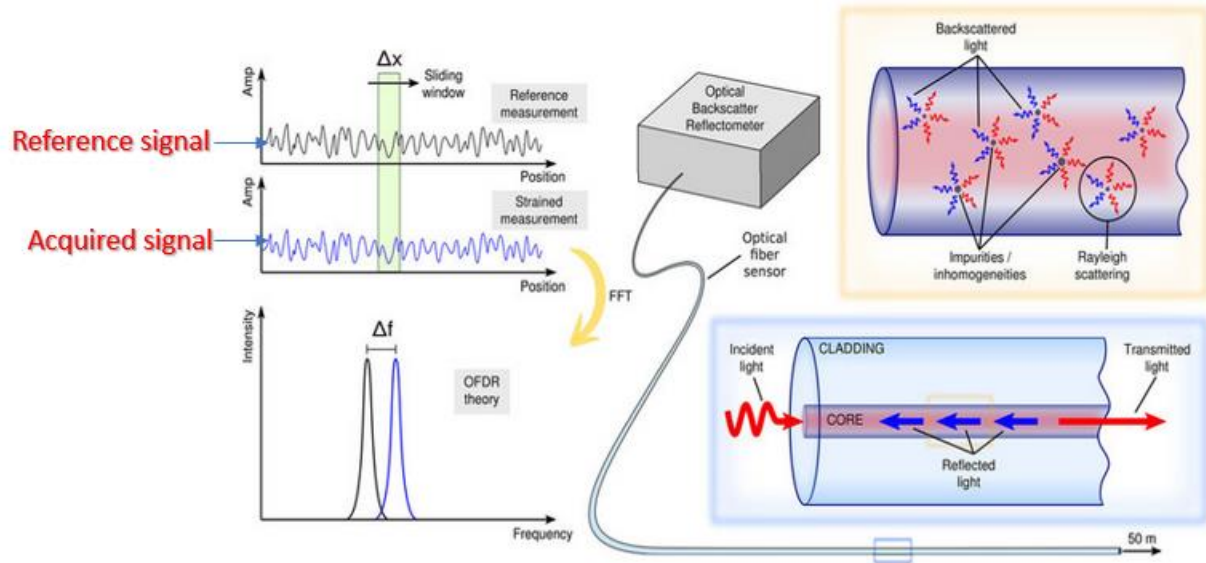


Figure 2.13-The Working Principle of DFOS Using Rayleigh Backscattering (Adapted from Berrocal et. al 2021)[110]

2.3.3.1. Rayleigh Scattering Principle

Several related optical phenomena occur within optical fibers, one of which is Rayleigh scattering (Palmieri & Schenato, 2013)[111]. This phenomenon takes place in various segments of the fiber and leads to variations in the local refractive index. Additionally, this effect is accompanied by backscattering, where the light beam is reflected by local imperfections in the glass structure and travels in the opposite direction to its original path.

With knowledge of the speed of light, data loggers, such as reflectometers, possess the capability to identify all occurrences, including micro-imperfections, with a spatial resolution on the order of millimeters (Sang et. al., 2011)[112]. The dispersion amplitude, while random, remains a consistent characteristic for a specific fiber and can be likened to a distinctive fingerprint (Buda-Ozog, 2022)[113].

Measurements based on Rayleigh scattering are responsive to alterations in both mechanical strains and temperatures, which induce modifications in the distances between local imperfections. This phenomenon manifests as shifts in Rayleigh frequencies between two consecutive measurement sessions (Buda-Ozog, 2022)[113].

Figure 2.14 below shows the spot gauges differences in comparison to DFOS sensors in an experimental test by Buda-Ozog et. al., (2022) [113].

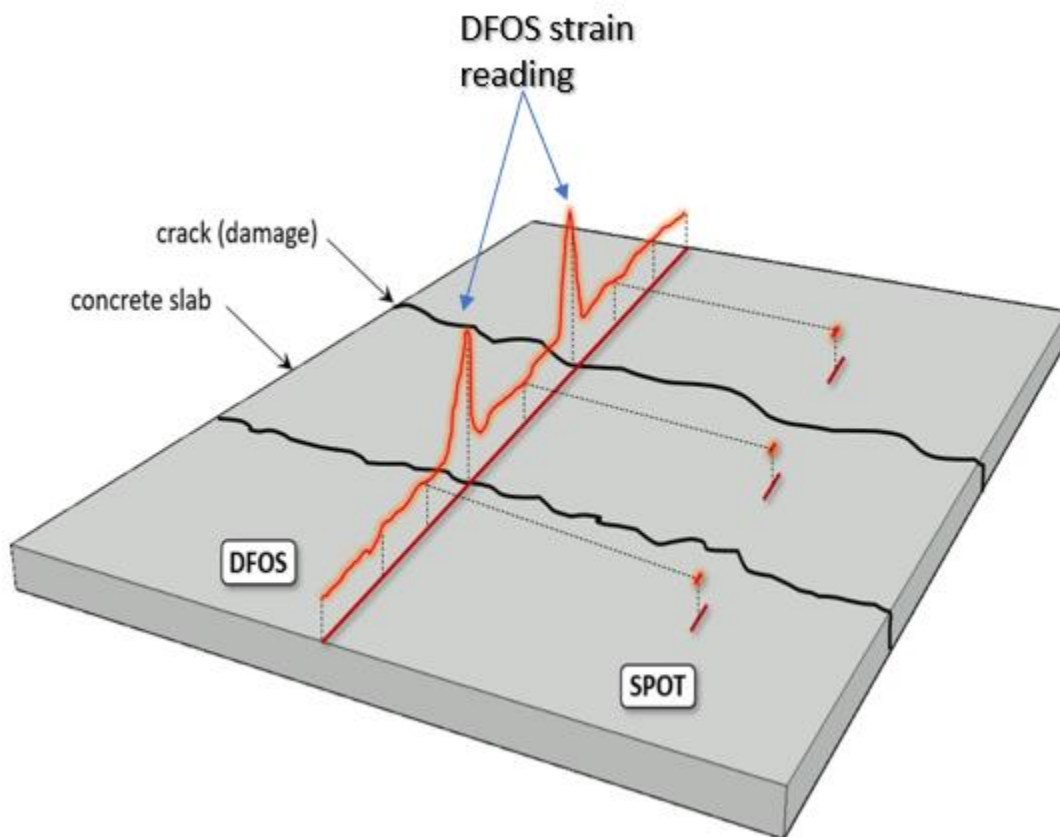


Figure 2.14-Spot Gauges Differences in Comparison to DFOS Sensors for a Slab (Adapted from Buda-Ozog et. al., 2022)[113]

2.3.4. Advantages of Distributed Fiber Optic Sensing vs Traditional Instrumentation Techniques

One significant advantage of optical fiber sensors is that they do not rely on electric current passing through the sensor. Consequently, optical sensors remain unaffected by electromagnetic interference, making them less susceptible to noise and ensuring greater stability compared to electrical instruments. Additionally, because glass fibers lack electrical conductivity, they are immune to damage from lightning strikes, making them suitable for use in structures like bridges or dams located in open areas. Optical fibers serve as low-loss waveguides for light, which is advantageous for remote sensing applications requiring a long communication link between the sensor and the demodulation unit. This characteristic is particularly beneficial for large structures such as bridges. (Leung, 2001)[102]

Another advantage of optical fibers is their potential for multiplexing. By employing a single signal demodulator shared by multiple sensors, the instrumentation cost for each sensor can be significantly reduced. Multiple sensors can be placed along a single optical fiber, simplifying the design of a sensor network, and streamlining sensor installation and connections to the demodulating system. (Leung, 2001)[102]

Optical fiber sensors exhibit remarkable versatility. They can be configured to measure various parameters and including the possibility of measuring two parameters simultaneously (e.g., both axial and transverse strains) using a single sensor.

To summarize, fiber optic sensors offer several advantages over electrical instruments in conventional monitoring applications. However, it is important to note that the current cost of an DFOS interrogator system, including optical sensors and associated optoelectronics equipment, is higher than its electrical counterpart. To make fiber optic sensors a direct replacement for electrical instruments in conventional applications, ongoing research and development efforts are needed to reduce both sensor and equipment costs. Nonetheless, innovative designs of fiber optic sensors can provide sensing capabilities beyond those of existing electrical instruments. Creative applications of these new sensors may lead to the development of more effective and reliable sensing schemes, potentially justifying their higher cost and encouraging adoption by forward-thinking clients.

2.3.5. Applications of DFOS Reinforced Concrete

The first structural strain monitoring system of this kind was proposed and demonstrated in 1999 (Demerchant et. al., 1999)[114]. Studies have since been conducted to monitor the structural strain of composite and concrete beams under limited load, reporting a linear relationship between the measured load and the average strain over the monitored spatial resolution (Zeng et. al., 2002)[115]. In 2001, a BOTDR system was used in a full-scale model of a river levee to demonstrate monitoring capabilities for potential collapse due to water penetration (Ohno, et. al., 2001)[116].

It is useful in the detection of cracks and corrosion in concrete structures (Goldfeld & Klar, 2013)[117]. Through their research, (Goldfeld & Klar, 2013) proposed an “iterative algorithm” which evaluates the different contributors to improve the curvature.

Another unique application is for bridge monitoring as seen in studies by Casas & Cruz, (2003)[118]; Enckell et al., (2011)[119]; Webb et al., (2017)[120]; Xu et al., (2016)[121]. Thereby showing how the values obtained were in the safe range or not.

DFOS can also be used for cable monitoring and discussed by Nazarian, et. al., (2016) who used distributed fiber optic sensors to detect tension loss in cables of cable-stayed bridges[122]. Another key application is seen in the Monitoring of composite structures, and this has been made possible through the use of DFOS. (Güemes, et. al., 2014)[123].

2.3.6. Identification of Gaps/Summary

Having done a thorough review on the different studies that are available on recycled aggregates, A few gaps have been identified which are well knitted to the objectives and the scope of this research. Therefore, I present the following gaps:

1. There is limited knowledge on the numerical evaluation of slabs made from recycled aggregate and supplemental materials.
2. Another significant gap is in the materials characterization and modeling of the two-way reinforced concrete slab which is a key objective and phase of this research work.

3. There is a gap in the study of the slab capacity of recycled concrete under varying elastic modulus. The estimation of the slab capacity at a given compressive strength and when the modulus of elastic for the different hardened concrete is ascertained. While also understanding the moment capacity of the section with the use of Response-2000.

This research therefore based on the above gaps, aims to fulfil the objectives of understanding the structural performance of recycled materials and the numerical evaluation by the use yield line, section analysis and specific deflection methods. A very unique and interesting study that aims to bridge some existing knowledge gaps and concerns.

2.4. Yield Line Analysis

A unique method for the assessment of the capacity of a slab and understand the behaviour of the slab with respect to its action under the application of load. Essentially, slabs that are loaded are analysed using yield line analysis. In specific, it is very useful in the examination of two-way slabs and for the determination of the plastic moment and the equivalent collapse load.

According to Kotteko et al., 2023, the yield line generally helps to provide the post-ultimate load and deformation relationship, which is obtained by deriving the plastic strain energy by utilization of a spatial mechanism due to the second-order displacement fields[124].

2.4.1. Principles of Yield Line Analysis

Caprani (2006) gives suggestions for the use of yield line for the determination of the plastic moment of slabs[125].

1. Utilize yield lines to divide the slabs into the regions that are rigid and will remain plane till collapse happens
2. The lines under consideration are straight
3. Rotation axes does lies in the support planes and passes over any columns
4. When adjacent regions are considered, the lines are made to pass the intersection points
5. Yield lines terminate at a slab boundary
6. Simple support attracts yield lines while continuous support repels yield lines

2.4.2. Procedure for Yield Line

Caprani(2006) gave a general procedure for the use of yield line in the analysis of two-way reinforced concrete slabs[125]. The assumptions are presented below.

1. Assume a collapse Mechanism
2. Estimate the load factor corresponding to the yield pattern
3. In reality failure occurs at the lowest collapse load factor

2.4.3. Identification of Yield Line Patterns

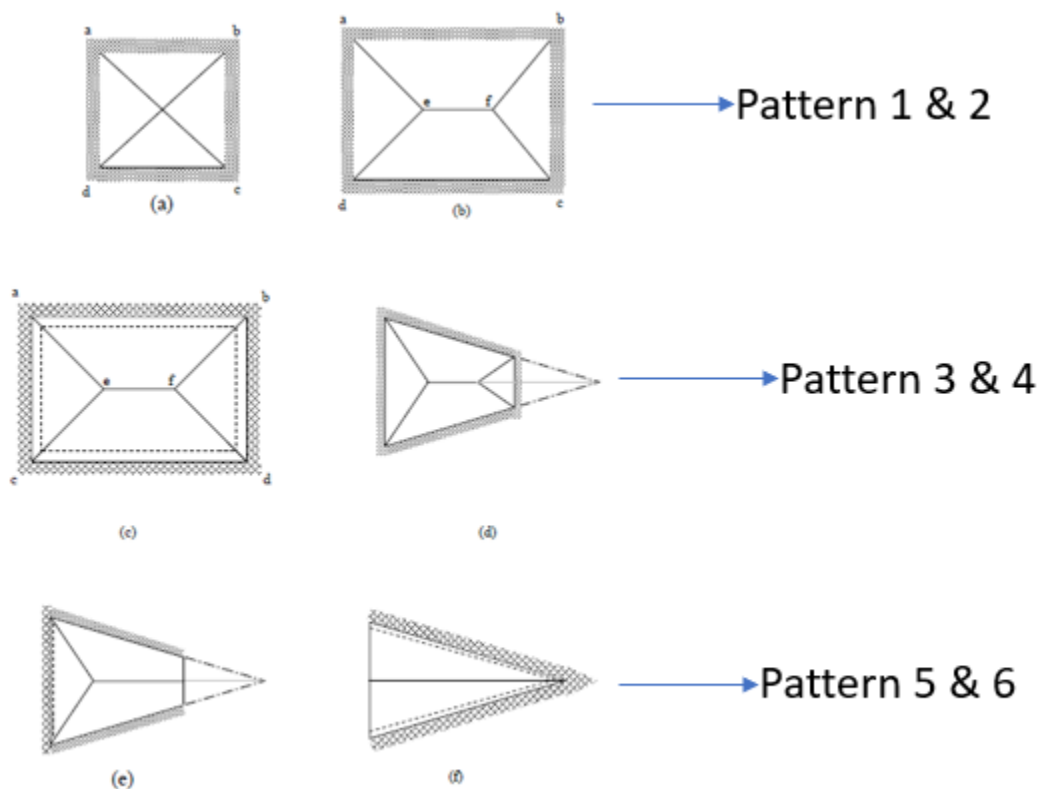


Figure 2.15-Some Possible Patterns (Adapted from Alasam, 2006)[126]

In the figure 2.16 below, it shows the possible yield line patters as illustrated by Alasam, (2006)[126].

2.4.4. Collapse Yield Moment and Slab Capacity Determination

To determine the moment and the capacity of the slab, we use the equation below:

$$M_r = \phi_s A_s f_y \left(d - \frac{a}{2} \right) / 10^6 \quad 2.5$$

Where M_r is the moment of resistance of the section, A_s is the area of steel mm/m, f_y is the strength of steel in MPa, d is the effective depth of the slab section in mm, a is the width of the loading plate in mm.

To compute the capacity of the slab section, it is

$$P = 8 \frac{M \times L}{L - a} \quad 2.6$$

Where M is the moment of resistance of the section in kNm, L is the clear span in meters, and a is the width of the loading plate or depth of neutral axis calculated in m.

2.4.5. Advantages of Yield Line over Linear Elastic Analysis

The yield line does have certain advantages as noted by Caprani (2006)[125]:

1. It is comparatively easier to use
2. The linear elastic method provides context on when the first yield will occur while the yield line estimates the ultimate capacity the slabs reach under load that and thus cause collapse.

2.4.6. Disadvantages of the Yield Line

Furthermore, Caprani (2006) gives the disadvantages of using the yield line method[125]:

1. The yield line generally requires experience to know what a possible failure mechanism could be
2. It is possible for dangerous designs to happen without proper checks and expert knowledge
3. It does not also provide information on the ideal service behaviour of the slab

It is important to note that the yield line does give the upper bound values in the estimation of the collapse load of the slabs.

2.5. Finite Element Analysis

2.5.1. Different Constitutive Models

2.5.1.1. Constitutive Model SBETA

The material model that constitutes SBETA involves the compression behaviour involving hardening and softening which is non-linear in nature. It also gives consideration to the behaviour

of the fractured concrete in the tension, the biaxial failure criteria based on strength, a consideration to the reducing concrete strength after cracking and reduced shear stiffness upon cracking and a fixed and rotated crack model. In addition to this it is assumed that a perfect bond is existing between the concrete and the reinforcement (Cervenka 2021)[127].

2.5.1.2. Fracture Plastic Constitutive Model

The fracture plastic model is a combination of the fracture and plastic behavior of the concrete in tension and in compression. This model is based off the smeared crack formulation which is classical orthotropic as well as the model of crack band. It further engages the use of the Rankine failure criterion of the exponential softening which could be used as rotated and fixed or could also be used as fixed crack model. The use return mapping algorithm is applied to integrate the constitutive equations. In particular, the hardening and the softening model for plasticity is based on the Menetrey-Willam failure surface. The combination of both algorithm is based on recursive substitution, and it does allow for the two model to be individually formulated and developed. Therefore, the model can simulate the cracking of concrete, high confinement crushing, as well as the closure of crack due to crushing in other directions of materials (Cervenka 2021)[127].

2.5.1.2.1. Menetrey-Willam Failure Surface

To better understand the failure mechanism used, the Menetrey-Willam failure surface is expatiated. This constitutive model is able to capture and simulate the mechanical behaviour of the concrete which includes the strength in tension, compression and as well as the non-linear softening, hardening parameters, and the dilatancy (Dmitriev et. al., 2020)[128]. The Menetrey-Willam surface utilizes a three-parameter function (Cervenka & Cervenka 2017)[129].

Based on the uniaxial compressive test, the relationship below in equation 2.7 shows the parameter $c \in < 0, 1 >$ which does evolve during the yielding and the crushing process (Cervenka & Cervenka 2017)[129]. The parameter is given below:

$$c = \left(\frac{f'_c(\epsilon_{eq}^p)}{f'_c} \right)^2 \quad 2.7$$

The blue dots in figure 2.16 clearly shows the Menetrey-Willam failure surface.

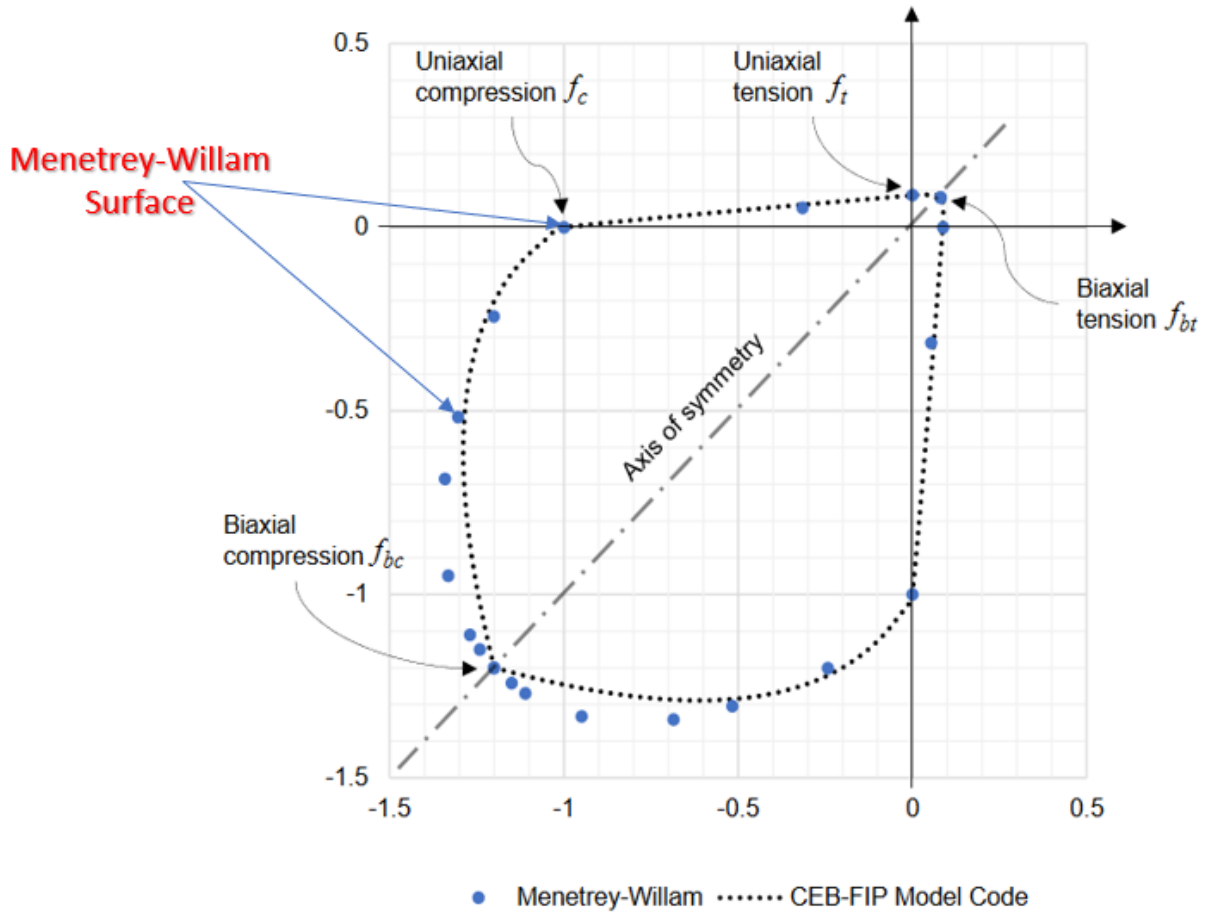


Figure 2.16-Menetrey-Willam Surface (Source: Adapted from Dmitriev et. al. 2020)[128]

2.5.1.3. Von Mises Plasticity Model

The Von Mises Plasticity Model is also referred to as the J_2 is based on the k parameter and as such

$$F^p(\sigma_{ij}) = \sqrt{J_2} - k(\epsilon_{eq}^p) = 0$$

Where J_2 is the stress deviator tensor for the second invariant. The descriptive parameter $k(\epsilon_{eq}^p) =$

$\sqrt{\frac{1}{3}} \sigma_y + (\epsilon_{eq}^p)$ is known as the maximal shear stress and σ_y is referred to as the uniaxial yield stress. A good application of the Von Mises Plasticity Model is for the cyclic steel behaviour (Cervenka, 2021).

2.5.1.4. Drucker-Prager Plasticity Model

The Drucker-Prager Plasticity model is also based on a formulation which is generic in nature. The function of the yield is defined as follows in equation 2.8 below:

$$F_{DP}^p(\sigma_{ij}) = \alpha I_1 + \sqrt{J_2} - k = 0 \quad 2.8$$

The parameters α and k are generally used to be able to define the shape of the failure surface. This can be obtained by matching it with the Mohr-Coloumb surface. When both surfaces agree in the meridian compressive plane, for $\theta=0^\circ$ then the formula is:

$$\alpha = \frac{2\sin\phi}{\sqrt{3}(3-\sin\phi)}, k = \frac{6\cos\phi}{\sqrt{3}(3-\sin\phi)} \quad 2.9$$

The failure surfaces are not fixed but rather do shift and this depends on what the value of the strain is. The value of the strain hardening is calculated based on the formular below, for $\theta=60^\circ$:

$$\alpha = \frac{2\sin\phi}{\sqrt{3}(3+\sin\phi)}, k = \frac{6\cos\phi}{\sqrt{3}(3+\sin\phi)} \quad 2.10$$

The equivalent plastic stain is calculated from the strain hardening as follows:

In general, the hardening and the softening in the Drucker-Prager Model is being determined by the k parameter which is selected in a way that the peak surface is able to pass through the uniaxial compressive strength, while the changes follow the expression below, (Cervenka 2021)[127]:

$$\Delta \varepsilon_{eq}^p = \min (\Delta \varepsilon_{ij}^p) \quad 2.11$$

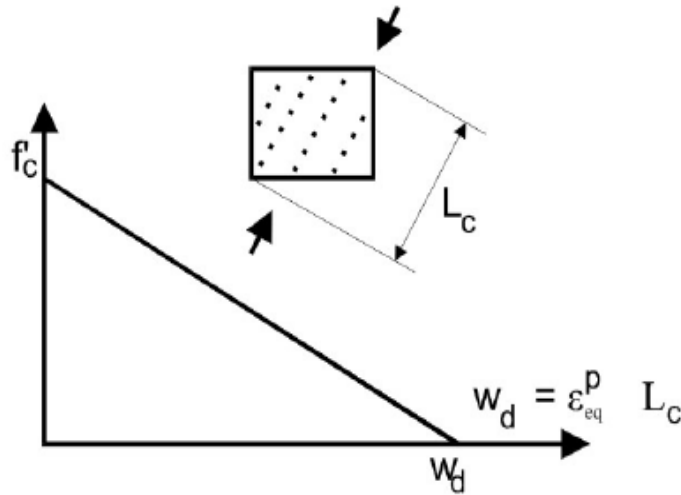


Figure 2.17-Linear Softening using the Drucker-Prager Modelling for Materials

2.5.1.5. User Material Model

In certain situations, none of the material models and in ATENA can be sufficient enough in the description of the behavior of the materials being used. While such cases can be handled by user defined laws in the fracture-plastic material model, such as CC3DNonLinCementitious2User.

The user material is built on the elastic isotropic material, the addition of material parameters and the stating of variables(Cervenka 2021)[127].

2.5.1.6. Interface Material Model

To simulate the contact surfaces between two material modes, the use of Interface Material Model can be used. A typical example of this is segment between two concrete and between foundation and a concrete structure. This particular model is based on the criterion of Mohr-Coulomb and cut off tension(Cervenka 2021)[127].

2.6. Studies that have Investigated the Modelling of Different Slabs

In the “Analysis and design of two-way slabs strengthened in flexure with FRCM”(Kadhim et al., 2022), findings showed that the ultimate load increases by the compressive strength and that the aspect ratio led to negligible achange in the failure load amongst other findings[130].

In the empirical and numeric study of UHPFRC two-way slab by Mahmud et. al., (2021), it was discovered that the numerical simulation in conjunction with the results obtained from the laboratory experiment were found to be in close alignment at the first cracking load and load carrying capacity as well as crack load location[131].

Akkaya et al., in 2022 studied the “Experimental, analytical, and numerical investigation of punching behaviour of two-way RC slab with multiple openings”. Findings revealed that FE results were in agreement to the experimental result and as such the values of the stiffness obtained reduces as the size of the lab openings increased[131].

3. CHAPTER THREE: METHODOLOGY & EXPERIMENTAL PROGRAM

3.1. Methodology Overview and Background

This research program was divided into three phases. As already mentioned in the previous chapter, the segments of the experimental program were designed to address the research objectives and the scope of this thesis.

In 2021, Santorsola developed a variety of LCC mixtures[11]. These mix designs contained a variety of materials in different proportion including fine and coarse RCAs, and ground granulated blast furnace slag. Santorsola focused on evaluating the fresh and hardened properties of various LCC mixtures which included, compressive strength, splitting tensile strength, as well as the density. While the objectives for validating the mixes was to obtain identical properties which were to be used for further study, the four mix designs had a target strength of 30MPa. In addition, Santorsola tested 12 reinforced concrete beams containing various LCC mixtures and evaluated the flexural strength and load-deflection response in comparison with current CSA A23.3-19 code provisions. Selected suitable materials such as the St. Mary's cement, recycled aggregates and blast furnace slag were used, and initial mix proportions were repeatedly tried for the database of low carbon concrete and then using guidelines such as the ACI and ASTM standards as a reference. Further iterations were done to optimize the desired properties with a focus on the compressive strength and the mixture slump without the addition of any admixtures or superplasticizers.

Secondly, in order to adopt some of these concrete mix designs developed by Santorsola, necessary corrections were made to the water cement ratio and was further validated to ensure that the target strength was achieved at 28 days following the ACI and CSA Standards. Therefore, this research seeks to continue the study of LCC as applicable for two-way reinforced concrete slabs.

In addition to this, the strength development curve for the different mixes were obtained with time and therefore the results are presented in the subsequent chapter of this thesis in details.

3.2. Experimental Program Overview

The program aims to address the objective in a solution-based oriented way to help navigate the research seamlessly. The initial process began with the characterization of the various concrete constituents and the mix design development which was based on Santorsola's work[11]. This entails selecting the ideal low-carbon concrete by batching from an existing database and altering

some of the water cement ratios and then validating. The second phase involved the use of ATENAGid for the modelling and the prediction of the behaviour of the two-way slab. The final phase involved the section analysis and the code comparison using the data of the slabs. Below is the figure 3.1 showing the summary of the experimental program.

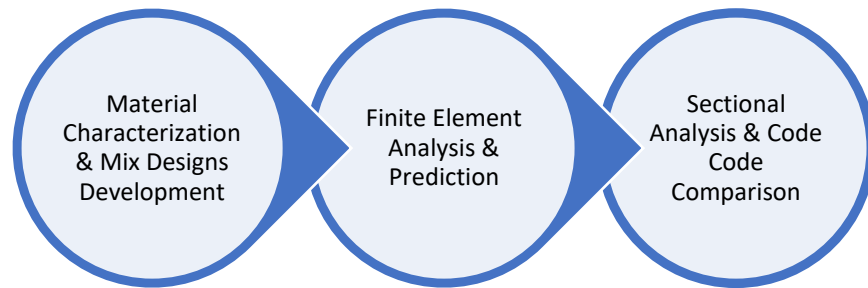


Figure 3.1-Experimental Program Phases

3.2.1. Aggregates Properties Testing

The first phase involved carrying out different materials test. Since the idea was to obtain low-carbon and environmentally friendly concrete, efforts were geared toward understanding the individual coarse RCA and the fine RCA in comparison with the natural coarse aggregate and natural fine aggregate denoted by CRCA, FRCA, NCA, NFA respectively in this thesis.

The certificate of analysis of the blast furnace granulated slag and the cement was obtained from the supplier and kept for record purposes. All the test for materials were performed by using the CSA A23.2-14 in conjunction with ASTM standards. Different properties were evaluated as follows:

1. Absorption
2. Sieve analysis
3. Moisture content
4. Bulk density

While these properties of the aggregates were essentially determined, the details of how the procedure was carried out is included in chapter four of this thesis for proper organization of ideas and thoughts.

3.3. Concrete Mixture Design Development and Fresh and Hardened Properties Testing

A key experimental phase of this research involved selecting existing low carbon concrete from a pool/data base of low carbon concrete developed by Jordan Santorsola[11], the reason for the selection was to achieve the desired properties as well as the workability and the target strength of 30MPa for each of the mixes considered without necessary altering the content of the cement or the aggregates ratio. To comply to this, a small percentage of the mix had their water/cement ratio adjusted while others were kept constant, while verify the ideal slump of the mix in question. For clarity, at the 28 days of the testing of the slabs and the test date, the following parameters were obtained: compressive strength, modulus of elasticity and Poisson's ratio based on CSA A23.2-19 standards.

The mixtures have been developed using the CSA A23.1-149 absolute volume method both for the control mixture which contains natural aggregates and the LCC mixtures which contains the combinations of coarse and fine RCA and slag cement.

Upon obtaining the properties of the concrete, necessary steps were taken to optimize the strength properties in cases where there was a lag or lead, which was attributed to the difference in the source of the original database mixes materials different from the latter. Another important thing to note is that a consistent mixing approach was adopted for all the mixes inclusive of the trial batches and the validated batches. The reason for this is to ensure consistency and eliminate any discrepancies that may arise due to mixing or batching processes.

4. CHAPTER FOUR: FRESH & HARDENED PROPERTIES TESTS & DISCUSSIONS

4.1. Concrete Mix Design & Process

Data obtained showed early strength gained in the initial phase which was attributed to free water and partly hydrated cement. However, there was consistency in the data obtained with the new cement which was procured and of course the ideal mixes were selected. The section 4.1.1, and 4.1.2 below explains the absolute volume method use in the experimental program, the mixing process, and the mechanical and fresh properties of the concrete, and then methods and procedures adopted for homogeneity.

In addition, table 4.1 and 4.2 below shows the mix designs adopted for this research, and the basic fresh and hardened properties of the concrete.

Table 4.1- Low Carbon Concrete Mix Designs(kg/m³)

ID	W/C	Water	Cement	Slag	NCA	NFA	CRA	FRA
NC-01	0.64	196.00	305.20		1035.30	752.40		
LC-C	0.58	177.00	305.20			751.00	935.40	
LC-CF	0.42	213.00	507.10				929.10	382.20
LC-CFS	0.42	213.00	253.50	253.50			836.00	490.60

Table 4.2-Fresh & Hardened Properties of the Low-Carbon Concretes

ID	Slump(mm)	f 'c @ 7days (MPa)	f 'c @ 28 days (MPa)	f _{ct} (MPa)
NC-01	90	18.82	28.65	3.80
LC-C	70	24.90	30.82	3.36
LC-CF	85	25.97	31.72	2.37
LC-CFS	110	27.12	31.56	2.61

It is also worthy to note that the potential which sets these low-carbon concrete different from the normal or conventional concrete is that the carbon footprints or carbon emissions have been considerable reduced due to the replacement with construction demolition waste (CWD) also known as recycled aggregates in the context of this thesis.

4.1.1. Mix Design by Absolute Volume Method

The absolute volume method of mix design often referred to as CSA A23.1-14 often begins with the initial design of the mix and satisfying or selecting the requirements, this includes the workability as well as the class of exposure[96]. The suitability of the materials to be used were

checked, evaluating the individual fine, coarse and recycled aggregates for the quality and standards of which sieve analysis was one which was also carried out for the aggregates used[96]. To achieve this, the volume in cubic meters of the entire slab, 12 cylinders, and 10% additional was calculated; in this volume was the weight of the individual materials such as the normal coarse aggregates the normal fine aggregates, the recycled coarse and fine aggregates, the cement, slag, and water.

The next thing was to compensate for the overall mixing water to account for in-situ aggregate moisture and absorption capacity by using the right proportion of aggregates, cement, and slag necessary to give the desired target strength and the slump. Upon achieving the wanted properties, the parameters are noted which gave the results and further used to cast the slabs.

4.1.2. Concrete Mixing Process

The CSA A23.1-14 which specifies the guidelines for concrete mixing and construction was used in conjunction with obtainable industry standards[96].

To begin, all materials required for the mixing were weighed in their different proportions a day before the maxing day and stored in sealed containers indoors at the High Bay Laboratory of York University Keele Campus. A 300-litre concrete high-shearing pan mixer was prepared and used by rinsing and patting dry with a with a slightly damp paper towel. The total volume of concrete (in cubic meters) required for each slab specimen was divided into two parts so as not to exceed the mixer capacity.

Another thing that was done was further dividing the half batch into two during the actual mixing. This implied that each batch was mixed independently on the next batch and as such, the constituent materials were allowed to mix thoroughly while water was gradually added to the cement and the aggregate mixture.

This was done to achieve homogeneity of the low-carbon materials being used and also facilitate control of the materials been added throughout the mixing process. Figure 4.1 and 4.12 below depicts the mixing and mixed concrete respectively using the large pan mixer in High-Bay Lab of York University.



Figure 4.1-The Mixing of the Concrete Constituent Materials



Figure 4.2-Preparation to Pour the Mixed Concrete

4.2. Aggregate Characterization

The characteristics of the aggregates being used to produce concrete are typical granular materials which include normal fine aggregate referred to sand, normal coarse aggregate referred to as gravel. In the case of recycled aggregates, recycled coarse and recycled fine aggregates were used. Other cementitious materials such as blast furnace granulated slag were also used for the experiment, and water was also used. Details of these materials are discussed briefly in the relevant sections below.

4.2.1. Mixing Constituents

4.2.1.1. Limestone

Crushed limestone also referred to as limestone was use as the natural coarse aggregate for the control concrete mixtures and granite known to be a dense type of rock will be able to provide some strength characteristics to the concrete in combination with a well matched sand and cement.

Similarly, for the recycled aggregate, the coarse aggregates were sieved into large bags and kept under controlled conditions in the high bay.

4.2.1.2. Natural Fine Aggregate

Also referred to as fine aggregate was used in the mixture to aid the workability and help in filling the voids of the mix since it was properly graded to provide good friction as well compaction during the mixing and the placement of the concrete.

4.2.1.3. Cement

St. Mary Cement Type GU-Ordinary Portland Cement was used for the concrete trial batches, validation, and the actual specimen casting.

4.2.1.4. Water

The available portable water in the Bergeron facility was used in all the concrete mixtures.

4.2.1.5. Recycled Aggregates

The recycled aggregates were obtained as a donation from Lafarge Canada Inc. The specification was OPSS Granular A and was pre-tested by default before arriving the Bergeron facility. Details of the material properties is discussed in the section of the particle size distribution and the analysis. The fine aggregate was sieved to ensure that the correct particle size distribution was achieved.

In general, for the testing of the aggregates and the concrete, the ASTM Standards have been used in conjunction with the ACI-318[87].

The role of the aggregates in the concrete is to provide the structural materials support upon which other constituents could be embedded or mixed to achieve the desired properties. Thus, enhancing the materials bond characteristics and compressive strength.

4.2.1.6. Blast Furnace Granulated Slag

This is often referred to as slag and it is used as a supplementary or cementitious materials in concrete. The slag was in ground form and was provided as an in-kind donation through Ashgrove.

4.2.2. Moisture Content Test

Aggregate moisture was measured in accordance with ASTM C 566, is the “Standard Test Method for Total Evaporable Moisture Content of Aggregate by Drying”[132]. The apparatus

used for test include a sensitive weighing balance, applicable source of heat in this case was an oven; which was used to oven dry the samples.

To begin, the mass of the samples for the coarse natural aggregates and coarse RCA and for the fine natural aggregate and fine RCA were first determined by placing the 500 grams of each sample into the pan container and putting it on the sensitive weighing balance. The mass of the empty pan was first recorded, then the mass of the pan is set to zero. Then placing the aggregates gently until the mass hits 500 grams required for the test. Thereby, obtaining an accurate measurement and placing in the oven to dry for 24 hours As a note, the oven was kept constant at a temperature of 115°C. The formula for calculating the percentage moisture content evaporable in the samples which were investigated is give as follows:

$$p = \frac{100(W-D)}{D} \quad 4.1$$

Where p = the moisture content evaporable of the sample (in percent)

W = the original mass of the sample (in grams)

D = mass of the oven dried sample (in grams)

Table 4.3 below shows the sampling sizes based on the ASTM standards and the percentage moisture content obtained for the different aggregates, While table 4.4 shows the percentage moisture content of the aggregates.

Table 4.3-Aggregate Sample Size for Test Based on C 566-97 (2000)[132]

Maximum Aggregate Size (mm)	Mass of Sample
4.75	0.5
9.5	1.5
12.5	2
19.0	3
25.0	4
37.5	6
50	8
63	10
75	13

90	16
100	25
150	50

Table 4.4-Percentage Moisture Content

Sample	1 (%)	2 (%)	3 (%)	Ave. (%)
NCA	2.00	2.05	2.07	2.04
NFA	4.05	4.10	4.15	4.10
CRA	3.55	3.50	3.51	3.52
FRA	2.62	2.60	2.65	2.62

According to table 4.4 above, the results shows that the moisture content of the recycled aggregates were significantly higher than the natural aggregate. The high percentage of moisture in the normal aggregate was accrued of the fact they were exposed to the natural effect of weather and as such could not assume the similar condition of the recycled aggregates which were kept in York University High Bay laboratory storage space.

While considerations were given to the adjustable moisture content in the aggregates particularly the normal fine aggregates. Care was taken not to alter the volumetric ratios of the cement. In this case the water content/cement ration was adjusted by simply adjusting the ratio of water present and accounted for in the aggregate, thereby having a minimal impact on the optimum strength of the concretes in consideration. Figure 4.3 and 4.4, and 4.5 shows the laboratory sampling process that was involved in obtaining the moisture content of the aggregate.



Figure 4.3- Determining the Moisture Content of the Recycled Fine Aggregate



Figure 4.4- Determining the Moisture Content of the Recycled Coarse Aggregate



Figure 4.5-Determining the Moisture Content of the Normal Coarse Aggregate

4.2.3. Absorption Test

The absorption test for the aggregates were carried out in accordance with ASTM International Standards Standard Test Method for Density, Relative Density (Specific Gravity), and Absorption of Fine Aggregate[133]. The standard defines the following terms as it relates to the mass of the aggregate particles in consideration:

OD → is the mass of oven dry sample the aggregates have been heated in a oven for up to 110+/- 5°C, thereby allowing it to reach a constant mass

SSD→The condition in which the “permeable pores of aggregate particles” are saturated with water to the level attained by immersing them in water for the specified duration, while not having any excess free water on the surface of these particles.

Three samples each for the natural coarse aggregate, natural fine aggregates and the fine aggregate and the coarse RCA were measured weighting 1000 grams. The specimens were placed in an oven and kept at a constant heat of 110°C for up to 24 hours until the mass became constant. The specimens were then allowed to completely cool at room temperature.

The specimen was the coved with water completely and allowed to stand for up to 24 hours. Then they were decanted by removing the excess water present in the aggregate without removing the

particles itself in a gently manner. In particular, the coarse aggregates were padded dry with a paper towel. The specimen was then distributed in a small sampling tray and a hot air gun for surface during the specimens. Proper stirring was continuously done at intervals alongside checks for surface moisture. To verify according to C 128 – 07a, a metal mould liked to be a frustum cone was used with dimensions of 40mm internally and 90mm externally with 75 mm height, alongside with a metal tamping rod of 25mm tamping face and 0.8mm in total thickness. With the larger diameter at the base, a portion of the sample was placed into the cone allowing git to overflow and cupping with fingers while holding the mould. The aggregates were then tamped lightly 25 times, starting the drop in height of the tamping rod at 5mm from the aggregate surface. The excess particles are removed from the bottom of the cone and in cases were the mould shape was regained, further drying was done, and adjustments were made to obtain the desired results and the weight in mass of the aggregates were recorded on a spreadsheet otherwise known as Microsoft excel workbook for easily calculations and plots were applicable. Figure 4.6 below shows the water absorption determination process in the laboratory, while table 4.5, 4.6, 4.7, 4.8 shows the different water absorption rate in percentages for the aggregates. Below is the expression for the determination of the absorption rate of fine aggregates which could also be used for coarse aggregates.

$$Absorption \% = 100 \left[\frac{S-A}{A} \right] \quad 4.2$$

Where:

S = mass of the saturated surface dried sample expressed in grams

A = mass of the oven dried sample expressed in grams



Figure 4.6-Initial Sample for Absorption of Fine & Coarse Aggregates

Table 4.5-Values for Percentage Water Absorption Content of NFA

Sample	M	S	A	% Absorption	AVE
1	1000.00	1008.01	982.01	2.64%	2.62%
2	1000.00	1006.52	985.35	2.14%	
3	1000.00	1010.54	980.44	3.07%	

Table 4.6-Values for Percentage Water Absorption Content of NCA

Sample	M	S	A	% Absorption	AVE
1	1000.00	1012.00	980.17	3.23	3.56%
2	1000.00	1016.00	980.10	3.60	
3	1000.00	1018.00	980.20	3.85	

Table 4.7-Values for Percentage Water Absorption Content of RFA

Sample	M	S	A	% Absorption	AVE
1	1000.00	1070.00	960.00	11.46	11.44%
2	1000.00	1078.01	962.01	12.05	
3	1000.00	1065.05	961.00	10.82	

Table 4.8-Values for Percentage Water Absorption Content RCA

Sample	M	S	A	% Absorption	AVE
1	1000.00	1020.23	975.70	4.56	5.21%
2	1000.00	1025.56	970.25	5.70	
3	1000.00	1028.66	976.10	5.38	

From the results obtained below, it was evident, that the recycled fine aggregates had a higher absorption rate than that of other aggregates used for the concrete mixtures. Specifically, the natural fine aggregates had the lowest absorption rates of 2.62% and recycled fine aggregate having a maximum value of 11.44%. Findings from literature such as Sartorsola (2021) have shown that the recycled aggregates have higher absorption rates and have linked this characteristic to the presence of the adhered mortar on the particles of the aggregate, thereby creating bonds and voids and making the aggregate to become more porous and permeable. In particular, Sartorsola found that absorbed values were around 25-32.2% lower than the AC₂₄ computed values. [11]

4.2.4. Relative Density

CSA A23.2-09 defined relative density as the ratio of the mass of a substance per unit volume to a same volume of distilled water that is gas-free at a stated temperature, while the initial volume is the impermeable portion of aggregate at a stated temperature to the mass in air of [96]. Density is generally expressed as:

$$D = \frac{M}{V} \quad 4.7$$

Where:

D = the density of the concrete materials which are the aggregate in kg/m³

D = mass of the substance considered in kilograms

V = Unit volume of the substance in cubic meters

Table 4.9 and 4.10 shows the density per 0.015m^3 of each concrete mix and the total mass and the total density required for each slab cast per mix. The data obtained show that the normal concrete had the highest density and the density further decreased with increasing replacement of the recycled aggregate or supplementary materials. Therefore, for situations that would typically warrant a light-weight concrete where a very high strength is not of paramount importance, the use of low-carbon concrete can be a suitable alternative to be able to reduce the self-weight of the slab or the structural element in consideration.

The materials that comprised the concrete were weighed in kilograms for each of the mixes. The total kilograms required for each of the mixing constituents such as the fine aggregate, the coarse aggregate, the slag, the fine recycled aggregate, and the coarse recycled aggregate, were summed up for each individual mix required in the 0.0173m^3 of concrete, as the total mass. The volume required was taken as the product of the length, width, and the thickness of the slab, which was 1.2m-by-1.2m-by-0.12m.

Further trend and relationship between the density and the compressive strength of the cylinder as well as the density and replacement percentage of recycled content is shown in figure 4.7 and 4.8.

Table 4.9-Cylinder Density per m^3 of the Concrete Mixes

ID	Density (kg/m³)
NC	2464
LC-C	2293
LC-CF	2201
LC-CFS	2098

Table 4.10-Total Mass of Materials (Aggregates + Supplementary Materials) in kg & Density per 0.1728m³ for the Slab

ID	Total Mass of Materials (Aggregates + Supplementary Materials) in kg	Density (kg/m ³)
NC	392.23	2268.52
LC-C	374.68	2168.28
LC-CF	351.01	2031.30
LC-CFS	309.84	1793.05

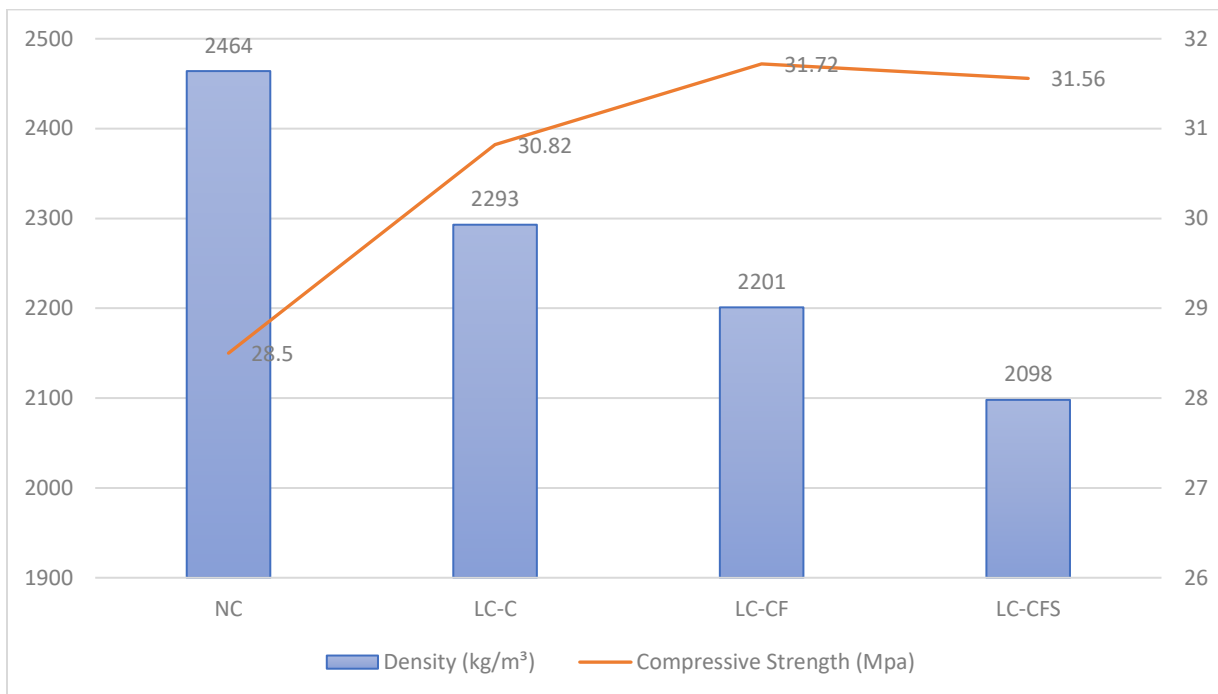


Figure 4.7-Relationship between Density & Compressive Strength for 0.015m³ of Concrete

From the figure 4.7 above, the density of concrete kept decreasing with the increment in the compressive strength. However, at the point of the addition of slag as a cementitious material, the density therefore decreased.

The density and compressive strength relationship was sustained enough up to the point of addition of the slag content as a supplemental material, this therefore beats down the chance to indirectly related them by proportionality.

However, this therefore mans that an attempt to improve or decrease the density of concrete by altering the percentage of the ratio of the mix constituent materials will tend to also affect the compressive strength of the concrete as evident in the above figure.

As more supplementary materials will be added or removed the compressive strength will tend to be affected. This situation can therefore be systematically managed by paying a close attention to the concrete slump, and the water/cement ratio. This is because of the existing relationship between the concrete slump and the water/cement ratio.

Therefore, it is on this existing relationship of density and compressive strength and density and replacement ratio, an hypothesis has been made, which is subject to a more extensive study.

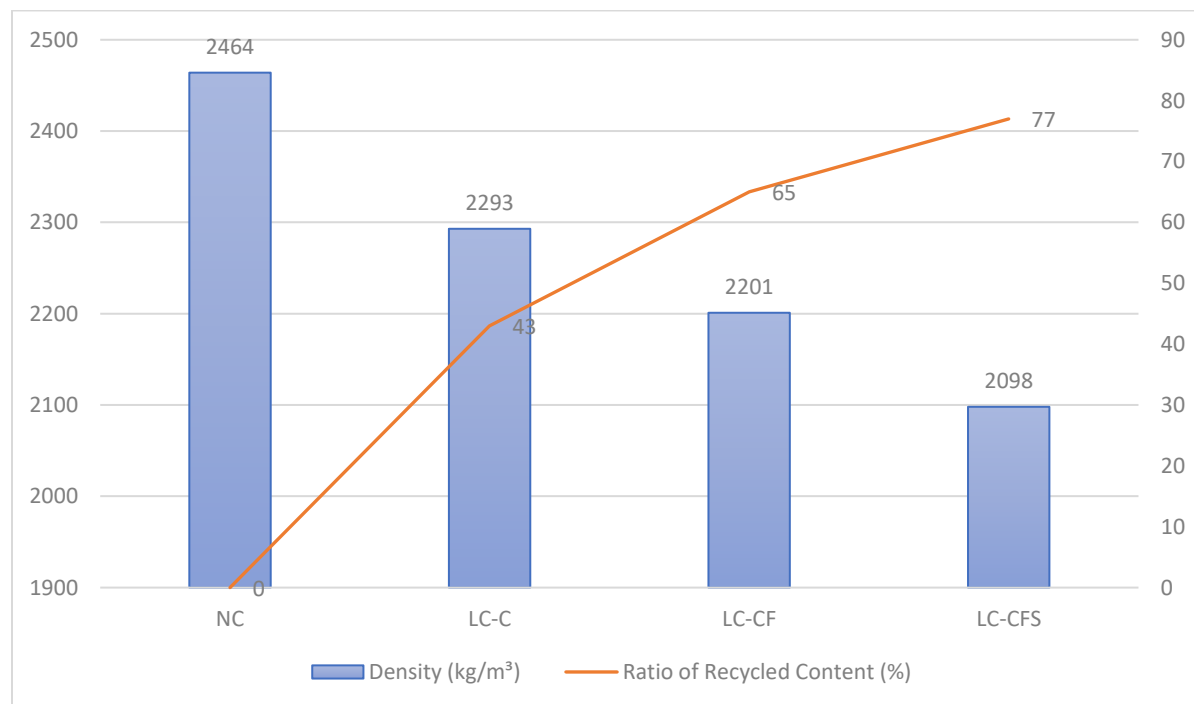


Figure 4.8-Relationship between Density & Replacement Percentage

The relationship between density and replacement percentage is shown in the figure 4.8 above. Just like it depicts a scissors-shape, it explains the indirect proportional relationship between both variables. The density was at its peak when the replacement ratio was zero and furtherly decreased

as the replacement percentage was increased. The maximum density was obtained where the replacement ratio was at its highest value of 77%.

Therefore, based on this information, it is clearly established that density is inversely proportional to replacement percentage. On this basis, the following equations is being proposed.

$$D = \frac{1}{R} C \quad 4.8$$

Where:

D = Density of Concretes

R = replacement ratio

C is a varying constant or multiplication factor

4.2.5. Sieve Analysis & Particle Size Distribution

The sieve analysis for the aggregate was carried out using CSA A23.2-2A, and ASTM C136-[96][134]. The weighing balance has an accuracy of 0.01g, and the sieves were stacked into each other, in an order of decreasing size other before the sieving operation started.

First, the ASTM Standards specifies 300g for the fine aggregate to be sieved, the 19mm nominal size the use of 5000g and for coarse and large fine aggregate meditate the same as 5000g was used for the coarse aggregate in accordance with the conformity standards as seen in table 4.20. All the sample materials were properly dried to a constant mass at 115°C and weighed. The next thing was the selection of the sieve sizes for use asl it applies to both the coarse aggregate and the fine aggregate.

The material was then pored into the sieve set as shown in figure 4.9 below and then placed into the mechanical sifting machine in the laboratory as shown in figure 4.10 and 4.11. This was programmed to shake for 10minutes which was sufficient time to allow the materials to be agitated and to reach the bottom of the pan in a homogeneous way.

The material contained in each of the pan was carefully poured into an empty pan and a brush was used to further empty the pan to ensure no residue of the material was to remain. According to the ASTM Standard, not more that 1% of material retained would pass through that sieve.

During the sieve analysis for the larger size, the minimum sieve said that was used was the 4.75mm. By appropriately following the procedures, it was ensured that no material was lost to the surrounding sieves and tabletops.

Upon completion of the agitation. The next procedure is to obtain the percentage of material that were retained by the sieve for the fine aggregate, for the coarse aggregate and for the recycled aggregate. The sample increments were computer and cumulative percentage retained forth different samples.

According to CSA A23.2-2A, the mass of each fraction is computed as follows:

$$A = \left(\frac{W_1}{W_2} \right) * B \quad 4.9$$

Where

A = size fraction mass on a total sample basis

W₁ = mass of sample that is finer than the selected sieve in the total sample

W₂ = mass of sample that is a reduce portion finer than the selected sieve actually sieved

B = mass of size fraction in reduced portion sieved

Upon completion of the test and weighing the content retained, the applicable date was collected and a graph of percentage passing versus the sieve size was plotted. The graph obtained form the sieve analysis of recycled coarse aggregate is shown in the figure 4.12. While Table 4.11 below shows the tests samples for conformity.

Table 4.11-Test Samples for Conformity

Nominal Maximum Size (mm)	Test Sample Size (kg)
9.5	1
12	2
19.0	5
25.0	10
37.5	15
50	20
63	35
75	60
90	100



Figure 4.9-Sieve Set



Figure 4.10-Lab Sifter



Figure 4.11-The Sifter Undergoing the Mechanical Shaking of the Sieve Set

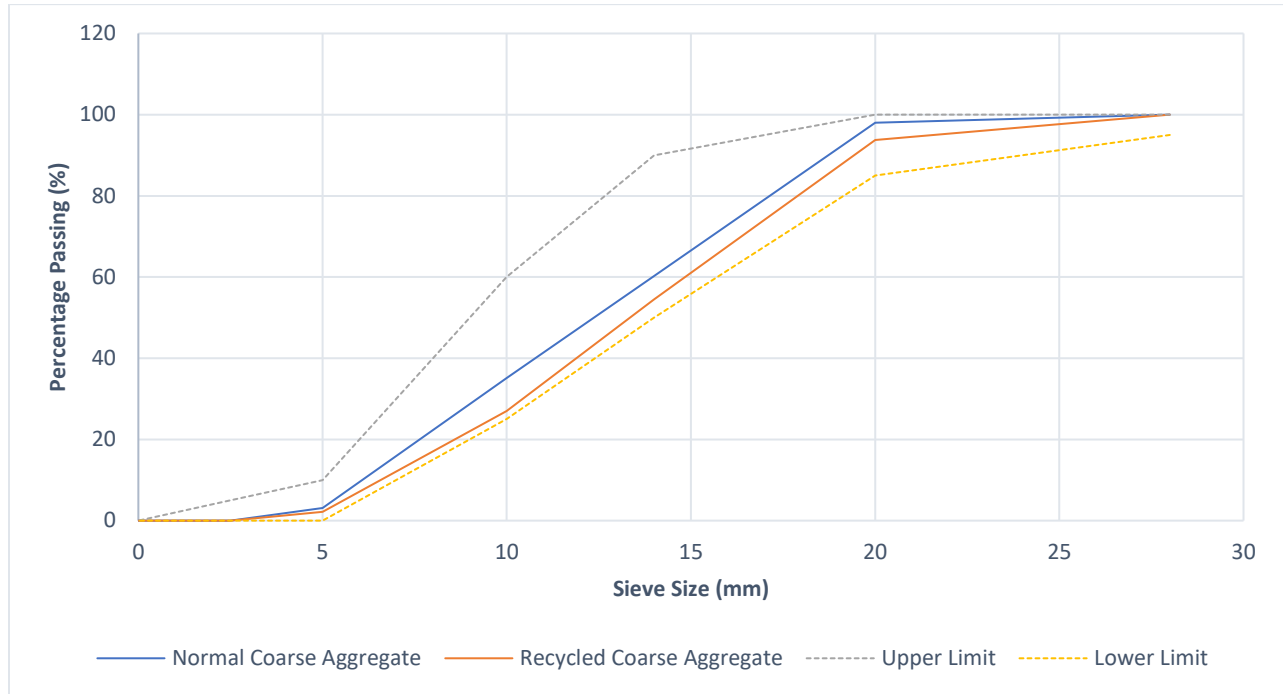


Figure 4.12-Sieve Analysis Chart for the Normal Coarse Aggregate and the Recycled Coarse Aggregate

From figure 4.43 it is evident that the recycled coarse aggregate and the normal coarse aggregates were within the limits of the CSA A23.2-2A Standards obtained from table 11, and as such were suitable for use in the production of the concrete.

According to the sieve analysis grading limits for the aggregate, embedded in table 10 of CSA A23.1- 09, in conjunction with the ASTM C 33/C 33M – 08 limits for the specified sieve sizes; and the graph above was obtained to be within the limits of the standards[96][135].

4.3. Tensile Tests on Reinforcing Steel

To understand the behaviour of the steel used in this research by critically produce and observing the stress strain response of the material and to be able to accurately utilise the properties of the steel for the finite element modelling. A comprehensive test of the steel was carried.

Firstly, the 10mm rebar were cut into 3 different specimens of size 400mm using a measuring tape, and the diameter of the rebar was also checked using a calliper, these measurements were recorded and stored safely.

Secondly, the MTS Machine was used, and the reinforcement was placed in between the grip, with the axial extensometer at the middle and the grips at the top and the bottom. An extensometer

which could accurately measure the reinforcement strain. Both grips were closed, and test was set by zeroing the extensometer readings and the load output was also set to zero.

Next was to switch on the DAQ system and ensure a synchronisation between it and the MTS test machine. A tensile force was then applied and the computerized DAQ was made to acquire the actuator reading, the extensometer reading and also the load and time of the test. At a strain rate of 0.01mm/mm the MTS test was stopped and the steel bar in the grips was unloaded using the remote-control upward signal. The test was then made to continue, such that when the necking begins, the extensometer was removed and the pin in the extensometer was replaced, then the test was resumed until it eventually failed and fractured. The change in the length of the specimen was then calculated as the sum of the actuator reading and the extensometer reading, and the stress of the specimen was computed as the load divided by the area of the specimen, taken the diameter of the specimen as 11.2mm. The equation below was used to compute the stress and the strain of the tension test of the specimen are gen below. The Figures 4.13, 4.14, 4.15, 4.16, shows the experimental set-up for the test as well as the plots that were obtained for the experiment for the three different samples. However, table 4.12 and 4.13 shows the material specification and specimen dimensions.

$$\text{Tensile Stress } (\sigma) = \frac{F}{A} \quad 4.3$$

$$\text{Tensile Strain } (\epsilon) = \frac{\Delta l}{l} \quad 4.4$$

$$Y = \frac{\text{tensile stress}}{\text{tensile strain}} \quad 4.5$$

Where

L = is the total length of the specimen in mm

σ = is the tensile stress in N/mm²

A = is the cross-sectional area of the specimen in mm²

P = is the deforming or tensile force in kN

d = the diameter of the specimen in mm

Δl = the change of length of specimen undergoing deformation in mm

ϵ = is the strain at any point in time along the length of the member which is in mm/mm or dimensionless

Y = the young modulus of the material which is given in N/mm²

Table 4.12-Material Specification for Steel

Specification	High-yield Steel
Diameter	10M
Specified Yield Strength	478.78

Table 4.13-Specimen Dimensions

Parameters	Specimen No. 1	Specimen No. 2	Specimen No. 3
Diameter	10M	10M	10M
Original Length	400mm	400mm	400mm
Geometry	Round	Round	Round
Area	100mm ²	100mm ²	100mm ²



Figure 4.13-Extensometer and Reinforcing Steel Arrangement for the Test

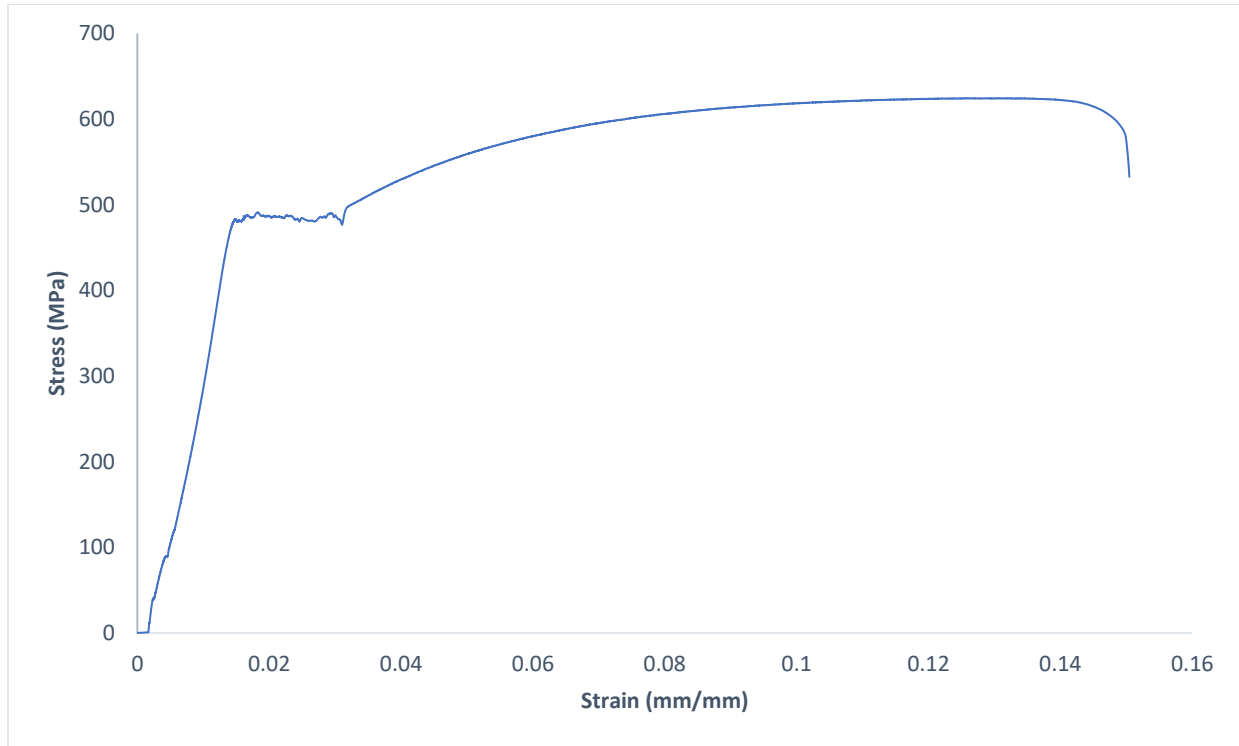


Figure 4.14-Stress/Strain Curve for Specimen 1

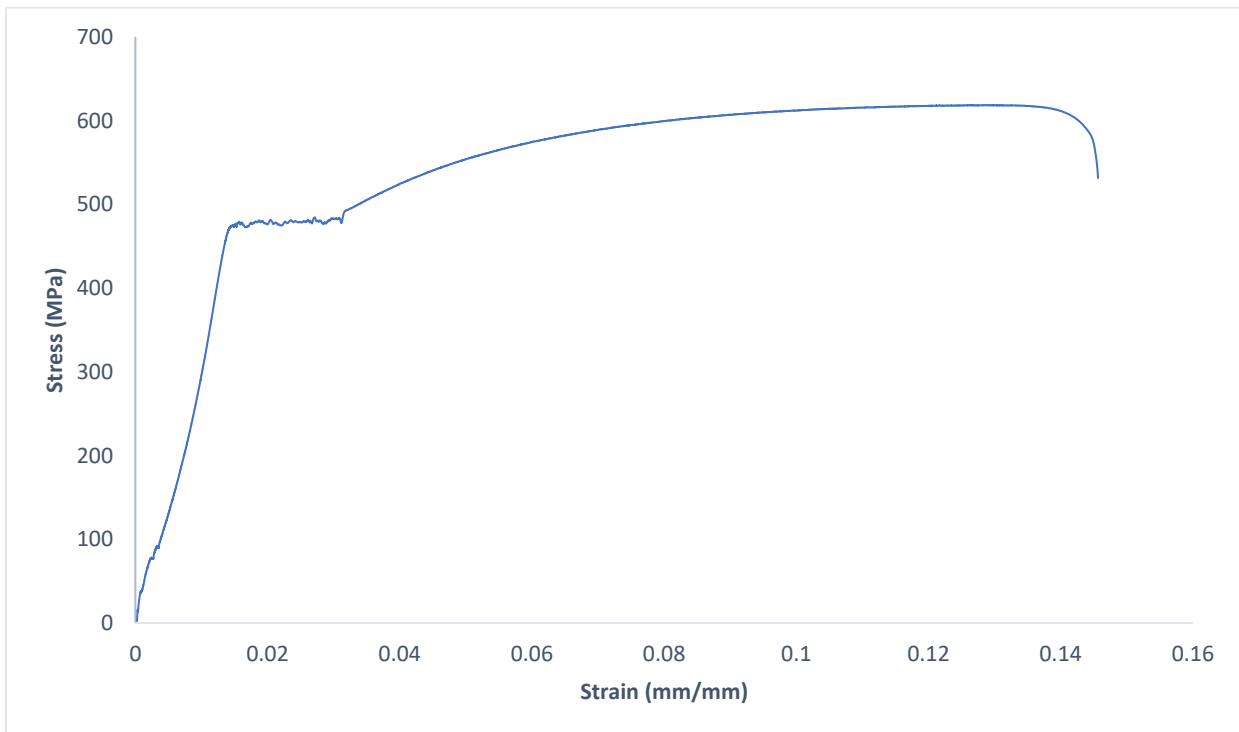


Figure 4.15-Stress/Strain Curve for Specimen 2

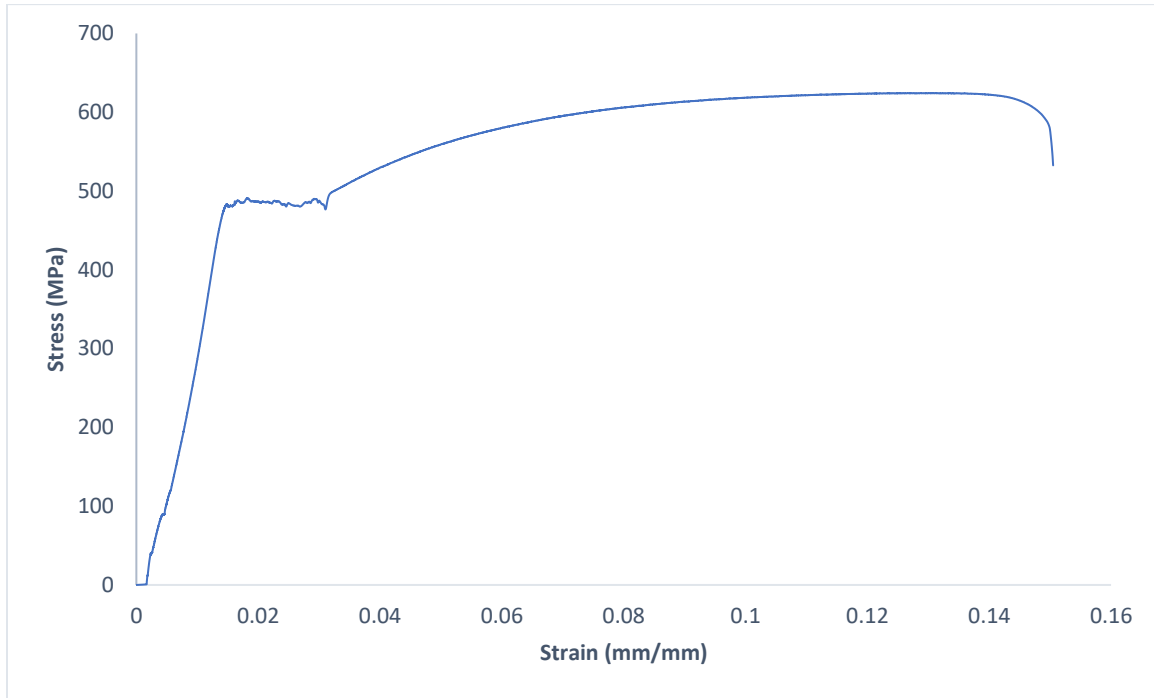


Figure 4.16-Stress/Strain Curve for Specimen 3

From Figure 4.14, 4.15, and 4.16, it was evident that the three specimens behaved in a similar manner. They first behaved like an elastic material when subjected to tensile forces. Upon reaching an average sustained stress of 482N/mm² and enters the plastic region where can take up more stresses and undergo further strains, as more energy is being harnessed, it reaches a peak stress or ultimate tensile strength of 620N/mm²; and beyond this point failure occurs and it the specimens break because of the continuous application of tensile force. A summary of the result is presented I table 4.14 below for further understanding.

Table 4.14-Tensile Test Result Summary

Test Parameters	Specimen 1	Specimen 2	Specimen 3	Minimum	Maximum	AVE
Diameter	10M	10M	10M	10M	10M	10M
Length (mm)	400	400	400	400	400	400
Area (mm ²)	100.00	100.00	100.00	100.00	100.00	100.00
Ultimate Stress (MPa)	619.00	624.00	624.00	619.00	624.00	622.0
Ultimate Strain (MPa)	0.15	0.15	0.15	0.15	0.15	0.15

4.4. Mechanical & Fresh Properties of Concrete

The mechanical properties and the fresh properties of the concrete used were determined in accordance with the ACI 318-19, CSA A23.1-19, and were also used in conjunction with ASTM International Standards.

4.4.1. Compressive Strength Results

Due to the properties of the recycled concrete aggregate, which is different from that of normal concrete, especially looking into the level of water absorbing properties.

The concrete cylinders were made using cylindrical plastic moulds. The concrete was placed in three different layers into the moulds and tapped 25 times in each layer. The surface was then lightly rodded off with the tamping rod.

A power operated compression machine was used for the determination of the compressive strength of the normal concrete and the low-carbon concrete. The specimens had a diameter of 100mm and a height of 200mm respectively. The diameter was used to compute the area of the specimen. The machine was set at a loading rate of 0.15MPa/s and there was no adjustment during the test. For each test an average of 6 cylinders were cast for both the mix validation and the slab concrete samples. The specimen was loaded to failure and the pattern of the failure was observed and recorded. The majority of the specimens showed a type 2 vertical crack with a conical shape and some spalling.

The compressive strength is calculated as the load divided by the cross-sectional area of the specimen. Typical failure patterns are given by ASTM 39/C 39M-01 in the figure 4.17 below[136]. The figure 4.18 illustrates the laboratory compressive strength test for concrete. Figure 4.19 and 4.20 shows the failure patterns for the normal concrete and the recycled concrete.

In addition, figure 4.21, 4.22, 4.23, and 4.24 shows the compressive strength development profile for the different concrete mixtures. The normal concrete has a similar strength gain profile to the low-carbon concrete that contained RCAs. Therefore, it is important to mention that this might be linked to a slow inner curing mechanism in both concrete and therefore it could be linked to the presence of the adhered mortar in the aggregates and as well as the slag content in combination

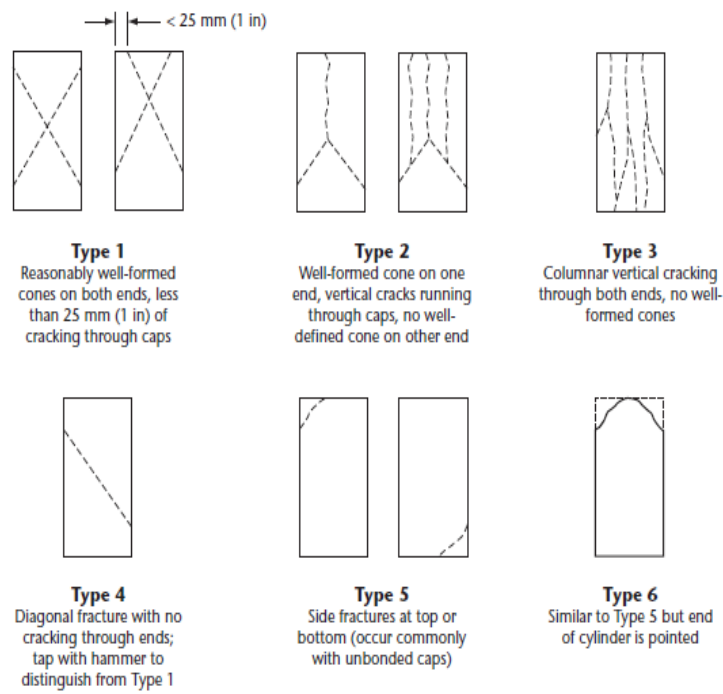


Figure 4.17-Typical Fracture Patterns by ASTM 39/C 39M-01[136]



Figure 4.18-Compressive Strength Test on Concrete



Figure 4.19-Failure Specimen for the Normal Concrete



Figure 4.20-Failure Specimens for the Low-Carbon Concrete LC-C

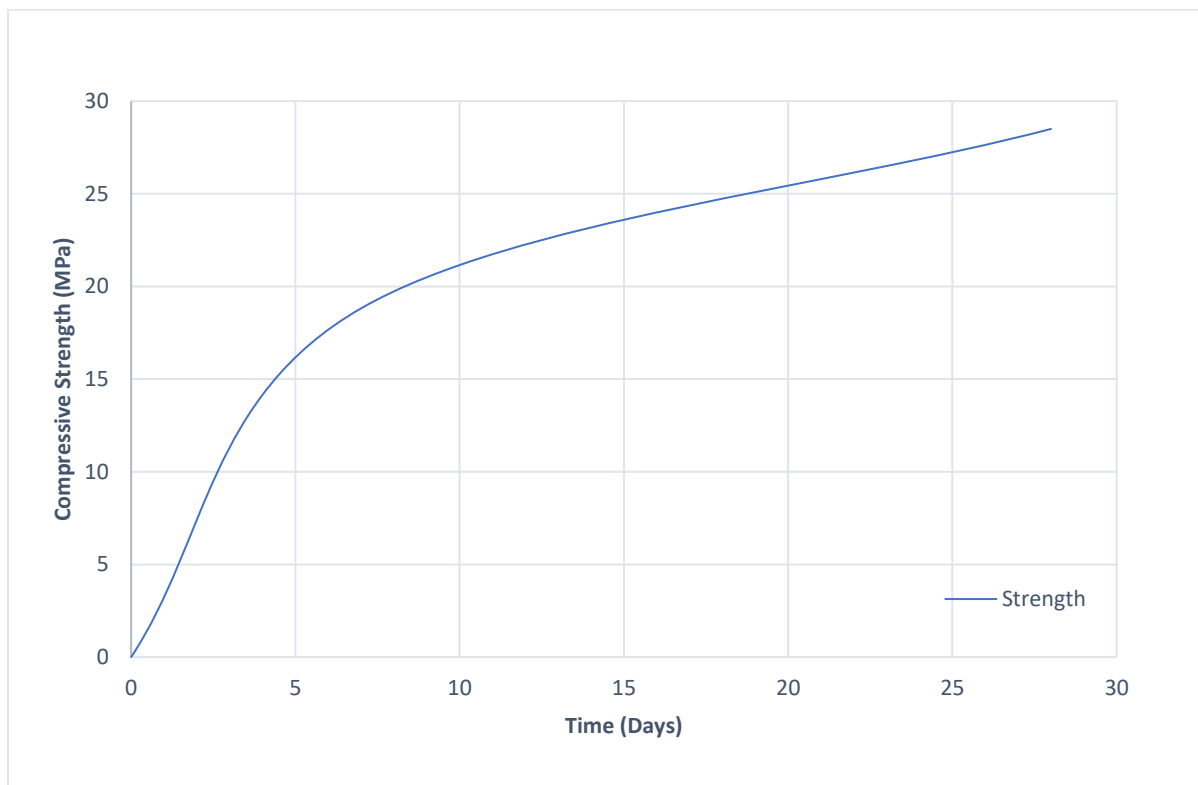


Figure 4.21-Compressive Strength Development Profile for Normal Concrete up to 28 days

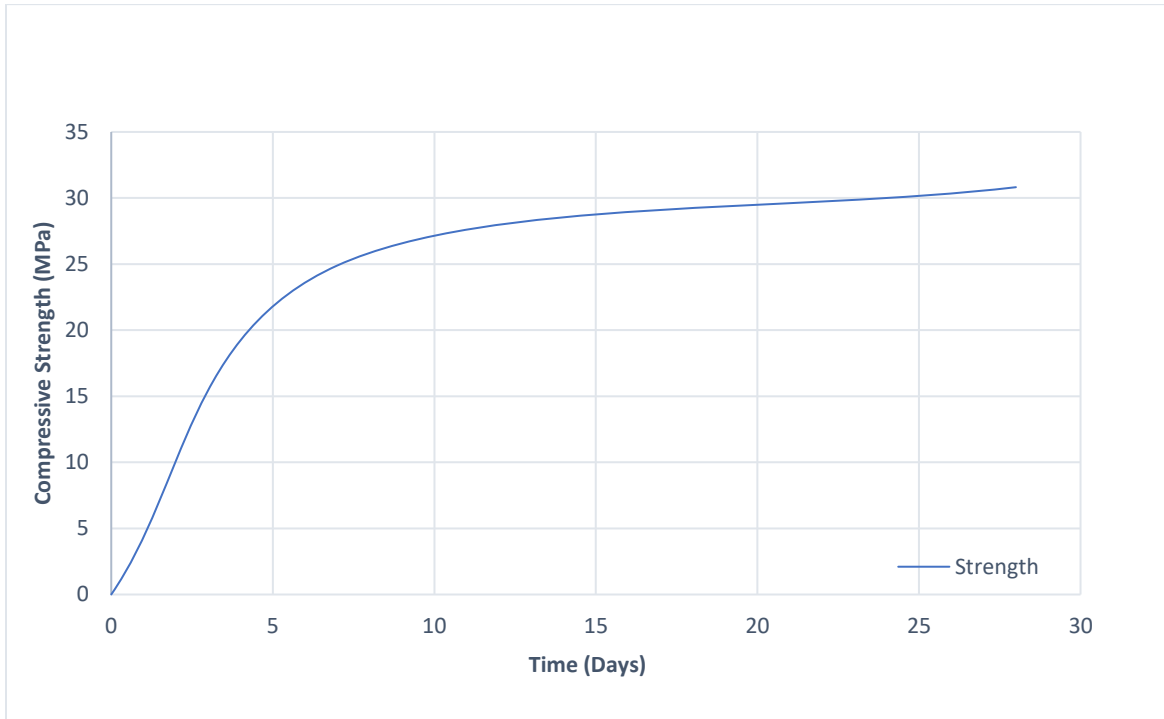


Figure 4.22-Compressive Strength Development Profile for LC-C Concrete up to 28 days

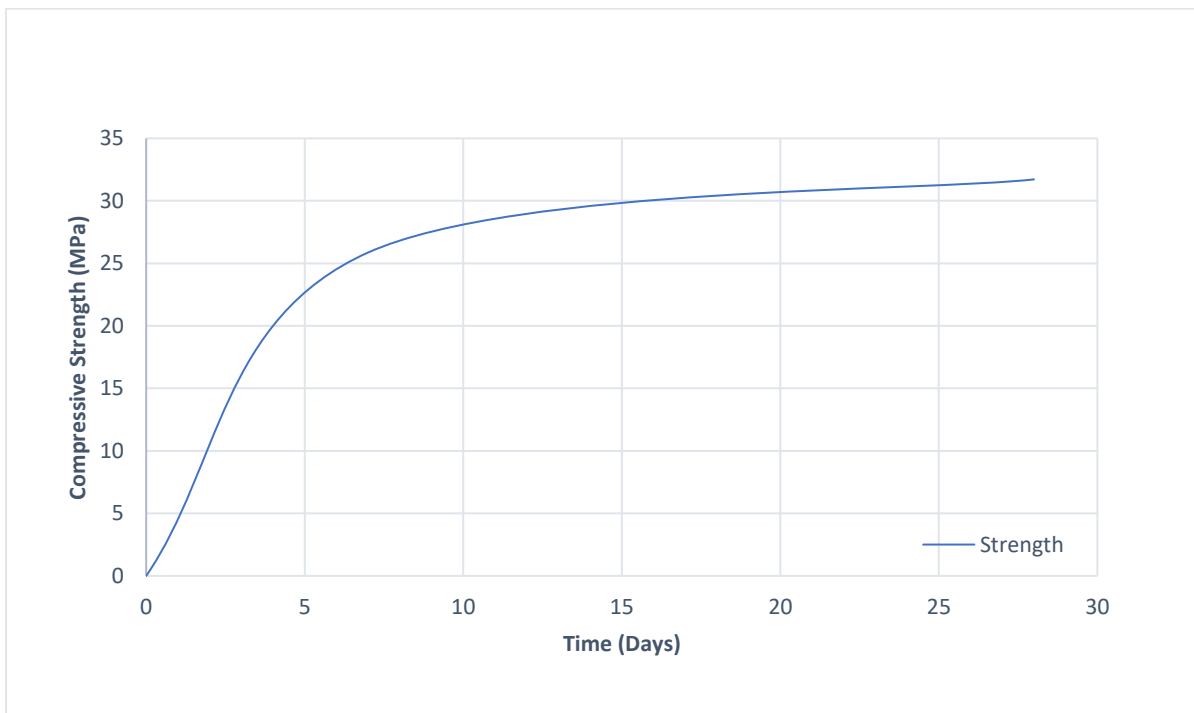


Figure 4.23-Compressive Strength Development Profile for LC-CF Concrete up to 28 days

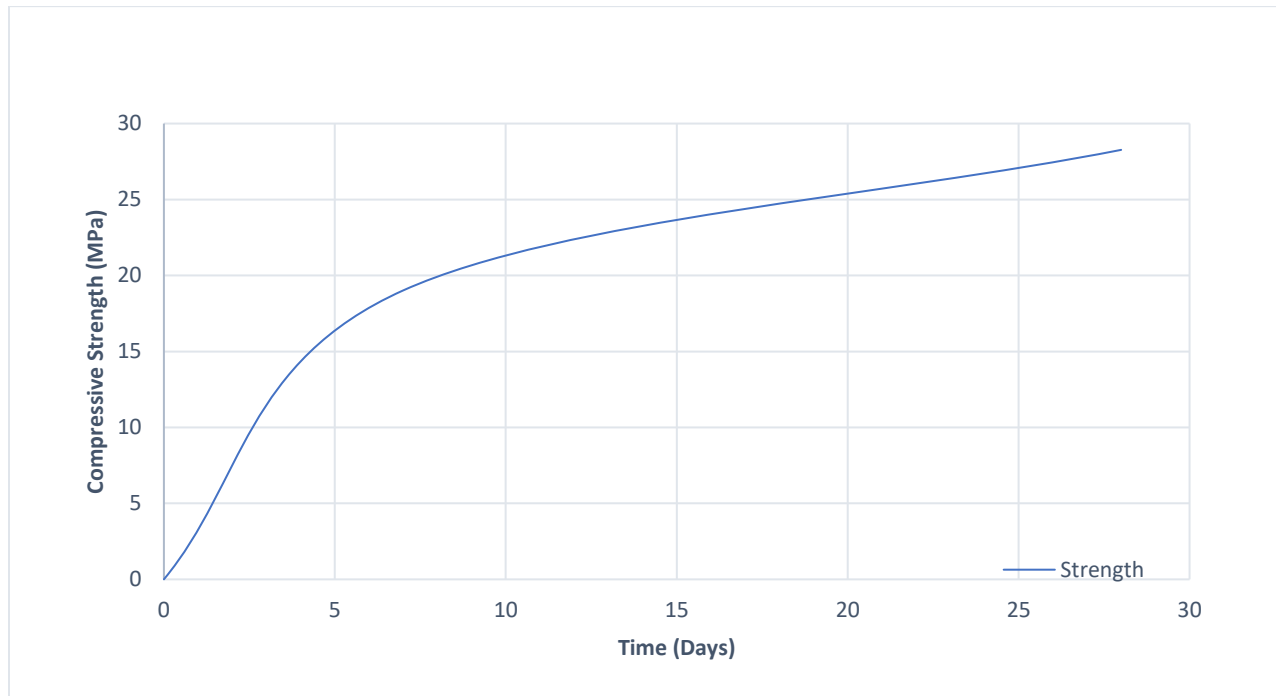


Figure 4.24-Compressive Strength Development Profile for LC-CFS Concrete up to 28 days

Based on the results obtained, it was observed that the peak compressive strengths were quite similar; however early strength gain was noted at 7 days for the recycled concretes. Table 4.15 below summarizes these results.

Table 4.15-Table of Replacement Percentage Cylinder Strength and Water Content

ID	Replacement Percentage (%)	Cylinder Strength (MPa)	W/C
NC	0	28.50	0.64
LC-C	43	30.80	0.58
LC-CF	65	31.70	0.42
LC-CFS	77	31.60	0.42

Where:

NC- Normal Concrete

LC-C-Low-Carbon Concrete with Coarse Recycled Aggregate as Replacement

LC-CF-Low-Carbon Concrete with Coarse & Fine Aggregate as Replacement

LC-CFS- Low-Carbon Concrete with Coarse & Fine Aggregate as Replacement & Slag

In order to clear doubts in the similarities of the strength profile obtained from the tests. Two samples from the tests namely: the replacement percentages and the water cement ratio were actually analysed using regression analysis to observe the trend and to know the correlation of the percentage replacement when it was compared to the water/cement ratio of the different concrete mix. The scatter plot was obtained and the equation $y = -0.0031x + 0.6585$ was obtained, with $R^2 = 0.9756$; taking the replacement percentage as the x-axis and the water/cement ratio on the y-axis as shown in figure 4.25 below. In addition, the degree of association measured by the correlation coefficient, somewhat referred to as the Pearson's coefficient was $r = -0.9357$ and showed that there was almost positive correlation between both variables and therefore the regression line intercepts the y-axis at 0.6585 and also with a slope of -0.0031 analytically obtained and matching that from the regression plot. Therefore, for every unit increase in the level of replacement expressed as percentage, the water/cement ratio will drop down by 0.0031. It also means that if the replacement percentage becomes 0% as we do have, we would have water/cement ratio of 0.6585.

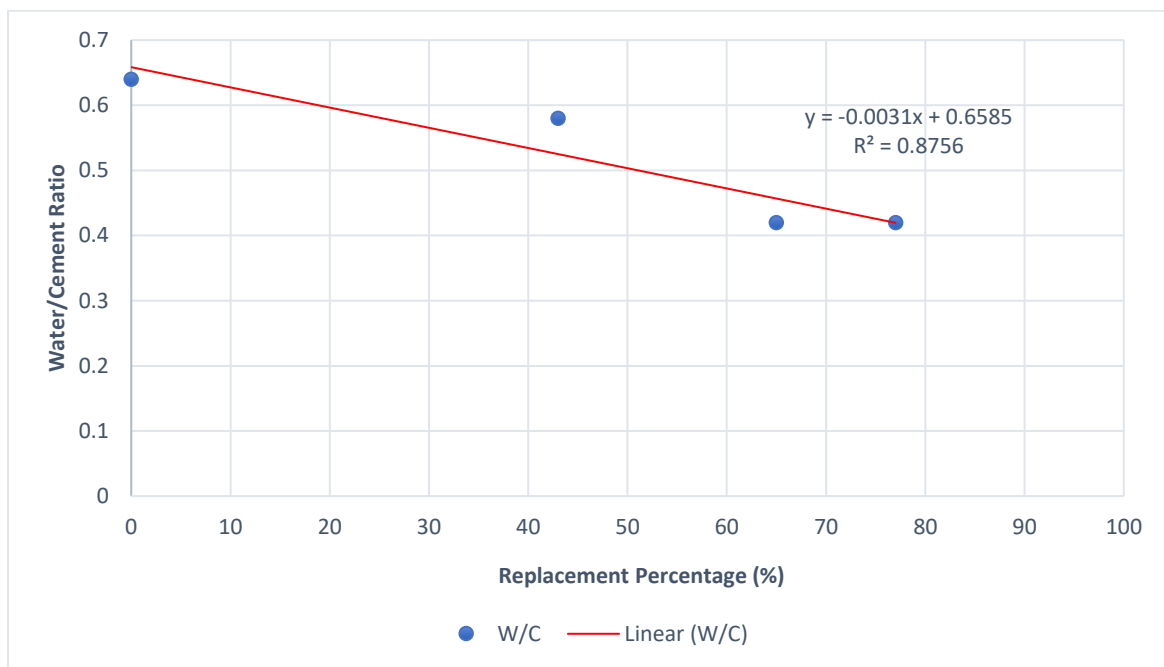


Figure 4.25-Linear Relationship between Water/Cement Ratio & Replacement Percentage

4.4.2. The Spitting Tensile Tests

The concrete cylinders of 100mm diameter by 200mm diameter were a representative of the different mixtures and were prepared in accordance with CSA A23.2-09. Two wooden bearing strips were placed at the bottom and the top of the specimen plates and both having a width of 25mm. All specimens were moist cured in a curing tank for 28 days. The cylinder was then positioned in the between the jig and the load was continuously applied at a loading rate of 700kPa/min until failure. The splitting tensile strength was then calculated and the load at failure and stresses are tabulated in table 4.16, 4.17, 4.18, and 4.19 respectively, based on the following equation:

$$T = \frac{2P}{\pi ld} \quad 4.6$$

Where:

P is the failure load in kN

d is the diameter of the specimen in mm

l is the length of the specimen in mm

Table 4.16-Splitting Tensile Test Results for LC-C

PARAMETER S FOR NC-	NC₁	NC₂	NC₃	NC₄	NC₅	NC₆	AVE STS @28days (MPa)
Diameter(mm)	100	102	100	101	102	101	3.80
Height(mm)	200	199	200	200	199	198	
Force(kN)	120.4	122.0	123	121	120.2	120.4	
STS(MPa)	3.72	3.77	3.91	3.81	3.77	3.83	

Table 4.17-Splitting Tensile Test Results for LC-C

PARAMETERS FOR LC-C	LC-C₁	LC-C₂	LC-C₃	LC-C₄	LC-C₅	LC-C₅	AVE STS @28days(MPa)
Diameter (mm)	100.5	101	100	100	102	102.5	3.36
Height (mm)	200	200	198	199	200	197	
Force (kN)	96.5	114.1	116.5	119.3	104.0	87.9	
STS(MPa)	3.06	3.60	3.68	3.82	3.25	2.77	

Table 4.18-Splitting Tensile Test Results for LC-CF

PARAMETER S FOR RC-CF	LC- CF ₁	LC- CF ₂	LC- CF ₃	LC- CF ₄	LC-CF ₅	LC-CF ₅	AVE STS @28days (MPa)
Diameter(mm)	101	103	101	104	102	101	2.37
Height(mm)	198	200	200	190	200	199	
Force(kN)	57.8	62.5	85.1	91.0	70.7	83.3	
STS(MPa)	1.84	1.93	2.68	2.93	2.21	2.64	

Table 4.19-Splitting Tensile Test Results for LC-CFS

PARAMETER S FOR LC-CFS	LC- CFS ₁	LC- CFS ₂	LC- CFS ₃	LC- CFS ₄	LC- CFS ₅	LC- CFS ₆	AVE STS @28days (MPa)
Diameter(mm)	101	101	101	101	101	100	2.61
Height(mm)	202	203	200	204	206	202	
Force(kN)	82.0	91.8	98.8	83.7	73.1	74.4	
STS(MPa)	2.56	2.85	3.11	2.59	2.24	2.32	

The figure 4.26 and 4.27 below shows the laboratory set up for the splitting tensile test for concrete cylinders and the split cylinder sample, while the figure 4.28 shows the graphical comparison of the different splitting tensile strength for the different mix ID's vs the percentage replacement.



Figure 4.26-Experimental Set-Up of Splitting Tensile Test



Figure 4.27-Split Specimen

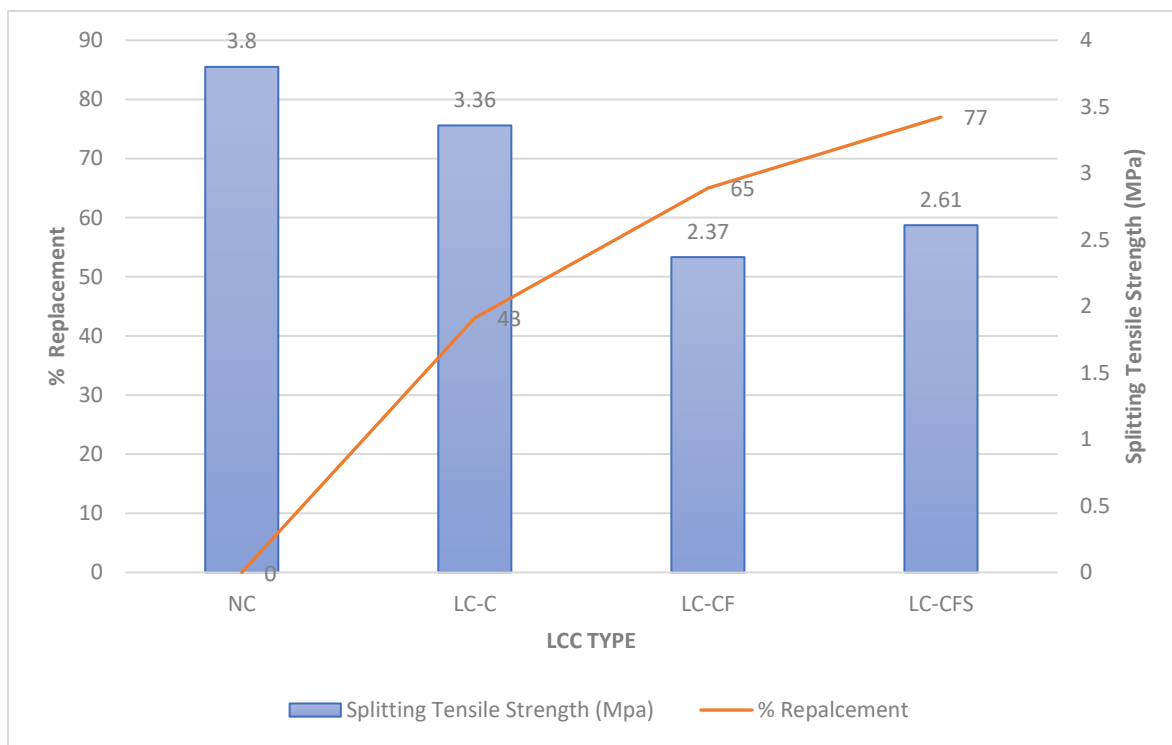


Figure 4.28-Summary Splitting Tensile Strength for Normal Concrete, and Low-Carbon Concretes vs Percentage Replacement

Upon evaluation of the splitting tensile strength using equation 4.6 above, the mean values for the test were taken as the average value, and the values obtained are well presented in figure 4.28 above; which shows the splitting tensile strength for the different concrete mixers. It can be then said that the incremental ration of replacement let to a decrease in the splitting tensile strength of the concrete. However, the only mix ID not fulfilling the criteria was the LC-CFS, which has a supplemental slag material and therefore recorded a slight increase in the value when compared to LC-CF.

The presence of the slag as a cementitious material could possibly the cause of an incremental splitting tensile test in the case of the LC-CFS, which was very unlikely of the other 3 mixes since there were no slag, a steady increment was otherwise recorded Because of this singular disparity, the compressive strength obtained from the different concrete and the splitting tensile strength were corelated together by the use of regression analysis and the plot of the splitting tensile strength(STS)versus the water/cement ratio was also obtained for the 28 days of both specimens.

Details of the plots obtained are shown in figure 4.29 and 4.30 below.

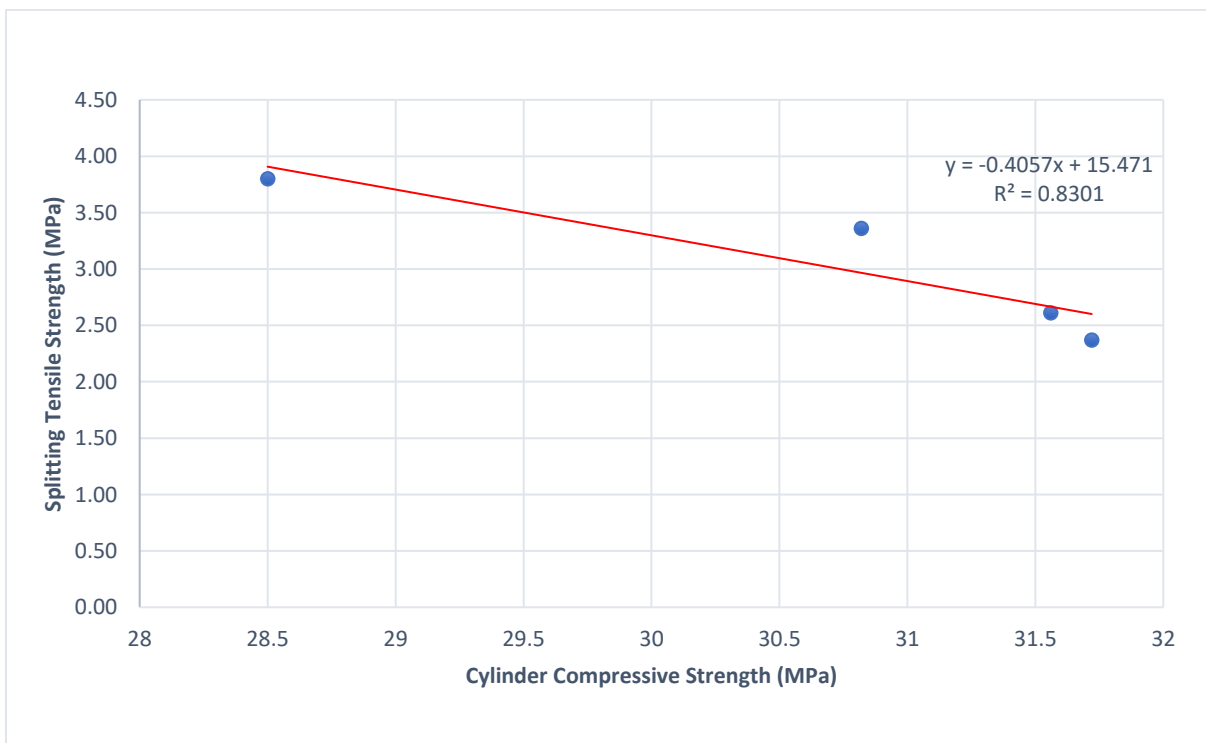


Figure 4.29-Splitting Tensile Strength versus Cylinder Strength using Linear Regression

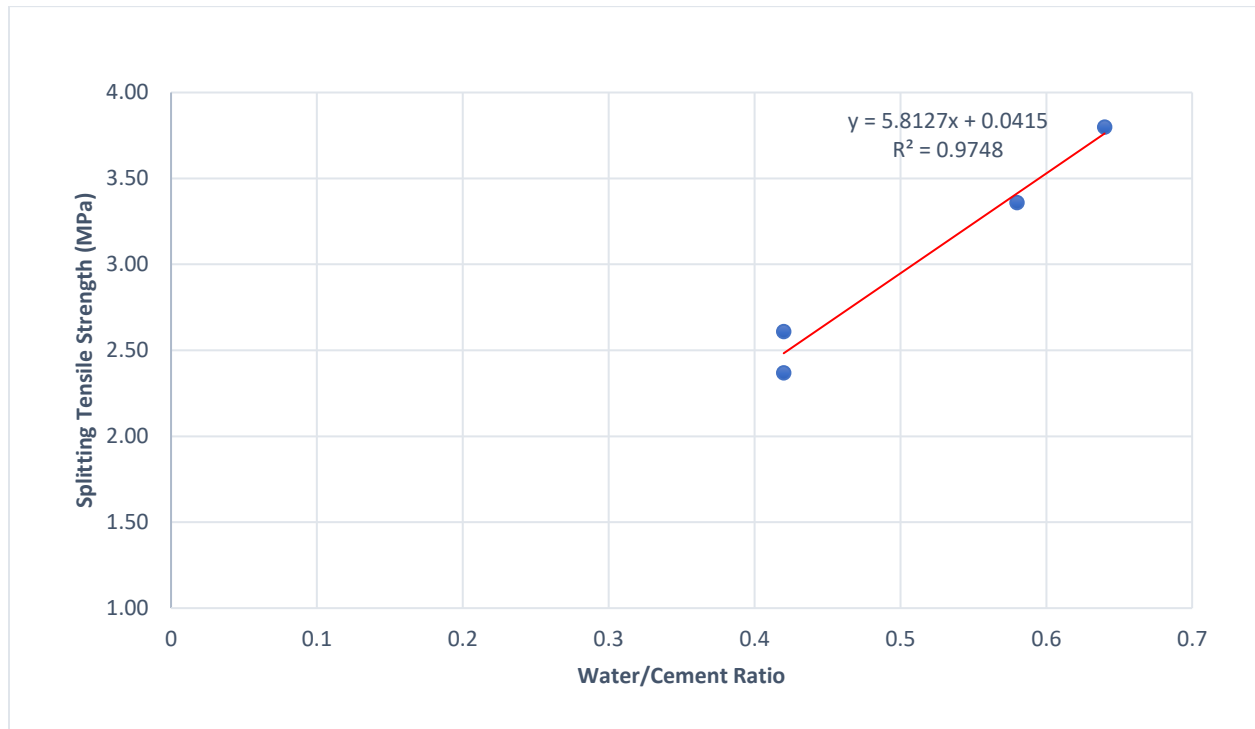


Figure 4.30-Splitting Tensile Strength versus Water/Cement Ratio using Linear Regression

In particular, from figure 4.30, a Pearson correlation coefficient of +0.99 was approximately obtained which showed almost a 100% complete relationship and strong relationship of how the variables were related and obtaining a slope of 5.812, and an intercept of 0.041 respectively.

In general, the splitting tensile strength for all the low carbon mixtures were far lower than that of the normal concrete. It was also evident that changes in the water cement ratio also influence compressive strength properties of the cylinder, that it does on the tensile properties of the concrete. As a matter of fact, from the data obtained, the water cement ration was directly proportional to the splitting tensile strength of the concrete, with the exception of the LC-CFS, and it is attributed to the slag content. The graph of the splitting tension tests, and the normalized cylinder strength is shown in the figure 4.31 below.

Therefore, more investigation is recommended on how certain incremental percentages of slag content can lead to changes in the splitting tensile strength of the concrete, without necessarily altering the durability of the concrete.

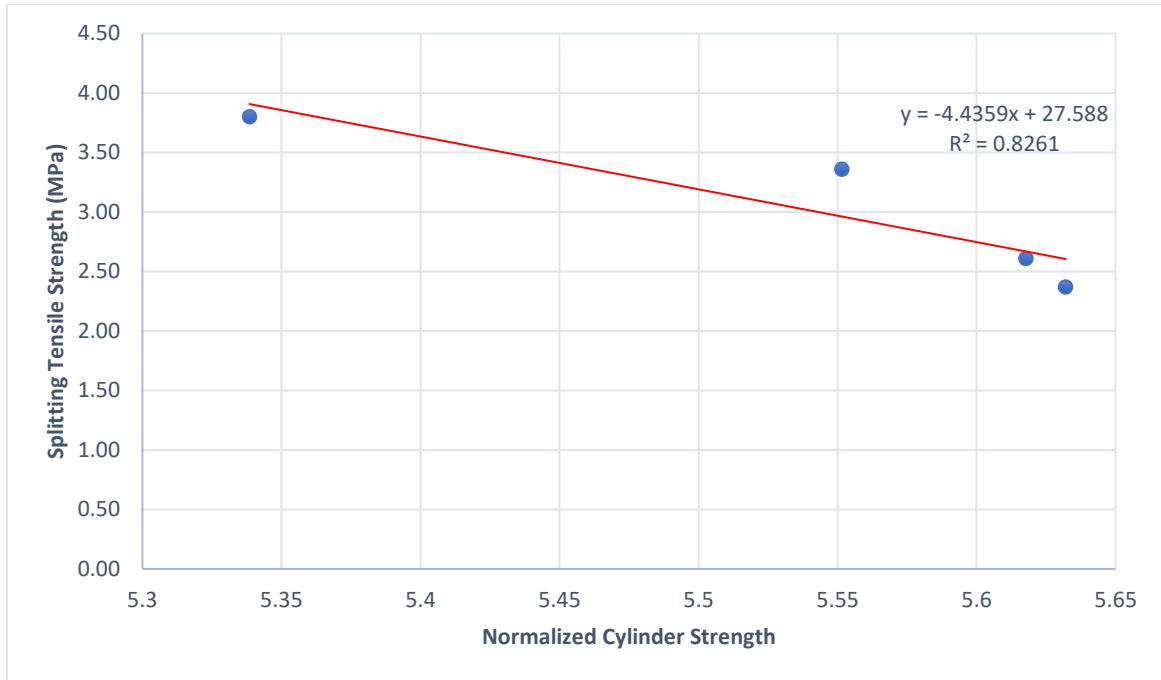


Figure 4.31-Splitting Tensile Strength vs Normalized Cylinder Strength

4.4.3. Workability (Slump)

Since the cylinder were consistent in their sizes and in their diameters, the slump of the fresh concrete was carried out by the use of CSA A23.2-5C[96]. A frustum cone was used with 100mm top diameter, 200mm in base diameter and 300mm in height. The mould had a separate base and handle in conjunction with a steel rod of about 16mm for the purpose of tamping the concrete into 3 different layers. The concrete sample was taken as a representative of the entire batch of concrete by the use of a scoop, and each layer was stroked 25 times, and each layer were rodded through their depth each. Care was taken during the last layer to ensure sufficient concrete could be heaped and still able to smoothen and strike out using the rod. The excess concrete was then removed from the base and the concrete slump mould was withdrawn from the top steadily (in five seconds) in such a way that lateral and torsional movement were fully restricted.

The normal concrete had the highest slump when it was compared to the other aggregates, and this is due to the water/cement ratio present in the concrete. Similar to this slump was that of LC-CFS obtain during the casting for the slab and the trail mixes that were validated. The target slump was to a maximum of 130mm.

The values obtained during the test procedure were rounded to the nearest 5mm in such that there were no decimals. Results from the slump test are presented in Table 4.20 below, while the actual slump test operation is shown in figure 4.32 and 4.33 below.

Table 4.20-Results of the Slump Test for the Different Mix ID's

ID	NC	LC-C	LC-CF	LC-CFS
Date	22 nd June 2023	22 nd June 2023	8 th June 2023	8 th June 2023
Slump (mm)	120	70	100	110



Figure 4.32-Slump Test Illustration



Figure 4.33-Measurement of the Concrete Slump

4.4.4. Modulus of Elasticity

The elastic modulus of concrete often referred to as the static modulus of elasticity of concrete was determined using ASTM C469 which gives the standard method and procedures for the determination of the elastic modulus and Poisson's ratio in the laboratory[137].

This test methods gives an opportunity to obtain the stress to strain ratio which is a measure of the elastic modulus of the concrete. To begin the procedure the cylinders of dimensions 100mm-by-200mm were first grinded on the bottom and the top faces and was tapped tried using a white paper towel. The next thing was the compressometer parts were assemble together and place in alignment by slightly elevating form the even surface using an elevation trapezoidal rod of about

10mm. The specimen was placed into the compressometer and aligned by carefully loosening and tightening the adjustment knobs of the compressometer. The test machine was set to a test speed of 0.002. The dial gauges were set to zero and the set-up was placed into the compression machine and ensuring the specimen and the compressometer were properly aligned and the specimen was first loaded to 40% of the initial ultimate load obtained from the compressive strength test, and the data was not recorded. The specimen was then loaded in three consecutive cycles taking note of the readings in the transverse and the longitudinal dial gauges. An average of the 3 sets of data was taken for the test and the average of three specimens was taken for the entire test as a representative sample for the test. While the details of the formula is shown below, the results from the modulus of elasticity tests as well as the pictures from the test are presented in table 4.21, 4.22, 4.23, and 4.24 respectively.

$$E = \frac{(S_2 - S_1)}{(\epsilon_2 - 0.000050)} \quad 4.10$$

Where

E is the chord modulus of elasticity given in GPa

S₂ is defined as the stress that corresponds to 40% of the ultimate load

S₁ is defined as the stress that corresponds to a longitudinal strain of 50 millionths psi

ε₂ is the longitudinal strain that is produced as a result of the stress S₂

4.4.5. Poisson's Ratio

The Poisson's ratio was also obtained using the second dial gauge during the test and it was thus calculated as follows:

$$E = \frac{(\epsilon_{t1} - \epsilon_{t2})}{(\epsilon_2 - 0.000050)} \quad 4.11$$

The data obtained for the test is presented below in table 4.21, 4.22, 4.23, 4.24:

Table 4.21-Elastic Modulus Data Set for NC

Parameters	Cylinder 1	Cylinder 2	Cylinder 3	Ave.
Elastic Modulus (GPa)	33.3	31.5	32.4	32.4
Height (mm)	200.0	200.0	198.0	199.3
Diameter (mm)	102.0	101.0	100.0	101.0
Force (kN)	104.1	104.3	104.7	104.4

Stress (MPa)	12.8	12.8	12.8	12.8
---------------------	------	------	------	------

Table 4.22-Elastic Modulus Data Set for LC-C

Parameters	Cylinder 1	Cylinder 2	Cylinder 3	Ave.
Elastic Modulus (GPa)	28.9	28.3	27.3	28.2
Height (mm)	200	198	200	199.3
Diameter (mm)	100	100	100	100
Force (kN)	99.2	100.0	99.9	99.7
Stress (MPa)	12.2	12.2	12.2	12.2

Table 4.23-Elastic Modulus Data Set for LC-CF

Parameters	Cylinder 1	Cylinder 2	Cylinder 3	Ave.
Elastic Modulus (GPa)	18.7	19.9	21.1	19.9
Height (mm)	200.0	200.0	198.0	199.3
Diameter (mm)	100.0	100.0	103.0	101.0
Force (kN)	103.2	103.3	103.4	103.3
Stress (MPa)	13.1	13.3	13.3	13.2

Table 4.24-Elastic Modulus Data Set for LC-CFS

Parameters	Cylinder 1	Cylinder 2	Cylinder 3	Ave.
Elastic Modulus (GPa)	16.9	15.3	15.3	15.8
Height (mm)	200.0	200.0	198.0	199.3
Diameter (mm)	102.0	101.0	100.0	101.0
Force (kN)	104.1	104.3	104.7	104.4
Stress (MPa)	12.8	12.8	12.8	12.8

From the data obtained for the elastic modulus of the concrete and the Poisson's ratio at 28 days, It is evident that as more replacement content was being added in place of natural aggregate the

elastic properties of the concrete also referred to as the chord modulus of elasticity was found to be higher for the concrete that had no replacement content or 0% recycled content. For the low-carbon concrete that had a percentage of recycled aggregates, elastic modulus was found to be increasing as the level of replacement content by weight was increasing, from coarse aggregate alone, to coarse and fine aggregate, to coarse aggregate, fine aggregate and additional cementitious material which was slag. Therefore, the replacement ratio was inversely proportional to the elastic modulus of the concrete. Figure 4.34 vividly shows this relationship of the mean elastic modulus in GPa for the NC, LC-C, LC-CF, LC-CFS, and the replacement ratio; the graph of elastic modulus of the concrete versus the strength by the use of regression analysis, and the graph of the elastic modulus of the concrete versus the density of the concrete. In addition, figure 4.35, 4.36, 4.37 and 4.38 shows the laboratory set up for the elastic modulus and the Poisson's ratio test.

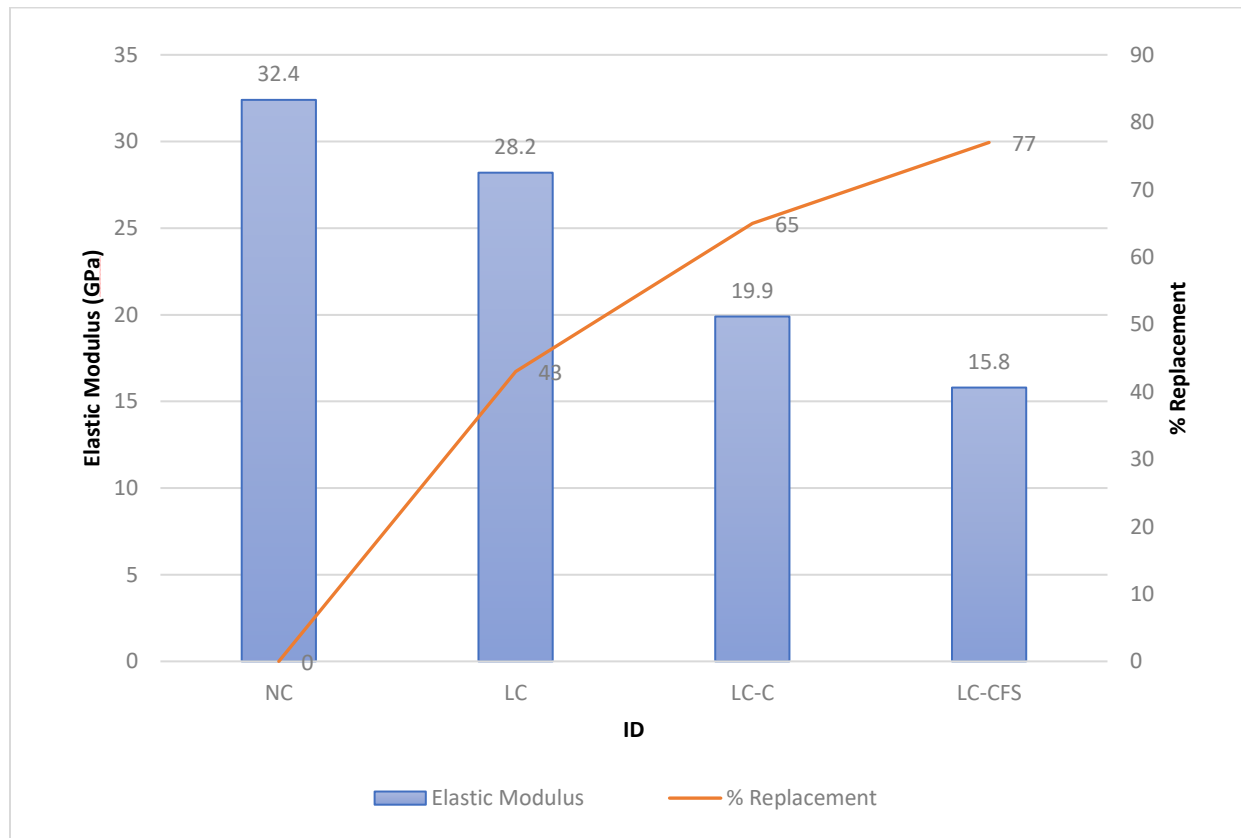


Figure 4.34-Elastic Modulus vs Percentage Replacement



Figure 4.35-Compressometer



Figure 4.36-Cylinder Positioning inside the Compressometer



Figure 4.37-Alignment of the Specimen and the Compressometer



Figure 4.38-Elastic Modulus & Poisson's Ratio Test-Set-Up

5. CHAPTER FIVE: THE REINFORCED CONCRETE SLABS DESIGN METHODOLOGY

This chapter discusses the design of the two-way reinforced concrete slabs. The further detailed procedures and checks are included in subsequent section of this chapters while figure 5.1 below presents the general slab layout.

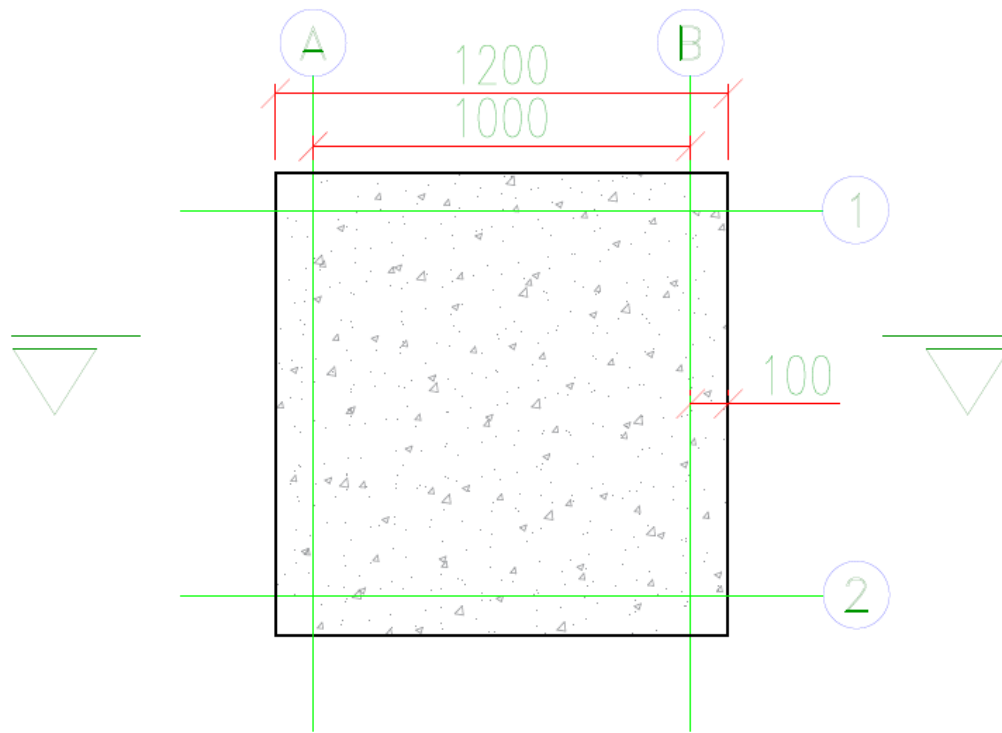


Figure 5.1-Slab Layout

5.1. The Design of the Slabs According to CSA A23.3-04

The design of the slabs was carried out in accordance with the ACI Code and the CSA Design Handbook. The slabs were designed to resist bending in both x and y planes by two way actions solely. Majorly the equivalent frame method was used for the analysis of the slabs and relevant checks were carried out by the use of analytical codes equations. Firstly, was the selection of the type of slab which was two-way slab. The next thing was to establish the governing design equations and design criteria of the slab.

A critical step in the design was to select the slab thickness for the anticipated load condition and the boundary conditions. Where applicable, the moment and the sharing forces for the slabs were

obtained and the deflection criteria as well as the reinforcement details and shear were checked to be in conformity of the code.

5.1.1. Selection of Slab Thickness & Effective Depth

Prior to the selection of the slab thickness. The definition of the slab ration that helps to select the choice of the design that was to be used was carried out. It was based on the fact that we have both axis x and y of the slab measuring 1200mm and 1200mm respectively and therefore they were designated as the L_y to L_x , which is the ratio of the long span to the ration of the short span. The slabs were designed for flexure without beams and based on this the ACI code permits the design of the slabs using the direct design method or the equivalent frame method. Since the ratio of $\frac{L_y}{L_x}$ is lesser than or equal to 2, therefore the slab is designed to be a two-way spanning slab for the purpose of the classification. Chapter 8 of the ACI 318-19 code provides the guidance for the selection of the thickness for two-way slabs. It categorically states that the slab thickness is not depended on the elastic modulus of the concrete and the loading. Although these lab tests are being carried out however, it is irrelevant to the selection of the slab thickness.

Clause 13.2.1 of the CSA A23.3-04 gives the minimum thickness of a slab to be $h_s=120mm$. However, where requirements are to be met and the minimum thickness inadequate for slabs without drop panels, the equation below shall be used so that the deflection and the cracking widths does not exceed the limits[138]. Table 5.1 gives further details on the minimum thickness based on the CSA A23.3-04.

$$h_s = \frac{l_n(0.6 + \frac{f_y}{1000})}{30} \quad 5.1$$

5.1.2 The Reinforcement Ratio

For the selected slabs in consideration, 10M bars were used which their typical diameter is 11.3mm and 4-10M bar were used in the x and in the y-direction, the reinforcing ratio for the four reinforced concrete slab was found to be 0.007/0.71%. The details of the design and reinforcement provision is in the appended section. The reinforcement ratio was calculated as thus:

$$\rho(\%) = \frac{A_s}{bd} \quad 5.2$$

5.1.2. Reinforcement Spacing

Based on the reinforcing ratio obtained, provisions were made for the transverse and longitudinal steel reinforcement taking into account the code requirements and other considerations such as the slab thickness, the concrete strength, the diameter of the reinforcing bars used, and the expected capacity of the slab obtained analytically and by the use of the finite element analysis. As a reference the CSA A23.3-04 was used to obtain the requirements for the spacing for the slabs as given in the table 5.3 below, with exceptions for ribbed slabs and the cellular constructions. Given the above mentioned, a spacing of 387mm was provided for the transverse and the longitudinal reinforcement.

Table 5.1-Spacing Requirements for Slabs

Negative reinforcement in the band defined by b_b	$1.5 h_s$, but $s \leq 250mm$
Remaining negative moment reinforcement	$3 h_s$, but $s \leq 500mm$
Positive moment reinforcement	$3 h_s$, but $s \leq 500mm$

From the above table, since $s \leq 500$ in both the positive and the negative reinforcement for the transverse and the longitudinal section; the provision of spacing of 387mm is adequate and satisfied the code provision.

5.1.3. Detailing of the Reinforcement & Slabs

Based on the details and spacing obtained during the analytical design of the slabs, the specification for the slab such as the reinforcement, the spacers, as well as the corner details were provided by the use of AutoCAD for convenience. The anchorage length was developed with applicable codes. In the figure 5.2 below, shows the reinforcing steel details, spacing and dimension for the 1.2m by 1.2m by 0.12m reinforced concrete slab.

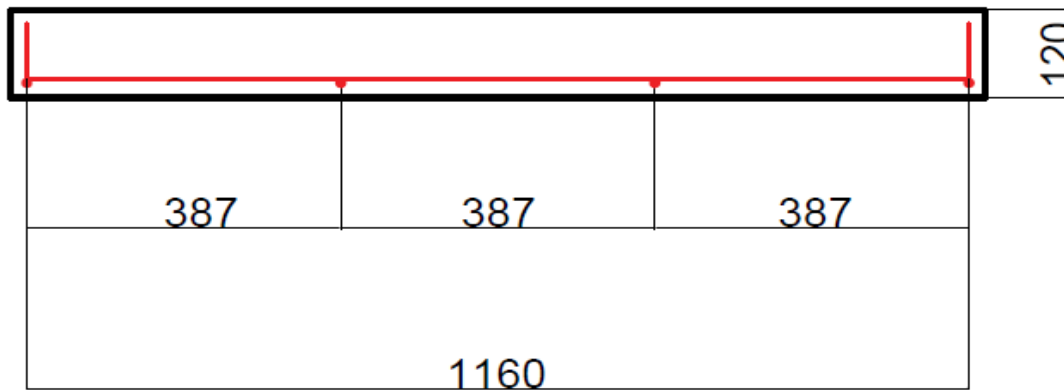


Figure 5.2-Reinforcing Bar Details

5.1.4. Provision of Corner Reinforcement to Slabs

The use of corner reinforcement or special type of shear reinforcement was not justified. This is because based on slab deformations and existing twisting corners, CSA A23.3-04, recommend the use of special reinforcement due to the presence of high twisting moments leading to bottom and top tension in the slabs. Since the slab is not subject to twisting, and the slab does not have a beam between the supports and has been supported on the four sides this condition is not justified for use. This is based on Clause 13.12.5 and N13.12.5. However, it is worthy to note that the main purpose of providing the corner reinforcement or curtailment is to be able to control crack around the three regions of the slab, which are the edges and the middle of the slab.

5.1.5. Provision of Cover to the Reinforcement

The edge spacing between the bars and the concrete were as same as 20mm providing sufficient cover to all reinforcement from the four sides and the bottom. Table 20.5.1.3.1 of ACI 318-19 gives the concrete cover specified for cast-in-place non-prestressed concrete members. CSA A23.1 also provides cover requirements for 20mm applicable to interior exposed slabs. To provide a suitable cover for the RC slab, a plastic 3D printed chair of height 20mm was placed at the bottom of the longitudinal reinforcing steel. Further information on the selection of the cover and exposure conditions are provided in the table 5.2 below.

Table 5.2-Cast-in-Place Non-prestressed Concrete Members Specified Concrete Cover (Source ACI 318-19)

Concrete Exposure	Member	Reinforcement	Specified Cover (in inches)
Cast against and permanently in contact with ground	All	All	3
Exposed to weather or in Contact with ground	All	No. 6 through No. 18 bars	1-1/2
		No. 5 bar, W31 or D31 wire, and smaller	1-1/2
	Slabs, joists, and walls	No. 14 and No. 18 bars	1-1/2
Not exposed or weather or in contact with ground	Beams, columns, pedestals, and tension ties	No. 11 bar and smaller	3/4

Based on the above specifications, the cover falls into the category of $\frac{3}{4}$ inches or 18.9mm which is approximately 20mm, therefore a concrete cover of 20mm was used for the bottom, top and the sides of the reinforcing deformed steel bars.

5.1.6. Check for Shear Requirements

The next procedure in the design of the slabs was to check for the load at which the slab shear will occur which is also the ultimate load at failure. Based on the equation provided in the calculation sheet attached to the appendix, by CSA A23.3-04, the obtained shear value was found to be $V_c = 129kN$.

5.1.7. Factored Moment Computation

In the case of the factored moment computation for the two-way slabs of 1200mm-by-1200mm. Based on the equation for the total statical moment $Mo = q_u l_{2a} l_n^2 / 8$, the total statical moment obtained was found to be **0.86kNm**. The value of the l_{2a} was taken to be 1.2m since the length of both sides of the slab are the same and the clear span was 1.0m between the supports. Table 5.3 and 5.4 and 5.5 provide the details for the distribution of the moments by utilizing the factored

statical moment obtained for the slab, and the obtained factored moment for the slab based on the values from the tables.

Table 5.3-Negative & Positive Factored Moment

Negative factored moment at the face of support	0.65
Positive factored moment at mid-span	0.35

Table 5.4-Distributed Factors using Total Factored Static Moment

Moment	Exterior edge unrestrained	Slabs with beams between all supports	Slabs without beams between interior supports	Exterior edge fully restrained
Interior negative factored moment	0.75	0.70	0.70	0.65
Positive factored moment	0.66	0.59	0.52	0.35
Exterior negative factored moment	0	0.16	0.26	0.65

Based on the distribution factors for the factored static moment. Exterior edge fully restrained applied to the slab and therefore the obtained static moment values shall be multiplied in accordance with these provisions to obtain the factored static moments for the slab. As already mentioned, table 5.5 present the findings of the moments obtained for the first exterior region and for the middle positive factored moment region of the reinforced concrete slab.

Table 5.5-The Factored Moments Obtained

Moment	Values (kNm)
1 st exterior negative factored moment	0.559
Positive factored moment	0.301
2 nd Exterior negative factored moment	0.559

Based on the above table, the negative factored moments were found to be 0.559kNm respectively on both sides of the slab and the positive factored moment was found to be 0.301kNm. Therefore, the moment plot obtained is shown in the figure below.

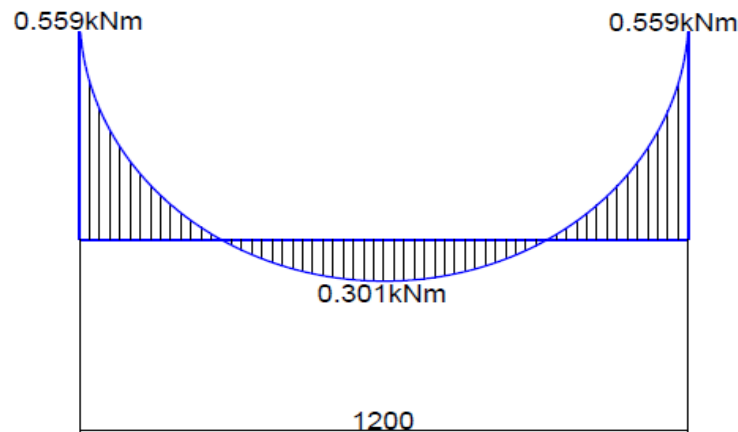


Figure 5.3-Factored Moment Diagram for the Two-Way Slab

5.1.8. Permissible Deflections

Based on the maximum permissible deflection requirements for floors not supporting or attached to non-structural elements likely to be damaged by deflections that are large, the permissible deflection in the slab was found to be 4mm.

In general, two way slabs are not usually subjected to deflections, however, to ensure that the computed deflection is with the limit, a basic check is carried out on the basis of the sustained load deflection which is given in Clause 9.8.2.5 of the CSA A23.3-04, and by using the ACI code crossing beam method a value of 4mm is obtained.

Table 5.6-Maximum Permissible Deflection Requirements

Type of Member	Deflection Consideration	Deflection Limitation
Flat roofs not supporting or attached to non-structural elements and likely to be damaged by deflections that are large	Immediate deflection due to specified live load L, or snow load, S	$\frac{l_n}{180}$
Floors not supporting or attached to non-structural elements likely to be damaged by deflections that are large	Immediate deflection due to specified live load L	$\frac{l_n}{360}$
Roof or floor construction supporting or attached to non-structural elements likely to be damaged by deflections that are large	Part of total deflection after attachment of non-structural element (long-term deflection due to sustained load and plus immediate deflection due to any additional live load)	$\frac{l_n}{480}$
Roof or floor construction supporting or attached to non-structural elements not likely to be damaged by deflections that are large	Part of total deflection after attachment of non-structural element (long-term deflection due to sustained load and plus immediate deflection due to any additional live load)	$\frac{l_n}{240}$

5.2. Yield Line Analysis of the Two-Way Slab

In the yield line analysis of the slab, the aim is to be able to estimate the lower bound values for the slab capacity. Firstly, to able to establish this, a particular collapse mechanism was assumed for the slab, taking into consideration the geometry of the slab.

This mechanism will help to estimate the load carry capacity of the slab when it is under the action of a concentrated load. In this case, the solution to the problem is obtained by solving for the moment of resistance of the slab, also known as the Mr. Upon obtaining the Mr, the capacity of

the slab was then calculated, and this was a function of the plastic moment, the clear span, the loading area in consideration.

The figure 5.4 given below shows the assume yield line pattern for the two-way slab. Failure is assumed to follow a diagonal cracking pattern towards the middle of the slab.

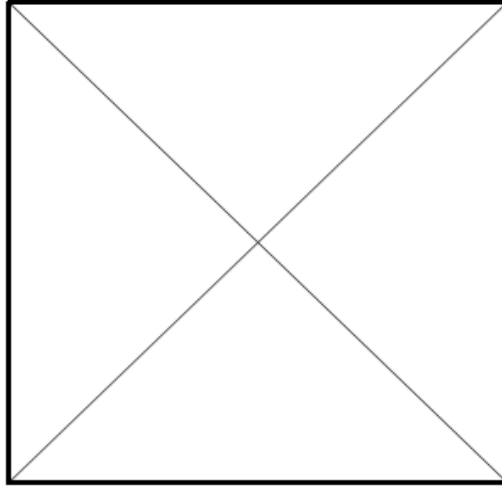


Figure 5.4-The Slab Assumed Yield Line Pattern

5.2.1. Evaluation of the Slab Capacity based on the Moment of Resistance

The equation below was used to obtain the initial capacity for the slabs:

$$M_r = \phi_s A_s f_y \left(d - \frac{a}{2}\right) / 10^6 \quad 5.3$$

ϕ_s is the material resistance factor for steel which in this case is taken as unity and A_s is the area of steel in mm^2 , f_y is the strength of steel in MPa, d is the effective depth of the slab, and $a=0.25$, is the width of the loading plate in meters. The M_r is therefore obtained as follows:

$$M_r = 1 * 333 * 400 \frac{94.4 - \frac{0.25}{2}}{10^6} = 12.56 \text{ kN.m}$$

The estimation of the load at failure is then calculated using the equation as below:

$$P = \frac{8 * M_p * L}{L - a} \quad 5.4$$

$$= 133.97 \text{ kN}$$

Therefore, based on the assumed slab failure pattern of the slab, the predicted capacity of the slab is 133.97kN. This particular load is also referred to as the collapse load for the two-way recycled RC slab.

5.2.2. ACI Crossing Method for Deflection

The computation of the deflection for the different slabs was carried out by the use of ACI crossing beam analogy method. In considering the elastic modulus for the natural aggregate concrete and for the concretes obtained from recycled materials, the data for the elastic modulus and the moment of inertia was use for the computation of the deflection for the reinforced concrete two-way slab. The equation 5.5 below was used to obtain the deflection for all the slabs.

$$\delta = \frac{K}{384} * \frac{wl_n^4}{E_c I_c} \quad 5.5$$

Where K is boundary condition factor and taken as 1.4 for interior panels, while E_c is the elastic modulus of concrete and I_c is the moment of inertia in mm^4 , l_n is taken as the clear span for the slab.

Give the above equation, the deflections are calculated as follows:

$$\delta \text{ for NC} = \frac{K}{384} * \frac{7.05 * 1000^4}{32.4 * 144 * 10^6} = 5.5\text{mm}$$

$$\delta \text{ for LC} - C = \frac{K}{384} * \frac{7.05 * 1000^4}{28.2 * 144 * 10^6} = 6.3\text{mm}$$

$$\delta \text{ for LC} - CF = \frac{K}{384} * \frac{7.05 * 1000^4}{19.9 * 144 * 10^6} = 8.9\text{mm}$$

$$\delta \text{ for LC} - CFS = \frac{K}{384} * \frac{7.05 * 1000^4}{15.8 * 144 * 10^6} = 11.28\text{mm}$$

The table 5.7 below gives the summary for the deflection values for the natural concrete and the recycled concretes.

Table 5.7-Summary of the Deflection of the Natural Concrete Slab & Low-Carbon Concrete

Slab ID	$\Delta_{mid}(mm)$
NC	5.50
LC-C	6.30
LC-CF	8.90
LC-CFS	11.28

In general, the concrete slabs showed predicted mid-span deflection as 5.50mm, 6.30mm, 8.90mm and 11.28mm using the ACI crossing beam analogy method. Based on this analogy, it was evident that increasing the percentage of replacement content led to larger mid span deformation or deflection.

In comparison with the code limits of ACI which is $1/240=5mm$, the slabs generally had higher deflection values; however, when compared to the FEA analysis, the NC and LC-C slabs and the LC-CF and LC-CFS were within the limits of the code. The FEA seems to have given more predictive analysis when compared to the deflection limits. This is summarized in table 5.8 and 5.9 below with the percentage (%) errors.

Table 5.8-Deflection Comparison for FEA with Limiting Value

Slab Type	FEA Deflection(mm)	ACI limit(mm)	% Error
NC	4	5	25
LC-C	4	5	25
LC-CF	5	5	0
LC-CFS	5	5	0

Table 5.9-Deflection Comparison for FEA with Limiting Value

Slab Type	Crossing Beam Predicted Deflection(mm)	ACI limit(mm)	% Error
NC	5.50	5	10
LC-C	6.30	5	26
LC-CF	8.90	5	78
LC-CFS	11.28	5	125.6

6. CHAPTER SIX: FINITE ELEMENT MODELLING OF TWO-WAY LOW-CARBON CONCRETE SLABS

Studies that have accurately investigated slabs that are made from recycled concrete aggregates are limitedly available. This is owing to the limitations in modelling of the aggregate's materials properties, and other factors such as bond effect of the aggregates. Therefore, it is worthwhile to investigate the behaviour of the slabs in conjunction with field laboratory work and to know to what extent does the Gid models the slab correctly in terms of predicting the failure of the slab and the load capacity owing to the constraints imposed.

The finite element modelling for the two-way slab involved certain procedures which include the idealisation and the modelling of the two-way slab using ATENA Gid, a finite element software for the analysis of reinforced concrete structures. In the modelling of the slabs, the slab was taken as an isotopically reinforced such that the reinforcement was similar at all corners of the slabs. The numerical technique generally involved dividing the structural slabs into different finite elements for the purpose of understanding the behaviour of the slab and the entire structural system.

The slab model is to provide a predictive analysis and to be able to obtain the slab load capacity in kN and the maximum deformation that will occur under the impact of the load. Consequently, it does not give or propose any equation for the analysis or the modelling of the slab. On this basis, the model was investigated for certain properties and the behaviour and response of the model was judged from those properties. Therefore, the modelling of the slab involved four stages, namely, the creation of the model nodes and the surfaces which are a representative of the slab with and the slab height, the discreet modelling of the reinforcement and the generation of the slab volume, the material properties characterization, the imposition of the boundary conditions of the slab, the meshing, and the analysis of the slab by the use of ATENA 3D program for running and the visualization of the results of the Gid Model.

6.1. Scope & Motivation for Finite Element Modelling

In this research, the primary reason for the modelling of the concrete using a 3D non-linear finite analysis software is to obtain the behaviour of reinforced concrete under the influence of loads and by the use a loading plate. The model was made in accordance with the experimental set-up and therefore any difference would be clearly stated with reasons. The initial model was created using line and nodes making use of the ATENAGid Software and results were obtained from the ATENA

3D Studio Program (<https://www.cervenka.cz/>). The interest of utilizing finite element analysis was to be able to observe the level of cracks, slab capacity, deflection, as well as the strains in the concrete and that of the reinforcing bars.

6.2. ATENAGid Constitutive Model

Several models have existed that have been used to characterise the behaviour of concrete itself. However, some of these models, they tend to vary in how they have taken into consideration the performance of concrete and its entire properties during modelling. The model used from Cervenka et. al., (2021) attempt to describe the behaviour of concrete in detail[127]. In particular, the CC3DNonLinCementitious2User material which is without temperature, fatigue and fiber reinforcement, was used.

6.2.1. Reinforcement Stress Strain Laws

According to Cervenka (2021), reinforcement could either be modelled as discrete or smeared. At the initial stage the reinforcement was kept discrete and later meshed into the concrete, while uniaxial stress was assumed. This was achieved by assuming the multi-linear law which helps in the modelling of the different state of steel such as the elastic, yield, hardening and fracture[127]. Figure 6.1 below illustrates the multi-line law.

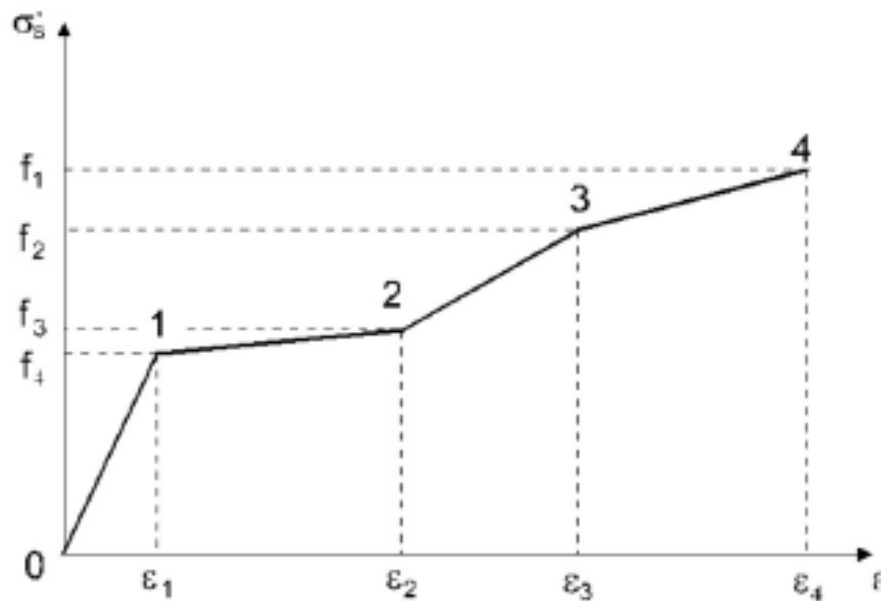


Figure 6.1-Stress-Strain Law for Reinforcement

6.2.2. Bond Strength of Concrete

In the preparation of the model, it is important to state that the model does not take into account the bond properties existing between the aggregates and therefore does not factor this into the capacity and the failure criteria of the slabs. While several models have attempted to provide information on the bond properties of recycled concrete for example a study by Liam (2016)[139]. This thesis in particular has exempted the bond investigation of the concrete involved in the study. Therefore, this gap is hereby acknowledged.

6.2.3. The Yield Mechanism of ATENA

The model was based on the formulation of smeared cracks and utilising the crack band. It was a combination of the fracture and the plastic model. The initial employs the Rankine failure criteria, the use of exponential softening and in particular rotated crack model, while the plasticity model was based on the Menetrey-Willam failure surface (Cervenka, 2021)[127].

6.3. The Slab Geometry

A discreet model and approach were used for the slab modelling. The concrete was first model, and the reinforcement was modeled in addition to it. The slab was modelled to the shape shown in figure 6.2 and 6.3 below:

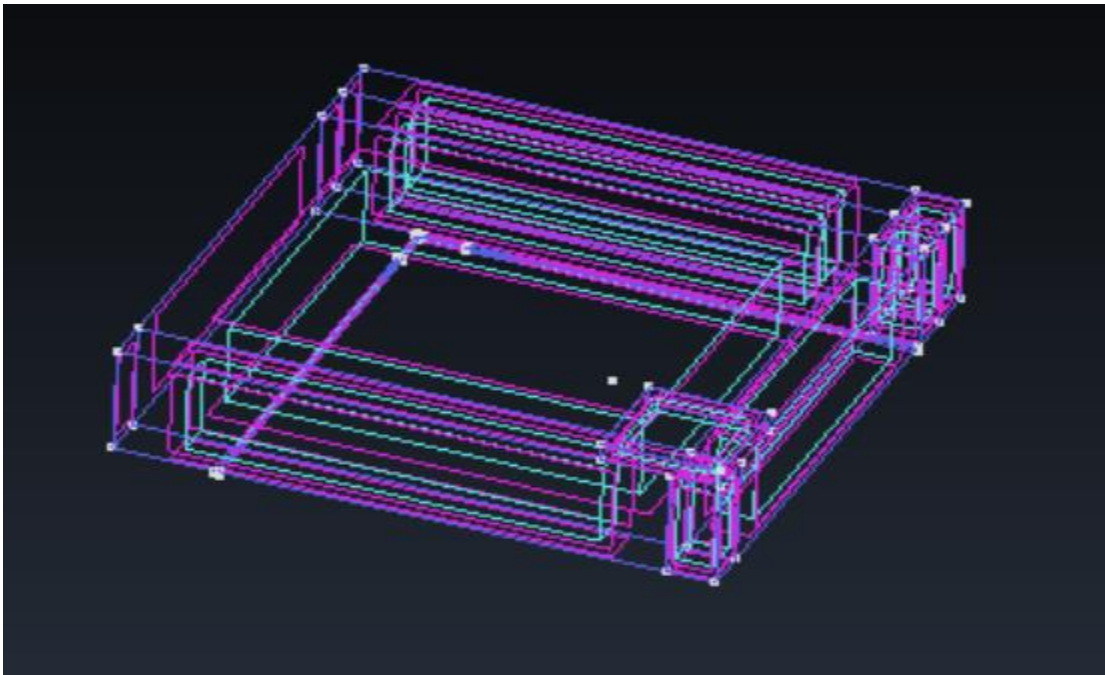


Figure 6.2-The Slab Model

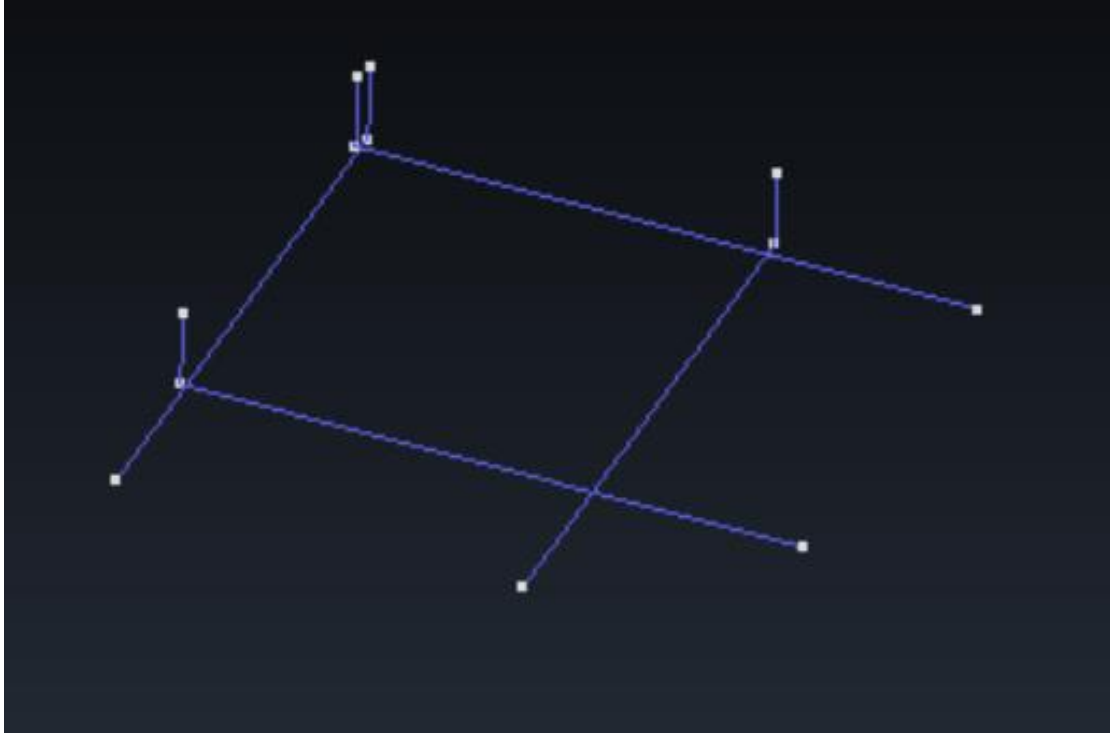


Figure 6.3-Discrete Model of the Reinforcement

6.3.1. The Use of Symmetry Condition

In the modelling of the slab, the use of symmetry condition was applied. For this purpose, only a quarter of the slab was modelled and analysed, this was the left upper quarter of the slab. While the values of the load obtained were obtained, they were multiplied by 4 to obtain the maximum load of the slab. Therefore, by enforcing the boundary conditions, the displacements obtained will be in the y-direction.

6.4. The Material Properties

Laboratory tests were conducted on the hardened concrete. This includes the modulus of elasticity of the concrete, and the compressive strength of the concrete. While other hardened parameters governing the normal concrete low-carbon concrete were obtained from the Fib Model Code (2010), and Choubey et al., (2016)[140][141]. Further details for the model properties are detailed below.

6.4.1. The Actual Elastic Modulus of Concrete & Recycled Concrete

The elastic modulus of the normal concrete and the recycled concrete that was used in the model were obtained experimentally by obtaining the elastic modulus property of the concrete. Since available equations from code considered elastic modulus as a function of the compressive strength and did not consider the relative stiffness of the concrete from the contributing material, it was therefore justified to utilise the experimental data for the modelling of the reinforced concrete two-way slabs.

6.4.2. Fracture Energy of Conventional and Low-Carbon Concrete

The fracture energy parameter of the concrete aims to estimate the absorption energy of the concrete during the failure phase which includes the cracking and the fracture of the concrete specimens. Several approaches can be used to obtain the fracture energy of concrete. However, fracture energy for the different concrete was obtain using Fib Model Code 2010 and Choubey et. al., (2016)[140][141]. The equation for the fracture energy G_F is given below.

$$G_F = 73 * f_{cm}^{0.18} \quad 6.1$$

$$G_F = b \frac{f_c}{E_c} * \left(\frac{d}{d_{20}}\right)^{b_1} * \left(\frac{t}{t_{30}}\right)^{b_2} * \lambda \quad 6.2$$

In the above equations f_c and f_{cm} are taken as the strength of the concrete, E_c is the elastic modulus of the concrete and b is taken as 85.93, b_1 is taken as 0.125, b_2 is taken as 0.211, d and t are the maximum size of the aggregate and curing age, d_{20} is taken as 20mm, and t_{30} is taken as 30 days, while the value of λ is taken to be unity.

Table 6.1-Fracture Energy Properties of the Concrete Mixes

ID	f_c (MPa)	Elastic Modulus (GPa)	Fracture Energy (G_f) @ 30 Days (N/mm)
NC	28.65	32.40	133.00
LC-C	30.82	28.20	93.31
LC-CF	31.72	19.90	136.09
LC-CFS	31.56	15.80	171.60

6.4.3. Tensile Strength of the Concrete

The tensile strength of the normal concrete was calculated based on the Fib Code (2010) which gives an equation to compute the tensile strength of normal weight concrete if the compressive strength alone was known[140]. In addition to this, Choubey et al., (2016) suggested an equation for the modelling of the fracture parameters for concrete made of recycled aggregate. Both equations are presented below respectively[140][141]:

$$f_{ctm} = 0.3(f_{ck})^{2/3} \quad 6.3$$

$$f_t = (0.24 - ar)f_{cu}^{\frac{2}{3}} \quad 6.4$$

Where

F_t is the concrete tensile strength MPa

F_{ctm} is the mean value of tensile strength in MPa

a is coefficient taken as 0.0006

r is the percentage replacement of RCA

f_{cu} is the cube compressive strength which in this case will be taken as the cylinder compressive strength

f_{ck} is the characteristic compressive strength

Table 6.2-Tensile Strength of Hardened Concrete Cylinders at 30 Days

ID	Tensile Strength (MPa)
NC	2.81
LC-C	2.35
LC-CF	2.35
LC-CFS	2.35

The above analytical equations have showed that normal concrete had a higher tensile strength when compared to the other concrete, while the tensile strength decreases with increasing

replacement of 100% RCA, showing 17% decrease compared to the tensile property of the natural aggregate concrete.

It is important to note that for the both concrete LC-CF and LC-CFS, since there is limited knowledge on the fracture energy in 100% combination with other constituent materials, and the tensile strength combined; the same equations for LC-C was applied.

6.4.4. Compressive Strength of Concrete

The compressive strength of the concrete f_{cu} was taken at 30 days also taken at 200 days respectively. Data obtained from the test was used for the material input during the modelling, further calculations done in previous section was based on the properties of the cylinder strength as it affects the tensile and the fracture energy property which was used in the model.

6.5. Reinforcing Steel Properties

The mechanical properties for the steel which was used in the model is presented in the table 6.3 below. The yield plateau was taken to be 550MPa and was selected to be more conservative in the modelling of the reinforced concrete slab, and therefore the yield strength of 500MPa was a round off value which was used based on test.

Table 6.3-The Reinforcement Properties

Parameters	Longitudinal Reinforcement X-Direction	Longitudinal Reinforcement Y-Direction
Yield Strength	500MPa	500MPa
Ultimate Strength	550MPa	550MPa
Maximum Strain	120mm/m	120mm/m
Reinforcement Ratio	0.035	0.035

Due to the reinforcement ratio in the slab, it was highly expected that the steel in the concrete was going to first be yielding before any crushing or material failure of the concrete will be occurring. Figure 6.4 below shows the material input parameters for the natural aggregate concrete. This included the prototype of the model, the modulus of elastic, which was varied based on the laboratory test results, the Poisson's ratio which was taken as an average value of 0.2 for all the concrete types due to unavailability of the data, the tension strength as indicated in the table 6.2, as well as the vary compression strength based on the compression tests at 28days.

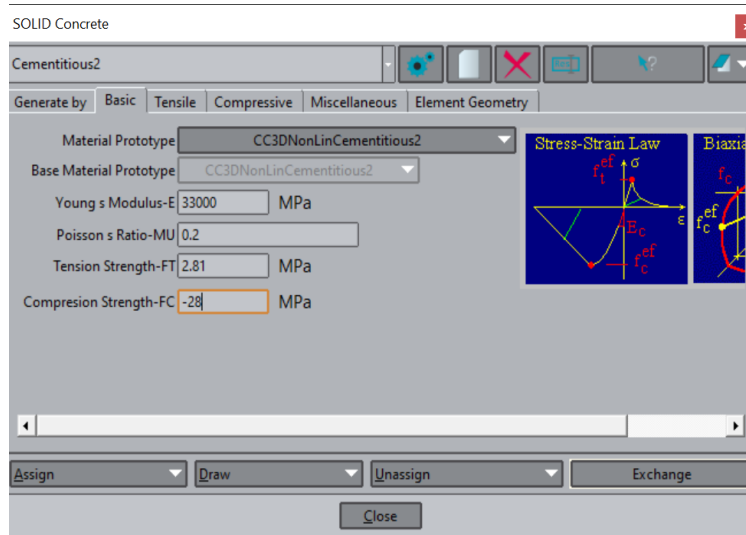


Figure 6.4-Input Material Properties of the Natural Concrete

6.6. Application of Boundary Conditions

In this section the boundary conditions used for the generation of the model is being described. To simulate ideal experimental condition. Two lines with end-end pints located at a span of 1000mm of the slab were positioned and 15mm high. The reason was to be able to get a similar situation such that the top plate of the slab was centrally and vertically loaded while a quarter of the slab was being modelled. This was to help obtain the load carry capacity of the slab and to obtain the predicted structural response that would be experimentally. During the non-linear FEA analysis, monitors were attached at specific points to obtain the forces, stresses, and the displacement occurs during the model execution. Therefore, symmetry condition was applied to be able to enforce the boundary conditions and to obtain the load carrying capacity of the two-way reinforced concrete slab model.

6.7. The Model Generation

The figure below shows the quarter slab model generated using line and points to form the structure.

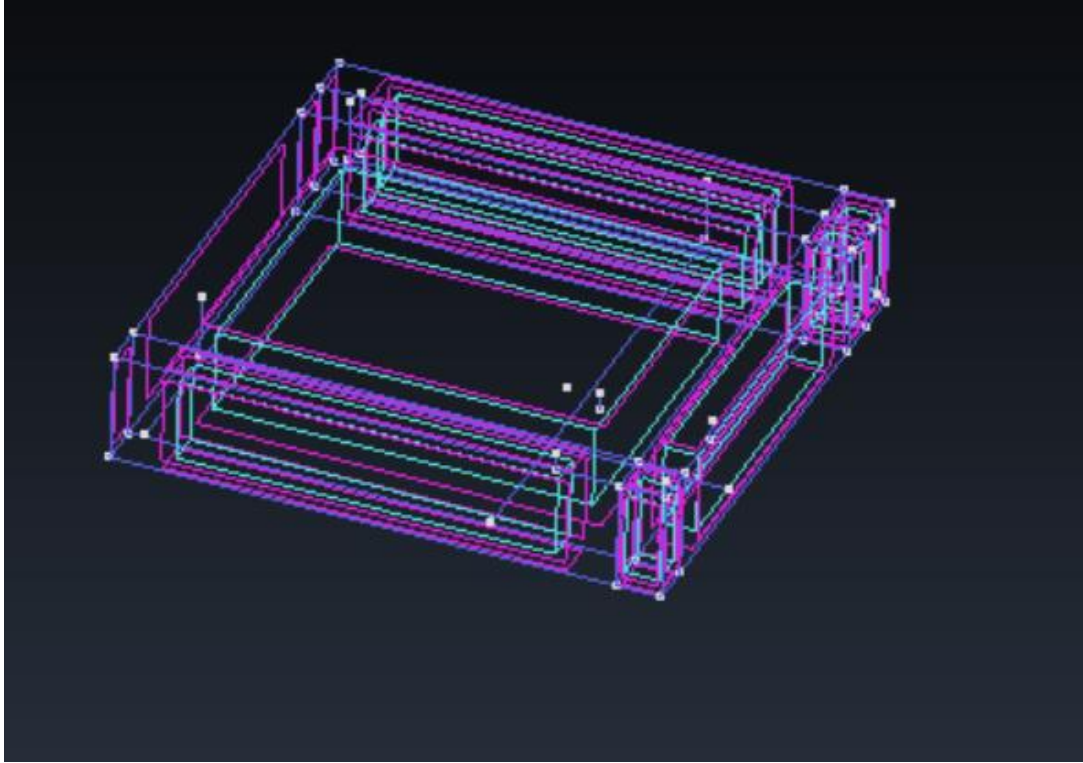


Figure 6.5-The Reinforced Concrete Slab Model

6.8. Meshing Parameters

In the meshing of the slab model, a meshing size of 0.05m was used to generate the finite element used for the analysis of the slab. In addition, hexahedral element was used for the generative meshing and analysis before the execution of the model. Figure 6.6 below shows the meshed generation for the models.

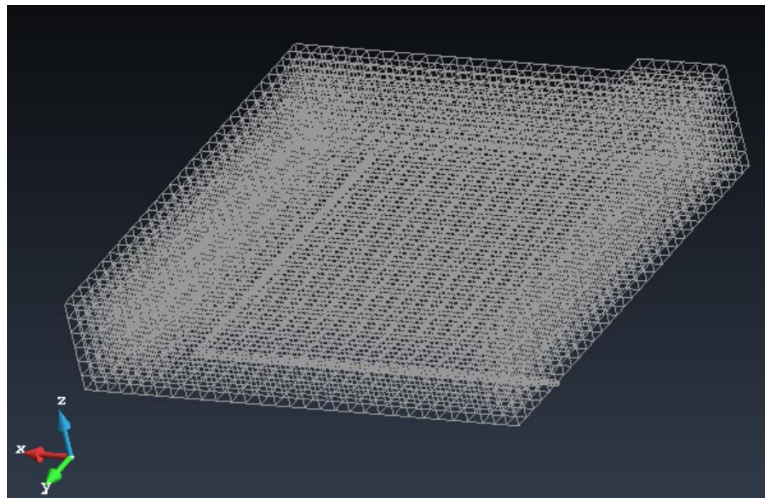


Figure 6.6-Mesh Generation for the Models

6.9. Slab NC

The normal concrete slab had an elastic modulus of 33GPa, a fracture energy of 130N/mm and therefore details for the slab is shown below

6.9.1. Load vs Displacement Curve

Figure 6.7 below shows the load displacement force for the natural concrete slab and the maximum load was 147.5kN

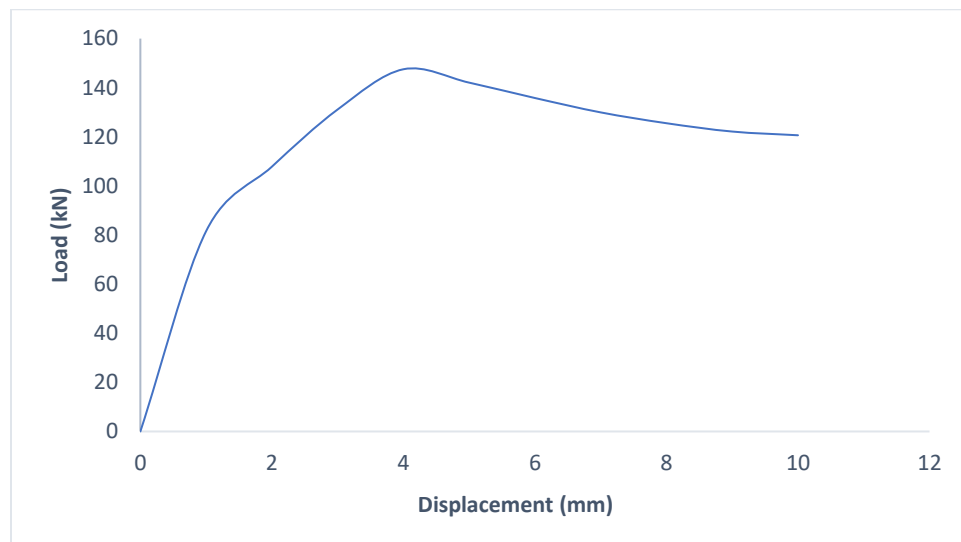
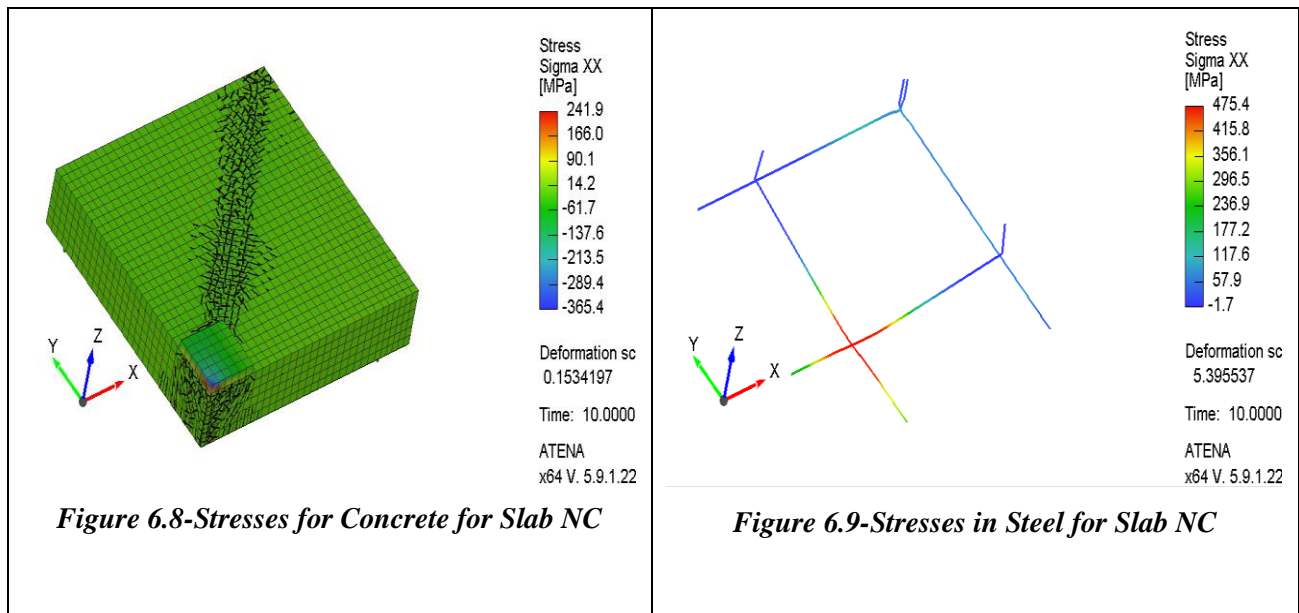
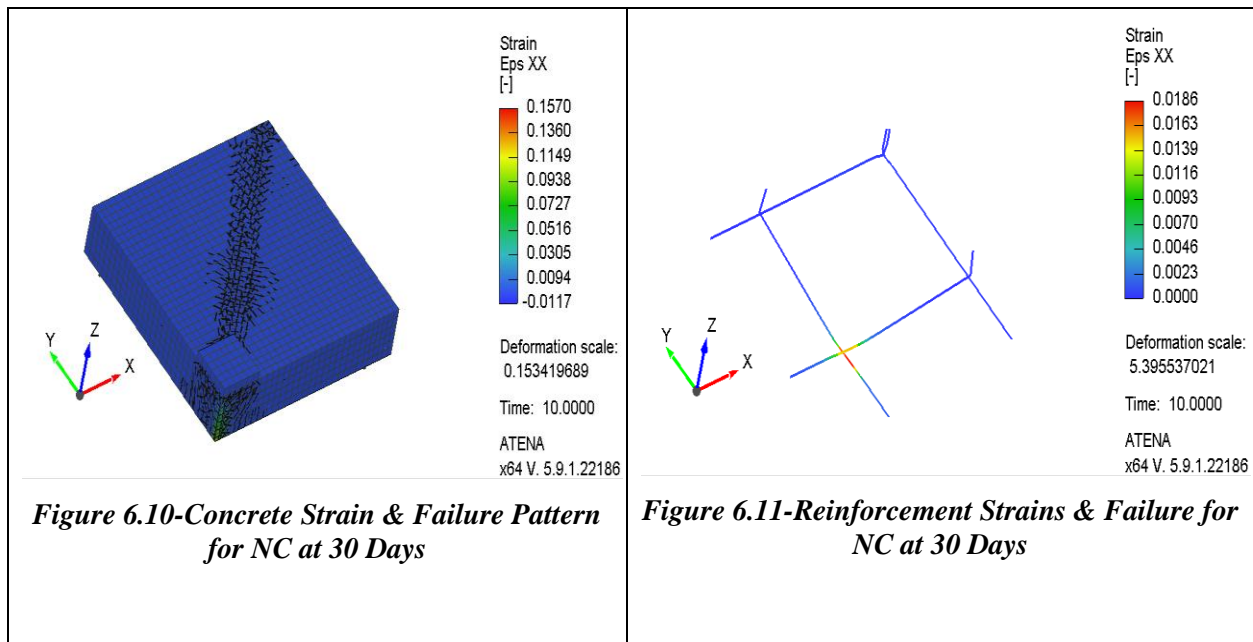


Figure 6.7-Load vs Displacement Curve for NC Slab

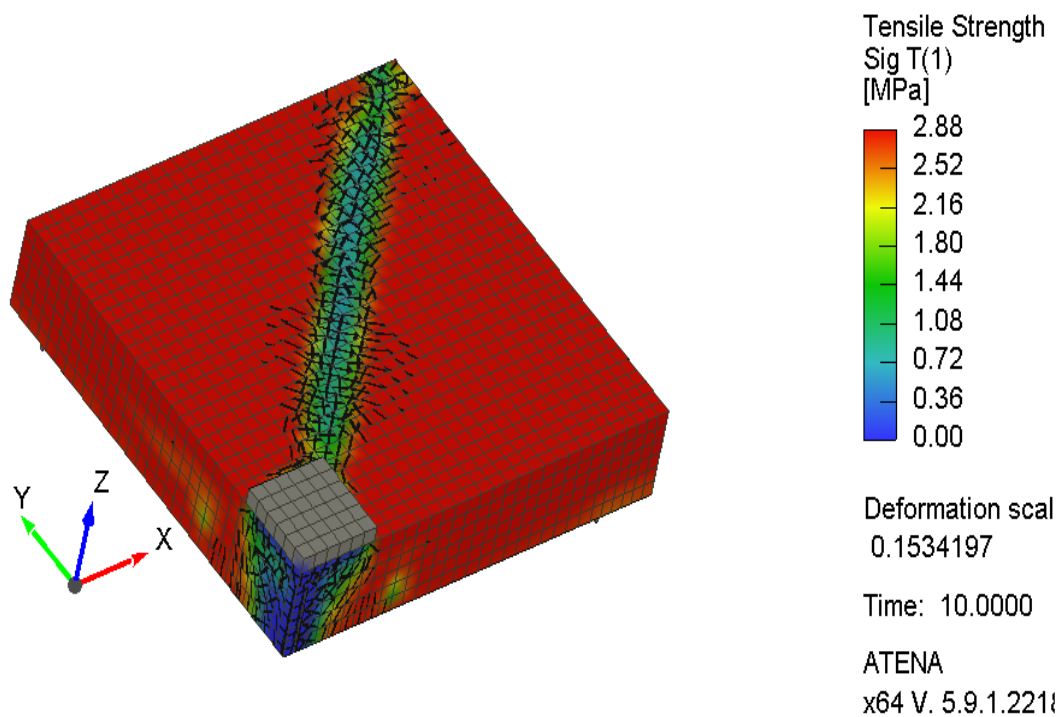
6.9.2. Stresses



6.9.3. Strains



6.9.4. Tensile Strength



6.9.5. Crack Patterns & Failure Mode

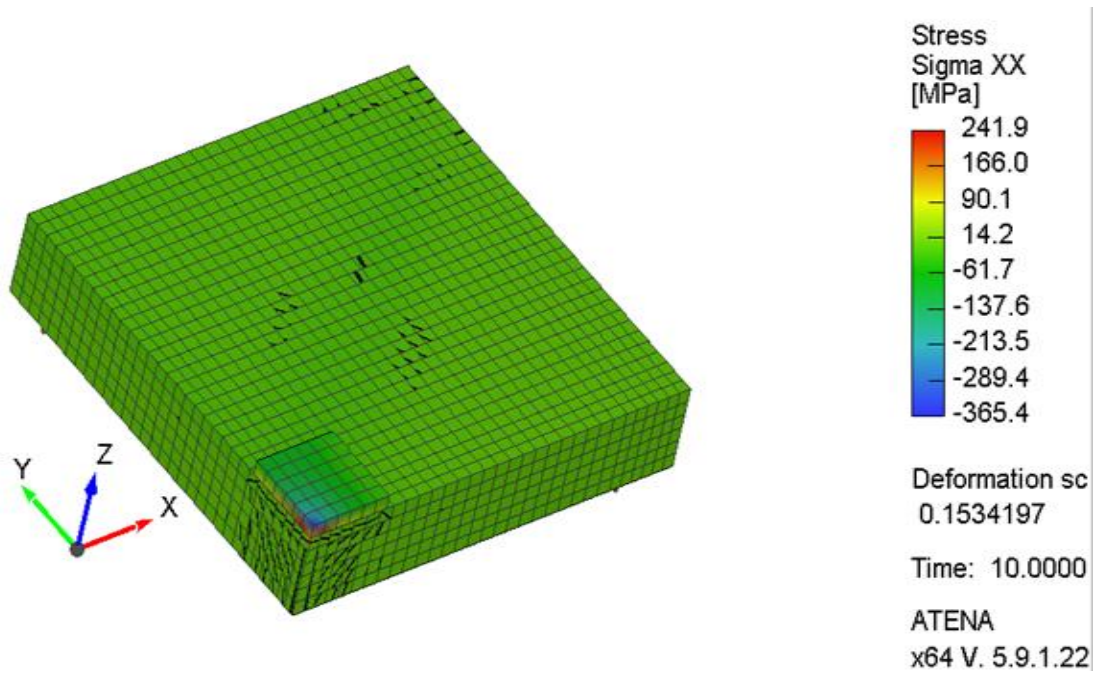


Figure 6.13-First Level Cracks

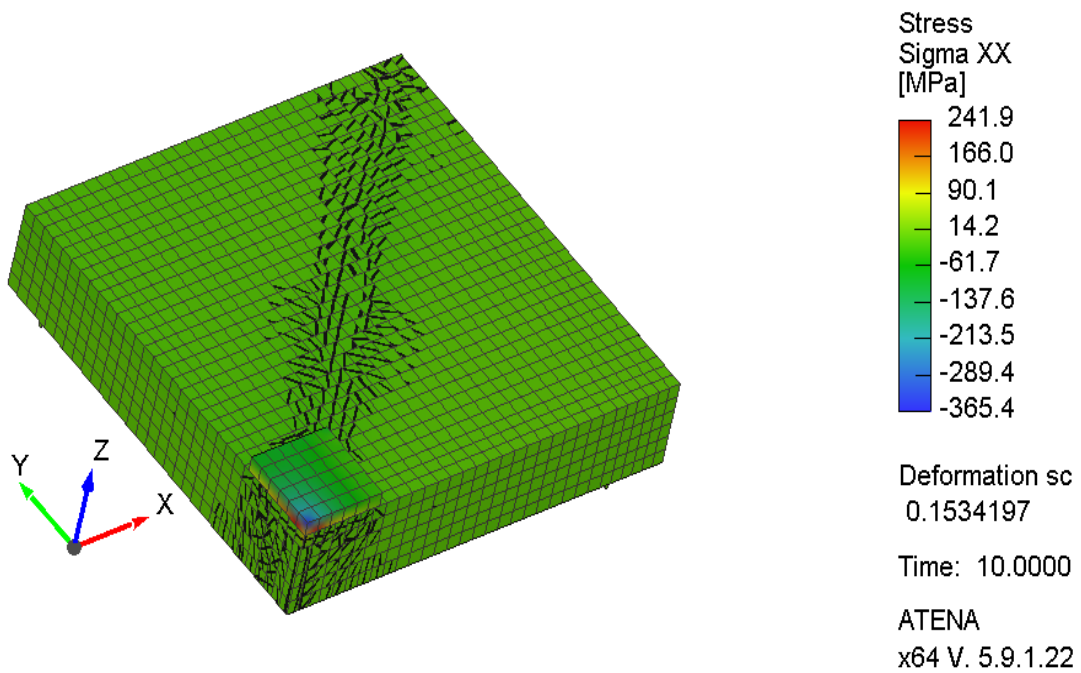


Figure 6.14-Second Level Cracks

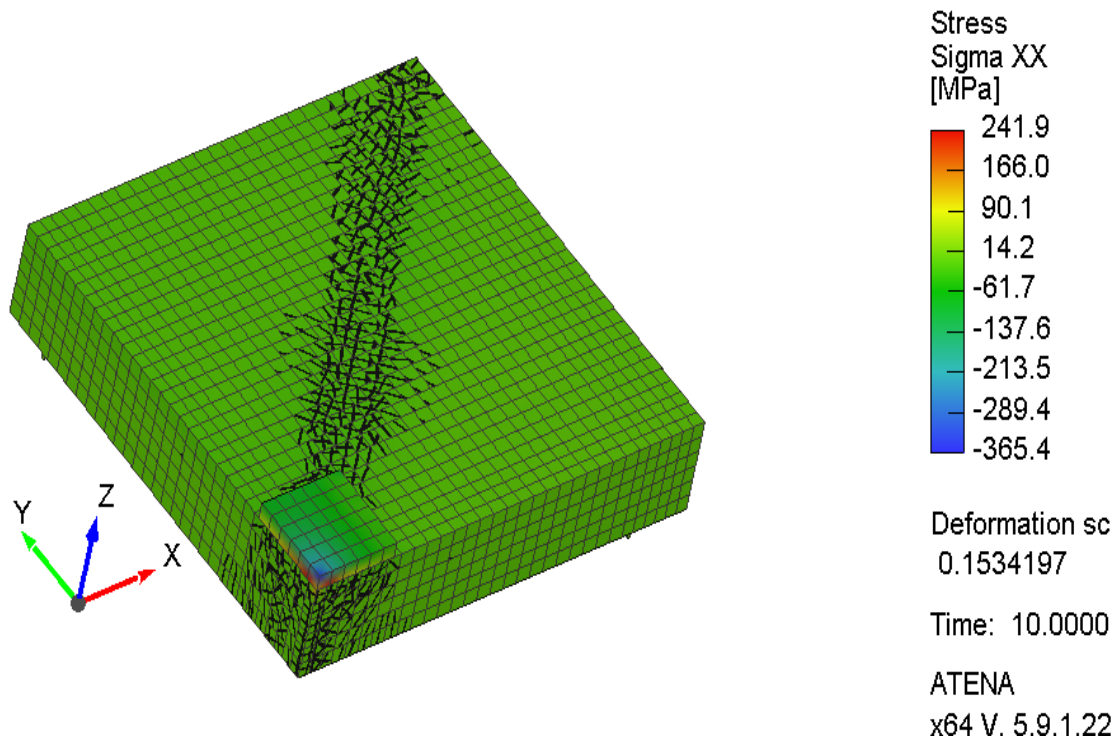


Figure 6.15-First Level Cracks

6.10. Slab LC-C

The LC-C Slab which had an elastic modulus of 28.2GPa at 28days and a fracture energy of 93N/mm alongside a concrete strength of 30.82MPa, had a maximum load of 140.82kN. This slab particularly required to a lower fracture energy compared to the normal concrete slab to produce a unit crack in the slab. While the cracks were more distributed towards the center and the edges of the slab. In addition, the failure patten of the yield line still governs for this slab. Figure 6.16, 6.17, 6.18, 6.19, 6.20, 6.21, 6.22, 6.23 and 6.24 shows the load vs displacement, stresses, strains, tensile strength, pattern of the failure, and the crack widths respectively.

6.10.1. Load vs Displacement Curve

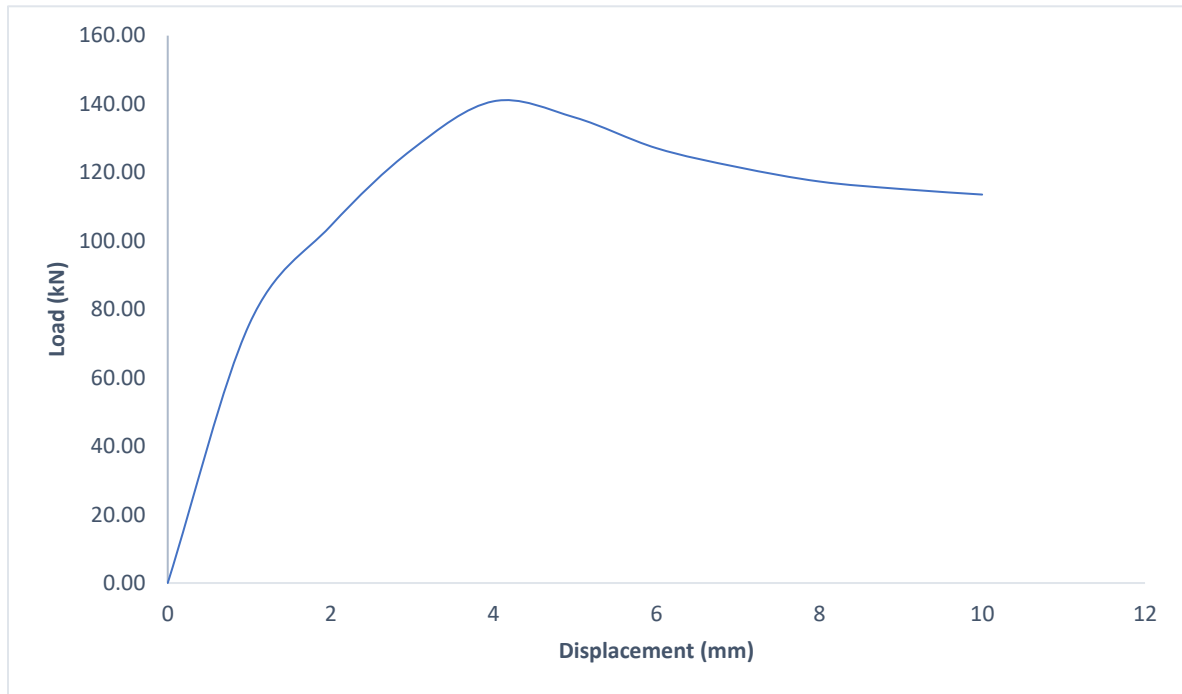
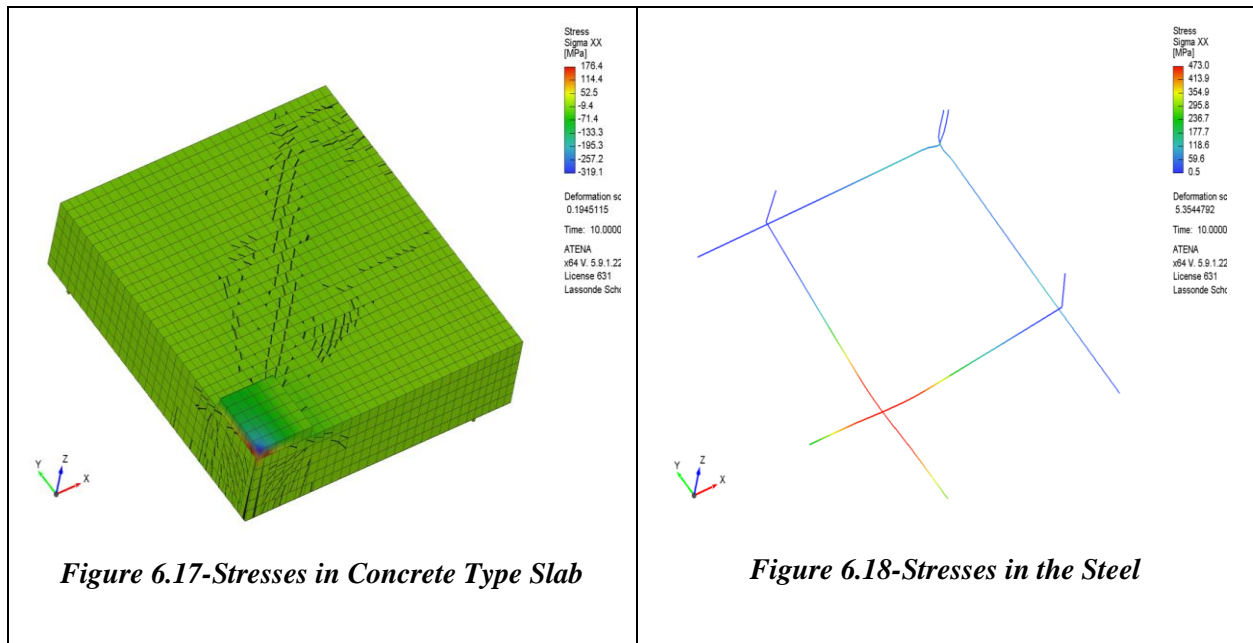
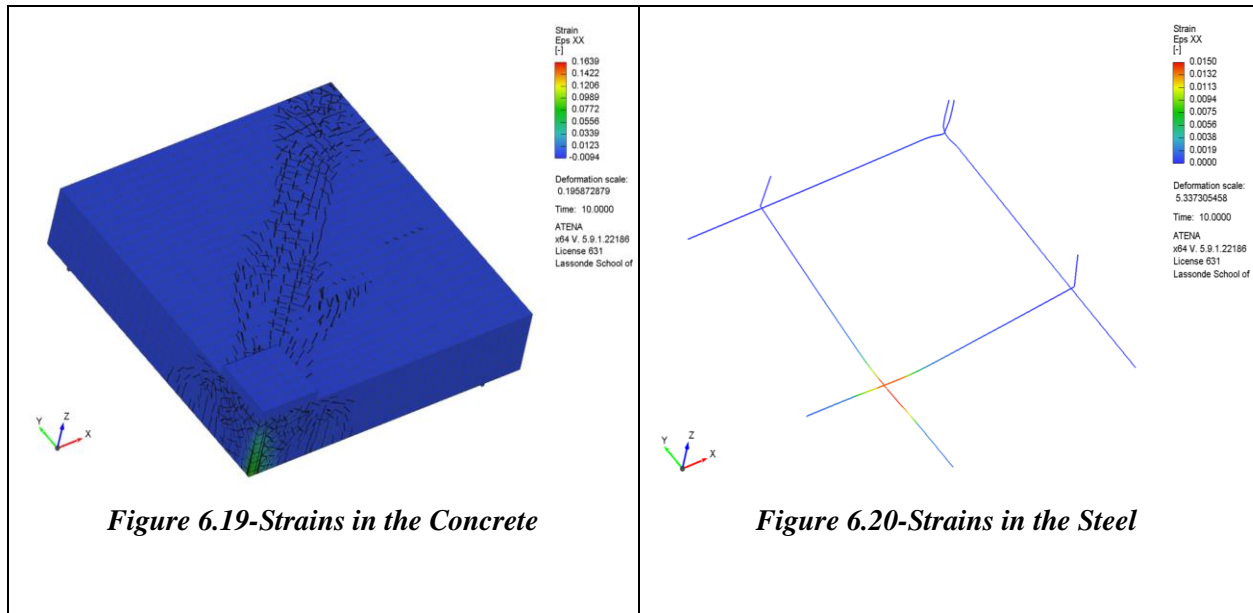


Figure 6.16-Load vs Displacement for the LC-C Concrete

6.10.2. Stresses



6.10.3. Strains



6.10.4. Tensile Strength

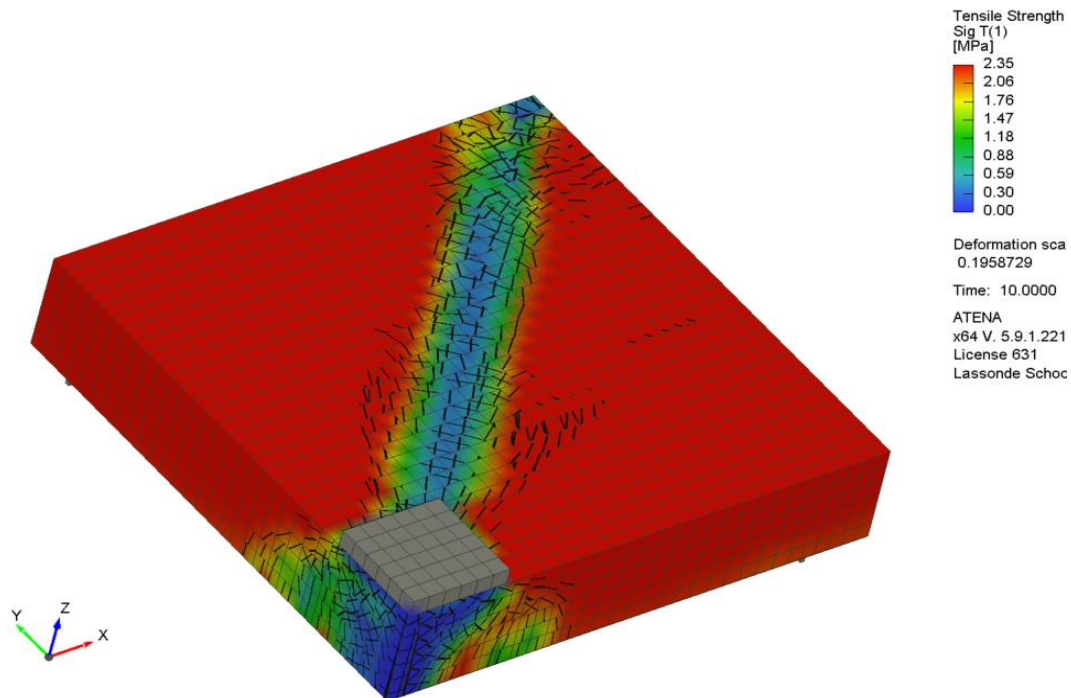


Figure 6.21-The Tensile Strength of the Reinforced Concrete Slab LC-CF

6.10.5. Crack Pattern & Modes of Failure

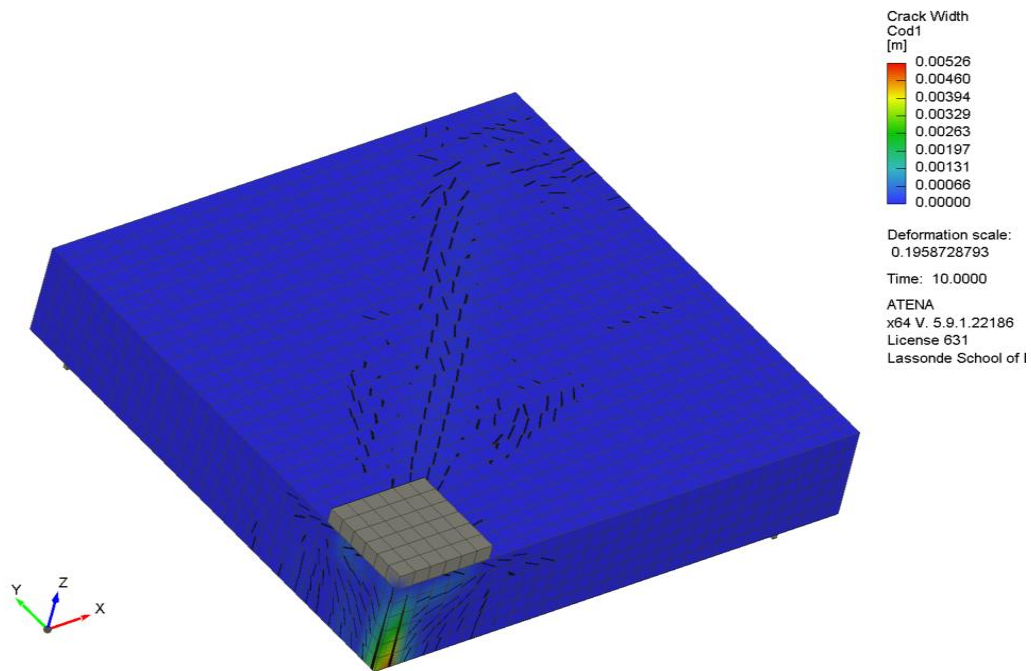


Figure 6.22-Level 1 Cracks

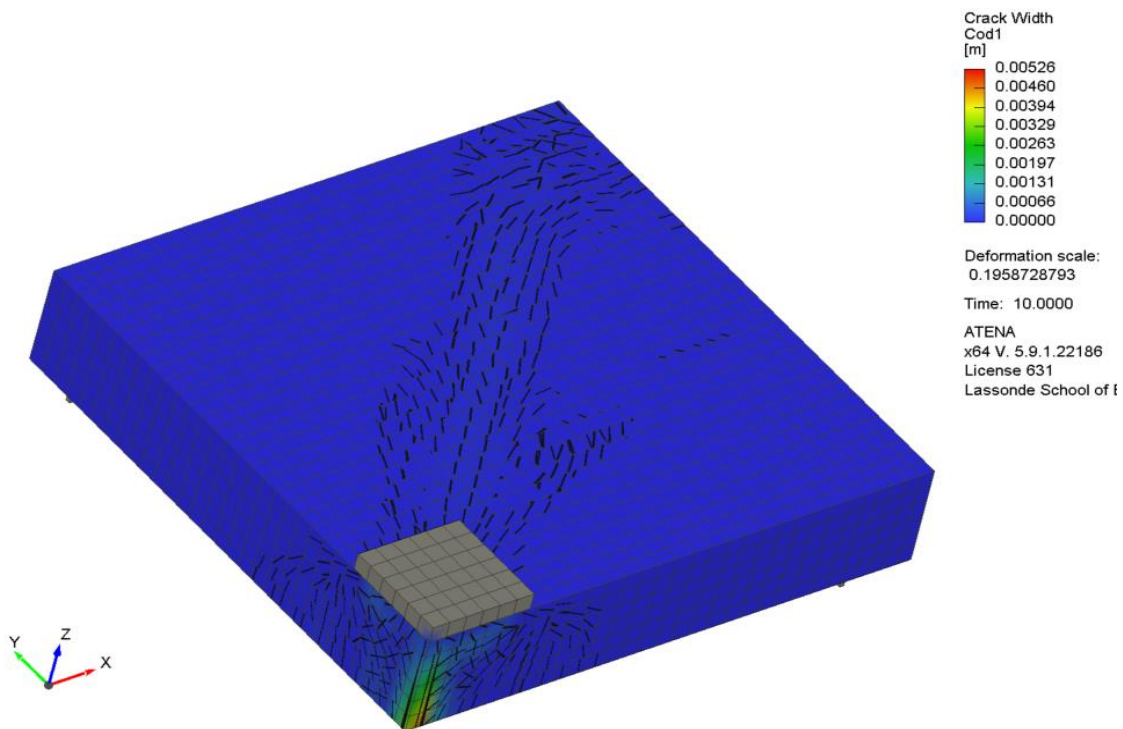


Figure 6.23-Level 2 Cracks

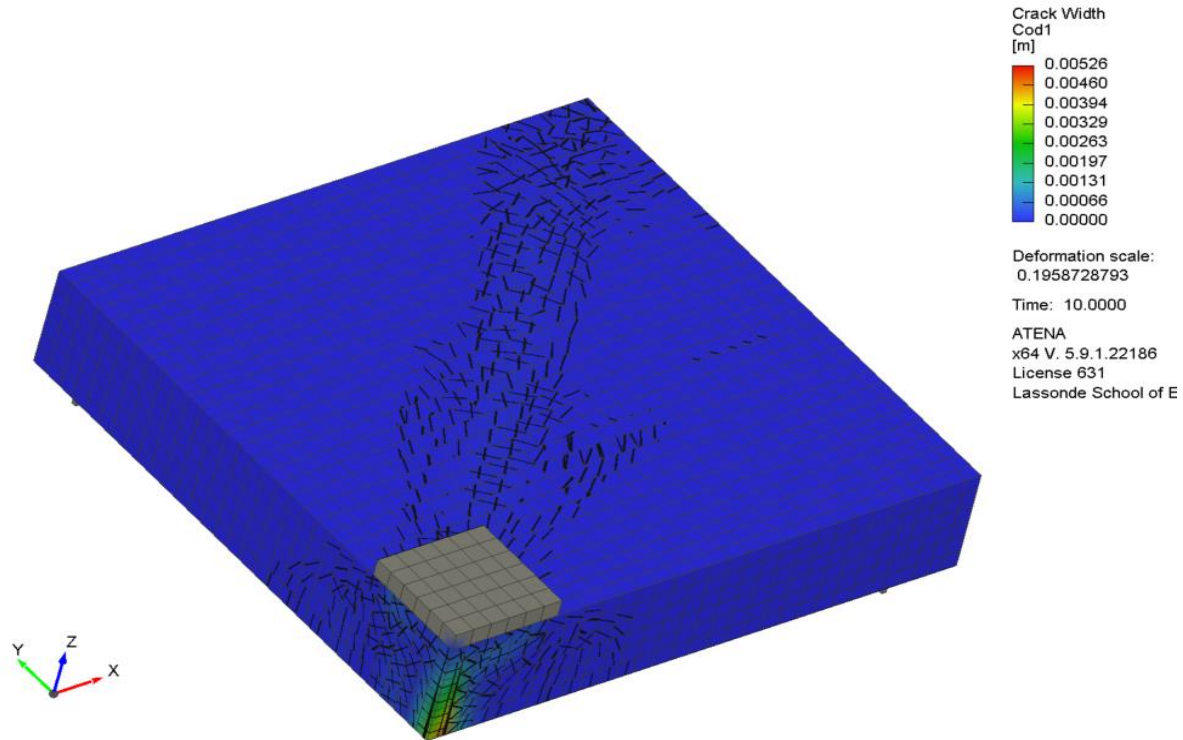


Figure 6.24-Level 3 Cracks

6.11. Slab LC-CF

This slab had a compressive strength of 31.72Mpa, and fracture energy of 136.09N/mm, as well as tensile strength of 2.35MPa and Figure 6.25, 6.26, 6.27, 6.28, 6.29, 6.30, 6.31, 6.32 and 6.33 shows the load vs displacement, stresses, strains, tensile strength, pattern of the failure, the cracking widths respectively.

6.11.1. Load vs Displacement Curve

Figure 6.25 below shows the load displacement curve for the LC-CF Slab. The peak displacement of the slab was 4mm and the maximum load was 134.56kN. This value obtained was higher than the control natural aggregate slab which had a displacement of 4mm and also the LC-CC which also had a peak displacement of 4mm respectively. This further illustrates that higher level of replacement and substitution with recycled materials led to greater peak displacement values of the FE model.

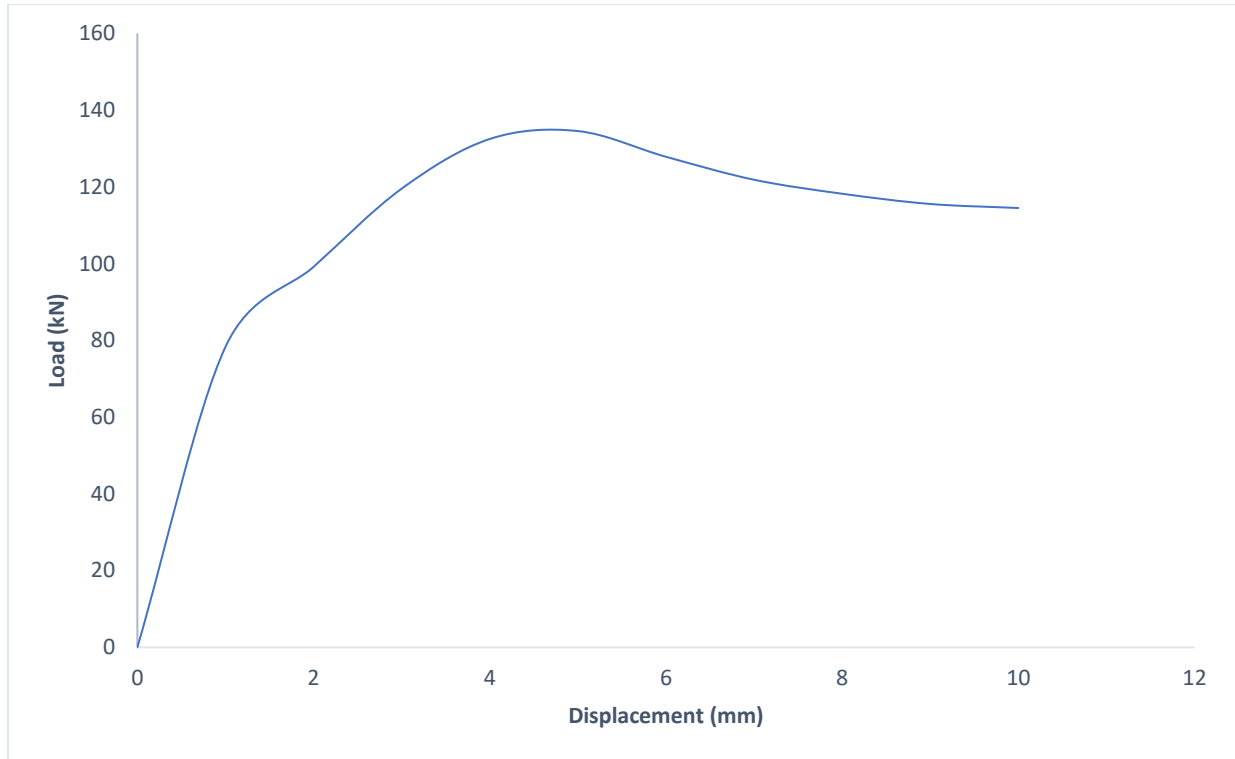
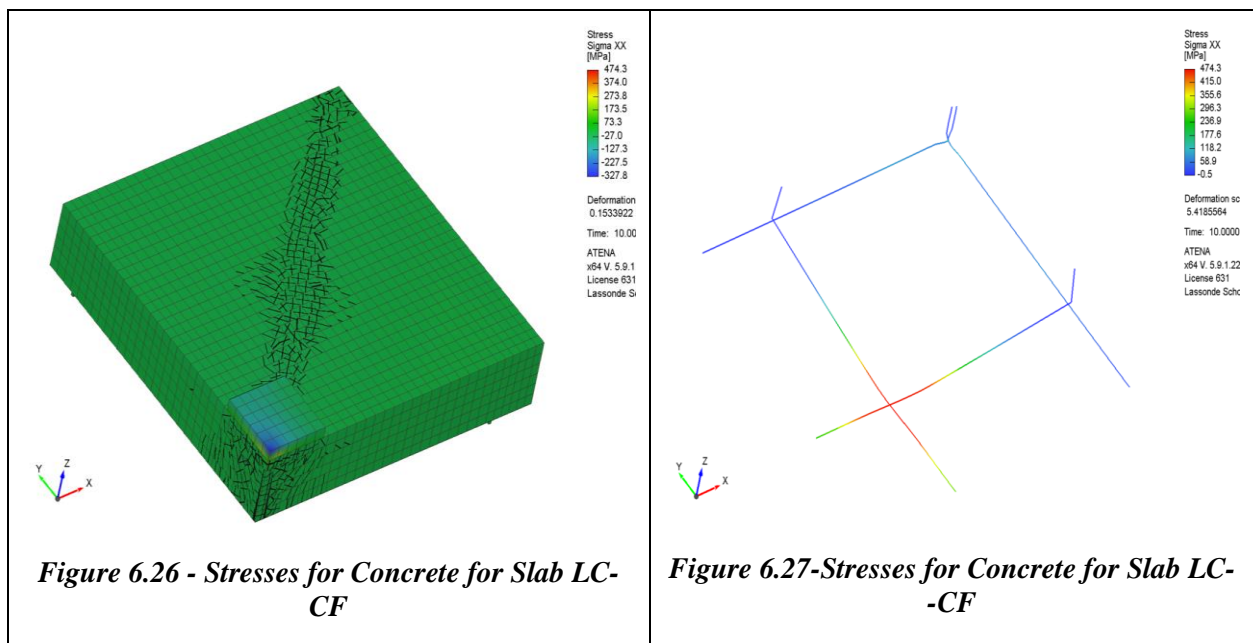
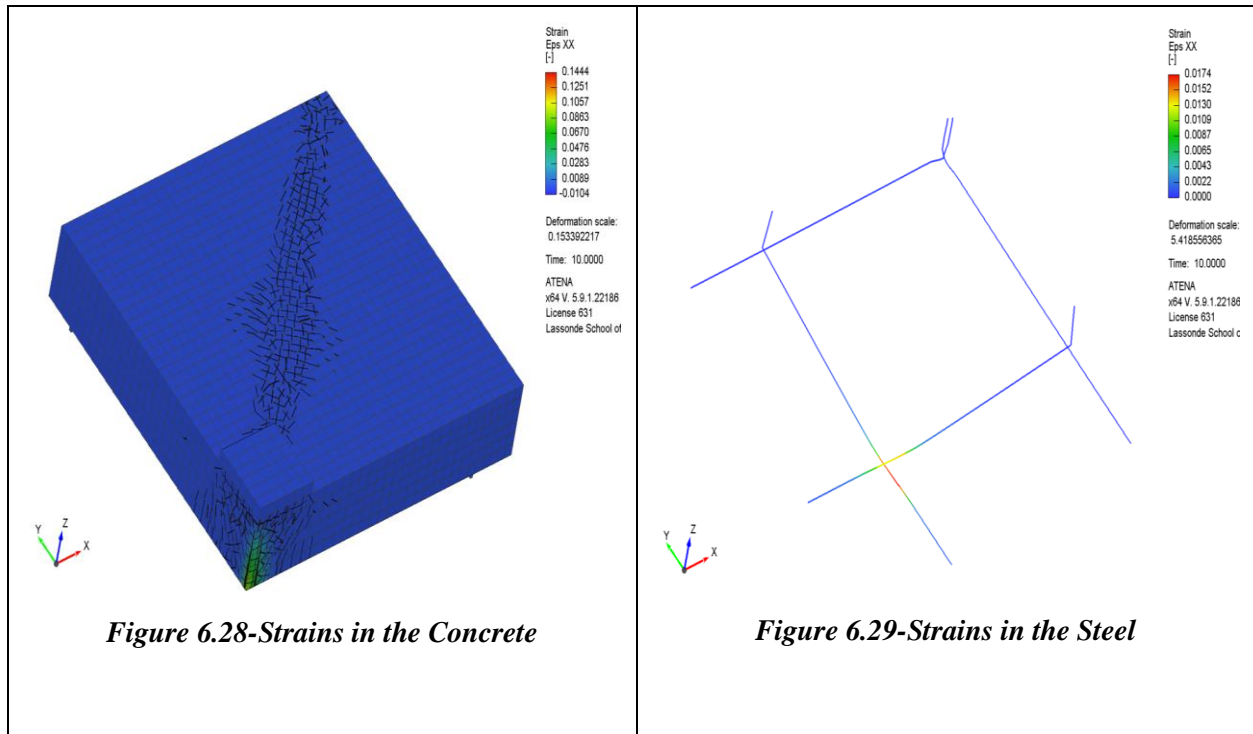


Figure 6.25-Load vs Displacement Curve for LC-CF

6.11.2. Stresses



6.11.3. Strains



6.11.4. Tensile Strength

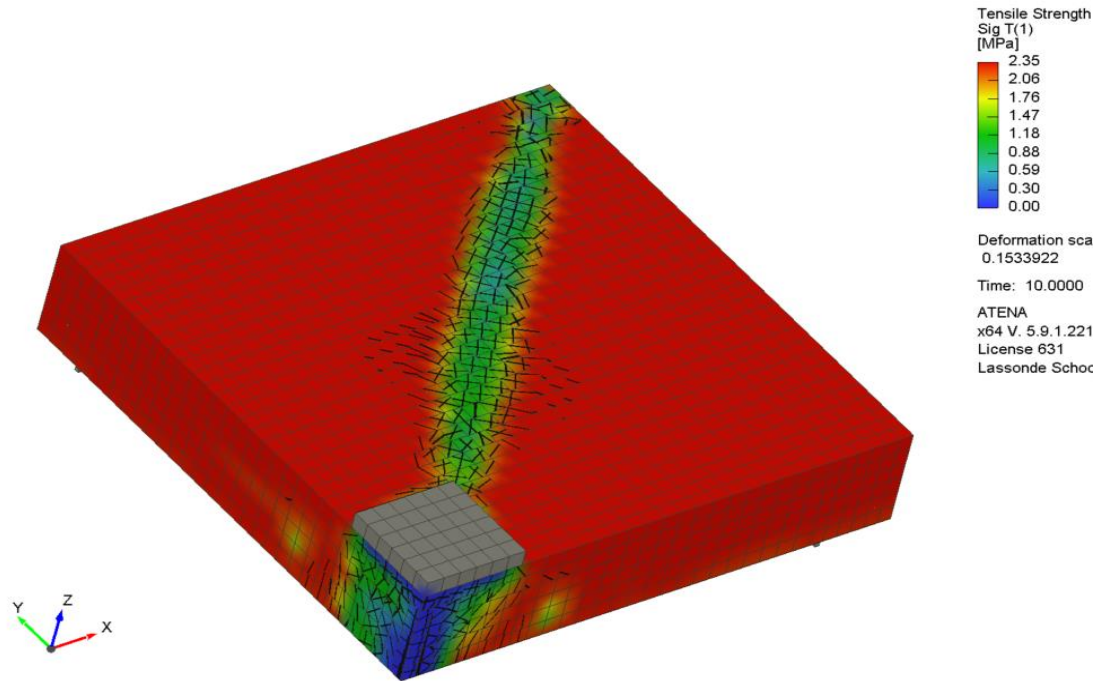


Figure 6.30-The Tensile Strength of the Reinforced Concrete Slab LC-CFS

6.11.5. Crack Patterns & Modes of Failure

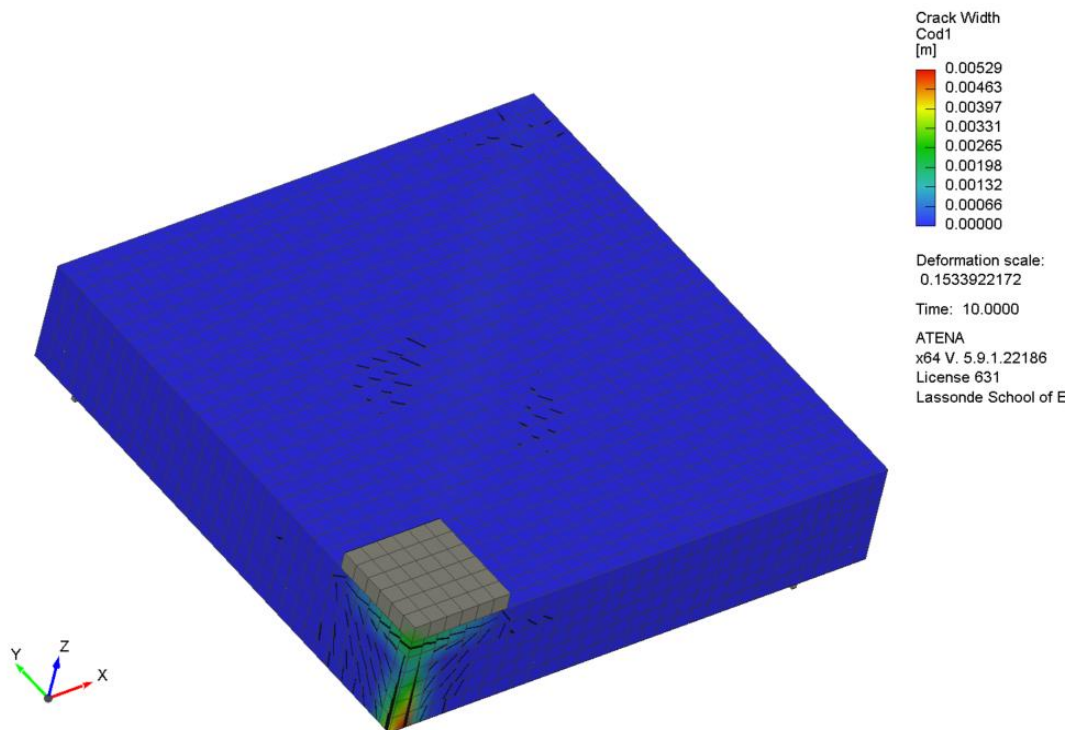


Figure 6.31-Level 1 Cracks

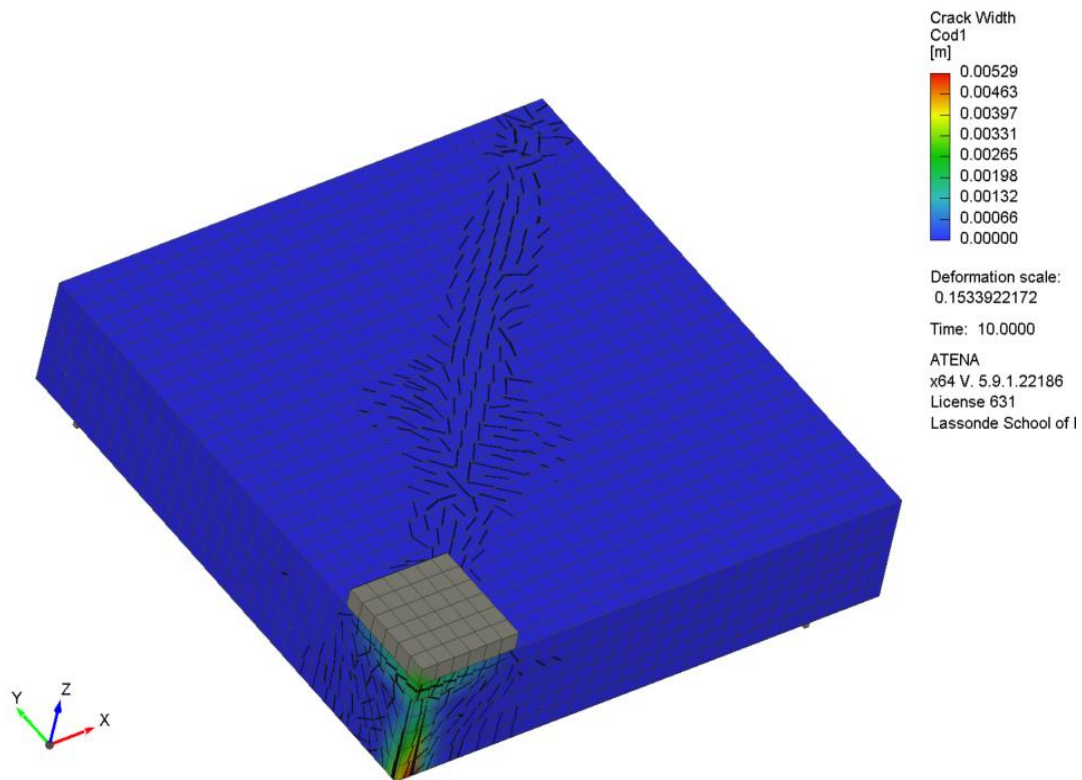


Figure 6.32- Level 2 Cracks

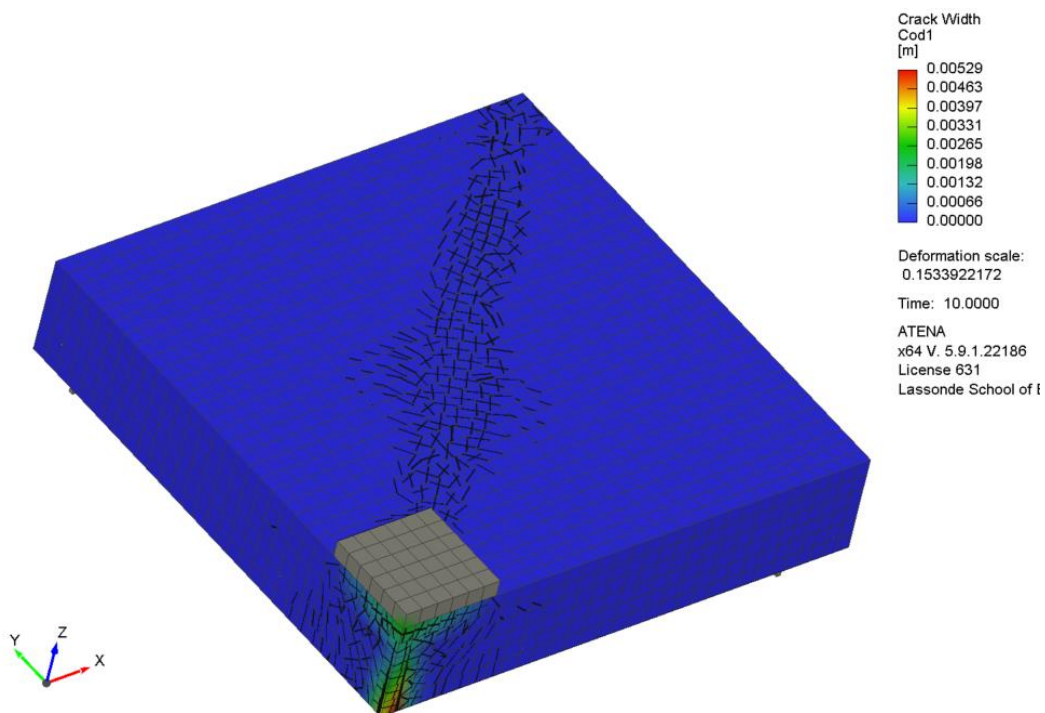


Figure 6.33-Level 3 Cracks

6.12. Slab LC-CFS

This slab had a compressive strength of 31.56Mpa, and fracture energy of 171.60N/mm, as well as tensile strength of 2.35MPa and Figure 6.34, 6.35, 6.36, 6.37, 6.38, 6.39, 6.40, 6.41 and 6.42 shows the load vs displacement, stresses, strains, tensile strength, pattern of the failure, the cracking widths respectively.

6.12.1. Load vs Displacement Curve

The figure 6.34 below shows the load displacement curve for the LCC-CFS Slab. The peak displacement of the slab was 5mm and the maximum load was 133.08kN. This value obtained was higher than the control natural aggregate slab which had a peak displacement of 4mm and also the LC-CF.

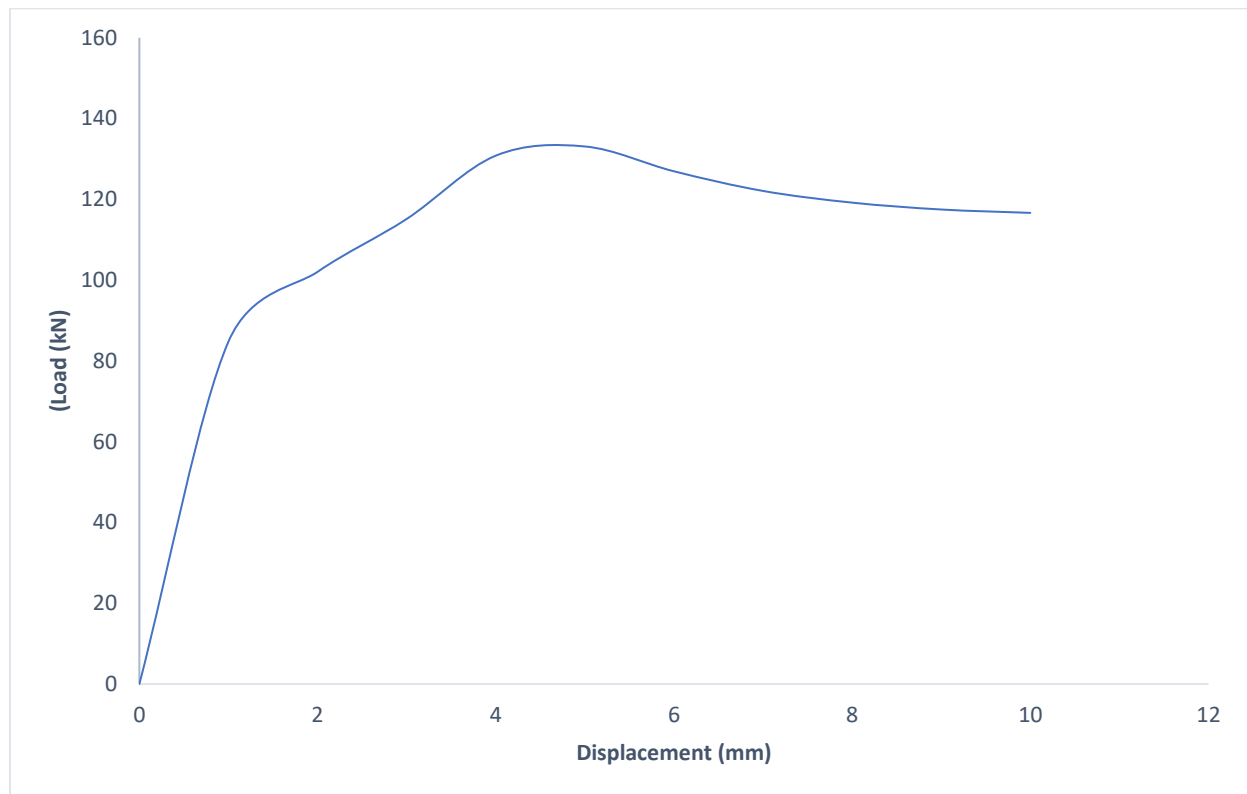
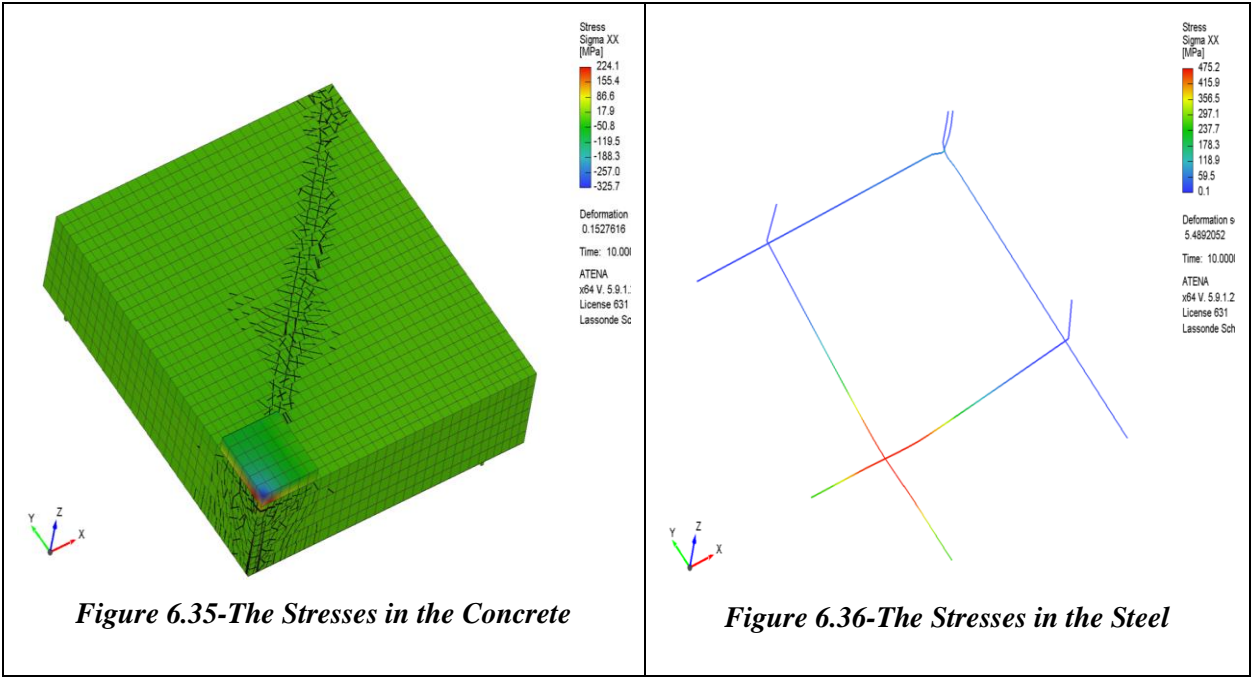
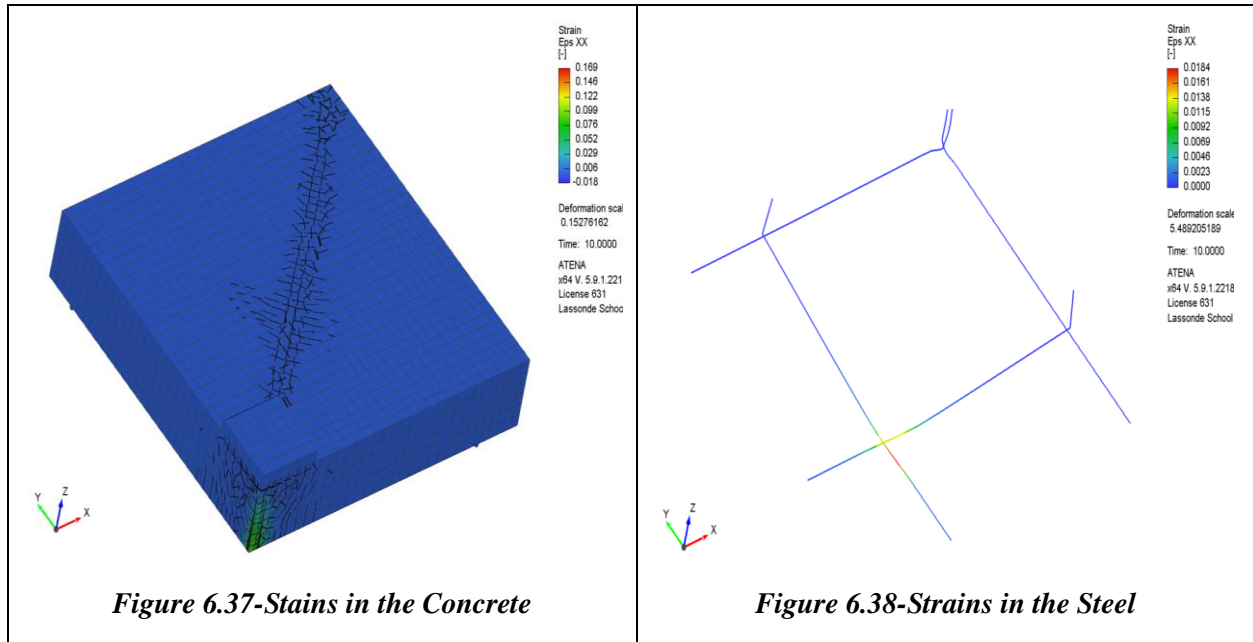


Figure 6.34-Load vs Displacement Curve

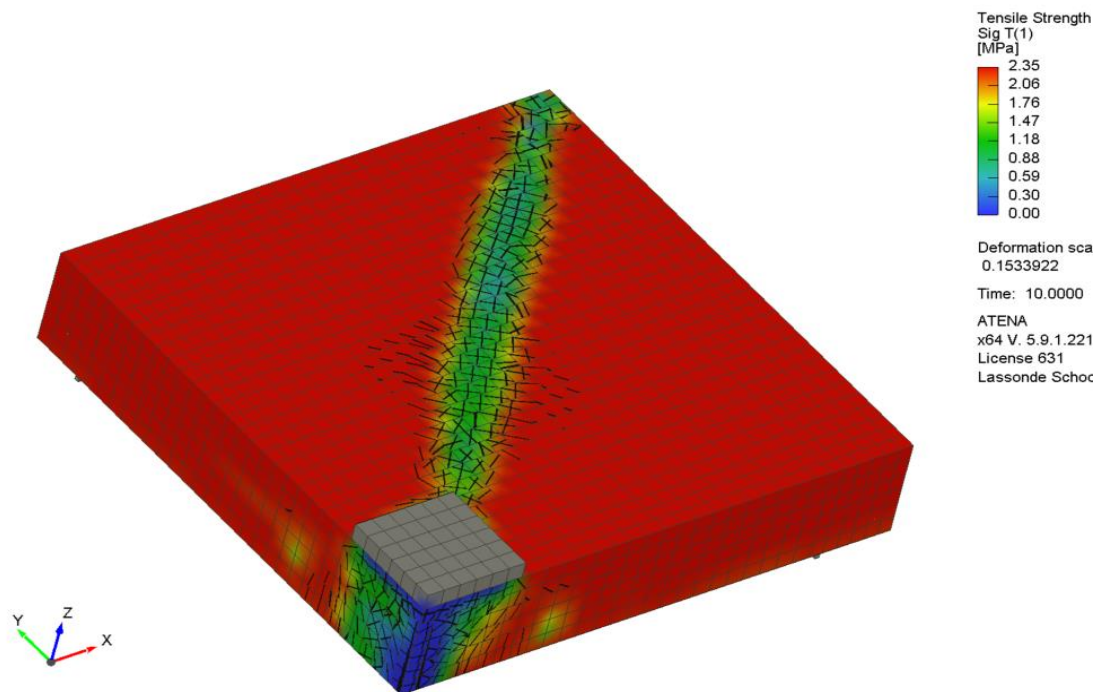
6.12.2. Stresses



6.12.3. Strains



6.12.4. Tensile Strength



6.12.5. Crack Patterns & Modes of Failure

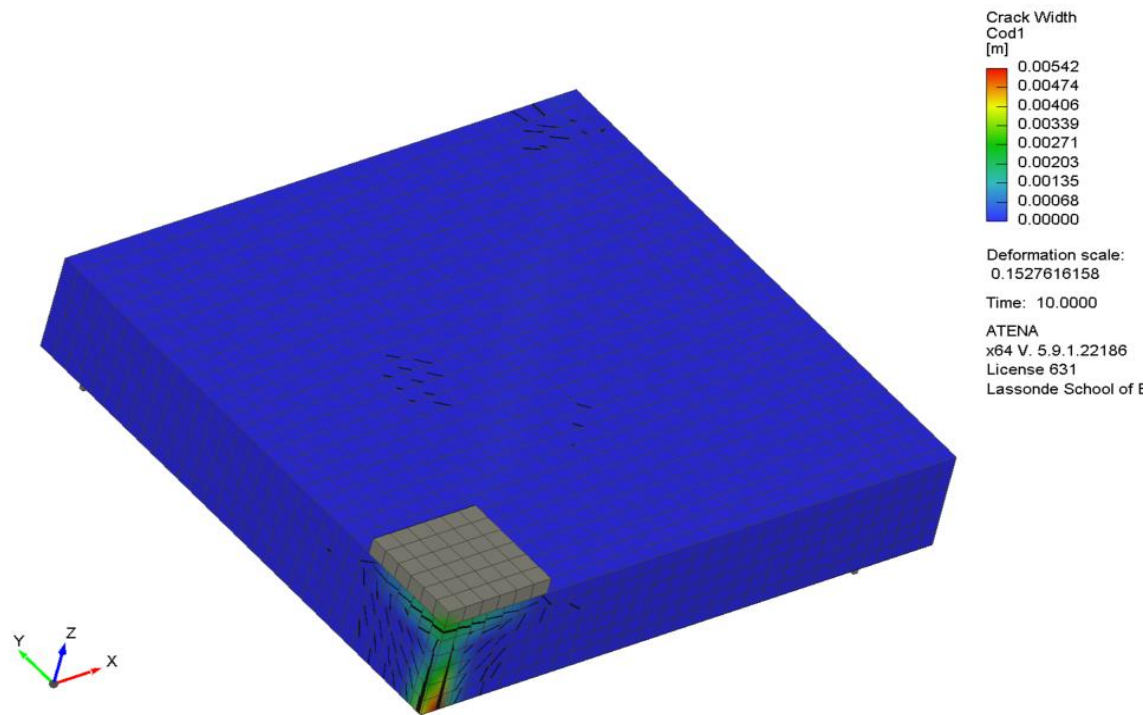


Figure 6.40-Level 1 Cracks

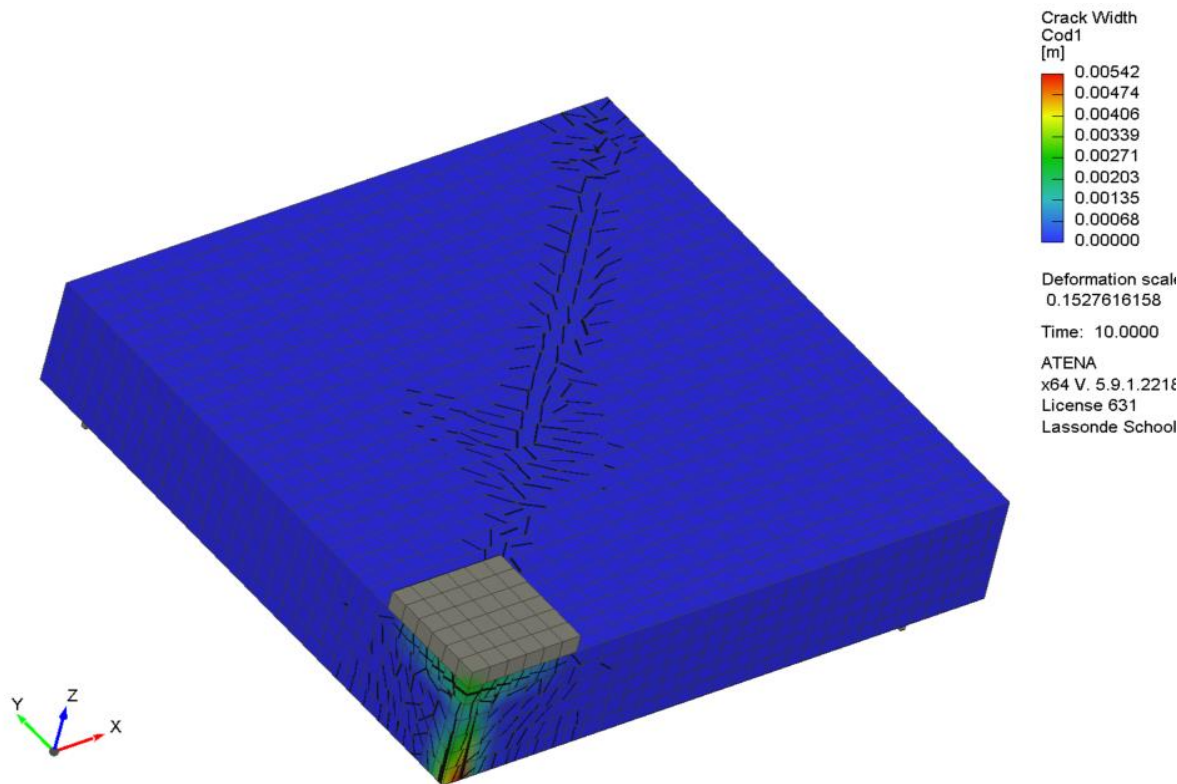


Figure 6.41-Level 2 Cracks

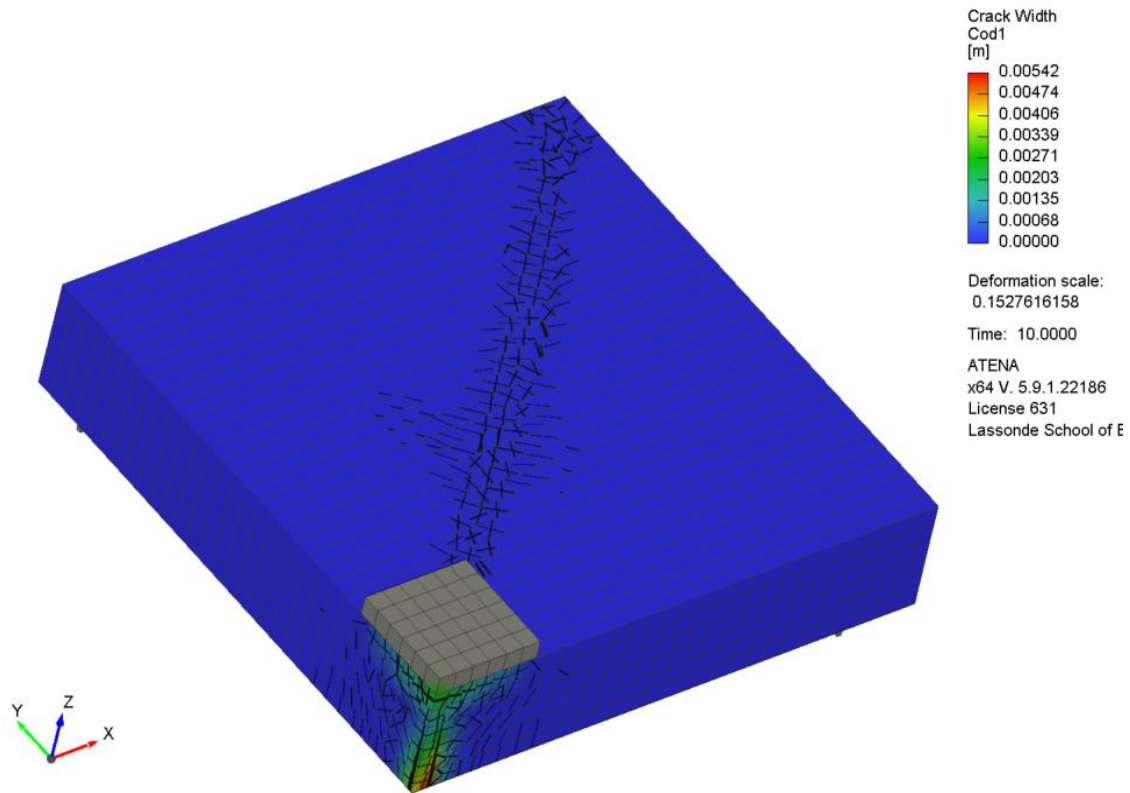


Figure 6.42-Level 3 Cracks

6.13. Summary of the FE Results

6.13.1. Maximum Load

Table 6.4 below shows the details of the maximum load obtained for the different slab and the percentage increase and decrease respectively. The control normal aggregate slab had the highest load of 147.52kN, and as the percentage of replacement content by weight increased, and the elastic modulus decreased, the maximum load was found to be decreasing. The minimum load was 133.10kN.

Table 6.4-Maximum Load Obtained

Slab ID	Maximum Load (kN)
NC	147.52
LC-C	140.82
LC-CF	134.60
LC-CFS	133.10

6.13.2. Peak Displacement of the Slabs

The peak displacement of the RC slab NC, LC-C, LC-CF, and LC-CFS is shown in the table 6.5 below.

Table 6.5-Peak Displacements

Slab ID	Peak Displacement (mm)
NC	4
LC-C	4
LC-CF	5
LC-CFS	5

6.13.3. Crack Width of the Slabs

The information on the maximum crack and comparison with the control natural aggregate slab widths and the different low-carbon concrete slab is presented below in table 6.6. Information from the table shows that the percentage difference was closer for the LC-CFS RC slab with 2% difference.

Table 6.6-FE Maximum Crack Width

Slab ID	Crack Width (mm)	Percentage Difference (%)
NC	5.53	Control
LC-C	5.26	5.00
LC-CF	5.29	4.43
LC-CFS	5.42	2.00

6.13.4. Percentage Decrease of the Slab Capacity

The information on the slab load capacity and the percentage increase and decrease is tabulated in the table 6.7 below. Information from the table shows that the LC-C slab had a load decrease of 4.6% when it was compared with the control slab, the LC-CF showed a decrease of 8.8% and finally, the LC-CFS slab showed the maximum load decrease of 9.8%. In general, load decrease was found to be within a range of approximately 10%.

Table 6.7-Percentage Decrease of the Slab Capacity

Slab ID	Slab	Percentage Decrease (%)
NC	147.52	Control
LC-C	140.82	4.55
LC-CF	134.60	8.76
LC-CFS	133.10	9.78

7. CHAPTER SEVEN: SECTIONAL ANALYSIS AND CODE COMPARISON

7.1. Section Analysis with the Use of Response-2000-Background

In the use of Response-2000 for sectional analysis of the slab, the analyses of the four different slabs were based on the modified compression field theory (MCFT), which is a program founded by Benz (2000)[142]. The assumptions for the MCFT includes uniform distribution of reinforcement within the element, application of load in a uniform pattern, existence of perfect bond between the concrete and the reinforcement, distribution of cracks, and that the principal stress and strains are coincident (Vecchio & De Lorenzi, 2009)[143]. In addition, the MCFT is based on compatibility conditions, considering the average values of strains; equilibrium conditions which considers the average value of stresses in the reinforcement and concrete; and the constitutive relations, which relate the average values of stress to strain. The purpose of utilizing Response-2000 was to be able to obtain the maximum moment of resistance of the slab that would lead to the maximum slab capacity. In view of the forementioned, the upper bound capacity of the slabs was obtained for the four different slabs which is presented in subsequent section of this chapter.

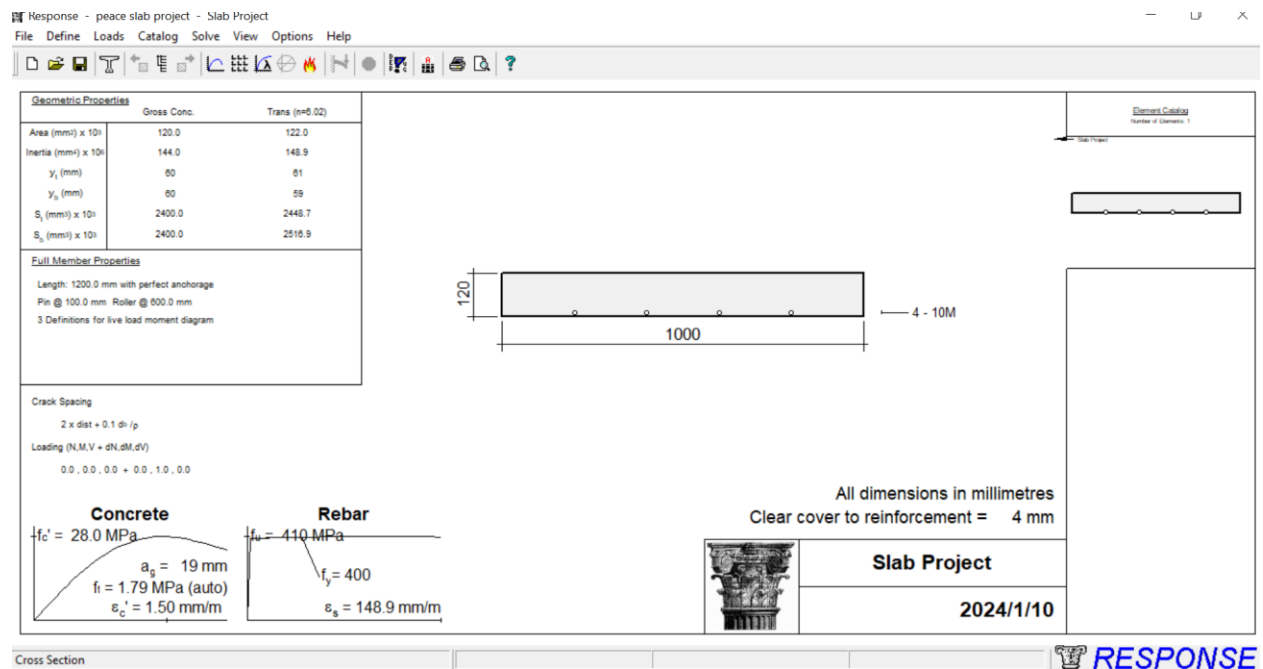


Figure 7.1-Section Geometric Properties

7.1.1. Material Properties, Full Member Properties, Material Reduction Factors

Definition of Section Properties for the members which included the per meter width of the slab, the boundary conditions and restraints, the material reduction factors and the concrete strength, the modulus of elasticity of the embedded steel and the dimensions of the member. Specifically for the purpose of the Response-2000 analysis, the material resistance factors for the steel and the concrete were taken as 1. The steel strength was generally taken as 400MPa and width of the section 1000mm and depth taken as 120mm. Specifically, 640mm of the full span was analysed. Table 7.1 to 7.16 shows the data obtained from the Response-2000 analysis and figure 7.1 to 7.63 shows the graphical representation of the section analysis and the member analysis showing the general plots, cracking widths and information, reinforcement plots, no shear plot, deformation and rotation, moment, and shear, as well as stiffness and axial plots obtained from Response-2000.

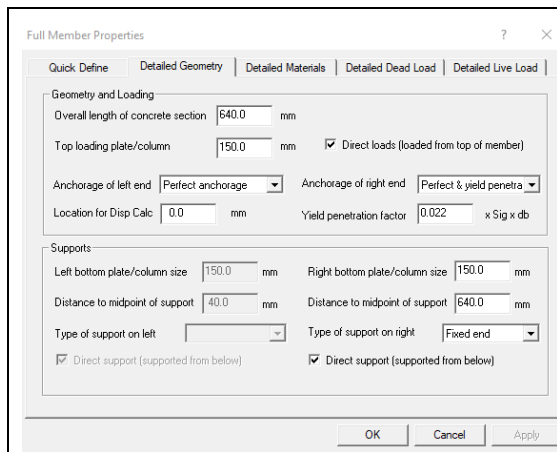


Figure 7.2-Full Member Properties

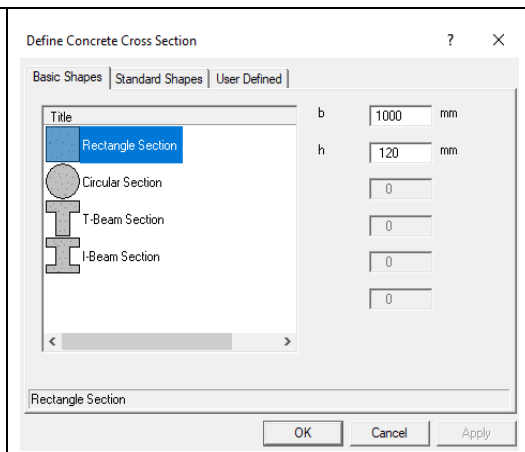


Figure 7.3-Cross-Section Properties

7.1.2. Analysis of the Slab Section NC

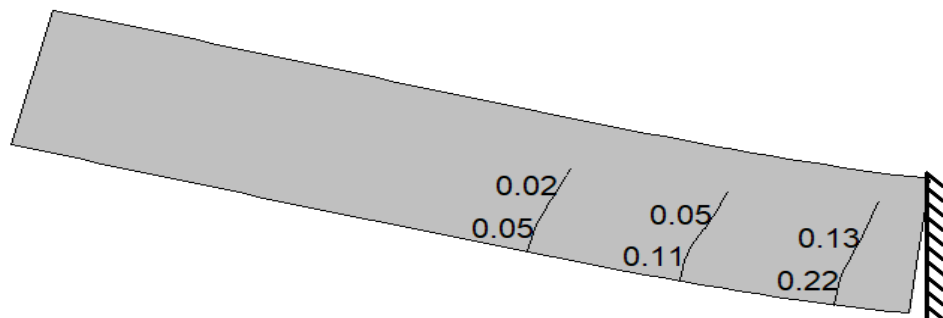


Figure 7.4-Slab Crack Pattern

7.1.2.1. Response-2000: General Plots

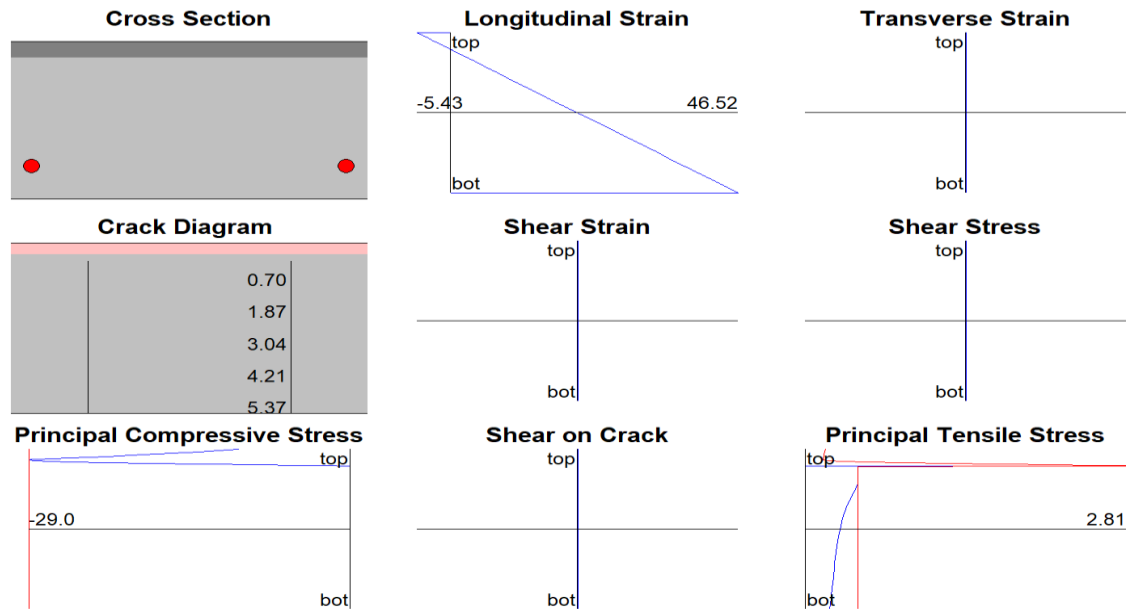


Figure 7.5-Reinforcing Steel Results

7.1.2.2. Response-2000: Cracking Information and Plots

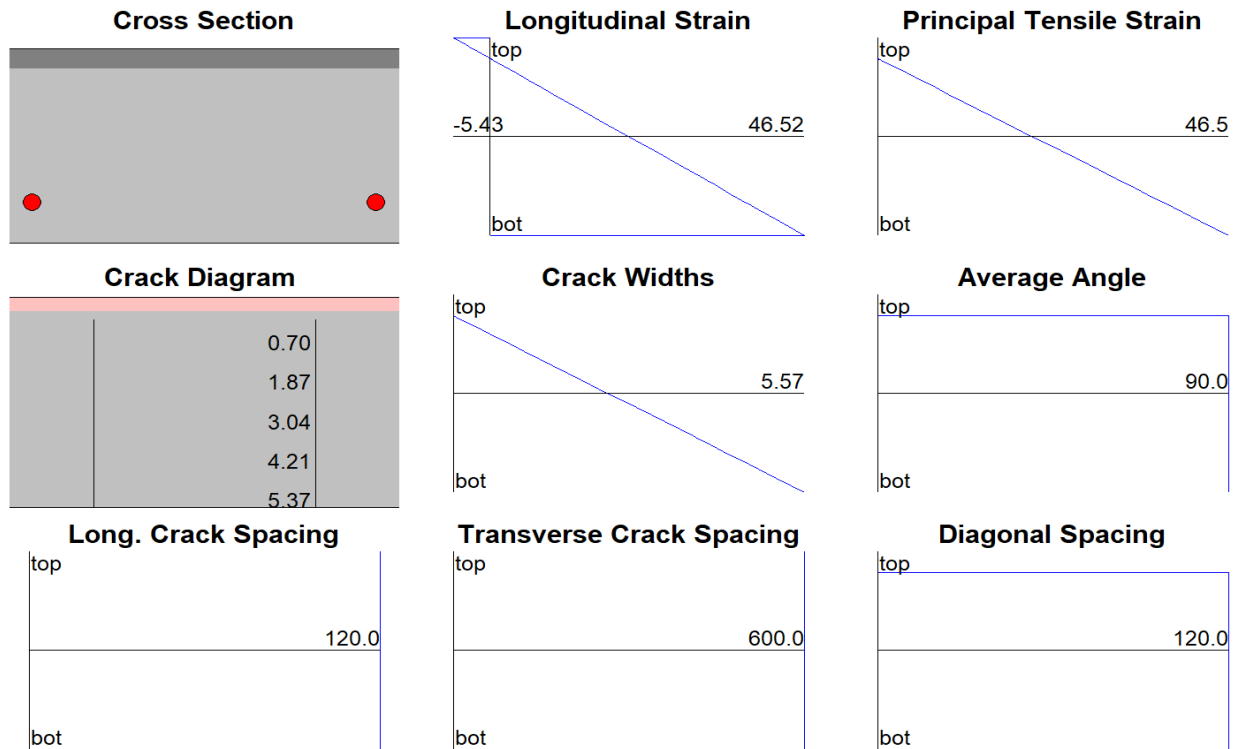


Figure 7.6-Member Crack Data, Max=5.56mm

7.1.2.3. Response-2000: Reinforcement Plots

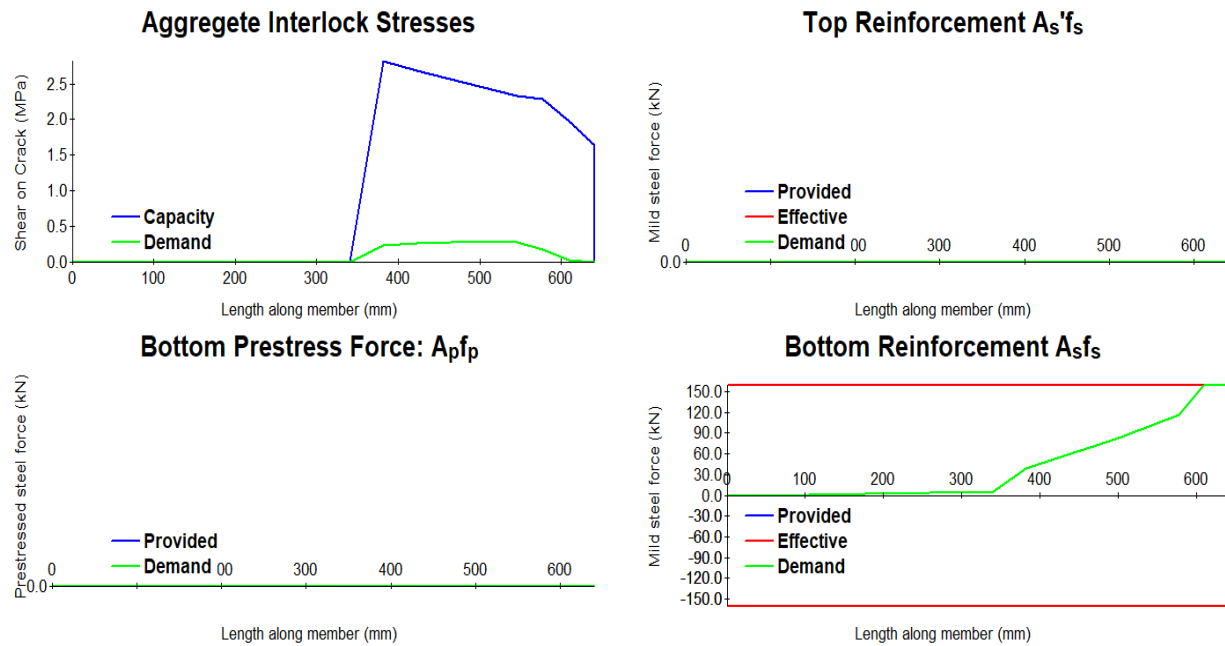


Figure 7.7-Bottom Reinforcing Details

7.1.2.4. Response-2000: No Shear Plots

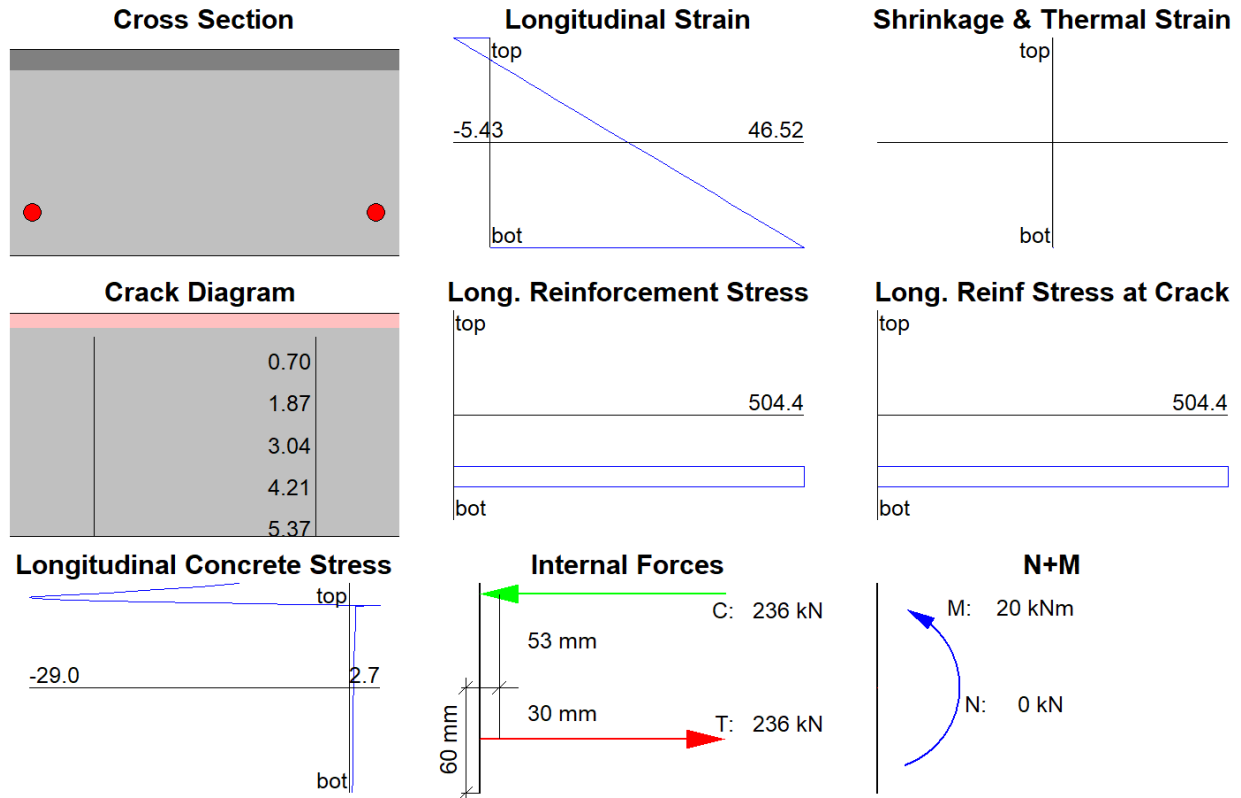


Figure 7.8-Concrete & Steel Stresses

7.1.2.5. Response-2000: Deformation & Rotation Plots

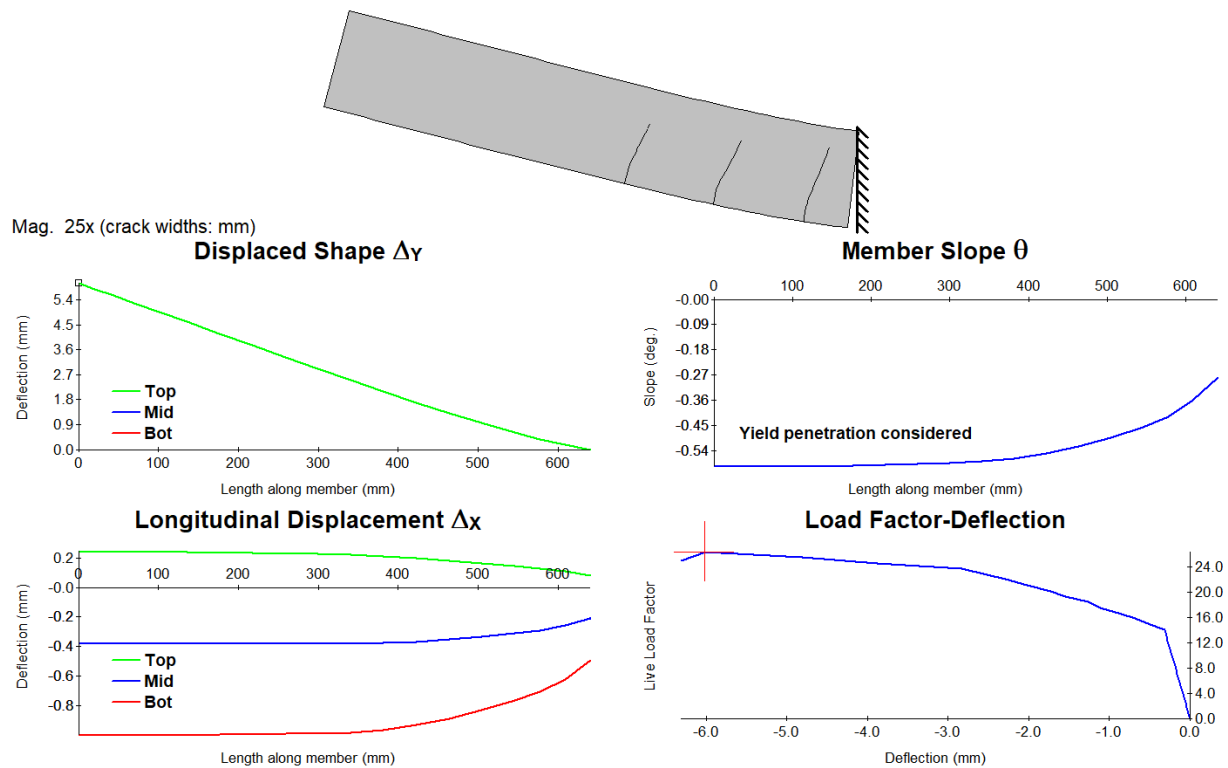


Figure 7.9-The Displacement of the Section, Max=6.37mm

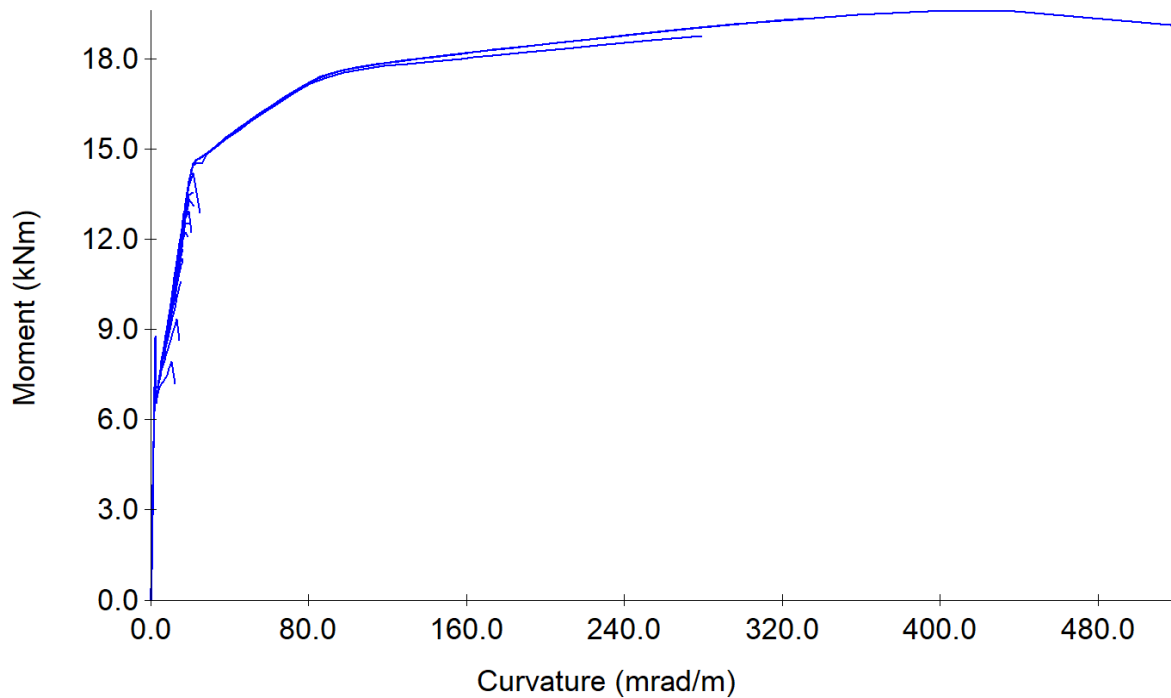


Figure 7.10-Moment vs Curvature, Max=19.09kNm & 521.36mrad/m

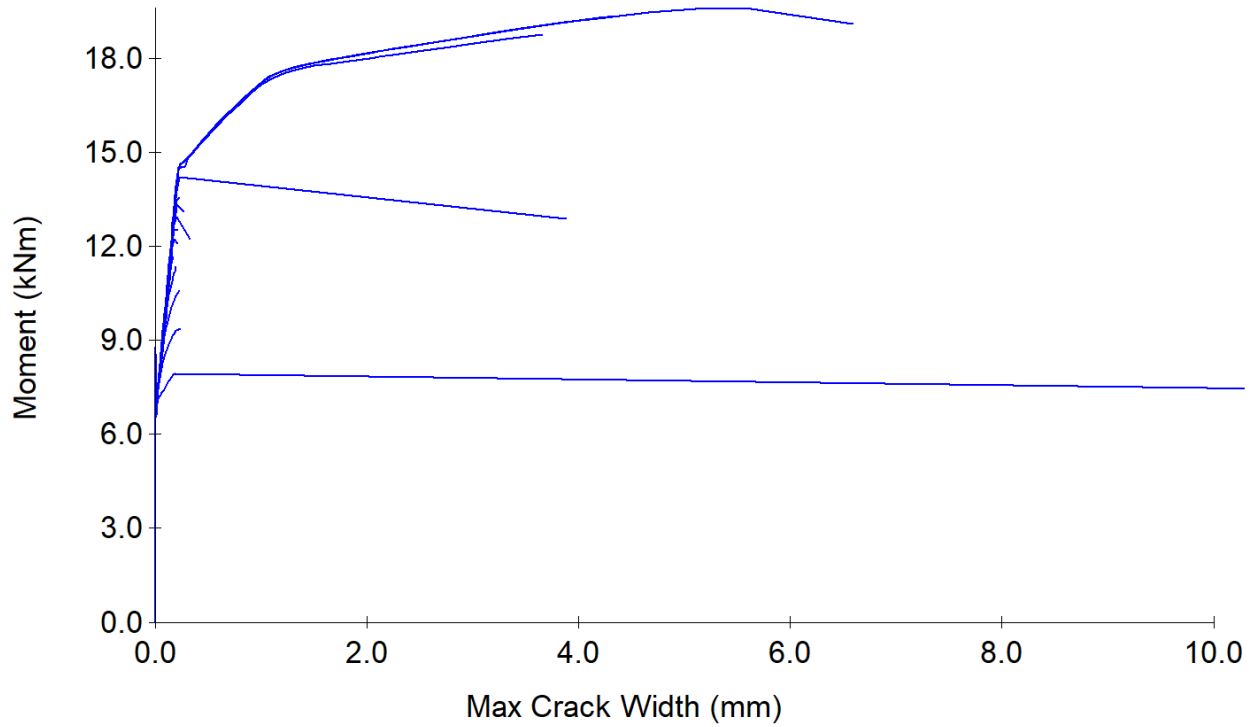


Figure 7.11-Moment vs Maximum Cracking Width, Max=6.58mm

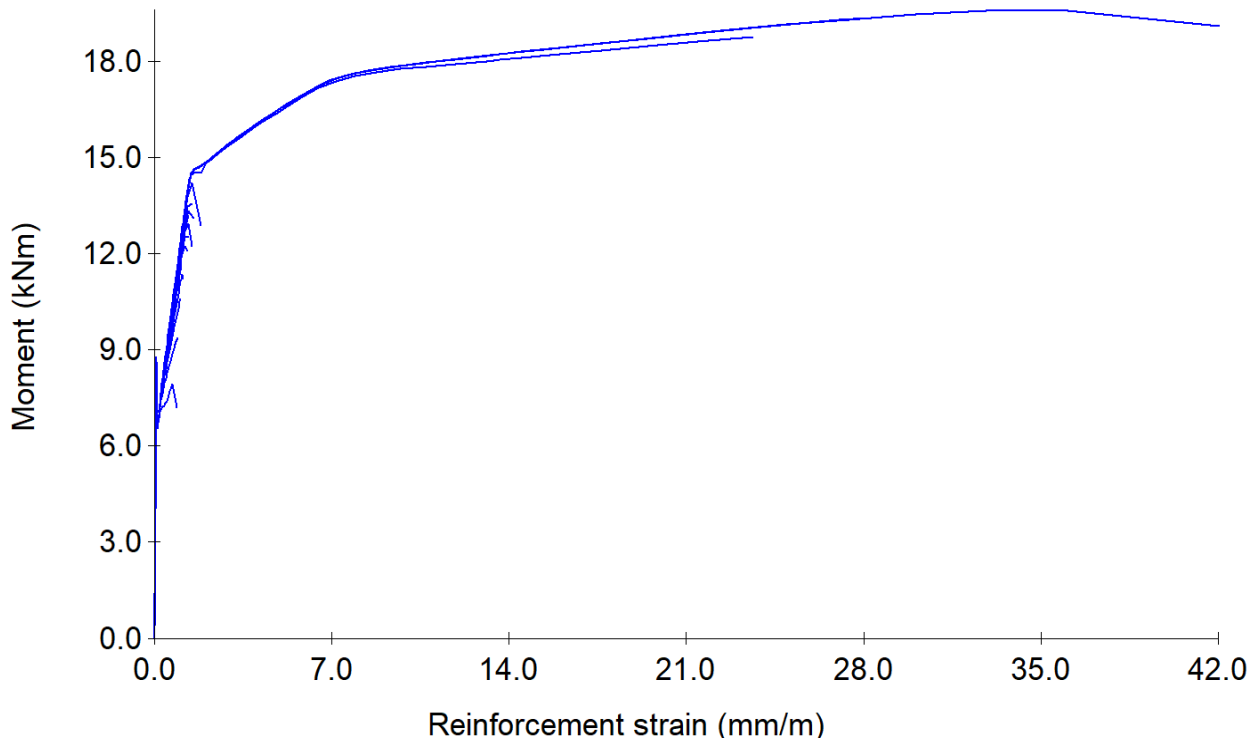


Figure 7.12-Moment vs Reinforcement Strain, Max=42mm/m

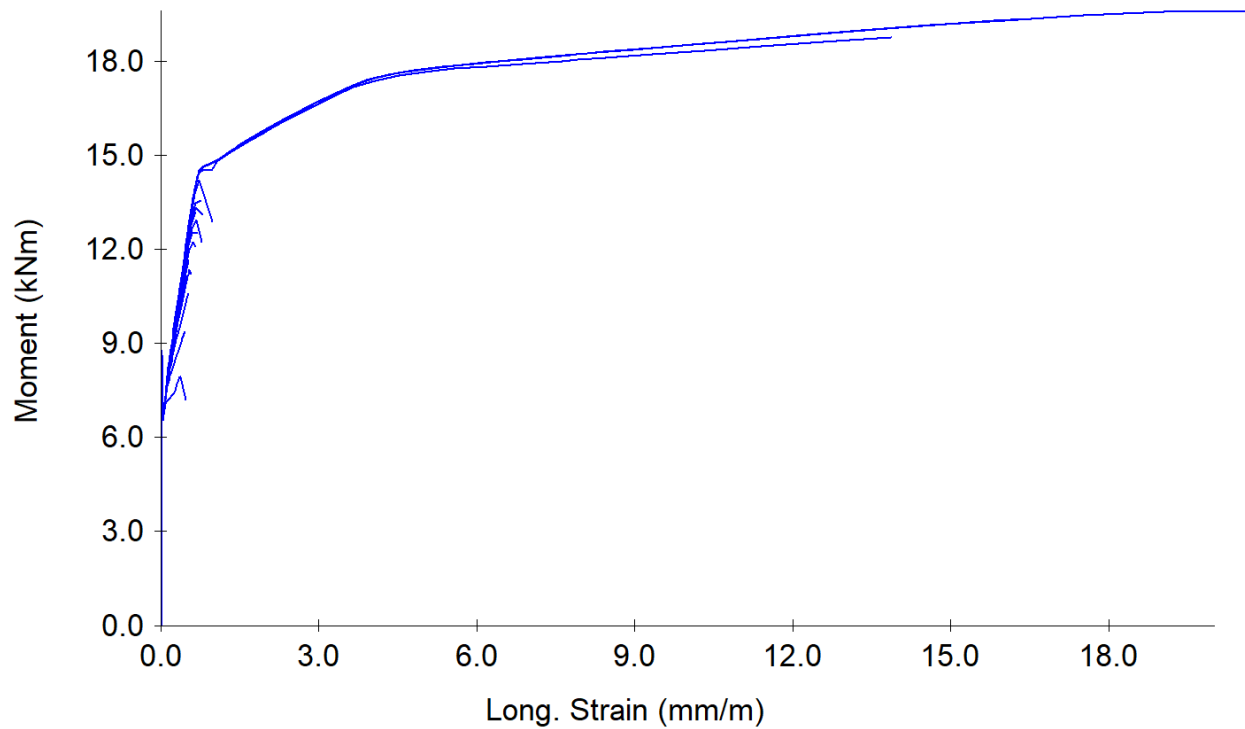


Figure 7.13-Moment vs Longitudinal Strain, Max=23.76mm/m

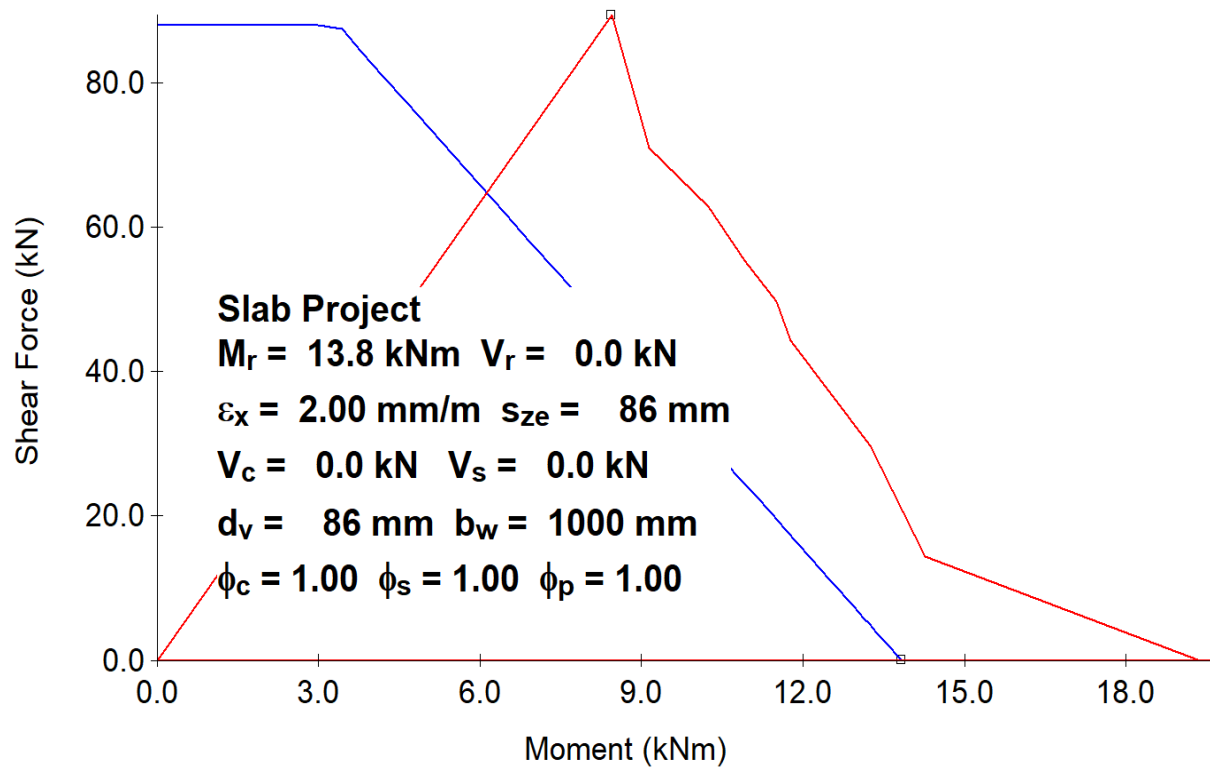


Figure 7.14-CSA 2014 M-V Interaction

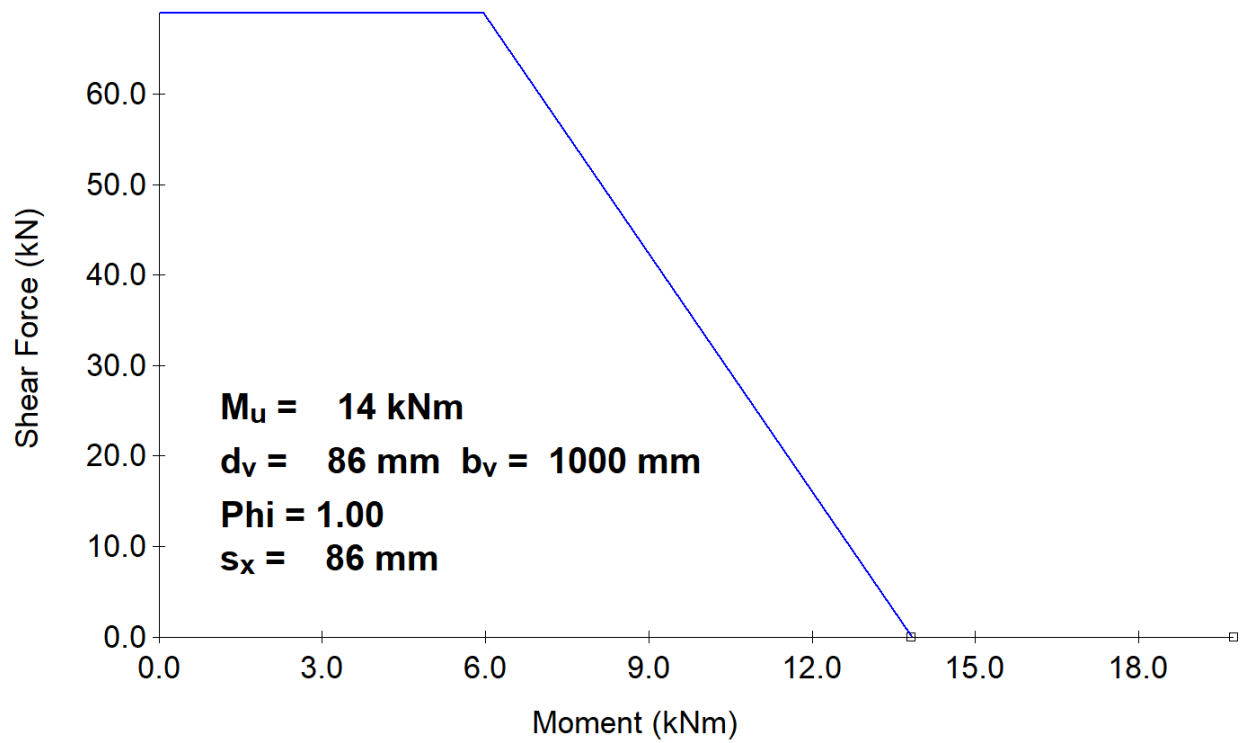


Figure 7.15-AASHTO-2000 M-V Interaction

7.1.2.6. Response-2000: Moment & Shear

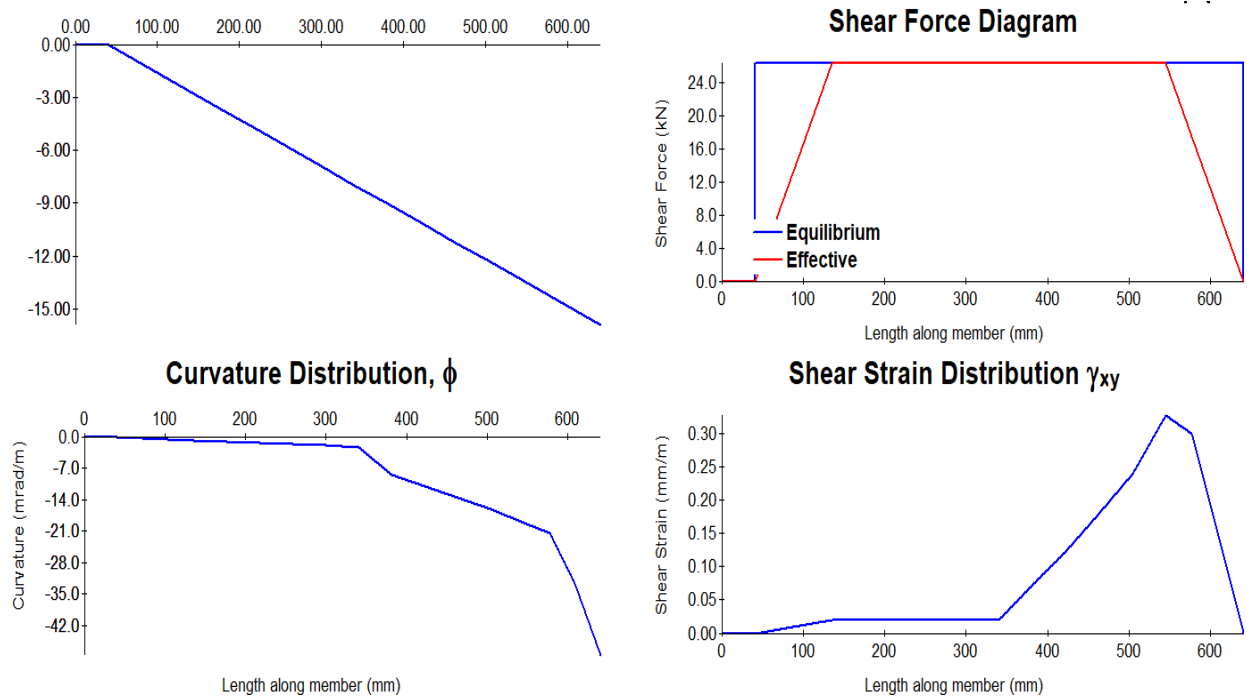


Figure 7.16-Moment & Shear Diagrams

7.1.2.7. Response-2000: Stiffness & Axial

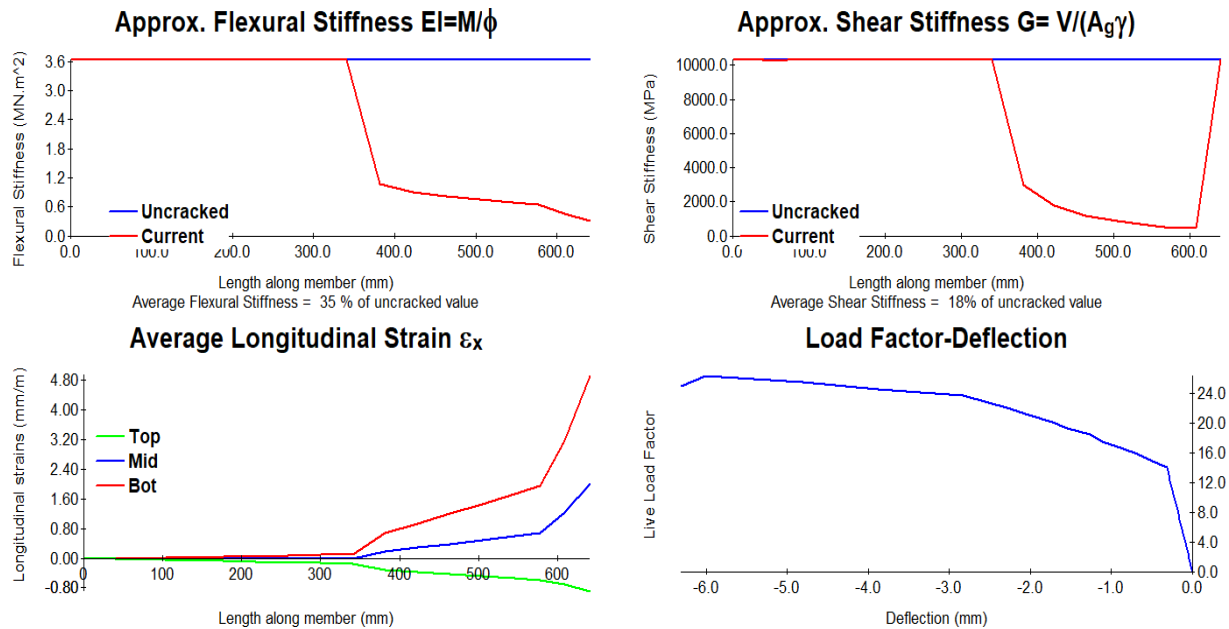


Figure 7.17-Stiffness & Axial Diagrams

7.1.3. Slab Capacity

7.1.3.1. Yield line Analysis Results for NC slab

The yield line method of analysis was used to obtain the slab capacity based. The M_r obtained for the slab with a compressive strength of 28.50 was found to be 19.4kNm.

7.1.3.2. Response-2000 Slab Capacity

In predicting the slab capacity with a compressive strength of 28.50MPa. Response-2000 sectional analysis found the moment of the slab to be 19.0kNm. which when back calculated, resulted into a capacity of 203.62kN.

7.1.3.3. FE Slab Capacity Comparison with Yield Line Analysis for NC Slab

The table below shows the predicted slab capacity when compared with the yield line analysis for the normal concrete strength.

Table 7.1-FEA vs Yield Line Comparison

Slab ID	FEA Capacity	Yield Line Capacity(kN)	% Difference
NC	147.520	112.54	26.901

7.1.3.4. FE Slab Capacity Comparison with Response-2000

Based on the slab capacity obtained at the maximum moment by the use of the Response-2000 program, it was found that the Response-2000 still gave a much higher capacity in comparison to the FEA capacity of the slab.

Table 7.2-FEA vs Response 2000 Comparison

Slab ID	FEA Capacity (kN)	Response-2000 Capacity (kN)	% Difference
NC	147.520	203.20	31.75

7.1.4. Slab Deflection

7.1.4.1. Slab Deflection Assessment with the Crossing Beam Method

The slab deflection for the normal concrete slab was compared to the ACI code and the sectional analysis using Response-2000 and the percentage difference for the both of them was obtained. In addition to this, all values were checked against the limiting value for deflection as per the ACI code.

7.1.4.2. FE Slab Deflection Comparison with ACI Code (Crossing Beam Method)

Table 7.3-FEA vs Response-2000 Comparison

Slab ID	FEA (mm)	Crossing Method (mm)	% Difference
NC	4.000	5.470	29.70

7.1.4.3. Crossing Beam Method Results Comparison with Sectional Analysis Results

Table 7.4-FEA vs Response-2000 Comparison

Slab ID	FEA (mm)	Response-2000 (mm)	% Difference
NC	4.000	6.370	45.71

7.1.5. Mohr Circles

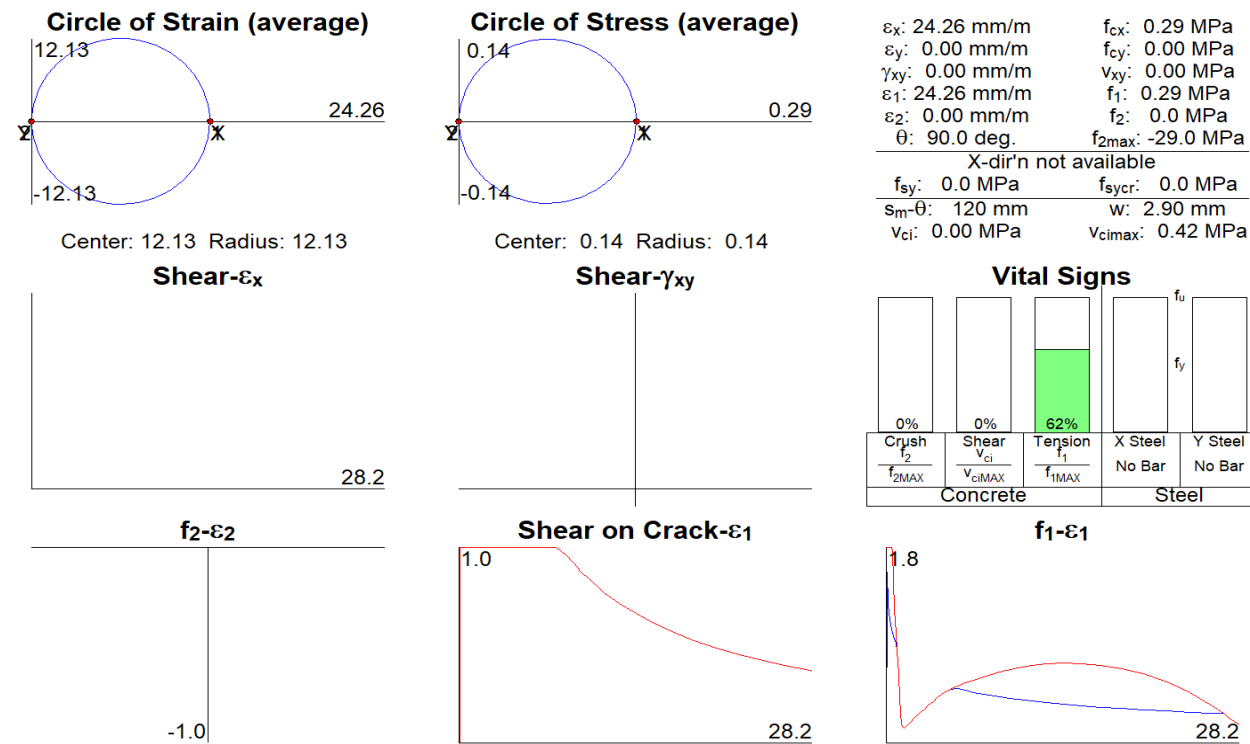


Figure 7.18-Mohr Circle

7.1.6. Analysis of the Slab Section LC-C

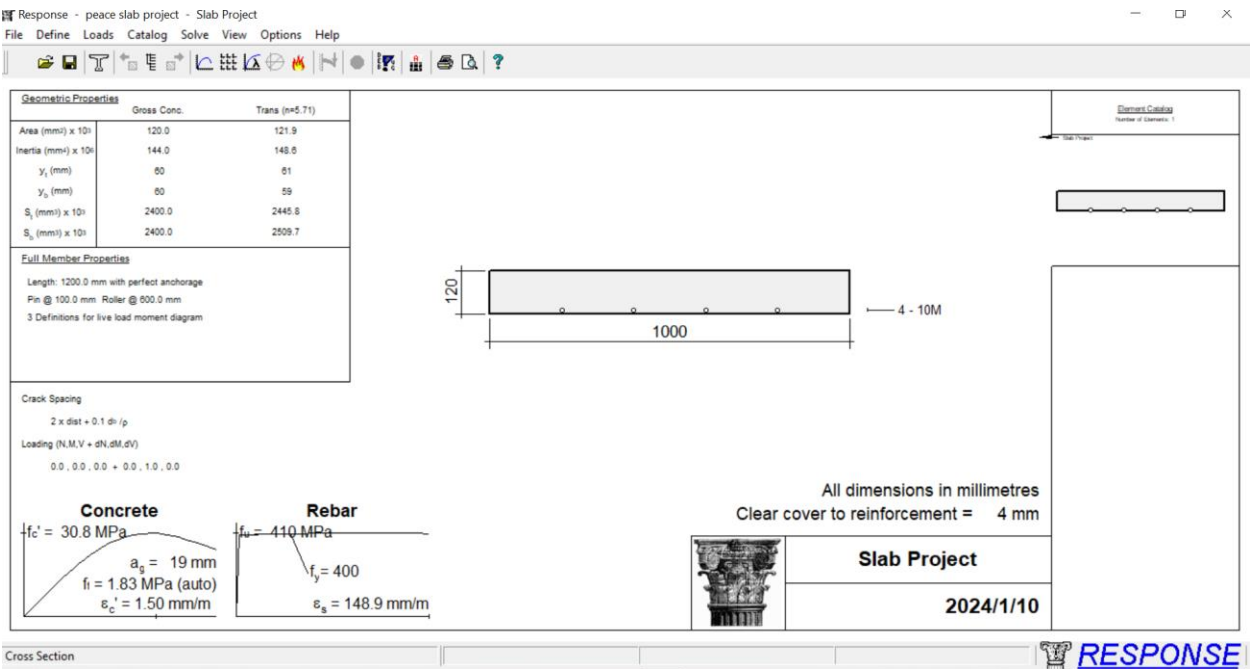


Figure 7.19-Section Properties

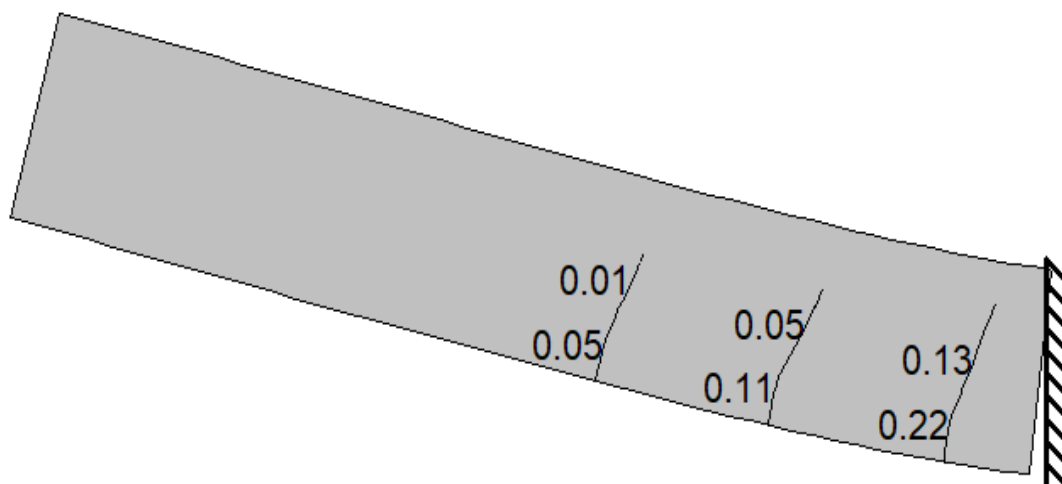


Figure 7.20-Slab Cracking Pattern

7.1.6.1. Response-2000: General Plots

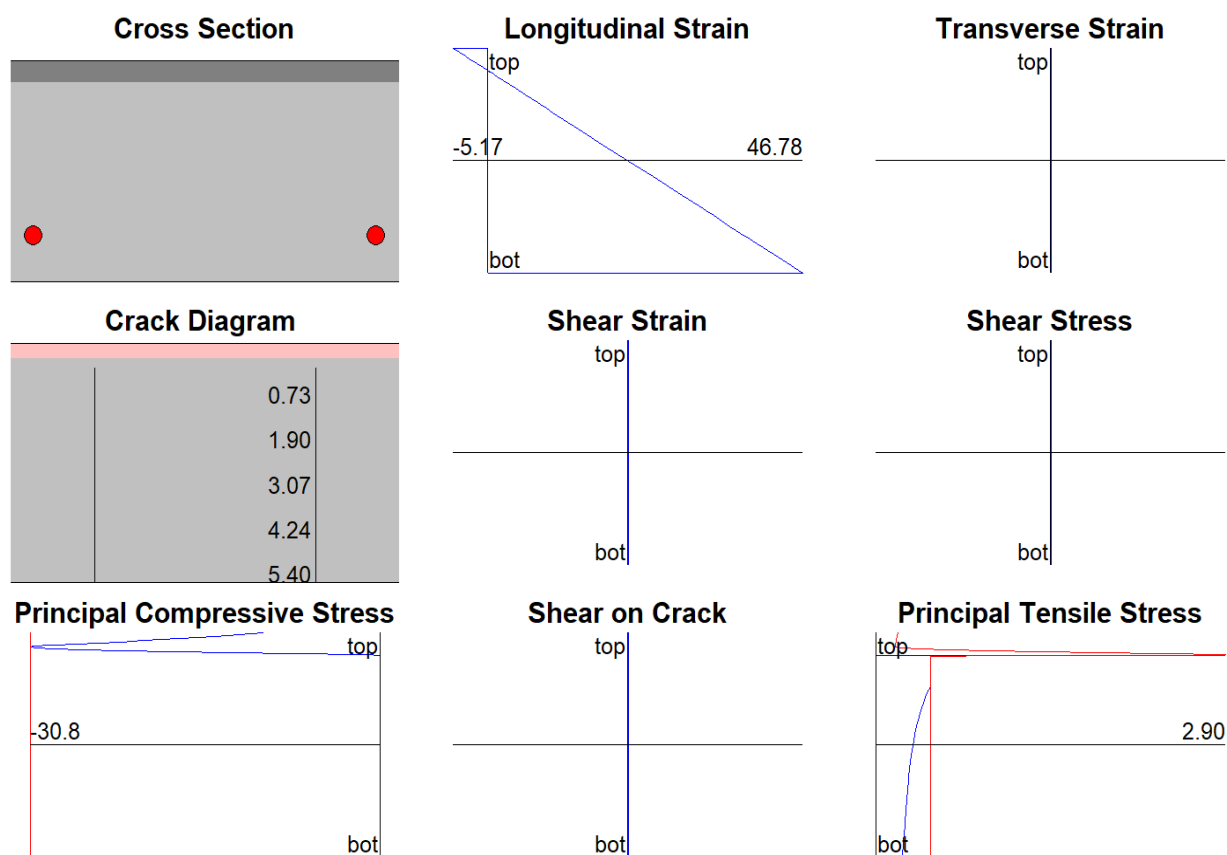


Figure 7.21-Compression & Tensile Results

7.1.6.2. Response-2000: Cracking Information and Plots

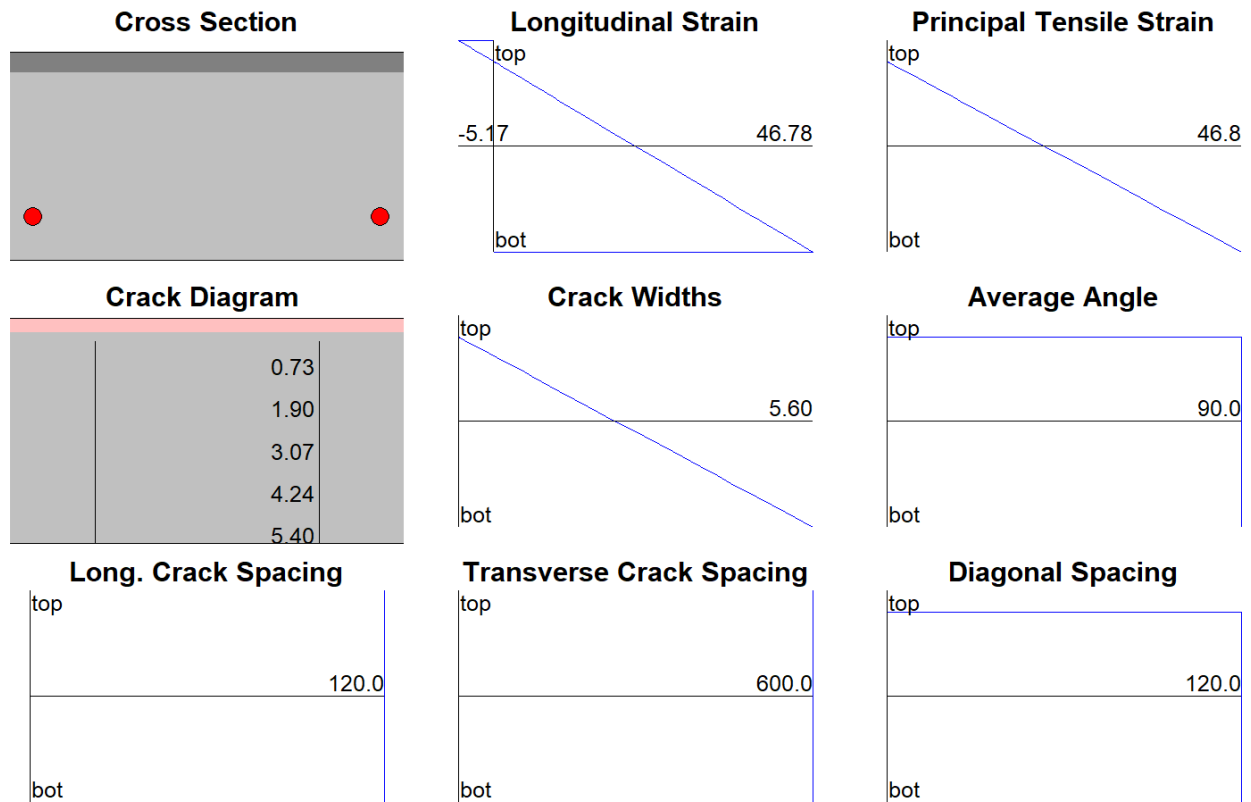


Figure 7.22-Member Crack Data, Max 5.60mm

7.1.6.3. Response-2000: Reinforcement Plots

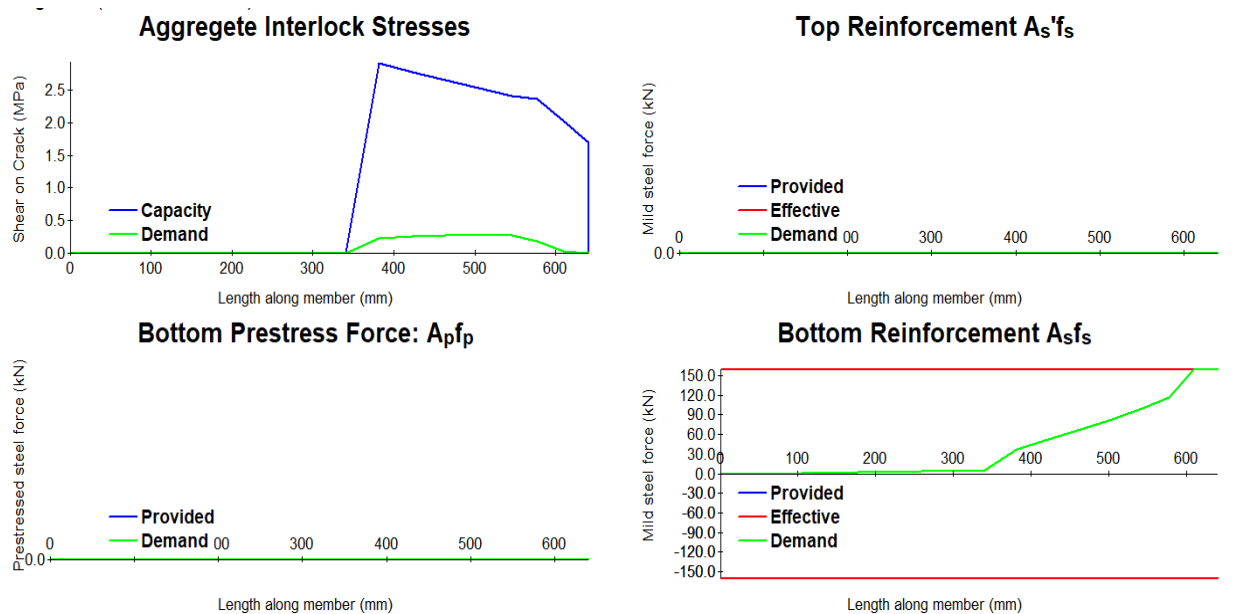


Figure 7.23-Bottom Reinforcing Details

7.1.6.4. Response-2000: No Shear Plots

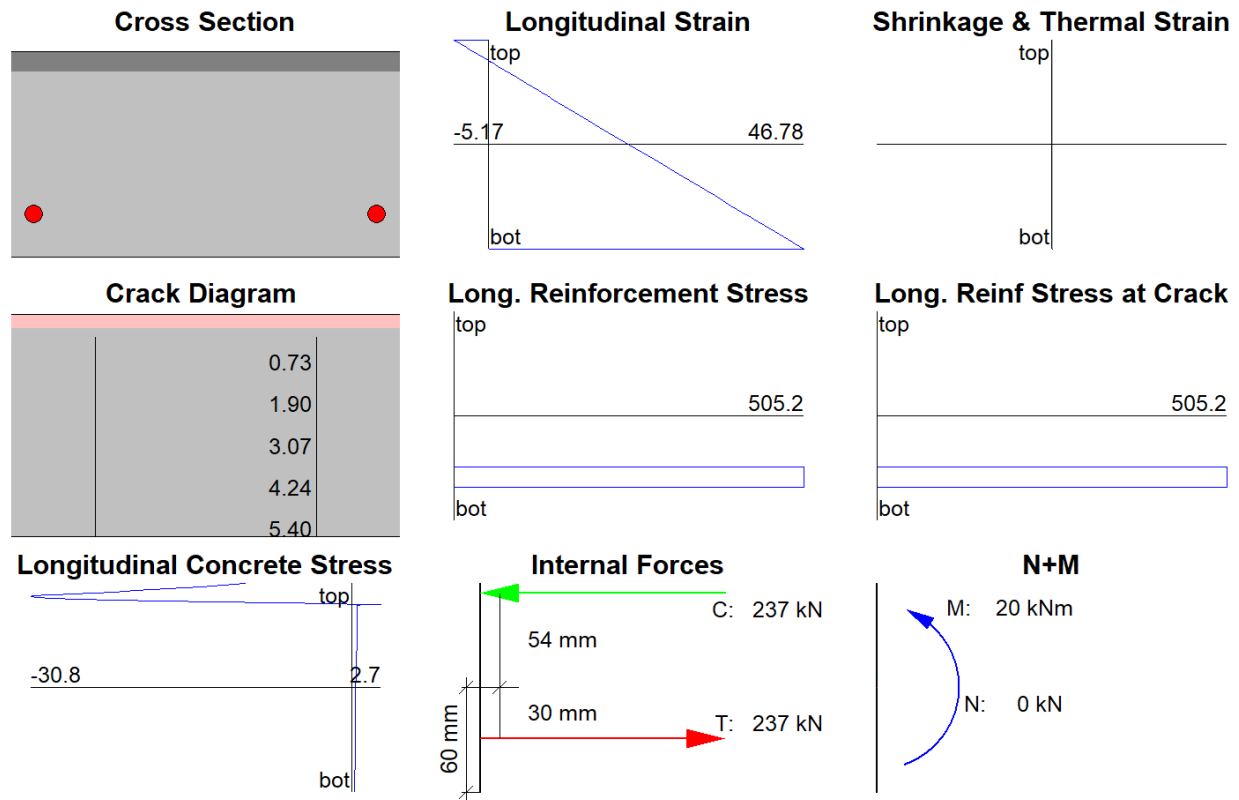


Figure 7.24-Concrete & Steel Stresses

7.1.6.5. Response-2000: Deformation & Rotation Plots

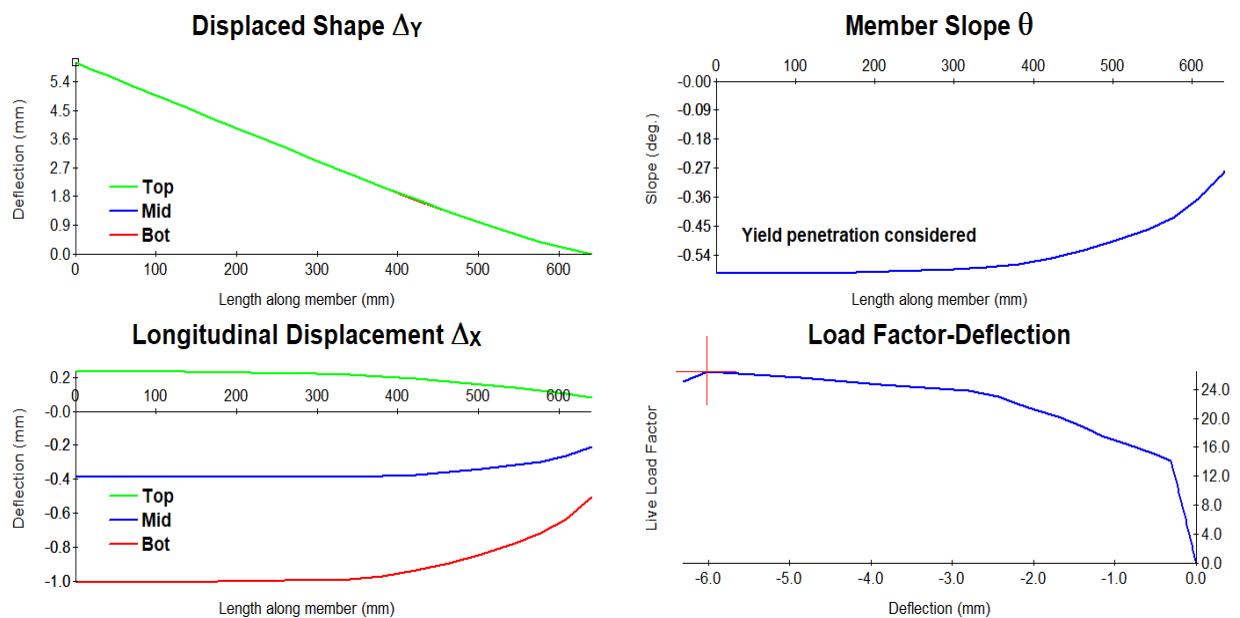


Figure 7.25-The Displacement of the Section, Max=6.32mm

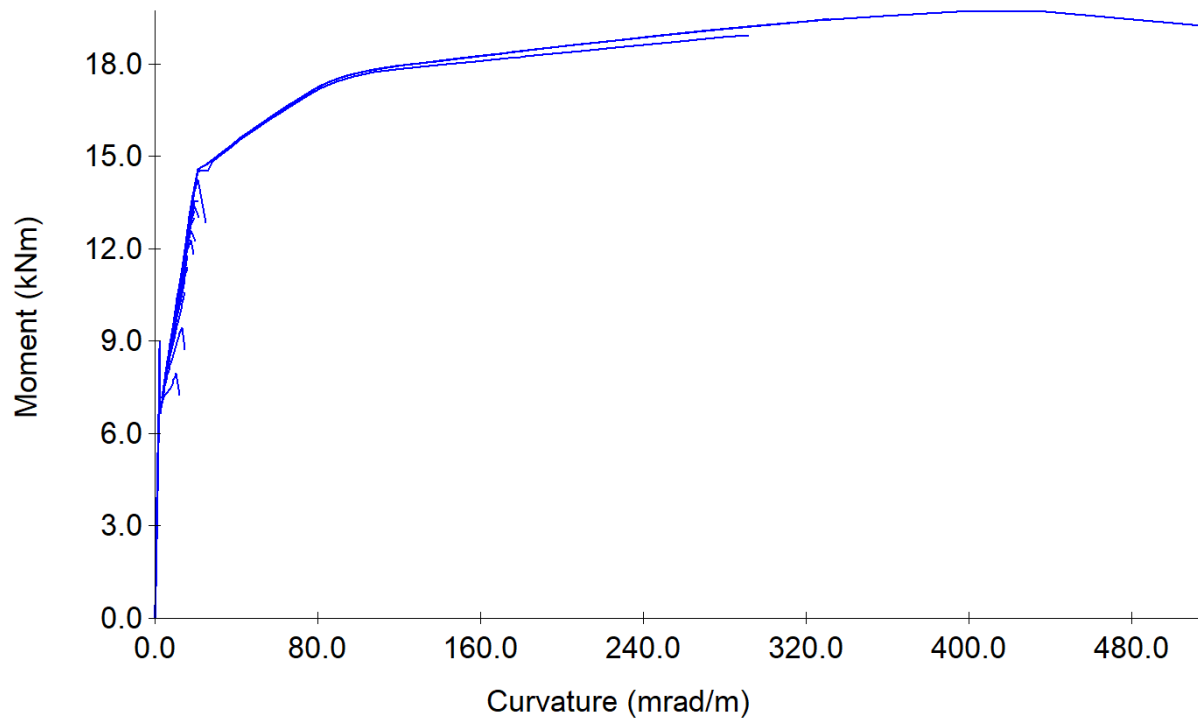


Figure 7.26-Moment vs Curvature, Max= 19.25kNm & 514.06mrad/m

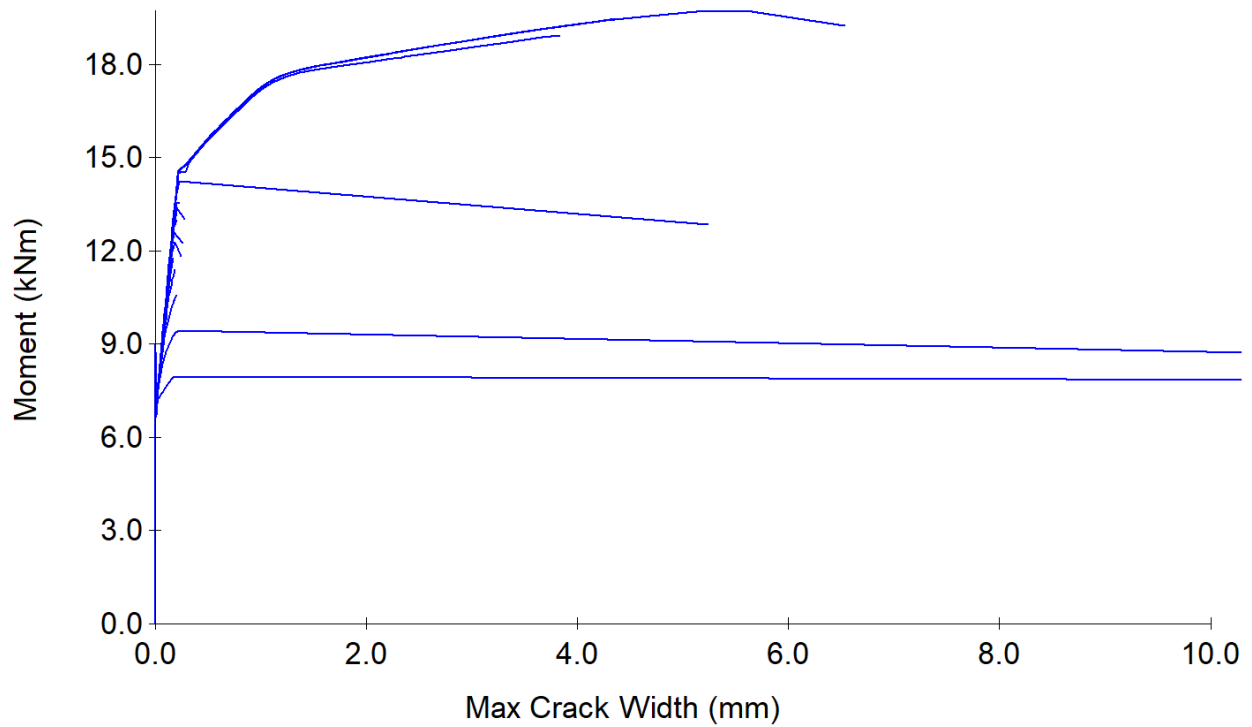


Figure 7.27-Moment vs Maximum Crack Width, Max=6.53mm

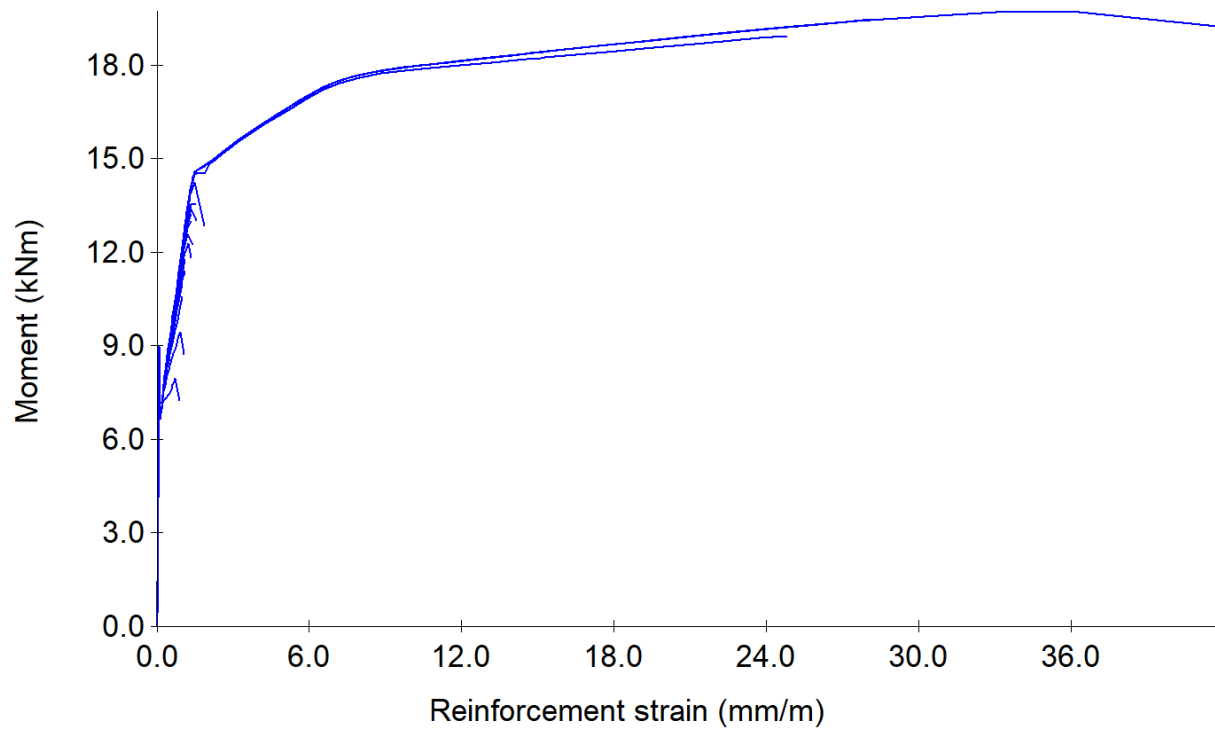


Figure 7.28-Moment vs Reinforcement Strain, Max=41.74mm/m

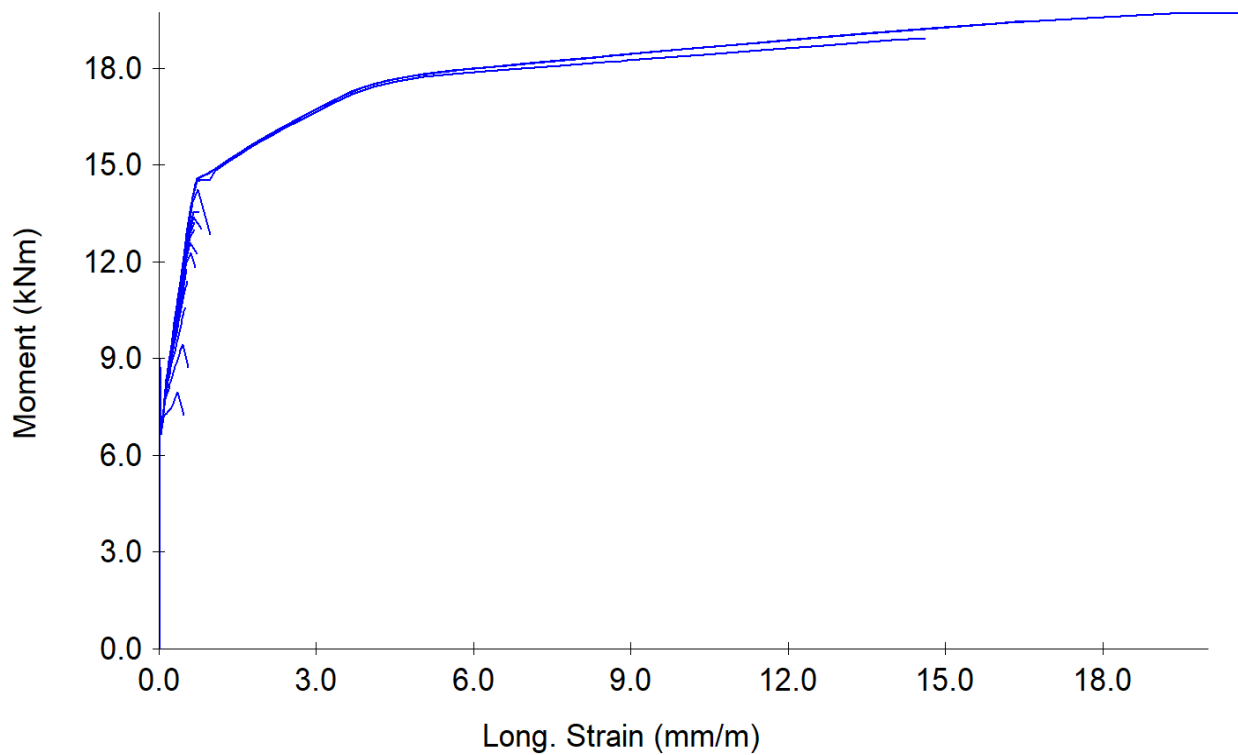


Figure 7.29-Moment vs Longitudinal Strain, Max=23.75mm/m

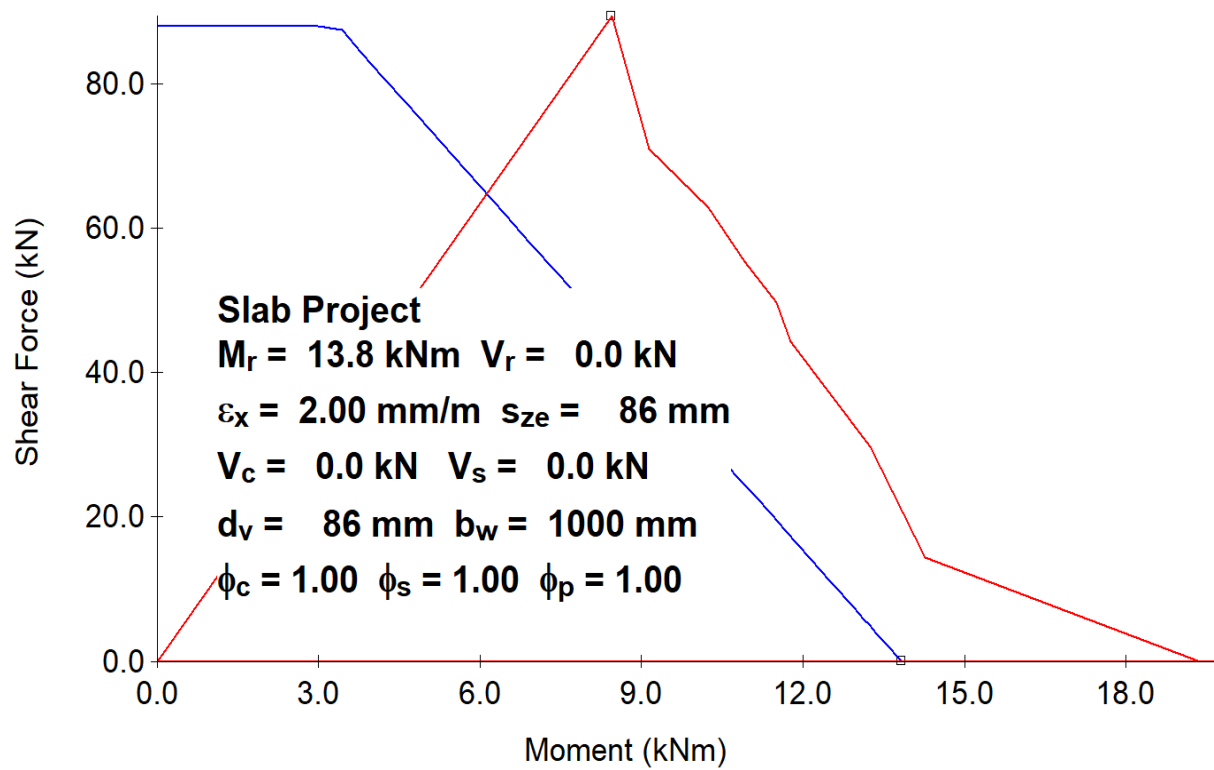


Figure 7.30- CSA 2014 M-V Interaction

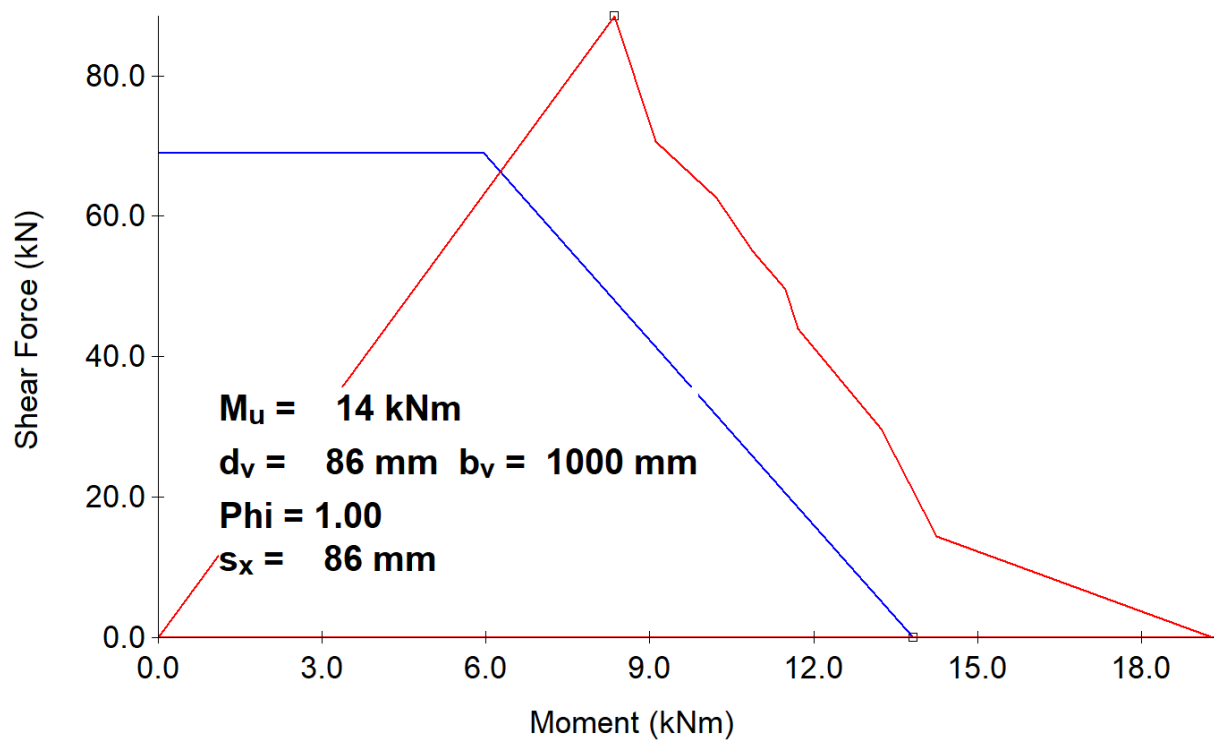


Figure 7.31-AASHTO-2000 M-V Interaction

7.1.6.6. Response-2000: Moment & Shear

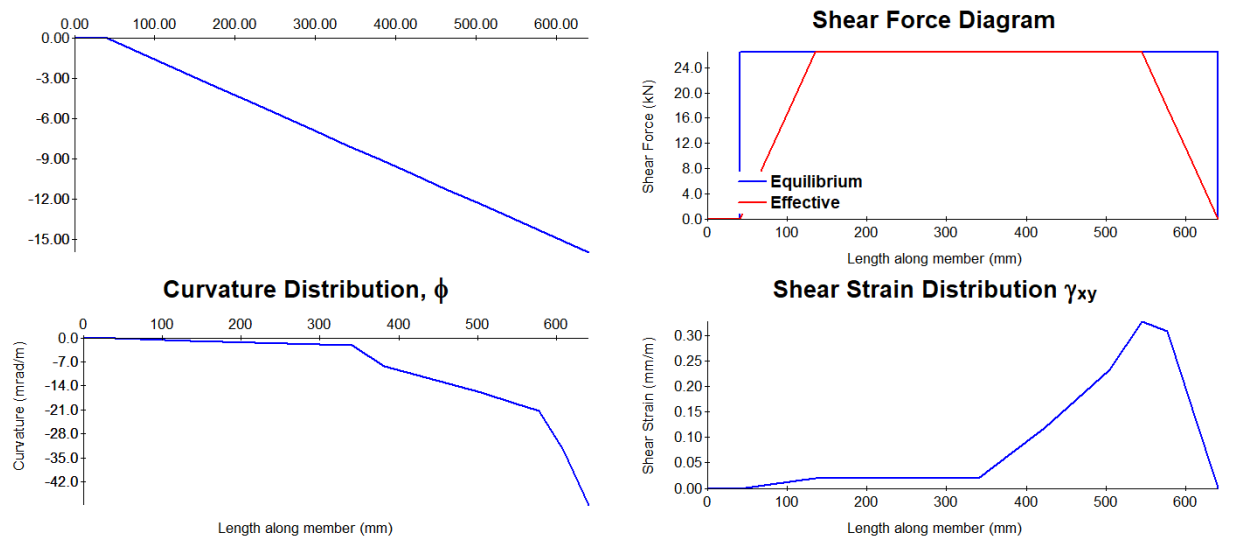


Figure 7.32-Moment & Shear Diagrams

7.1.6.7. Response-2000: Stiffness & Axial

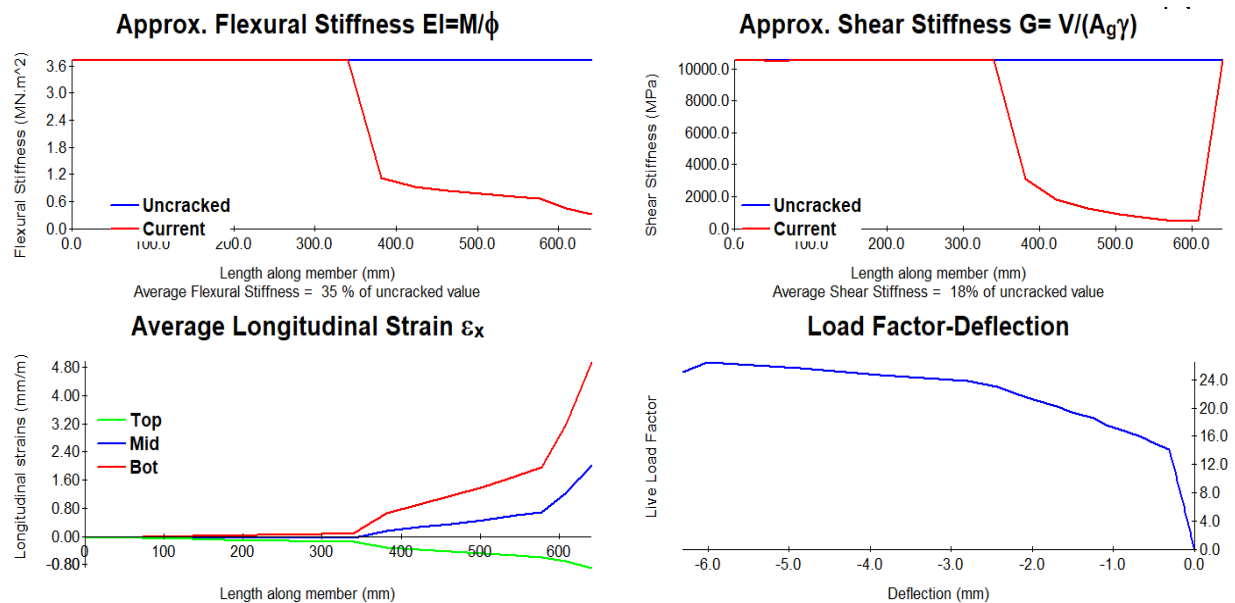


Figure 7.33-Stiffness & Axial Diagrams

7.1.7. Slab Capacity

7.1.7.1. Yield line Analysis Results for LC-C slab

The yield line results from the slab gave an M_r of 13.94kNm and capacity of the slab as 112.59kN.

7.1.8. Response-2000 Slab Capacity

In predicting the slab capacity with a compressive strength of 30.82MPa. Response-2000 sectional analysis found the moment of the slab to be 19.3kNm. which when back calculated, resulted into a capacity of 205.3kN.

7.1.8.1. FE Slab Capacity Comparison with Yield Line Analysis

Table 7.5-FEA vs Yield Line Comparison

Slab ID	FEA Capacity (kN)	Yield Line Capacity (kN)	% Difference
LC-C	140.820	112.590	22.280

7.1.8.2. FE Slab Capacity Comparison with Response-2000

Table 7.6-FEA vs Yield Line Comparison

Slab ID	FEA Capacity (kN)	Response-2000 (kN)	% Difference
LC-C	140.820	205.30	37.258

7.1.9. Slab Deflection

7.1.9.1. Slab Deflection Assessment with the Crossing Beam Method

The deflection of the slab was found to be 6.280mm based on the using the crossing method.

7.1.9.2. FE Slab Deflection Comparison with ACI Code (Crossing Beam Method)

Table 7.7-FEA vs ACI Code

Slab ID	FEA (mm)	Crossing Beam (mm)	% Difference
LC-C	4.000	6.280	44.36

7.1.9.3. Crossing Beam Method Results Comparison with Sectional Analysis Results

Table 7.8-FEA vs Response-2000

Slab ID	Crossing Beam (mm)	Response-2000 (mm)	% Difference
LC-C	6.284	6.320	0.571

7.1.10. Mohr Circles

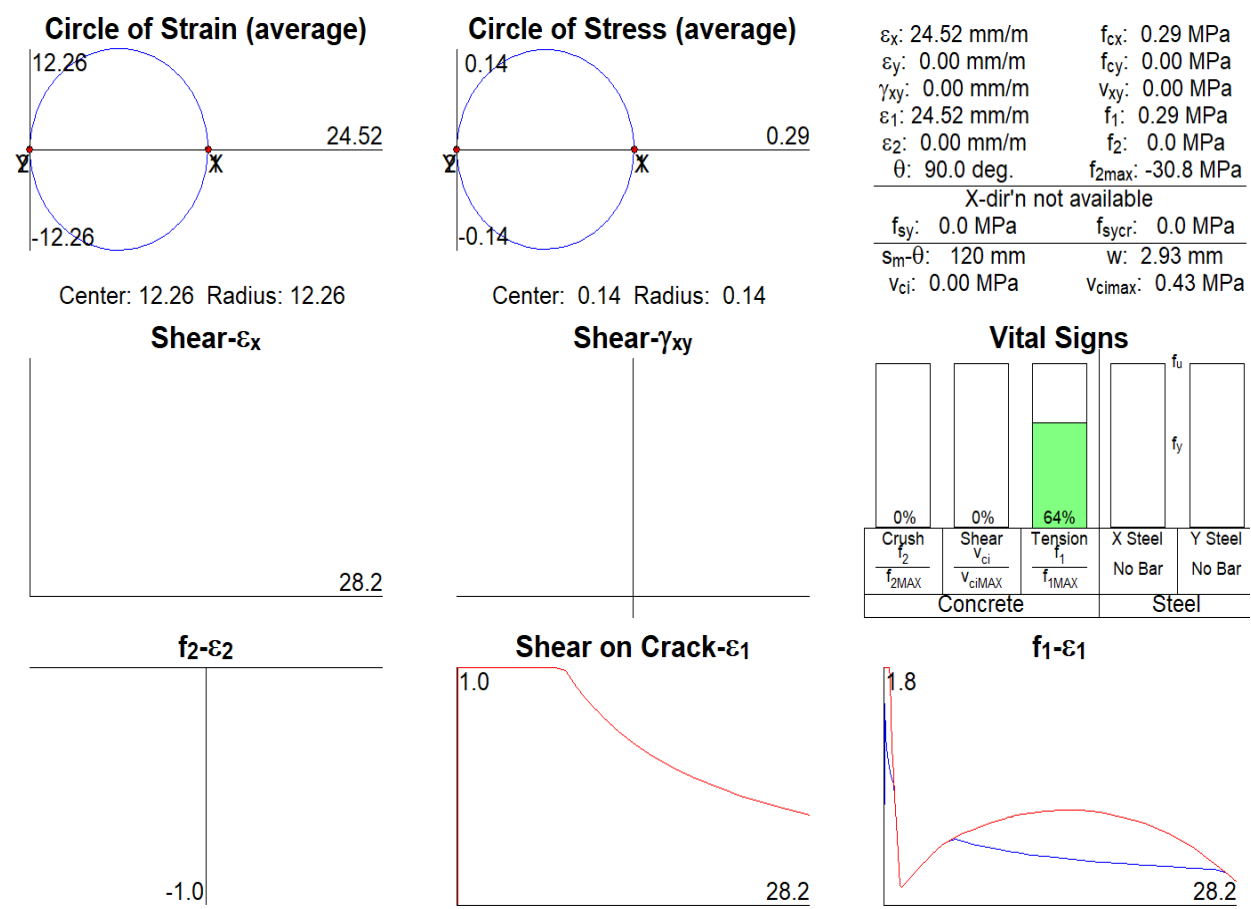


Figure 7.34-Mohr Circles

7.1.11. Analysis of the Slab Section LC-CF

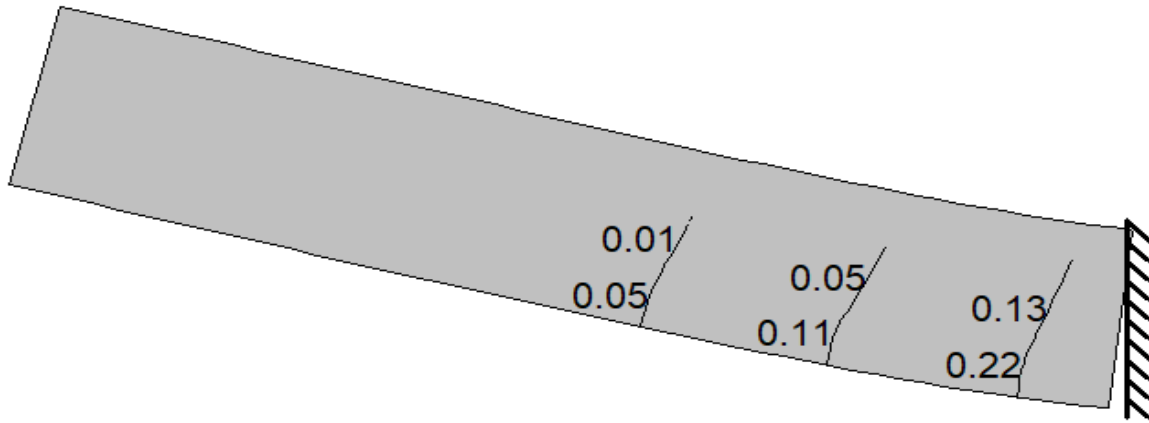


Figure 7.35-Slab Crack Pattern

7.1.11.1. Response-2000: General Plots

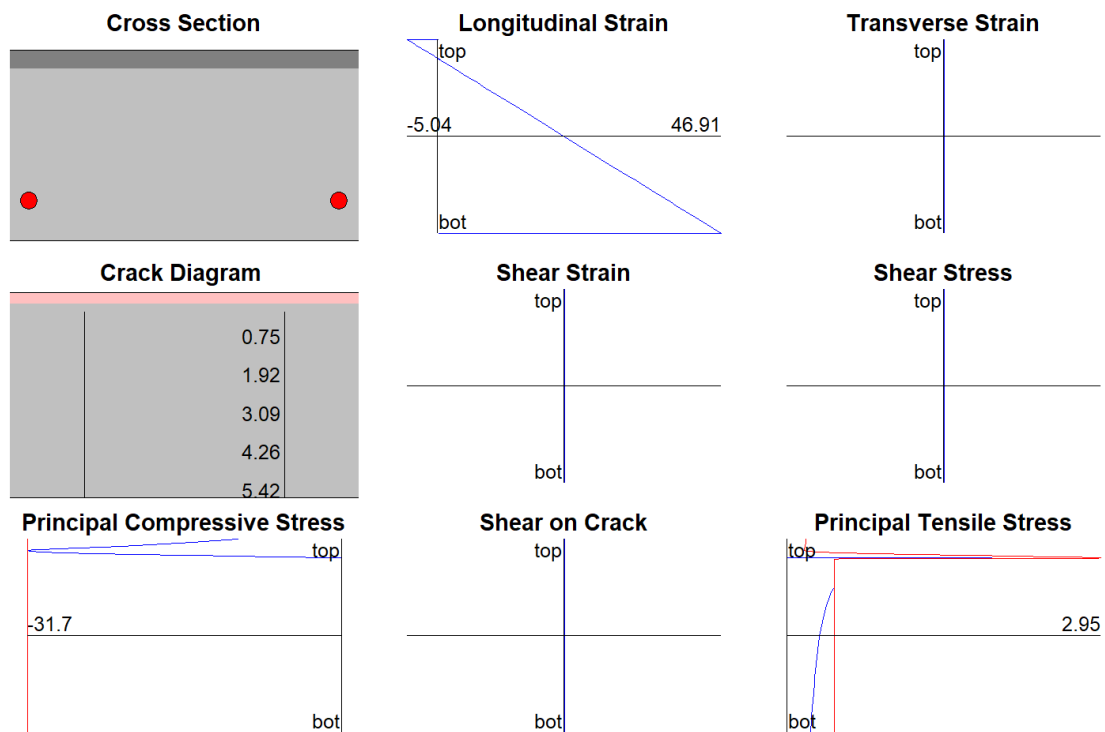


Figure 7.36-Compressive & Tensile Stresses

7.1.11.2. Response-2000: Cracking Information and Plots

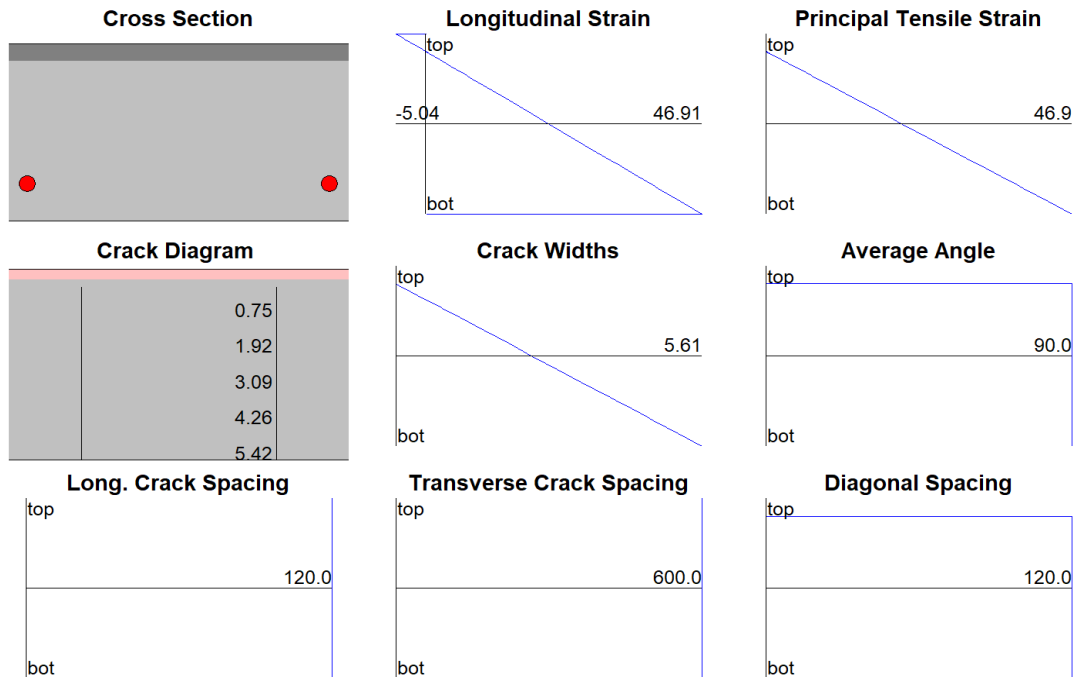


Figure 7.37-Member Crack Data, Max= 5.62

7.1.11.3. Response-2000: Reinforcement Plots

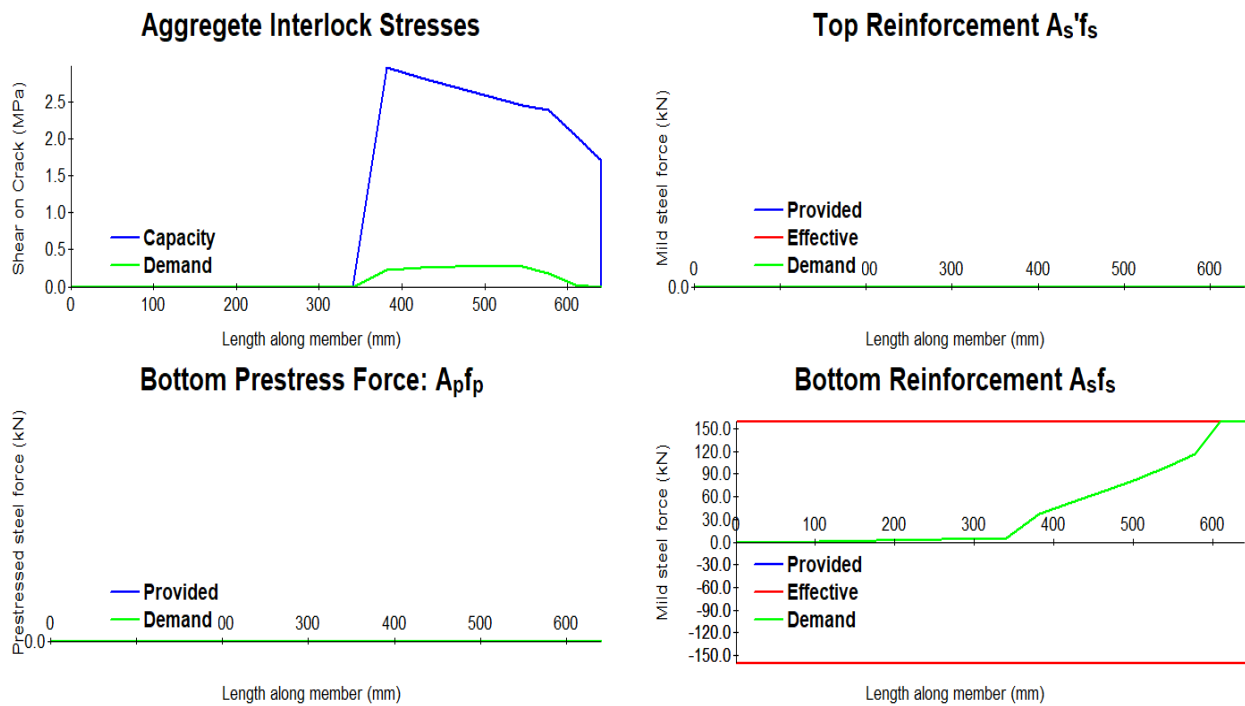


Figure 7.38-Bottom Reinforcing Details

7.1.11.4. Response-2000: No Shear Plots

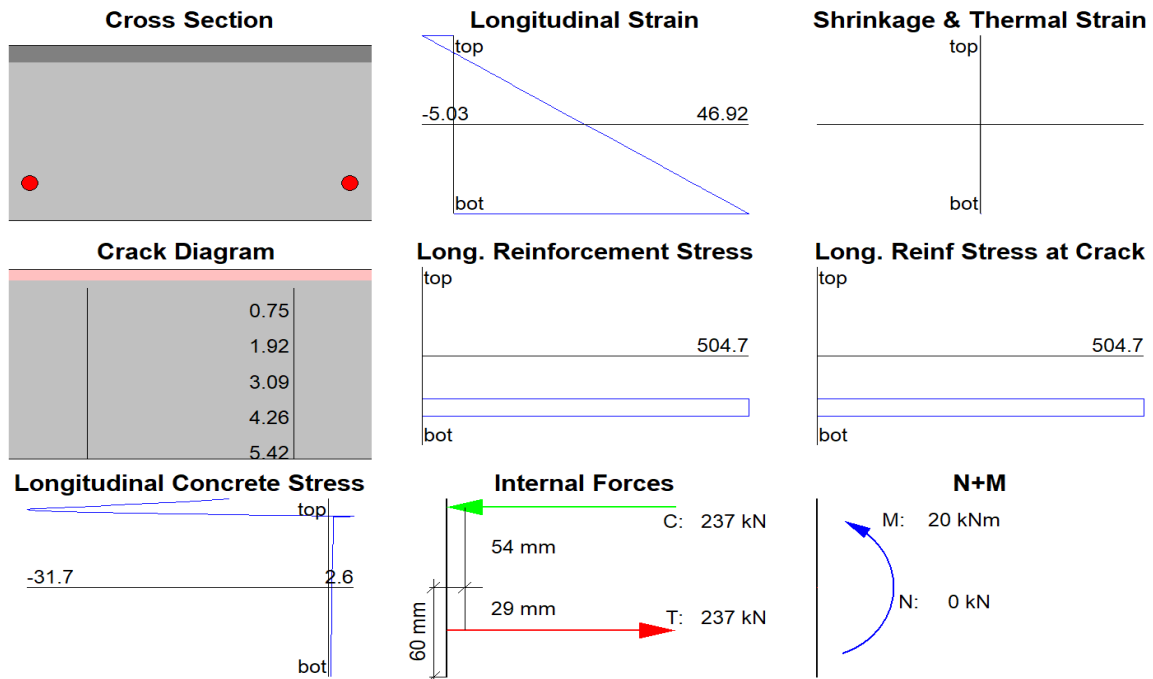


Figure 7.39-No Shear Plot

7.1.11.5. Response-2000: Deformation & Rotation Plots

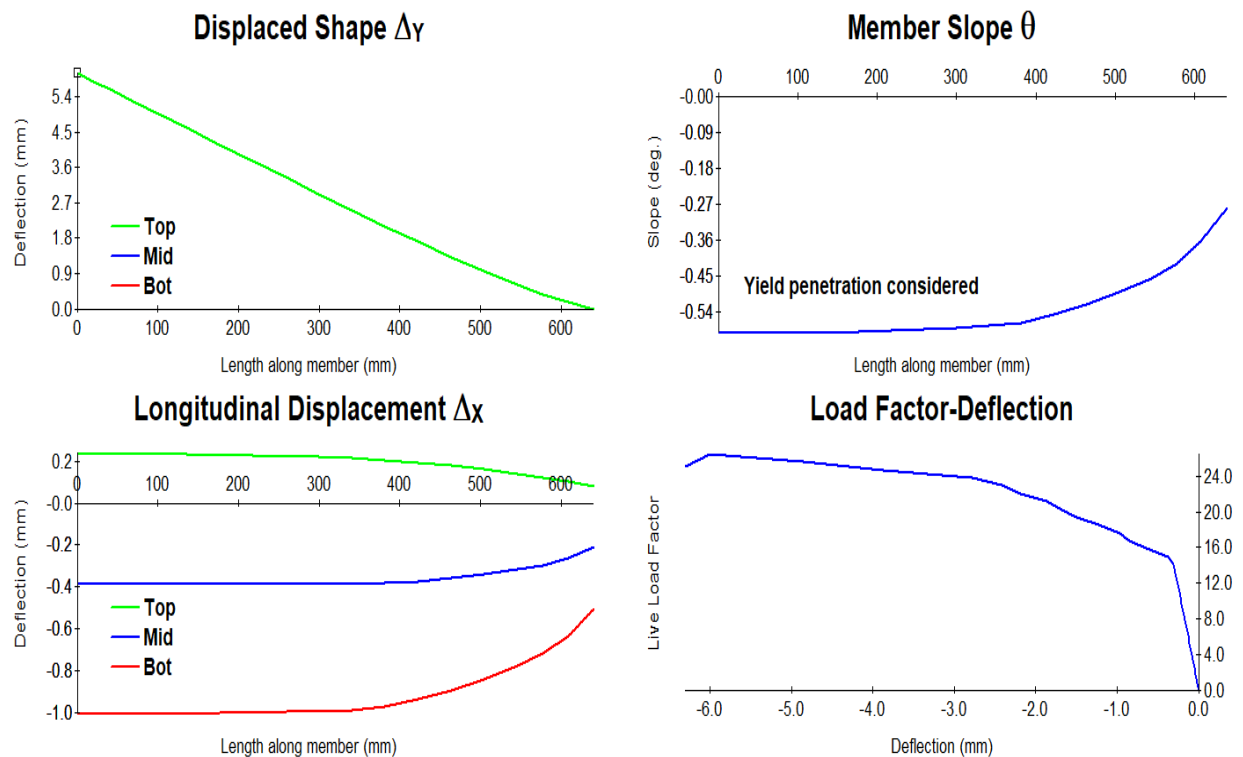


Figure 7.40-The Displacement of the Section, Max=6.31mm

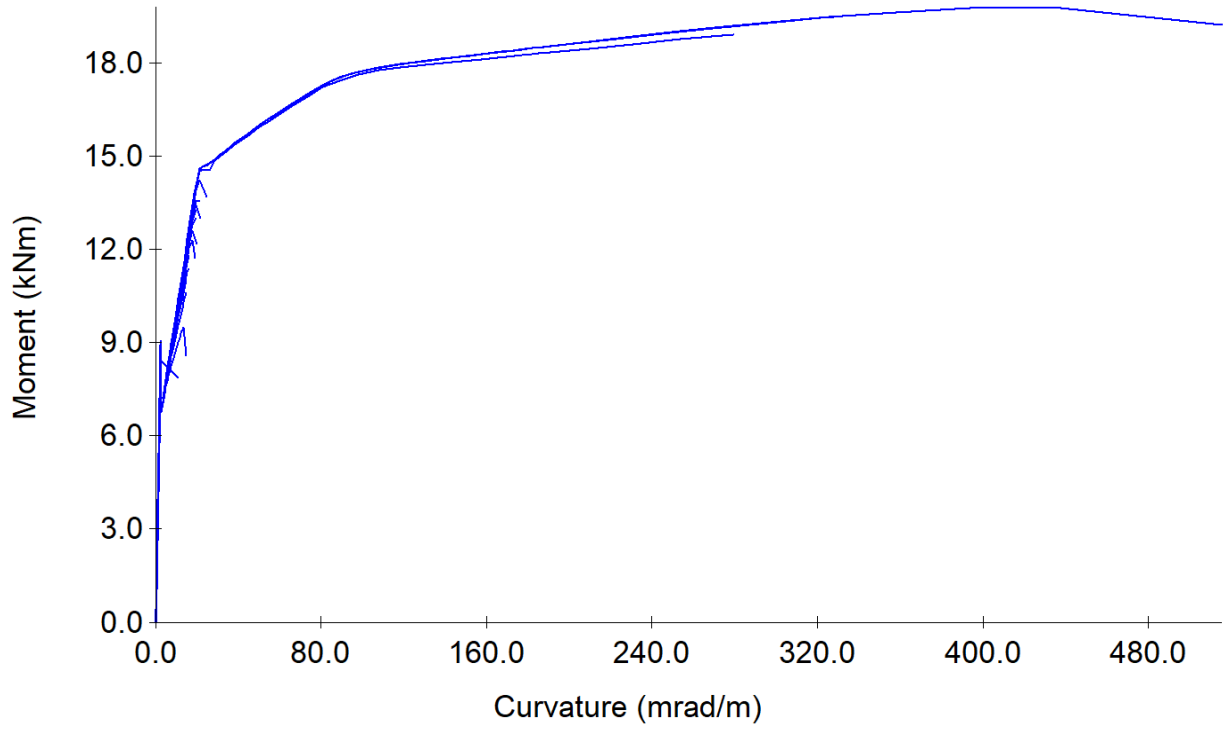


Figure 7.41-Moment vs Curvature, Max=19.22kNm & 515.34mrad/m

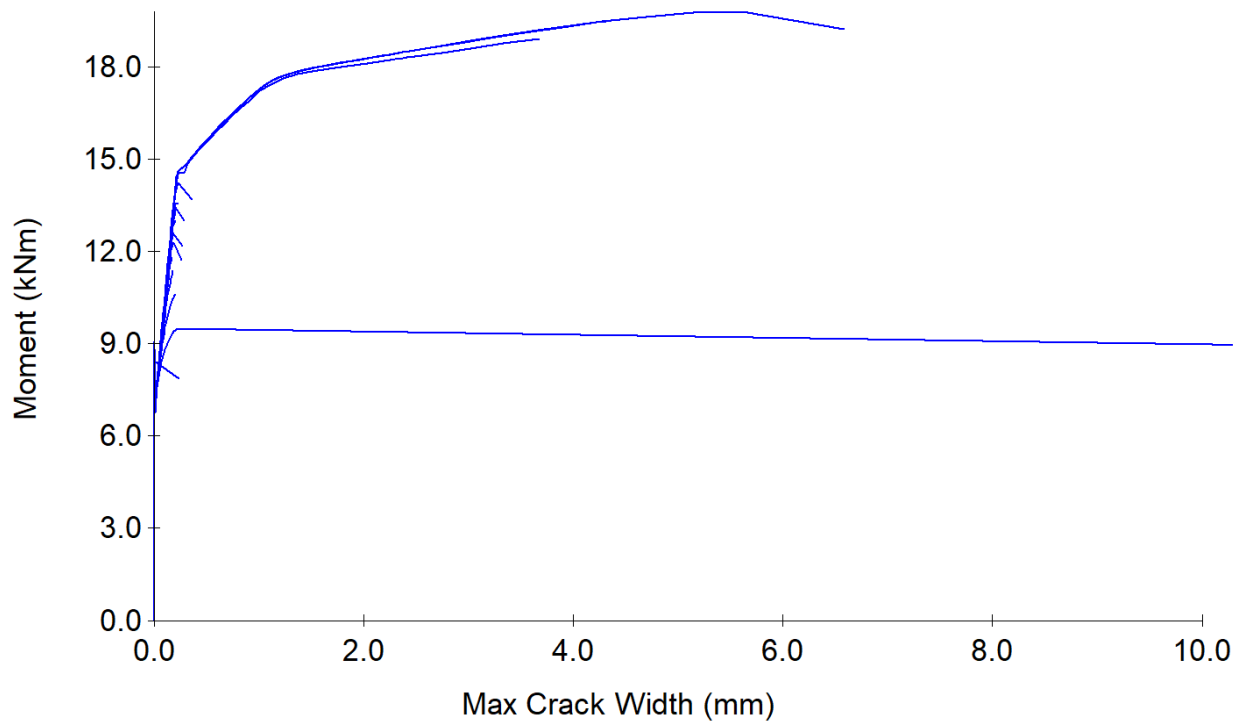


Figure 7.42-Moment vs Maximum Crack Width, Max=6.58mm

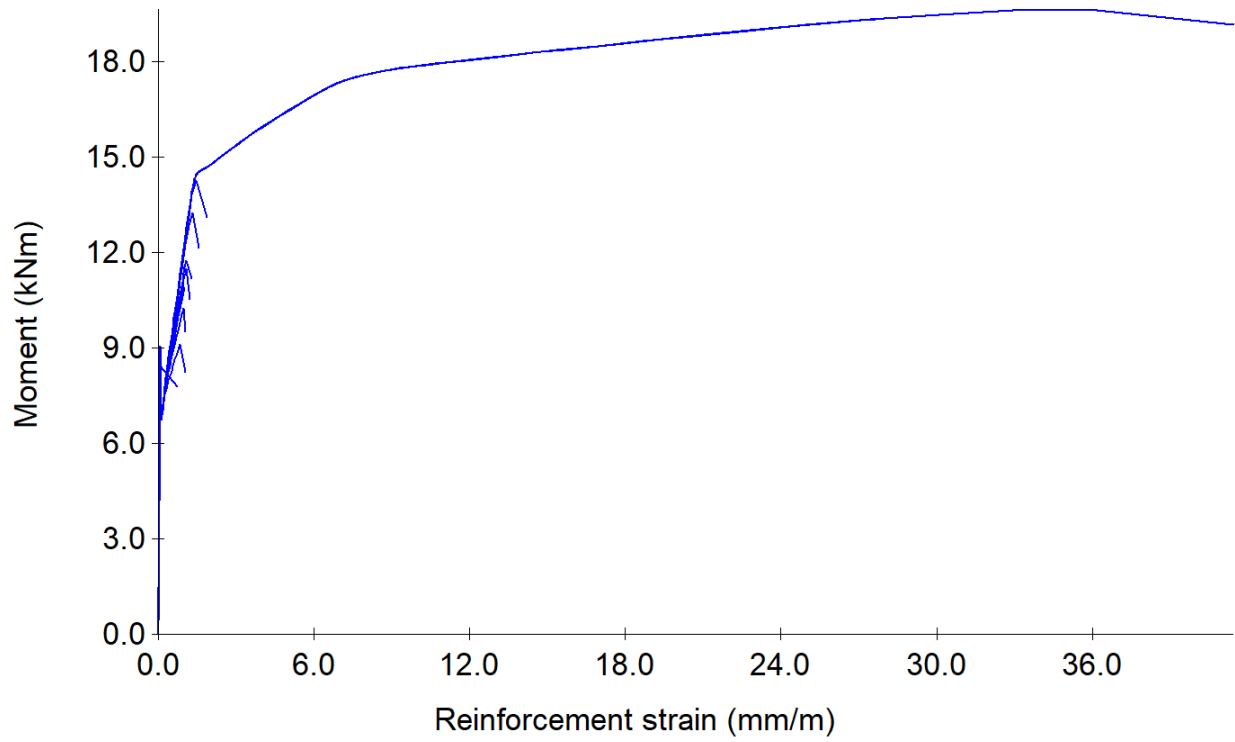


Figure 7.43-Moment vs Reinforcement Strain, Max=42.11mm/m

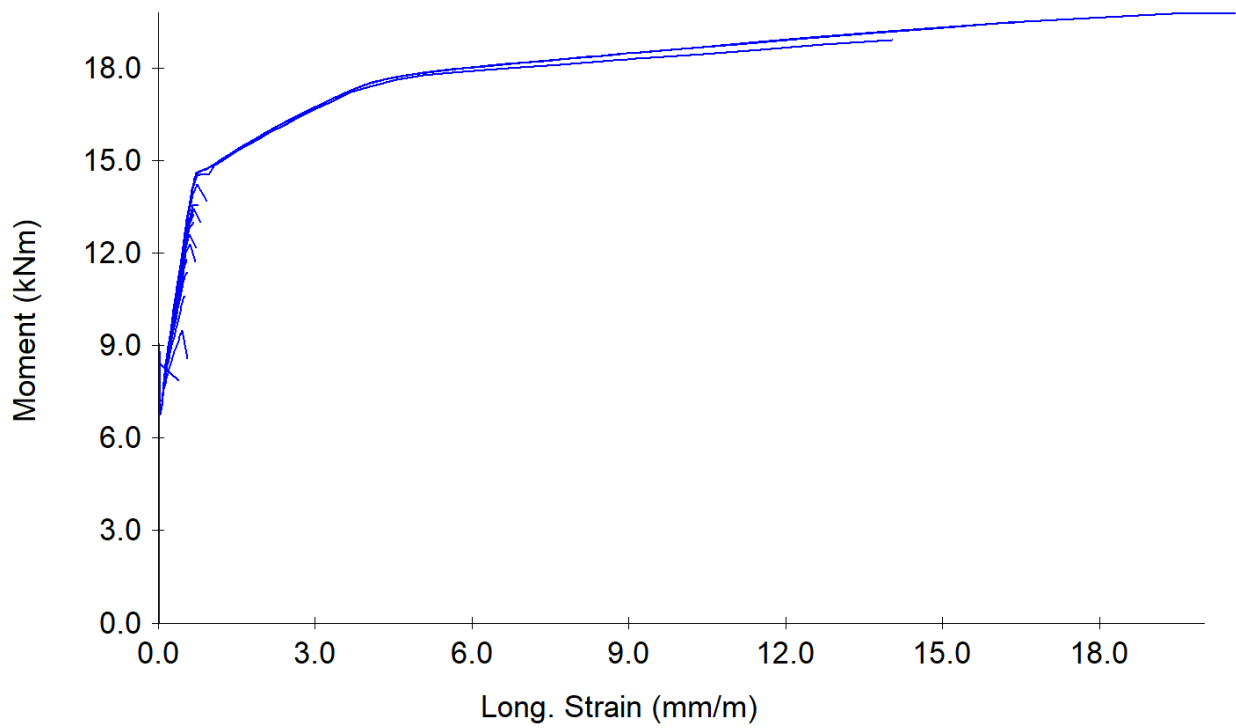


Figure 7.44-Moment vs Longitudinal Strain

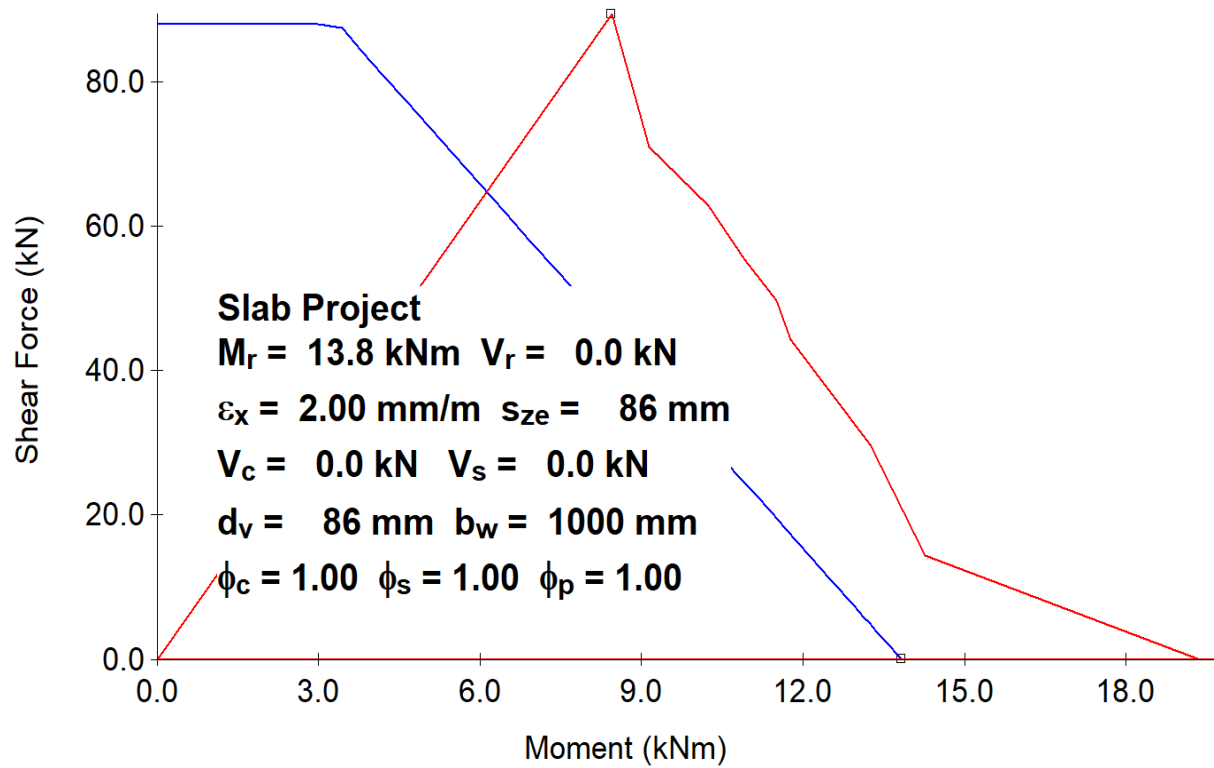


Figure 7.45-CSA 2014 M-V Interaction

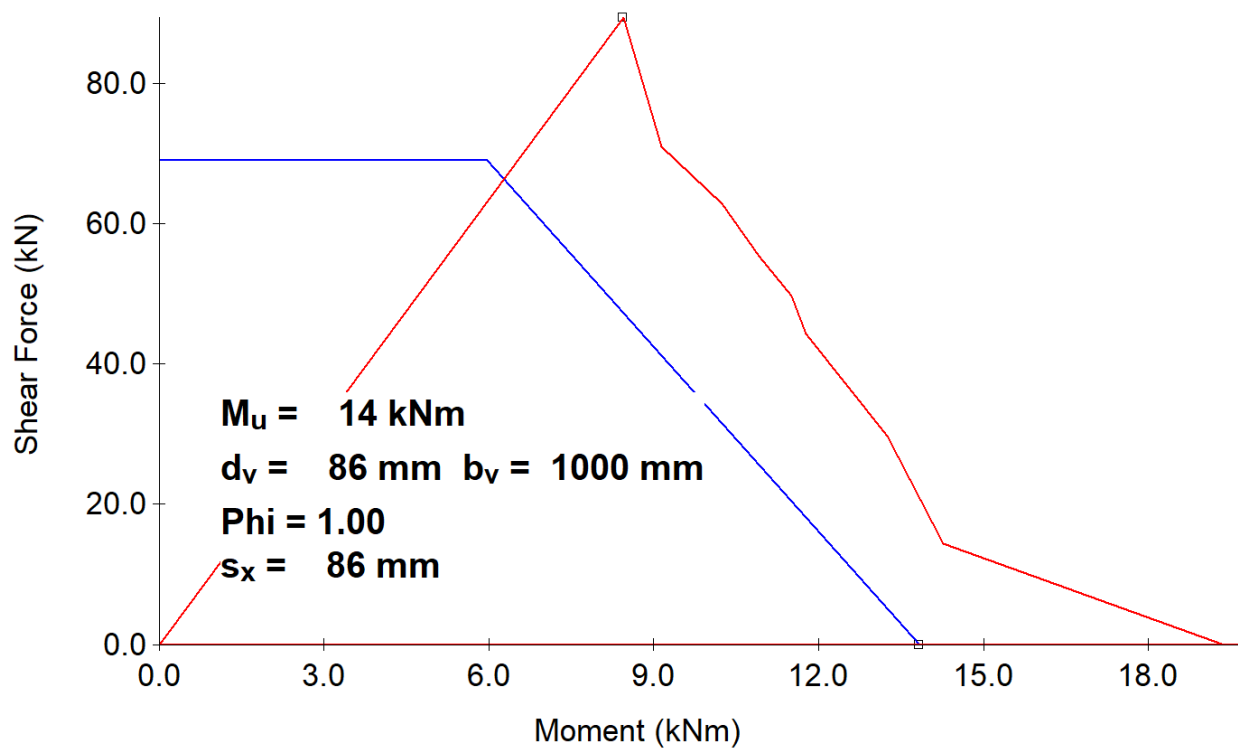


Figure 7.46-AASHTO-2000 M-V Interaction

7.1.11.6. Response-2000: Moment & Shear

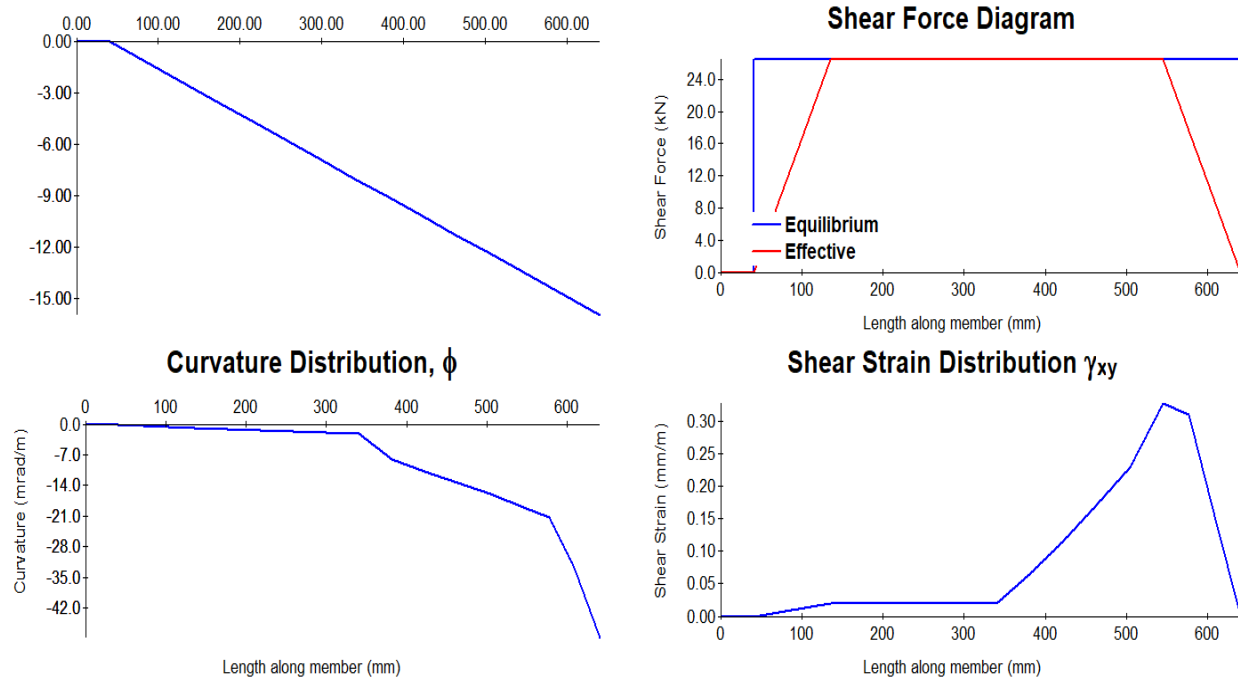


Figure 7.47-Moment & Shear Diagrams

7.1.11.7. Response-2000: Stiffness & Axial

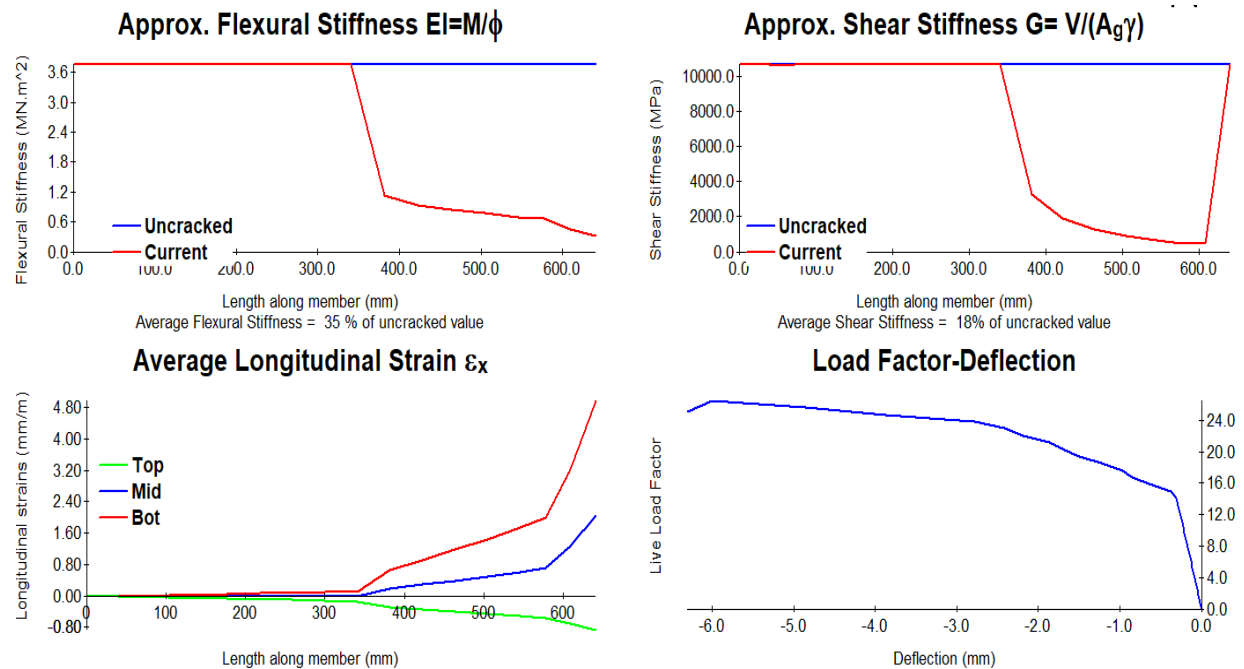


Figure 7.48-Stiffness & Axial Diagrams

7.1.12. Slab Capacity

7.1.12.1. Yield line Analysis Results for LC-CF slab

Upon yield line analysis, an M_r of 13.96kNm was obtained for the slab and a capacity of 112.41kN.

7.1.13. Response-2000 Slab Capacity

The capacity of the section as revealed for the moment of 19.2kNm was revealed to be 205.0kN.

7.1.13.1. FE Slab Capacity Comparison with Response-2000

Table 7.9-FEA vs Yield Line Comparison

Slab ID	FEA Capacity (kN)	Sectional Analysis (kN)	% Difference
LC-CF	134.600	205.010	41.465

7.1.13.2. FE Slab Capacity Comparison with Yield Line Analysis for LC-CF Slab

Table 7.10-FEA vs Response-2000 Comparison

Slab ID	FEA Capacity (kN)	Yield Line Capacity (kN)	% Difference
LC-CF	134.600	112.410	17.967

7.1.13.3. Slab Capacity Comparison with Response-2000

7.1.14. Slab Deflection

7.1.14.1. Slab Deflection Assessment with the Crossing Beam Method

The slab deflection assessment was found to be 8.905mm.

7.1.14.2. FE Slab Deflection Comparison with ACI Code (Crossing Beam Method)

Table 7.11-FEA vs Crossing Beam Method

Slab ID	FEA (mm)	Crossing Beam (mm)	% Difference
LC-CF	4.000	8.905	76.017

7.1.14.3. Crossing Beam Method Results Comparison with Sectional Analysis Results

Table 7.12-FEA vs Response-2000 Comparison

Slab ID	Crossing Beam (mm)	Response-2000 (mm)	% Difference
LC-CF	8.905	2.945	100.591

7.1.15. Mohr Circles

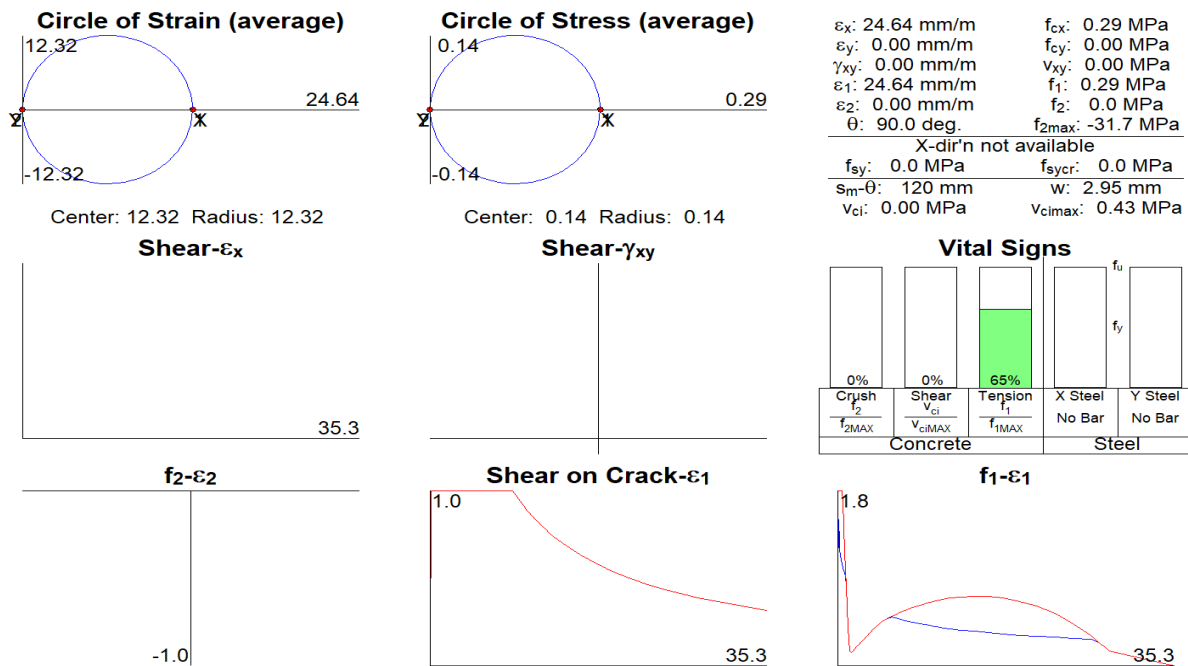


Figure 7.49-Mohr Circles

7.1.16. Analysis of the Slab Section LC-CFS

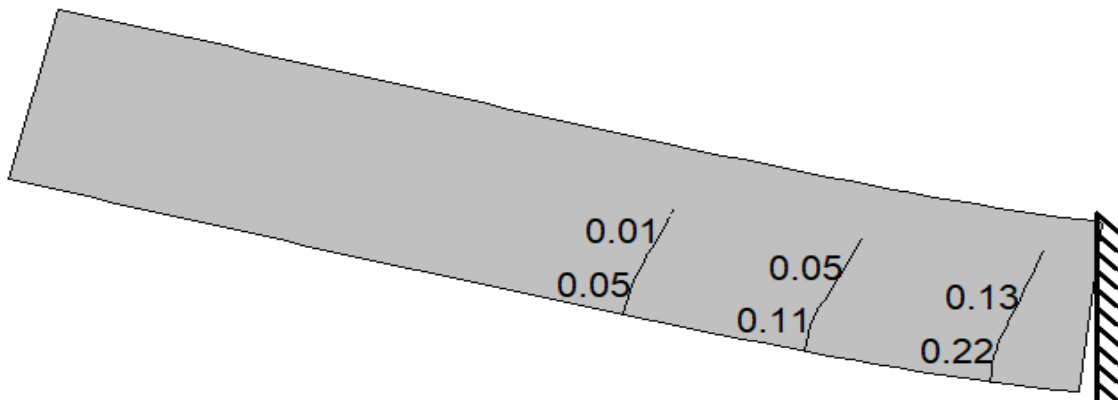


Figure 7.50-Slab Crack Pattern

7.1.16.1. Response-2000: General Plots

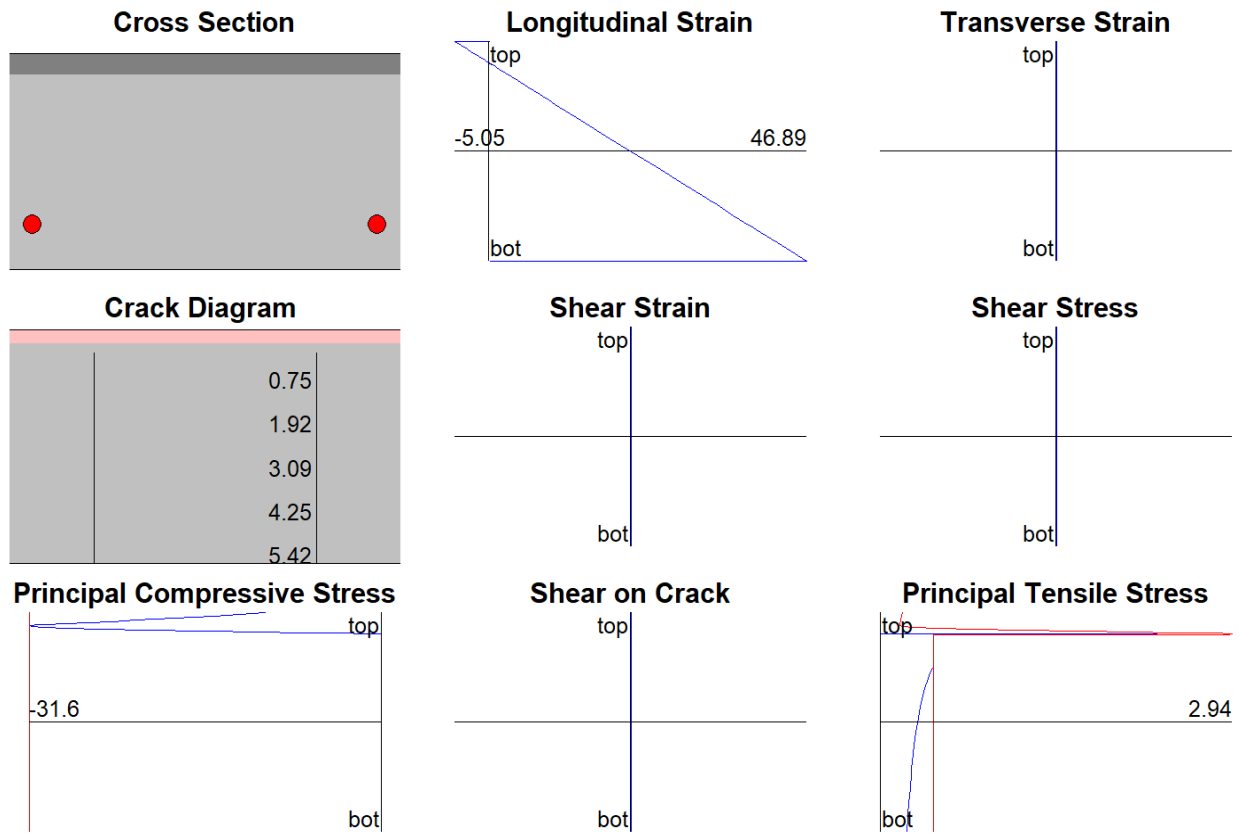


Figure 7.51-Compressive & Tensile Stresses

7.1.16.2. Response-2000: Cracking Information and Plots

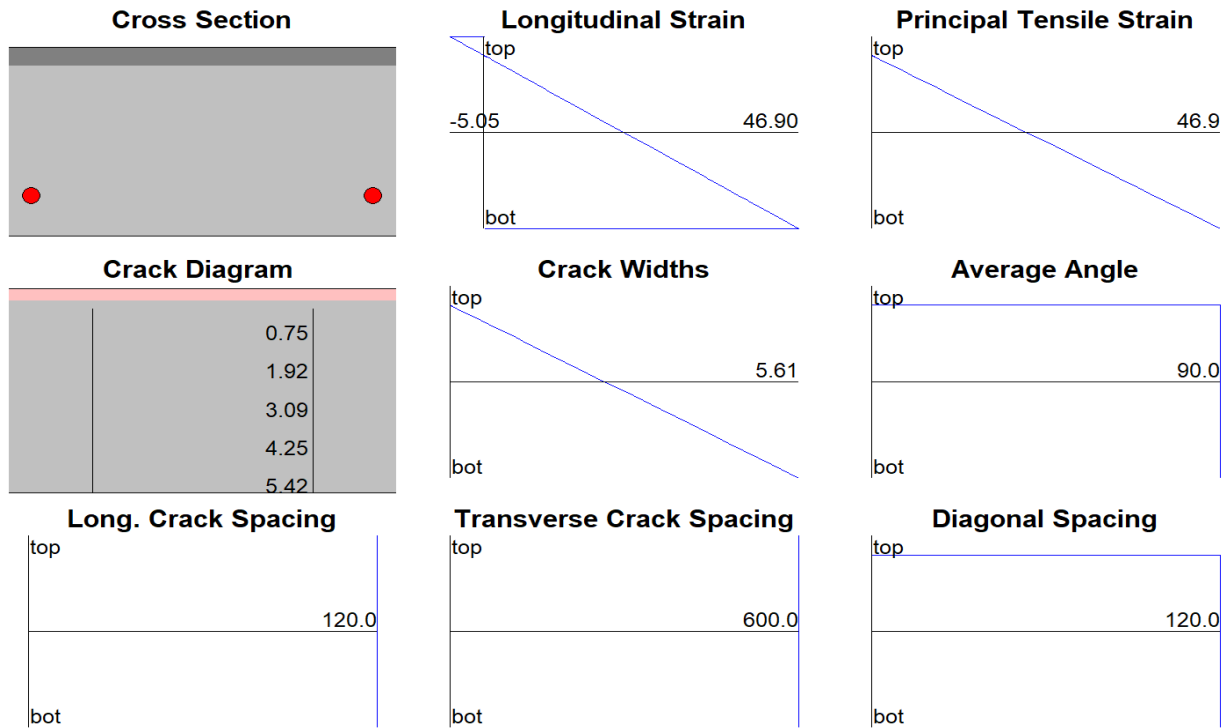


Figure 7.52-Member Crack Data

7.1.16.3. Response-2000: Reinforcement Plots

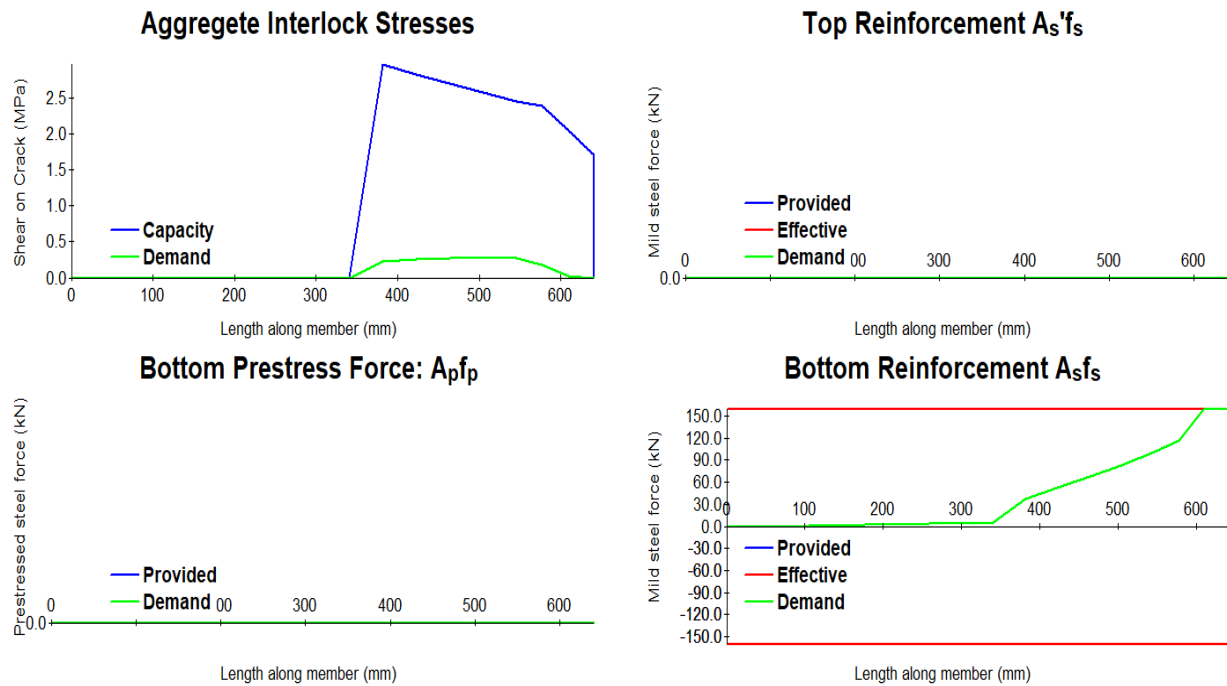


Figure 7.53-Bottom Reinforcing Details

7.1.16.4. Response-2000: No Shear Plots

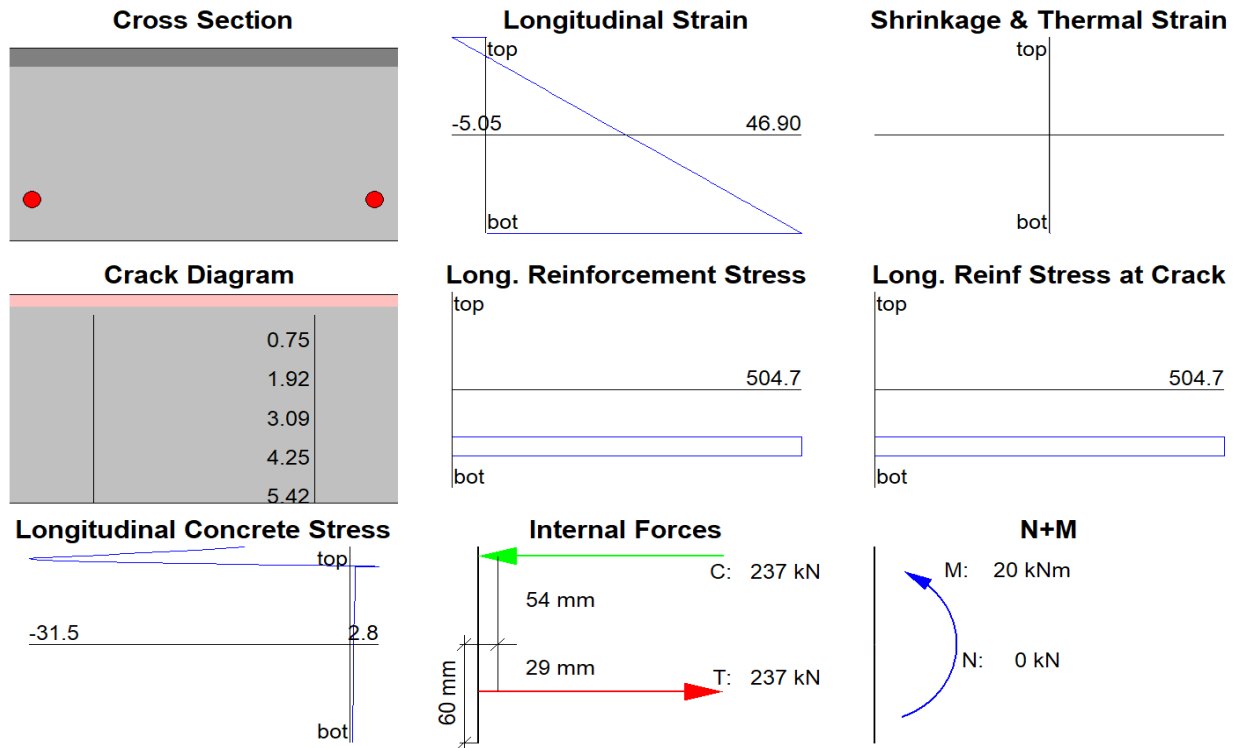


Figure 7.54-Concrete & Steel Stresses

7.1.16.5. Response-2000: Deformation & Rotation Plots

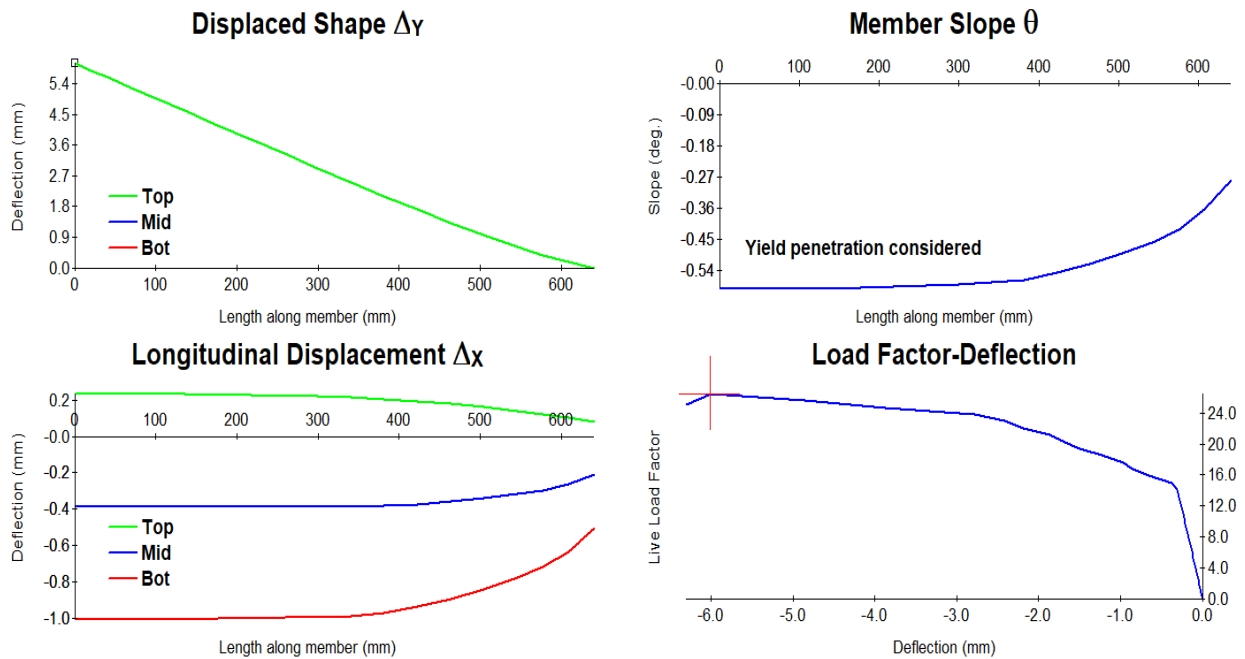


Figure 7.55- The Displacement of the Section, Max-6.01mm

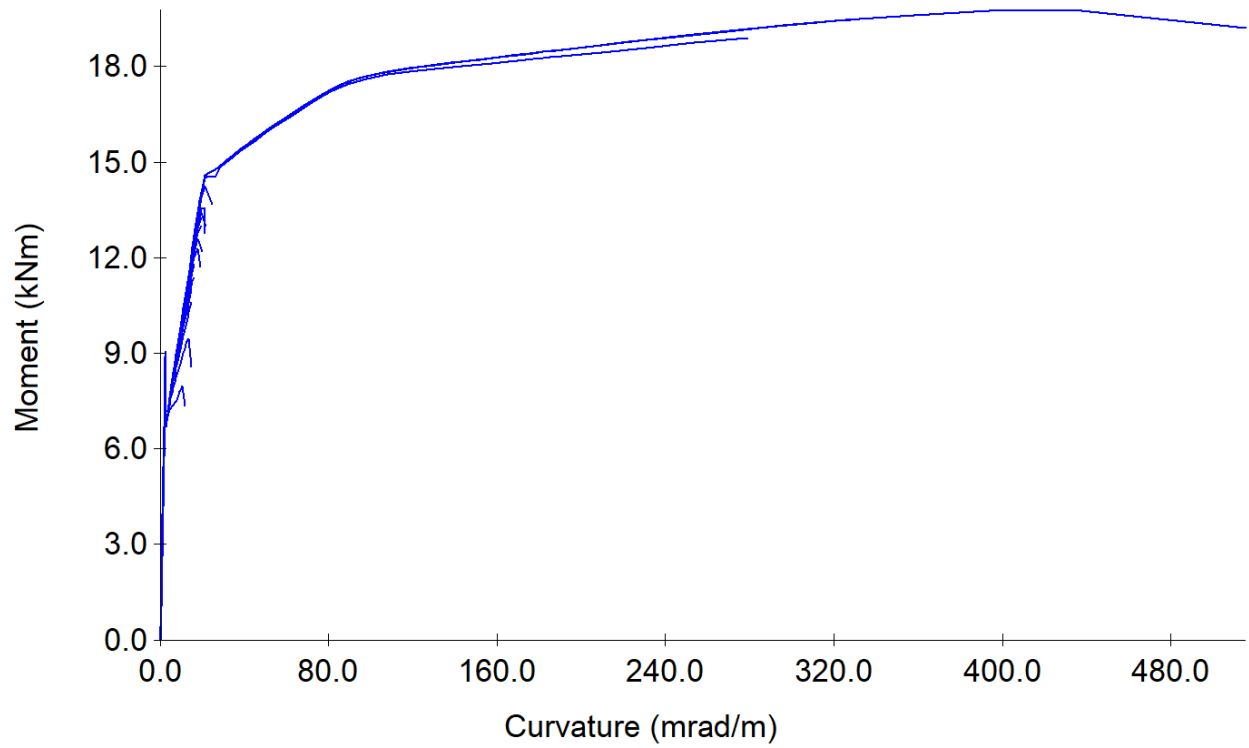


Figure 7.56-Moment vs Curvature, Max= 19.22kNm & 515.34

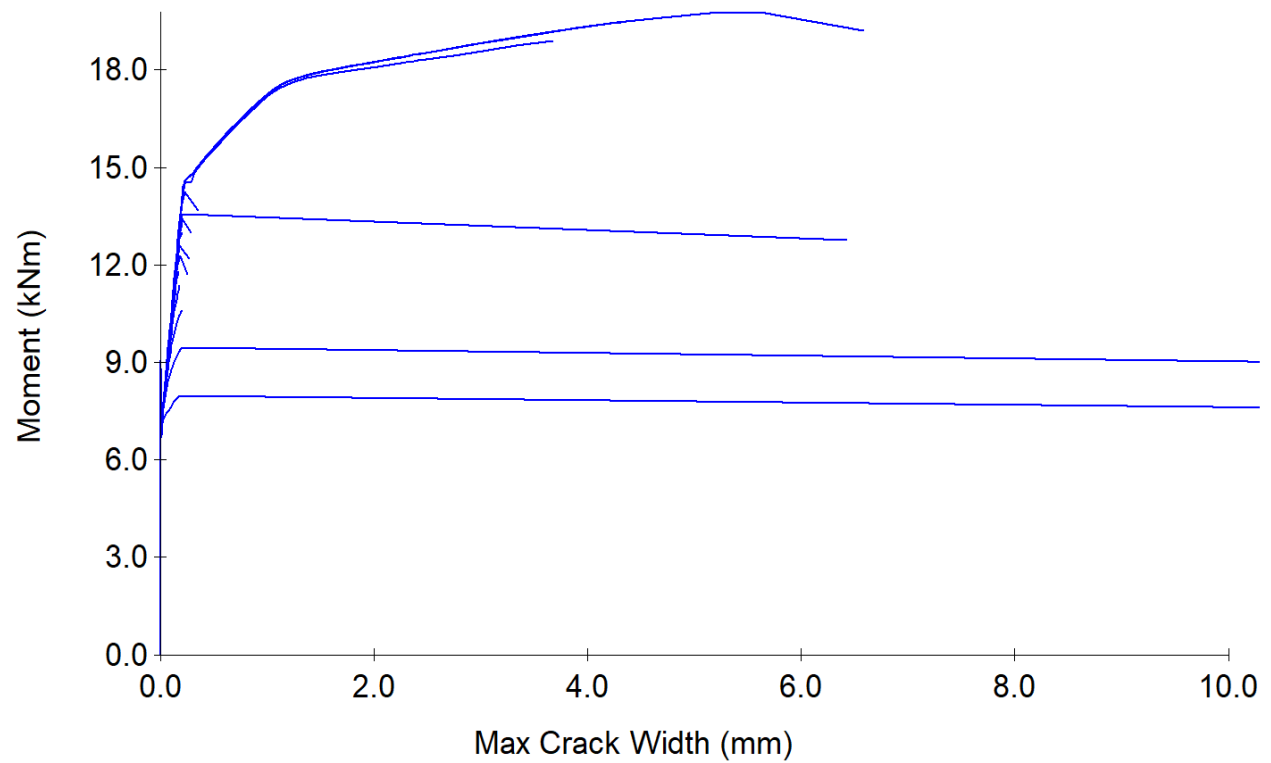


Figure 7.57-Moment vs Maximum Crack Width, Max=6.57mm

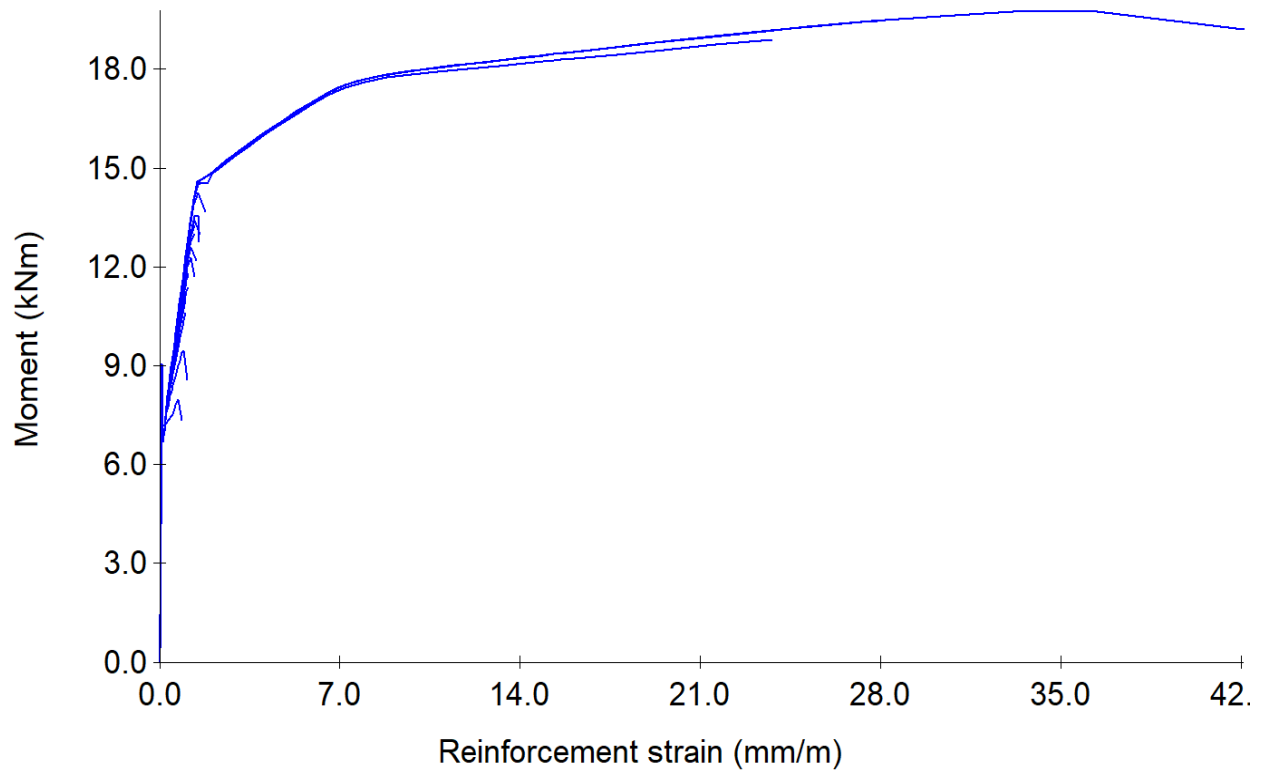


Figure 7.58-Moment vs Reinforcement Strains, Max=42.08mm/m

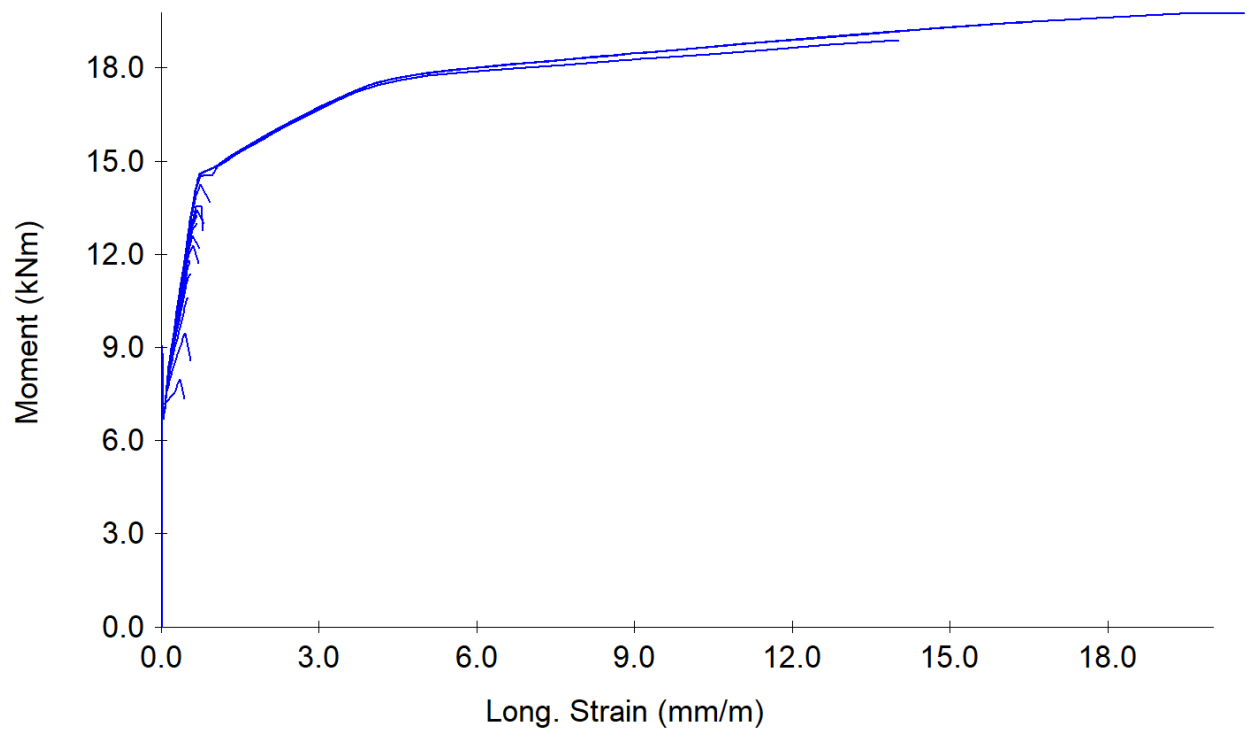


Figure 7.59-Moment vs Longitudinal strain, Max=24.04mm/m

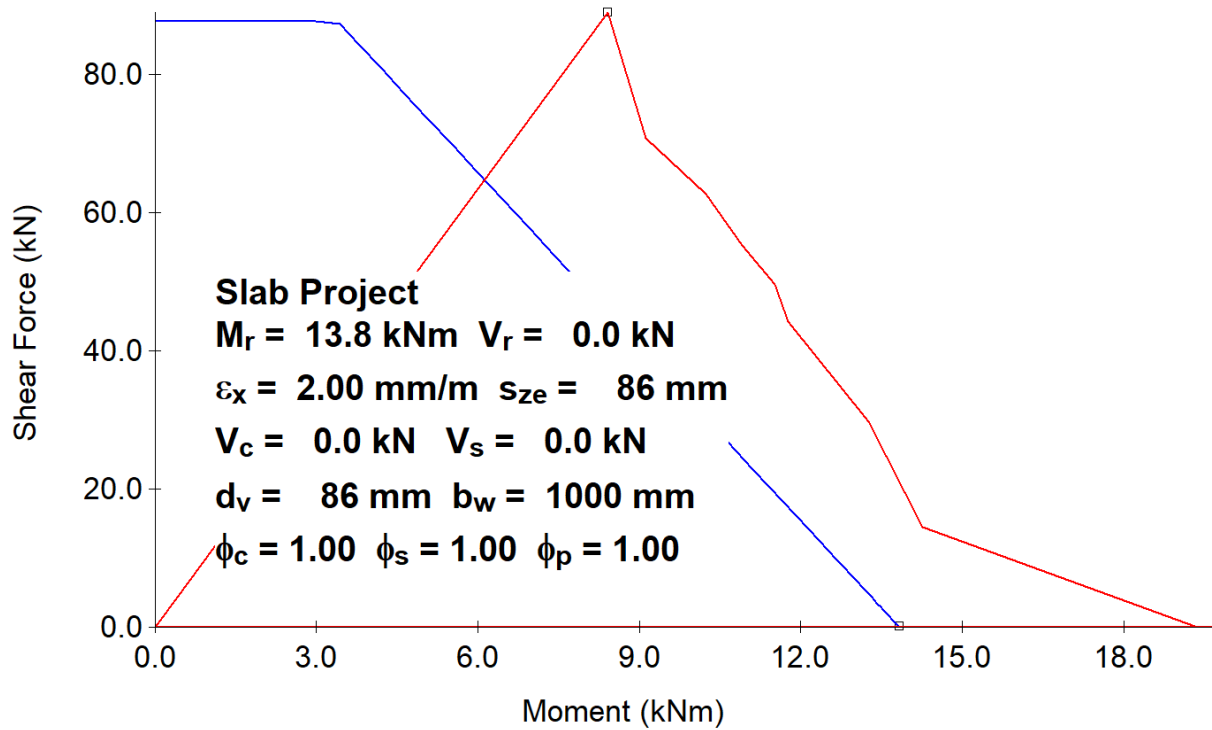


Figure 7.60-CSA 2014 M-V Interaction

7.1.16.6. Response-2000: Moment & Shear

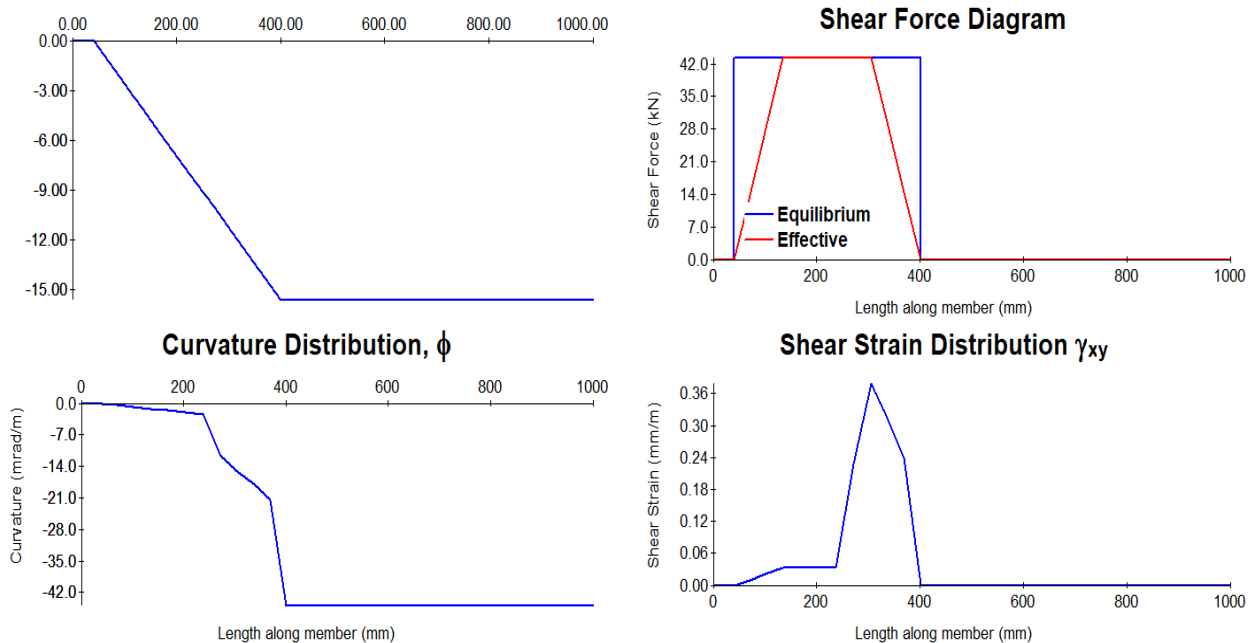


Figure 7.61-Moment & Shear Diagrams

7.1.16.7. Response-2000: Stiffness & Axial

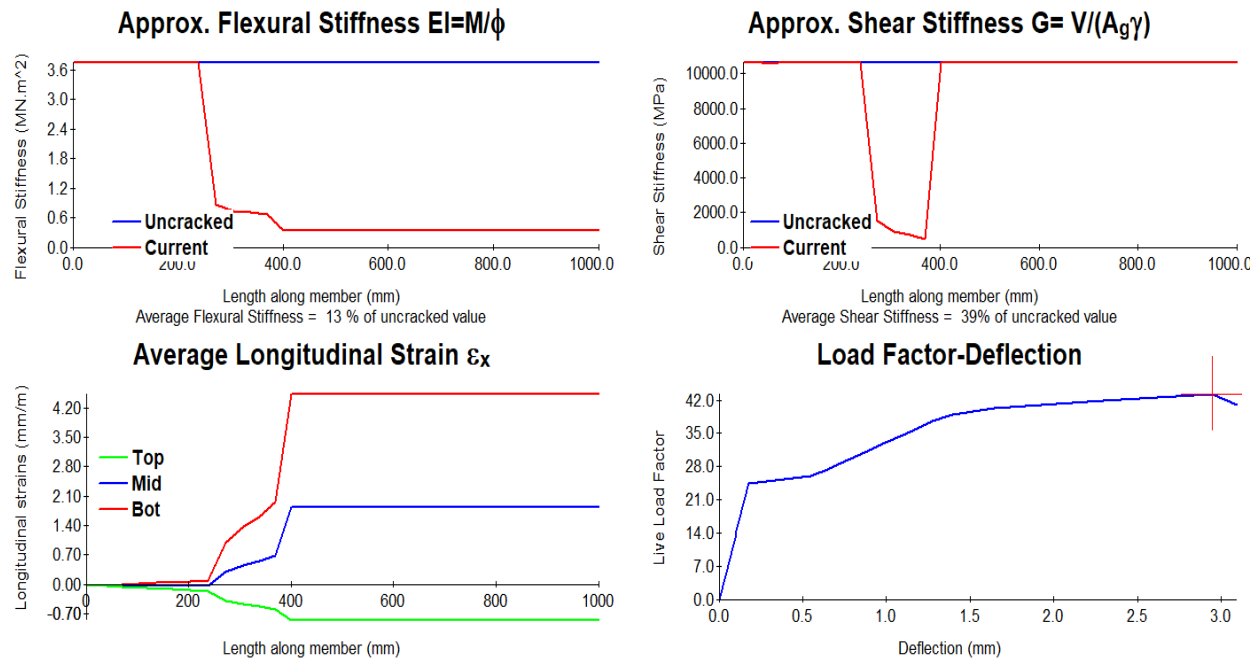


Figure 7.62-Axial & Stiffness Diagram

7.1.17. Slab Capacity

7.1.17.1. Yield line Analysis Results for LC-CFS slab

For LC-CFS slab, the M_r obtained was 13.95kNm. The yield line capacity was 112.57kNm. This is for a compressive strength of 31.56MPa.

7.1.17.2. Response-2000 Slab Capacity

The slab capacity obtained by using the maximum moment of 19.2kNm from the sectional analysis was found to be 205.01kN.

7.1.17.3. FE Slab Capacity Comparison with Yield Line Analysis for LC-CFS Slab

Table 7.13-FEA vs Yield Line Comparison

Slab ID	FEA Capacity (kN)	Yield Line Capacity (kN)	% Difference
LC-CFS	133.080	112.570	16.698

7.1.17.4. FE Slab Capacity Comparison with Response-2000

Table 7.14-FEA vs Yield Line Comparison

Slab ID	FEA Capacity (kN)	Response-2000 (kN)	% Difference
LC-CFS	133.080	205.010	42.550

7.1.18. Slab Deflection

7.1.18.1. Slab Deflection Assessment with the Crossing Beam Method

By using the crossing beam method to estimate the deflection, it found to be 11.217mm based on the given elastic modulus of the concrete.

7.1.18.2. FE Slab Deflection Comparison with ACI Code (Crossing Beam Method)

Table 7.15-FEA vs Response-2000 Comparison

Slab ID	FEA (mm)	Response-2000 (mm)	% Difference
LC-CFS	5.000	6.010	18.347

7.1.18.3. Crossing Beam Method Results Comparison with Section Analysis Results

Table 7.16-FEA vs Response-2000 Comparison

Slab ID	FEA (mm)	Crossing Beam (mm)	% Difference
LC-CFS	5.000	11.217	76.673

7.1.19. Mohr Circles

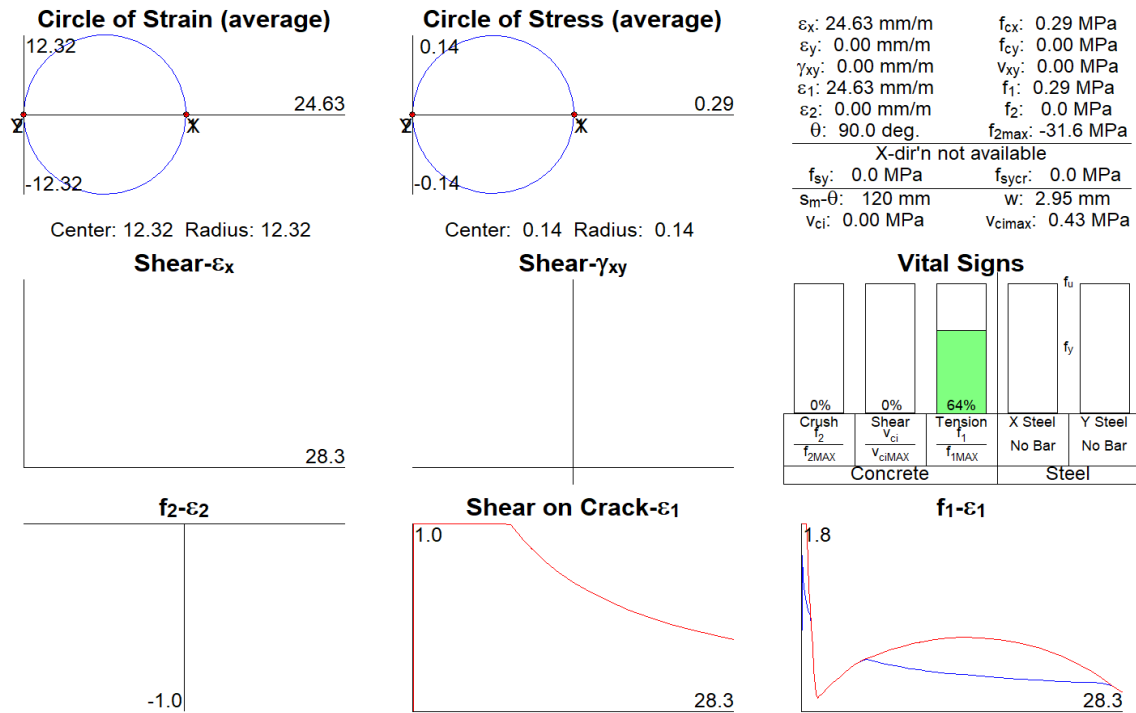


Figure 7.63-Mohr Circles

7.1.9 Summary of Conclusions

The maximum deflection using the crossing method was the slab LC-CFS with 11.217mm. This was more evident where the elastic modulus which indicates the stiffness of the concrete was decreasing and the deflection was increasing.

In general, the analysis from Response-2000 gave a maximum deflection value of 6.37 which was for the natural aggregate concrete slab and the LC-CF slab gave a maximum crack width of 6.58mm, details are shown in table 7.17.

7.1.20. Comparison of the Maximum Crack Widths

Table 7.17- Maximum Crack Widths Comparison of FE & Response-2000

Slab ID	FE Model (mm)	Response-2000(mm)	% Difference
NC	5.53	6.58	17.34
LC-C	5.26	6.53	21.54
LC-CF	5.29	6.58	21.74
LC-CFS	5.42	6.57	19.18

7.1.21. Collapse Load Summary

A summary of the details of the collapse load obtained from the FE Model, Response-2000, and the CSA comparison are presented below in table 7.18.

Table 7.18-Load Comparison

Slab ID	FE Pcol. (kN)	Response-2000 Pcol. (kN)	CSA Pcol. (kN)
NC	147.52	203.62	112.54
LC-C	140.82	205.30	112.59
LC-CF	134.60	205.01	112.41
LC-CFS	133.08	205.01	112.57

7.1.22. Deflection Comparison

A summary of the details of the deflections obtained from the FE Model, Response-2000, and the ACI crossing beam analogy methods are presented below in table 7.19. In addition, table 7.20 and 7.21 shows the summary of the percentage comparison with the FE and the Response-2000 results

Table 7.19-Deflection Comparison

Slab ID	FE δ_{peak} (mm)	ACI (mm)	Response-2000 (mm)
NC	4.00	5.50	6.37
LC-C	4.00	6.30	6.32
LC-CF	5.00	8.90	6.31
LC-CFS	5.00	11.28	6.01

7.1.23. Summary-Percentage Difference of FE Deflection & Response-2000

Table 7.20-Summary: Percentage Comparison of FE Results & Response-2000

Slab ID	FE δ_{peak} (mm)	Response-2000 (mm)	% Difference
NC	4.00	6.37	45.70
LC-C	4.00	6.32	44.96
LC-CF	5.00	6.31	23.17
LC-CFS	5.00	6.01	18.35

7.1.24. Summary-Percentage Difference of ACI Crossing Beam Analogy Deflection Result & Response-2000

Table 7.21- Summary: Percentage Comparison of FE Results & Response-2000

Slab ID	ACI (mm)	Response-2000 (mm)	% Difference
NC	5.50	6.37	14.65
LC-C	6.30	6.32	23.32
LC-CF	8.90	6.31	0.32
LC-CFS	11.28	6.01	60.96

8. CHAPTER EIGHT: CONCLUSIONS & RECOMMENDATIONS

8.1. Conclusions

8.1.1. Materials Characterization

1. In cases where light weight concrete is required, the use of LCC is a viable alternative by increasing the replacement ratio. This was evident in the values obtained for the density of the low carbon concrete.
2. The density of the LCC was found to be inversely proportional to the ratio of recycled materials content. Therefore, an attempt to increase the replacement ratio of the recycled content will subsequently reduce the density.
3. Based on the splitting tensile test result, the use of slag in LCC does not have the tendency to be able to increase the splitting property of the concrete. However, when LC-CF was compared to LC-CFS, with 100% replacement of its fine and coarse aggregate with slag as a supplementary material, the LC-CF showed a 9% decrease in its splitting tensile strength when compared to that of LC-CFS.
4. The elastic modulus of LCC was found to decrease as the replacement ratio of the recycled materials content increased.

8.1.2. Yield Line Analysis

1. The estimation from the yield line analysis based on the assumed failure pattern gave values in the lower bound compared to the FEA values and Response-2000 sectional analysis.
2. Since the collapse load is based on the plastic moment of the section, it does not account for other specific concrete and reinforcement parameters. In addition to this, it gave a lower bound value in comparison to the Response-2000 obtained values.

8.1.3. Finite Element Analysis

1. Results of the FEA analysis showed some agreement with the ACI code limits for deflection. In particular, 50% of the data obtained for the model deflection for the LC-CF and LC-FS showed 0% error when matched with ACI code limits.
2. The FE flexural capacity predictions for the LCC slabs resulted in a of 4.55%, 8.76% and 9.78% decrease in slab capacity as compared to the control slab for the LC-C, LC-CF, and

LC-CFS slabs respectively. Specifically for the NC, LC-C, LC-CF, and LC-CFS, the loads were 147.5kN, 140.8kN, 134.6kN and 133.1kN respectively for the model.

3. The maximum midspan deflections for the LC-CF and LC-CFS were approximately 5mm which were within current ACI code limits.
4. It was reasoned that for LCC slabs, the lower the elastic modulus, while taking cognisance of their increasing fracture energy values, it resulted in their proportional decrease (i.e., in proportional to the percentage of recycled/secondary material content) in maximum load capacity.

8.1.4. Sectional Analysis

1. It analyses the slab taking cognisance of the strength at the said curing date and establish a relationship on how the strength at the age of the concrete can affect other properties of the slab. Results showed that when compared to FEA and yield line, the values were highest and in the upper bound category.
2. It also provides an estimate of the cracking widths obtained in the LCC slabs.
3. The displacement values estimated using the sectional analysis method were found to be higher when compared to the code limits and FEA, and therefore represented an overestimate of deflection.

8.1.5. Deflections Using the Crossing Beam Analogy Method

1. The maximum midspan deflection values obtained using the crossing beam method produced varying values which were in proportion to the elastic modulus of the concrete. The deflection values obtained were 5.5mm, 6.3mm, 8.9mm and 11.2mm for NC, LC-C, LC-CF, and LC-CFS respectively. This therefore implied the decreasing elastic modulus led to larger deflections using the crossing beam analogy method.

8.2. Limitations and Shortcomings of this Research Study

1. The use of sectional analysis was not able to account for the fracture energy of the various LCC mixtures as well as the bond properties.
2. In the use of ATENAGid for the modelling, the bond effect was not also taken into consideration.

8.3. Application of the Research Findings

As a solution for reducing the carbon footprint of our built environment, the use of low carbon concrete in reinforced concrete floor slab systems could be a significant intervention, particularly in urban settings where natural materials must be transported long distances and potential sources of recycled materials are locally available.

8.4. Recommendations for Future Research

Several recommendations for future research have been proposed based on the findings of this research.

1. The punching shear of two-way slabs produced using different strengths of low-carbon concrete should be investigated.
2. Another area worth investigating is the effect of reinforcement bond for various low carbon concretes and its effect on the slab cracking failure pattern, flexural capacity and maximum midspan deflection.
3. Performing a comprehensive life-cycle assessment (LCA) on the use of low-carbon concrete in building floor slabs is recommended.
4. A long-term durability study should be undertaken on how various types of low-carbon concrete affect the durability of the resulting two-way slabs when subjected to freeze-thaw, carbonation, chloride-induced corrosion, etc.

REFERENCES

- [1] “Government of Canada and Cement Association of Canada launch Roadmap to Net-Zero Carbon Concrete by 2050 - Canada.ca.” <https://www.canada.ca/en/innovation-science-economic-development/news/2022/11/government-of-canada-and-cement-association-of-canada-launch-roadmap-to-net-zero-carbon-concrete-by-2050.html> (accessed Sep. 11, 2023).
- [2] O. Ortiz, J. C. Pasqualino, and F. Castells, “Environmental performance of construction waste: Comparing three scenarios from a case study in Catalonia, Spain,” *Waste Manag.*, vol. 30, no. 4, pp. 646–654, Apr. 2010, doi: 10.1016/J.WASMAN.2009.11.013.
- [3] M. L. Berndt, “Properties of sustainable concrete containing fly ash, slag and recycled concrete aggregate,” *Constr. Build. Mater.*, vol. 23, no. 7, pp. 2606–2613, Jul. 2009, doi: 10.1016/J.CONBUILDMAT.2009.02.011.
- [4] L. Ferreira, J. De Brito, and M. Barra, “Influence of the pre-saturation of recycled coarse concrete aggregates on concrete properties,” *Mag. Concr. Res.*, vol. 63, no. 8, pp. 617–627, Aug. 2011, doi: 10.1680/MACR.2011.63.8.617/ASSET/IMAGES/SMALL/MACR63-617-F15.GIF.
- [5] S. Kou, C. P.-C. and building materials, and undefined 2012, “Enhancing the durability properties of concrete prepared with coarse recycled aggregate,” *Elsevier*, Accessed: Aug. 07, 2023. [Online]. Available: <https://www.sciencedirect.com/science/article/pii/S0950061812001092>.
- [6] D. Pedro, J. De Brito, L. E.-C. and B. Materials, and undefined 2014, “Influence of the use of recycled concrete aggregates from different sources on structural concrete,” *Elsevier*, Accessed: Aug. 07, 2023. [Online]. Available: <https://www.sciencedirect.com/science/article/pii/S09500618140094>

- 16.
- [7] X. Li, “Recycling and reuse of waste concrete in China: Part I. Material behaviour of recycled aggregate concrete,” *Resour. Conserv. Recycl.*, vol. 53, no. 1–2, pp. 36–44, Dec. 2008, doi: 10.1016/J.RESCONREC.2008.09.006.
 - [8] J. Pacheco, J. De Brito, J. Ferreira, and D. Soares, “Flexural load tests of full-scale recycled aggregates concrete structures,” *Constr. Build. Mater.*, vol. 101, pp. 65–71, Dec. 2015, doi: 10.1016/J.CONBUILDMAT.2015.10.023.
 - [9] J. Pacheco, J. De Brito, J. Ferreira, D. S.-A. structural journal, and undefined 2015, “Destructive Horizontal Load Tests of Full-Scale Recycled-Aggregate Concrete Structures.,” *researchgate.net*, 2015, doi: 10.14359/51687800.
 - [10] J. Xiao, W. Li, Y. Fan, and X. Huang, “An overview of study on recycled aggregate concrete in China (1996–2011),” *Constr. Build. Mater.*, vol. 31, pp. 364–383, Jun. 2012, doi: 10.1016/J.CONBUILDMAT.2011.12.074.
 - [11] J. Santorsola and J. Santorsola, “Development and Structural Performance Assessment of Low-Carbon Concrete Using Recycled Concrete Aggregates and Secondary Materials,” no. November, 2021.
 - [12] D. Wimpenny, “Low Carbon Concrete – Options for the Next Generation of Infrastructure Concrete Solutions 09 Paper 4a-1,” *Concr. Solut. 09*, no. January 2009, pp. 1–10, 2009.
 - [13] D. Pedro, J. De Brito, and L. Evangelista, “Influence of the use of recycled concrete aggregates from different sources on structural concrete,” *Constr. Build. Mater.*, vol. 71, pp. 141–151, Nov. 2014, doi: 10.1016/J.CONBUILDMAT.2014.08.030.
 - [14] M. Malešev, V. Radonjanin, and S. Marinković, “Recycled Concrete as Aggregate for Structural Concrete Production,” *Sustain. 2010, Vol. 2, Pages 1204-1225*, vol. 2, no. 5, pp. 1204–1225, Apr. 2010, doi: 10.3390/SU2051204.

- [15] M. Gomes and J. De Brito, “Structural concrete with incorporation of coarse recycled concrete and ceramic aggregates: Durability performance,” *Mater. Struct. Constr.*, vol. 42, no. 5, pp. 663–675, Jun. 2009, doi: 10.1617/S11527-008-9411-9/FIGURES/9.
- [16] J. Xiao and T. Ding, “Research on recycled concrete and its utilization in building structures in China,” *Front. Struct. Civ. Eng.*, vol. 7, no. 3, pp. 215–226, Sep. 2013, doi: 10.1007/S11709-013-0212-Z/METRICS.
- [17] C. Hoffmann, S. Schubert, A. Leemann, and M. Motavalli, “Recycled concrete and mixed rubble as aggregates: Influence of variations in composition on the concrete properties and their use as structural material,” *Constr. Build. Mater.*, vol. 35, pp. 701–709, Oct. 2012, doi: 10.1016/J.CONBUILDMAT.2011.10.007.
- [18] “Government of Canada and Cement Association of Canada announce partnership to advance global leadership in low-carbon concrete production - Canada.ca.” <https://www.canada.ca/en/innovation-science-economic-development/news/2021/05/government-of-canada-and-cement-association-of-canada-announce-partnership-to-advance-global-leadership-in-low-carbon-concrete-production.html> (accessed Aug. 20, 2023).
- [19] N. Reis, J. de Brito, J. R. Correia, and M. R. T. Arruda, “Punching behaviour of concrete slabs incorporating coarse recycled concrete aggregates,” *Eng. Struct.*, vol. 100, pp. 238–248, Oct. 2015, doi: 10.1016/J.ENGSTRUCT.2015.06.011.
- [20] B. Fernandes, H. Carré, J. C. Mindeguia, C. Perlot, and C. La Borderie, “Effect of elevated temperatures on concrete made with recycled concrete aggregates - An overview,” *J. Build. Eng.*, vol. 44, p. 103235, Dec. 2021, doi: 10.1016/J.JOBE.2021.103235.
- [21] F. Stochino, L. Pani, L. Francesconi, and F. Mistretta, “Cracking of Reinforced Recycled Concrete Slabs,” *Int. J. Struct. Glas. Adv. Mater. Res.*, vol. 1, no. 1, pp. 3–9, Jan. 2017, doi: 10.3844/SGAMRSP.2017.3.9.
- [22] K. Bremer *et al.*, “Fibre Optic Sensors for the Structural Health

- Monitoring of Building Structures,” *Procedia Technol.*, vol. 26, pp. 524–529, Jan. 2016, doi: 10.1016/J.PROTCY.2016.08.065.
- [23] P. J. M. Monteiro, S. A. Miller, and A. Horvath, “Towards sustainable concrete,” *Nat. Mater.* 2017 167, vol. 16, no. 7, pp. 698–699, Jun. 2017, doi: 10.1038/nmat4930.
- [24] M. Etxeberria, A. R. Marí, and E. Vázquez, “Recycled aggregate concrete as structural material,” *Mater. Struct. Constr.*, vol. 40, no. 5, pp. 529–541, Jun. 2007, doi: 10.1617/s11527-006-9161-5.
- [25] A. M. Knaack and Y. C. Kurama, “Design of concrete mixtures with recycled concrete aggregates,” *ACI Mater. J.*, vol. 110, no. 5, pp. 483–493, 2013, doi: 10.14359/51685899.
- [26] M. Kabir, S. Arefin, and S. Fawzia, “Determination of creep behaviour of concrete made by brick chips in Bangladesh,” *Proc. Australas. Struct. Eng. Conf. 2012*, 2012.
- [27] H. Binici, “Effect of crushed ceramic and basaltic pumice as fine aggregates on concrete mortars properties,” *Constr. Build. Mater.*, vol. 21, no. 6, pp. 1191–1197, Jun. 2007, doi: 10.1016/J.CONBUILDMAT.2006.06.002.
- [28] B. S. Karen Henry, A. Member, and S. Hunnewell Morin, “Frost Susceptibility of Crushed Glass Used as Construction Aggregate,” *J. Cold Reg. Eng.*, vol. 11, no. 4, pp. 326–333, Dec. 1997, doi: 10.1061/(ASCE)0887-381X(1997)11:4(326).
- [29] A. O. Atahan and A. Ö. Yücel, “Crumb rubber in concrete: Static and dynamic evaluation,” *Constr. Build. Mater.*, vol. 36, pp. 617–622, Nov. 2012, doi: 10.1016/J.CONBUILDMAT.2012.04.068.
- [30] K. P. Verian, W. Ashraf, and Y. Cao, “Properties of recycled concrete aggregate and their influence in new concrete production,” *Resour. Conserv. Recycl.*, vol. 133, pp. 30–49, Jun. 2018, doi: 10.1016/J.RESCONREC.2018.02.005.
- [31] J. Xiao, *Modeled recycled aggregate concrete*. 2018.
- [32] H. Yan, Q. Shen, L. C. H. Fan, Y. Wang, and L. Zhang, “Greenhouse gas

- emissions in building construction: A case study of One Peking in Hong Kong,” *Build. Environ.*, vol. 45, no. 4, pp. 949–955, Apr. 2010, doi: 10.1016/J.BUILDENV.2009.09.014.
- [33] D. Wimpenny, “Low Carbon Concrete-Options for the Next Generation of Infrastructure.”
- [34] E. Gartner, “SCIENTIFIC AND SOCIETAL ISSUES INVOLVED IN DEVELOPING SUSTAINABLE CEMENTS,” *Role Cem. Sci. Sustain. Dev. - Proc. Int. Symp. Dedic. to Profr. Fred Glas. Univ. Aberdeen, Scotl.*, pp. 445–458, 2003, doi: 10.1680/ROCSISD.32460.0046.
- [35] P. Purnell and L. Black, “Embodied carbon dioxide in concrete: Variation with common mix design parameters,” *Cem. Concr. Res.*, vol. 42, no. 6, pp. 874–877, Jun. 2012, doi: 10.1016/J.CEMCONRES.2012.02.005.
- [36] D. J. M. Flower and J. G. Sanjayan, “Green house gas emissions due to concrete manufacture,” *Int. J. Life Cycle Assess. 2007 125*, vol. 12, no. 5, pp. 282–288, May 2007, doi: 10.1065/LCA2007.05.327.
- [37] P. J. Nixon, “37-DRC COMMITTEE ~ I Recycled concrete as an aggregate for concrete.”
- [38] K. Wesche and R. R. SCHULZ, “BETON AUS AUFBEREITETEM ALTBETON - TECHNOLOGIE UND EIGENSCHAFTEN,” *BETONTECHNISCHE BERICHTE*, no. 22, 1984.
- [39] A. D. Buck, “Recycled concrete as a source of aggregate,” *This Digit. Resour. was Creat. from scans Print Resour.*, 1976, Accessed: Jul. 15, 2023. [Online]. Available: <https://erdc-library.erdcdren.mil/jspui/handle/11681/11503>.
- [40] S. Frondistou-Yannas, “Waste Concrete as Aggregate for New Concrete,” *J. Proc.*, vol. 74, no. 8, pp. 373–376, Aug. 1977, doi: 10.14359/11019.
- [41] R. Sri, R. Bsc, and C. T. Tam, “Properties of concrete made with crushed concrete as coarse aggregate,” <https://doi.org/10.1680/mac.1985.37.130.29>, vol. 37, no. 130, pp. 29–

- 38, May 2015, doi: 10.1680/MACR.1985.37.130.29.
- [42] M. C. Limbachiya, E. Marrocchino, and A. Koulouris, “Chemical-mineralogical characterisation of coarse recycled concrete aggregate,” *Waste Manag.*, vol. 27, no. 2, pp. 201–208, 2007, doi: 10.1016/J.WASMAN.2006.01.005.
- [43] “Demolition Reuse Conc Mason V2 - Y Kasai - Google Books.” https://books.google.ca/books?hl=en&lr=&id=QXDEEEAAAQBAJ&oi=fnd&pg=PA585&dq=Ikeda+T,+Yamane+S,+Sakamoto+A.+Strengths+of+concrete+containing+recycled+aggregate.+In:+Proceedings+of+the+2nd+international+RILEM+symposium+on+demolition+and+reuse+of+concrete+and+masonry,+Tokyo,+Japan%3B+Nov+1988.+p.+7-11.&ots=8f70Mf5XW8&sig=PK3Hrd_laJfZ9G9iSXADgJtHbis&redir_esc=y#v=onepage&q&f=false (accessed Jul. 15, 2023).
- [44] T. C. Hansen, “Recycled aggregates and recycled aggregate concrete second state-of-the-art report developments 1945-1985,” *Mater. Struct.*, vol. 19, no. 3, pp. 201–246, May 1986, doi: 10.1007/BF02472036/METRICS.
- [45] R. S. Ravindrarajah, Y. H. Loo, and C. T. Tam, “Recycled concrete as fine and coarse aggregates in concrete,” <https://doi.org/10.1680/mac.1987.39.141.214>, vol. 39, no. 141, pp. 214–220, May 2015, doi: 10.1680/MACR.1987.39.141.214.
- [46] K. K. Sagoe-Crentsil, T. Brown, and A. H. Taylor, “Performance of concrete made with commercially produced coarse recycled concrete aggregate,” *Cem. Concr. Res.*, vol. 31, no. 5, pp. 707–712, May 2001, doi: 10.1016/S0008-8846(00)00476-2.
- [47] “Strength and durability characteristics of recycled aggregate concrete - ProQuest.” <https://www.proquest.com/docview/304271671/abstract/F703A63E254545FBPQ/1?accountid=15182> (accessed Jul. 15, 2023).
- [48] M. P. Adams and A. Jayasuriya, “Guideline Development for Use of Recycled Concrete Aggregates in New Concrete,” *ACi*, pp. 1–89, 2019,

- [Online]. Available:
https://www.acifoundation.org/Portals/12/Files/PDFs/ACI_CRC_18-517_Final_report.pdf.
- [49] M. N. Abou-Zeid, M. N. Shenouda, S. L. McCabe, and F. A. El-Tawil, "Reincarnation of Concrete," *Concr. Int.*, vol. 27, no. 2, pp. 53–59, Feb. 2005.
- [50] "Strength and durability characteristics of recycled aggregate concrete - ProQuest."
<https://www.proquest.com/docview/304271671/abstract/284766FDB8B043C9PQ/1?accountid=15182> (accessed Jul. 15, 2023).
- [51] C. Zhou and Z. Chen, "Mechanical properties of recycled concrete made with different types of coarse aggregate," *Constr. Build. Mater.*, vol. 134, pp. 497–506, Mar. 2017, doi: 10.1016/J.CONBUILDMAT.2016.12.163.
- [52] L. Evangelista and J. de Brito, "Mechanical behaviour of concrete made with fine recycled concrete aggregates," *Cem. Concr. Compos.*, vol. 29, no. 5, pp. 397–401, May 2007, doi: 10.1016/J.CEMCONCOMP.2006.12.004.
- [53] A. K. Padmini, K. Ramamurthy, and M. S. Mathews, "Influence of parent concrete on the properties of recycled aggregate concrete," *Constr. Build. Mater.*, vol. 23, no. 2, pp. 829–836, Feb. 2009, doi: 10.1016/J.CONBUILDMAT.2008.03.006.
- [54] M. Kikuchi, Y. Dosho, T. Miura, and M. Narikawa, "APPLICATION OF RECYCLED AGGREGATE CONCRETE FOR STRUCTURAL CONCRETE. PART 1 – EXPERIMENTAL STUDY ON THE QUALITY OF RECYCLED AGGREGATE AND RECYCLED AGGREGATE CONCRETE," *Sustain. Constr. Use Recycl. Concr. Aggreg.*, pp. 157–168, 1998, doi: 10.1680/SCUORCA.27268.0005.
- [55] A. Katz, "Properties of concrete made with recycled aggregate from partially hydrated old concrete," *Cem. Concr. Res.*, vol. 33, no. 5, pp. 703–711, May 2003, doi: 10.1016/S0008-8846(02)01033-5.

- [56] “Effects of Using Recycled Concrete as Aggregate on the Engineering Properties of Concrete | National Symposium on the Use of Recycled Materials in Engineering Construction: 1996; Programme & Proceedings.”
<https://search.informit.org/doi/epdf/10.3316/informit.724989685432808> (accessed Jul. 16, 2023).
- [57] A. M. Neville, “Aggregate Bond and Modulus of Elasticity of Concrete,” *Mater. J.*, vol. 94, no. 1, pp. 71–74, Jan. 1997, doi: 10.14359/287.
- [58] ASTM, “ASTM C 136-06: Standard Test Method for Sieve Analysis of Fine and Coarse Aggregates,” vol. 04, 2006.
- [59] T. C. Hansen, “Recycled aggregates and recycled aggregate concrete second state-of-the-art report developments 1945-1985,” *Mater. Struct.*, vol. 19, no. 3, pp. 201–246, May 1986, doi: 10.1007/BF02472036.
- [60] H. J. Chen, T. Yen, and K. H. Chen, “Use of building rubbles as recycled aggregates,” *Cem. Concr. Res.*, vol. 33, no. 1, pp. 125–132, Jan. 2003, doi: 10.1016/S0008-8846(02)00938-9.
- [61] K. Rahal, “Mechanical properties of concrete with recycled coarse aggregate,” *Build. Environ.*, vol. 42, no. 1, pp. 407–415, Jan. 2007, doi: 10.1016/J.BUILDENV.2005.07.033.
- [62] M. Etxeberria, E. Vázquez, A. Marí, and M. Barra, “Influence of amount of recycled coarse aggregates and production process on properties of recycled aggregate concrete,” *Cem. Concr. Res.*, vol. 37, no. 5, pp. 735–742, May 2007, doi: 10.1016/J.CEMCONRES.2007.02.002.
- [63] R. Movassaghi, “Durability of Reinforced Concrete Incorporating Recycled Concrete as Aggregate (RCA),” 2006.
- [64] A. Gokce, S. Nagataki, T. Saeki, and M. Hisada, “Freezing and thawing resistance of air-entrained concrete incorporating recycled coarse aggregate: The role of air content in demolished concrete,” *Cem. Concr. Res.*, vol. 34, no. 5, pp. 799–806, May 2004, doi: 10.1016/J.CEMCONRES.2003.09.014.

- [65] T. C. Hansen and H. Narud, "Strength of Recycled Concrete Made From Crushed Concrete Coarse Aggregate," *Concr. Int.*, vol. 5, no. 1, pp. 79–83, Jan. 1983.
- [66] J. Xiao and H. Falkner, "Bond behaviour between recycled aggregate concrete and steel rebars," *Constr. Build. Mater.*, vol. 21, no. 2, pp. 395–401, Feb. 2007, doi: 10.1016/J.CONBUILDMAT.2005.08.008.
- [67] V. W. Y. Tam and C. M. Tam, "Crushed aggregate production from centralized combined and individual waste sources in Hong Kong," *Constr. Build. Mater.*, vol. 21, no. 4, pp. 879–886, Apr. 2007, doi: 10.1016/J.CONBUILDMAT.2005.12.016.
- [68] ASTM Committee, "Standard Test Method for Total Evaporable Moisture Content of Aggregate by Drying, ASTM C566-97," *Annu. B. ASTM Stand.*, vol. 97, no. Reapproved 2004, pp. 5–7, 1997.
- [69] D. Sun *et al.*, "Effect of the Moisture Content of Recycled Aggregate on the Mechanical Performance and Durability of Concrete," *Mater.* 2022, Vol. 15, Page 6299, vol. 15, no. 18, p. 6299, Sep. 2022, doi: 10.3390/MA15186299.
- [70] C. S. Poon, Z. H. Shui, L. Lam, H. Fok, and S. C. Kou, "Influence of moisture states of natural and recycled aggregates on the slump and compressive strength of concrete," *Cem. Concr. Res.*, vol. 34, no. 1, pp. 31–36, Jan. 2004, doi: 10.1016/S0008-8846(03)00186-8.
- [71] M. C. Limbachiya, "Coarse recycled aggregates for use in new concrete," *Proc. Inst. Civ. Eng. Eng. Sustain.*, vol. 157, no. 2, pp. 99–106, 2004, doi: 10.1680/ENSU.2004.157.2.99.
- [72] A. Baikerikar, "Issue 6) JETIR (ISSN-2349-5162) JETIR1406019 Journal of Emerging Technologies and Innovative Research (JETIR) www.jetir," vol. 1, p. 472, 2014, Accessed: Jul. 22, 2023. [Online]. Available: www.jetir.org.
- [73] R. S. Paranhos, B. G. Cazaciu, C. H. Sampaio, C. O. Petter, R. O. Neto, and F. Huchet, "A sorting method to value recycled concrete," *J. Clean. Prod.*, vol. 112, pp. 2249–2258, Jan. 2016, doi:

10.1016/J.JCLEPRO.2015.10.021.

- [74] S. Khan, "Evaluation of Mechanical Properties of Recycled Aggregate Concrete," *Masters Theses*, Dec. 2005, Accessed: Jul. 22, 2023. [Online]. Available: https://scholarworks.wmich.edu/masters_theses/4742.
- [75] M. C. Limbachiya, T. Leelawat, and R. K. Dhir, "Use of recycled concrete aggregate in high-strength concrete," *Mater. Struct. Constr.*, vol. 33, no. 9, pp. 574–580, 2000, doi: 10.1007/BF02480538/METRICS.
- [76] L. Zhang, J. Zhang, G. Chen, and G. Lin, "Flexural behavior of hybrid FRP-recycled aggregate concrete-steel hollow beams," *J. Constr. Steel Res.*, vol. 200, p. 107650, Jan. 2023, doi: 10.1016/J.JCSR.2022.107650.
- [77] P. Visintin, L. Dadd, M. Ul Alam, T. Xie, and B. Bennett, "Flexural performance and life-cycle assessment of multi-generation recycled aggregate concrete beams," *J. Clean. Prod.*, vol. 360, p. 132214, Aug. 2022, doi: 10.1016/J.JCLEPRO.2022.132214.
- [78] W. C. Choi and H. Do Yun, "Compressive behavior of reinforced concrete columns with recycled aggregate under uniaxial loading," *Eng. Struct.*, vol. 41, pp. 285–293, Aug. 2012, doi: 10.1016/J.ENGSTRUCT.2012.03.037.
- [79] A. Raza, A. C. Manalo, U. Rafique, O. S. AlAjarmeh, and Q. uz Z. Khan, "Concentrically loaded recycled aggregate geopolymer concrete columns reinforced with GFRP bars and spirals," *Compos. Struct.*, vol. 268, p. 113968, Jul. 2021, doi: 10.1016/J.COMPSTRUCT.2021.113968.
- [80] L. Francesconi, L. Pani, and F. Stochino, "Punching shear strength of reinforced recycled concrete slabs," *Constr. Build. Mater.*, vol. 127, pp. 248–263, Nov. 2016, doi: 10.1016/J.CONBUILDMAT.2016.09.094.
- [81] P. R. L. Lima, J. A. O. Barros, A. B. Roque, C. M. A. Fontes, and J. M. F. Lima, "Short sisal fiber reinforced recycled concrete block for one-way precast concrete slabs," *Constr. Build. Mater.*, vol. 187, pp. 620–634, Oct. 2018, doi: 10.1016/J.CONBUILDMAT.2018.07.184.
- [82] K. Michaud, N. Hoult, A. Lotfy, and P. Lum, "Performance in shear of

- reinforced concrete slabs containing recycled concrete aggregate,” *Mater. Struct. Constr.*, vol. 49, no. 10, pp. 4425–4438, Oct. 2016, doi: 10.1617/S11527-016-0798-4/FIGURES/9.
- [83] H. Yuan, L. Zhu, M. Zhang, and X. Wang, “Mechanical behavior and environmental assessment of steel-bars truss slab using steel fiber-reinforced recycled concrete,” *J. Build. Eng.*, vol. 69, p. 106252, Jun. 2023, doi: 10.1016/J.JOBE.2023.106252.
- [84] D. Darwin and C. W. (Charles W. Dolan, *Design of concrete structures - 16 ed - international student edition*. 2021.
- [85] E. S. Hoffman, D. P. Gustafson, and A. J. Gouwens, “One-Way Reinforced Concrete Slabs,” *Struct. Des. Guid. to ACI Build. Code*, pp. 37–54, 1998, doi: 10.1007/978-1-4757-6619-6_3.
- [86] Y. L. Liu, J. Q. Huang, X. Chong, and X. G. Ye, “Experimental investigation on flexural performance of semi-precast reinforced concrete one-way slab with joint,” *Struct. Concr.*, vol. 22, no. 4, pp. 2243–2257, Aug. 2021, doi: 10.1002/SUCO.202000676.
- [87] ACI Committee 318, *Building Code Requirements for Structural Concrete*. 2014.
- [88] S. Alexander, “Strip Method for Flexural Design of Two-Way Slabs,” *Spec. Publ.*, vol. 183, pp. 93–118, May 1999, doi: 10.14359/5536.
- [89] H. MARZOUK, U. A. EBEAD, and K. W. NEALE, “FLEXURAL STRENGTHENING OF TWO-WAY SLABS USING FRPs,” pp. 427–436, Jun. 2003, doi: 10.1142/9789812704863_0039.
- [90] J. H. Chung, H. S. Jung, B. il Bae, C. S. Choi, and H. K. Choi, “Two-Way Flexural Behavior of Donut-Type Voided Slabs,” *Int. J. Concr. Struct. Mater.*, vol. 12, no. 1, pp. 1–13, Dec. 2018, doi: 10.1186/S40069-018-0247-6/FIGURES/13.
- [91] S. Lee, K. Hong, Y. Yeon, and K. Jung, “Flexural behavior of rc slabs strengthened in flexure with basalt fabric-reinforced cementitious matrix,” *Adv. Mater. Sci. Eng.*, vol. 2018, 2020, doi: 10.1155/2018/2982784.

- [92] A. J. Pawar, N. S. Mathew, P. D. Dhake, and Y. D. Patil, “Flexural behavior of Two-Way voided slab,” *Mater. Today Proc.*, vol. 65, pp. 1534–1545, Jan. 2022, doi: 10.1016/J.MATPR.2022.04.500.
- [93] H. A. Elgohary, “Supplementary span-to-depth ratio expressions for one-way slab complying with ACI-318 and SBC-304 deflection limits,” *J. Umm Al-Qura Univ. Eng. Archit.* 2023 141, vol. 14, no. 1, pp. 71–78, Mar. 2023, doi: 10.1007/S43995-023-00015-3.
- [94] H. A. Elgohary, “Supplementary span-to-depth ratio expressions for one-way slab complying with ACI-318 and SBC-304 deflection limits,” *J. Umm Al-Qura Univ. Eng. Archit.* 2023 141, vol. 14, no. 1, pp. 71–78, Mar. 2023, doi: 10.1007/S43995-023-00015-3.
- [95] J. Xiao, C. Sun, and X. Jiang, “Flexural behaviour of recycled aggregate concrete graded slabs,” *Struct. Concr.*, vol. 16, no. 2, pp. 249–261, Jun. 2015, doi: 10.1002/SUCO.201400008.
- [96] Csa a23.1-09/a23.2-09, *Concrete materials and methods of concrete construction/Test methods and standard practices for concrete*. 2009.
- [97] T. Galkovski, Y. Lemcherreq, J. Mata-Falcón, and W. Kaufmann, “Fundamental Studies on the Use of Distributed Fibre Optical Sensing on Concrete and Reinforcing Bars,” *Sensors* 2021, Vol. 21, Page 7643, vol. 21, no. 22, p. 7643, Nov. 2021, doi: 10.3390/S21227643.
- [98] K. Soga and L. Luo, “Distributed fiber optics sensors for civil engineering infrastructure sensing,” <https://doi.org/10.1080/24705314.2018.1426138>, vol. 3, no. 1, pp. 1–21, Jan. 2018, doi: 10.1080/24705314.2018.1426138.
- [99] J.-M. Hénault *et al.*, “Application of Distributed Fibre Optical Sensing in Reinforced Concrete Elements Subjected to Monotonic and Cyclic Loading,” *Sensors* 2022, Vol. 22, Page 2023, vol. 22, no. 5, p. 2023, Mar. 2022, doi: 10.3390/S22052023.
- [100] B. G. W Housner *et al.*, “Structural Control: Past, Present, and Future,” *J. Eng. Mech.*, vol. 123, no. 9, pp. 897–971, Sep. 1997, doi: 10.1061/(ASCE)0733-9399(1997)123:9(897).

- [101] S. Villalba and J. R. Casas, "Application of optical fiber distributed sensing to health monitoring of concrete structures," *Mech. Syst. Signal Process.*, vol. 39, no. 1–2, pp. 441–451, Aug. 2013, doi: 10.1016/J.YMSSP.2012.01.027.
- [102] C. K. Y. Leung, "Fiber optic sensors in concrete: the future?," *NDT E Int.*, vol. 34, no. 2, pp. 85–94, Mar. 2001, doi: 10.1016/S0963-8695(00)00033-5.
- [103] H. N. Li, D. S. Li, and G. B. Song, "Recent applications of fiber optic sensors to health monitoring in civil engineering," *Eng. Struct.*, vol. 26, no. 11, pp. 1647–1657, Sep. 2004, doi: 10.1016/J.ENGSTRUCT.2004.05.018.
- [104] M. Majumder, T. K. Gangopadhyay, A. K. Chakraborty, K. Dasgupta, and D. K. Bhattacharya, "Fibre Bragg gratings in structural health monitoring—Present status and applications," *Sensors Actuators A Phys.*, vol. 147, no. 1, pp. 150–164, Sep. 2008, doi: 10.1016/J.SNA.2008.04.008.
- [105] "Fiber Optic Sensors: An Introduction for Engineers and Scientists - Google Books." https://books.google.ca/books?hl=en&lr=&id=Xn_cOnModcMC&oi=fnd&pg=PR7&ots=SdHw2newOS&sig=pflzoVAfu7Fpf7oUkWFior7HuSc&redir_esc=y#v=onepage&q&f=false (accessed Aug. 27, 2023).
- [106] A. Barrias, J. R. Casas, and S. Villalba, "A Review of Distributed Optical Fiber Sensors for Civil Engineering Applications," *Sensors 2016, Vol. 16, Page 748*, vol. 16, no. 5, p. 748, May 2016, doi: 10.3390/S16050748.
- [107] T. G. Giallorenzi *et al.*, "Optical Fiber Sensor Technology," *IEEE Trans. Microw. Theory Tech.*, vol. 30, no. 4, pp. 472–511, 1982, doi: 10.1109/TMTT.1982.1131089.
- [108] "Fiber Optic Sensors - Google Books." https://books.google.ca/books?hl=en&lr=&id=5KdCOguH9CsC&oi=fnd&pg=PP1&ots=WODDAh-ymh&sig=zntoCeXR5nO1CWCW5Jh-rI4CPdE&redir_esc=y#v=onepage&q&f=false (accessed Aug. 27,

2023).

- [109] Z. Ding *et al.*, “Distributed Optical Fiber Sensors Based on Optical Frequency Domain Reflectometry: A review,” *Sensors* 2018, Vol. 18, Page 1072, vol. 18, no. 4, p. 1072, Apr. 2018, doi: 10.3390/S18041072.
- [110] C. G. Berrocal, I. Fernandez, and R. Rempling, “Crack monitoring in reinforced concrete beams by distributed optical fiber sensors,” *Struct. Infrastruct. Eng.*, vol. 17, no. 1, pp. 124–139, 2021, doi: 10.1080/15732479.2020.1731558.
- [111] L. Palmieri, “Distributed Optical Fiber Sensing Based on Rayleigh Scattering,” *Open Opt. J.*, vol. 7, no. 1, pp. 104–127, Jan. 2014, doi: 10.2174/1874328501307010104.
- [112] A. Sang *et al.*, “Millimeter resolution distributed dynamic strain measurements using optical frequency domain reflectometry,” <https://doi.org/10.1117/12.885946>, vol. 7753, no. 17, pp. 432–435, May 2011, doi: 10.1117/12.885946.
- [113] L. Buda-Ozóg *et al.*, “Distributed fibre optic sensing: Reinforcement yielding strains and crack detection in concrete slab during column failure simulation,” *Measurement*, vol. 195, p. 111192, May 2022, doi: 10.1016/J.MEASUREMENT.2022.111192.
- [114] X. Bao, T. Bremner, M. DeMerchant, and A. Brown, “Structural monitoring by use of a Brillouin distributed sensor,” *Appl. Opt. Vol. 38, Issue 13*, pp. 2755–2759, vol. 38, no. 13, pp. 2755–2759, May 1999, doi: 10.1364/AO.38.002755.
- [115] T. W. Bremner *et al.*, “Strain measurement in a concrete beam by use of the Brillouin-scattering-based distributed fiber sensor with single-mode fibers embedded in glass fiber reinforced polymer rods and bonded to steel reinforcing bars,” *Appl. Opt. Vol. 41, Issue 24*, pp. 5105–5114, vol. 41, no. 24, pp. 5105–5114, Aug. 2002, doi: 10.1364/AO.41.005105.
- [116] H. Ohno, H. Naruse, M. Kihara, and A. Shimada, “Industrial Applications of the BOTDR Optical Fiber Strain Sensor,” *Opt. Fiber*

- Technol.*, vol. 7, no. 1, pp. 45–64, Jan. 2001, doi: 10.1006/OFTE.2000.0344.
- [117] Y. Goldfeld and A. Klar, “Damage Identification in Reinforced Concrete Beams Using Spatially Distributed Strain Measurements,” *J. Struct. Eng.*, vol. 139, no. 12, p. 04013013, Dec. 2013, doi: 10.1061/(ASCE)ST.1943-541X.0000795/SUPPL_FILE/SUPPLEMENTAL_DATA_ST.1943-541X.0000795_GOLDFELD.PDF.
- [118] J. R. Casas, P. J. S. Cruz, and M. Asce, “Fiber Optic Sensors for Bridge Monitoring,” *J. Bridg. Eng.*, vol. 8, no. 6, pp. 362–373, Nov. 2003, doi: 10.1061/(ASCE)1084-0702(2003)8:6(362).
- [119] M. Enckell, B. Glisic, F. Myrvoll, and B. Bergstrand, “Evaluation of a large-scale bridge strain, temperature and crack monitoring with distributed fibre optic sensors,” *J. Civ. Struct. Heal. Monit.*, vol. 1, no. 1–2, pp. 37–46, Jun. 2011, doi: 10.1007/S13349-011-0004-X/FIGURES/10.
- [120] G. T. Webb, P. J. Vardanega, N. A. Hoult, P. R. A. Fidler, P. J. Bennett, and C. R. Middleton, “Analysis of Fiber-Optic Strain-Monitoring Data from a Prestressed Concrete Bridge,” *J. Bridg. Eng.*, vol. 22, no. 5, p. 05017002, May 2017, doi: 10.1061/(ASCE)BE.1943-5592.0000996/SUPPL_FILE/SUPPLEMENTAL_DATA_BE.1943-5592.0000996_WEBB.PDF.
- [121] J. Xu, Y. Dong, Z. Zhang, S. Li, S. He, and H. Li, “Full scale strain monitoring of a suspension bridge using high performance distributed fiber optic sensors,” *Meas. Sci. Technol.*, vol. 27, no. 12, p. 124017, Nov. 2016, doi: 10.1088/0957-0233/27/12/124017.
- [122] E. Nazarian, F. Ansari, X. Zhang, and T. Taylor, “Detection of Tension Loss in Cables of Cable-Stayed Bridges by Distributed Monitoring of Bridge Deck Strains,” *J. Struct. Eng.*, vol. 142, no. 6, p. 04016018, Jun. 2016, doi: 10.1061/(ASCE)ST.1943-541X.0001463/ASSET/C454C2Ao-118C-4D99-8F01-

17BDECEF6764/ASSETS/IMAGES/LARGE/FIGURE17.JPG.

- [123] A. Güemes, A. Fernandez-Lopez, and P. Fernandez, “Damage Detection in Composite Structures from Fibre Optic Distributed Strain Measurements,” 2014, Accessed: Sep. 10, 2023. [Online]. Available: <https://inria.hal.science/hal-01020392>.
- [124] V. Ungureanu, L. Czechowski, J. Jankowski, and A. Sanduly, “ULTIMATE STRENGTH OF TWCFS MEMBERS UNDER ECCENTRIC COMPRESSION – UPPER-BOUND ESTIMATION VIA,” pp. 1–12, 2023.
- [125] C. Caprani, “Civil Engineering Design (1) Analysis and Design of Slabs,” no. 1, pp. 1–40, 2006.
- [126] E. Mohammed Abdelgadir Ahmed Alasam Supervisor and E. El-Niema, “Yield Line Method Applied to Slabs with Different Supports Partial Fulfilment of requirements for the degree of M.sc. in Structural Engineering,” 2006.
- [127] V. Červenka, L. Jendele, and J. Č. Prague, “ATENA Program Documentation Part 1 Theory Written by,” 2021.
- [128] A. Dmitriev, Y. Novozhilov, D. Mikhalyuk, and V. Lalin, “Calibration and validation of the Menetrey-Willam constitutive model for concrete,” *Constr. Unique Build. Struct.*, vol. 88, no. 8804, p. 8804, 2020, doi: 10.18720/CUBS.88.4.
- [129] J. Červenka and V. Červenka, “Three Dimensional Combined Fracture-Plastic Material Model for Concrete including Creep and Rate Effect for dynamic Loading.”
- [130] M. M. A. Kadhim, A. Jawdhari, A. H. Adheem, and A. Fam, “Analysis and design of two-way slabs strengthened in flexure with FRCM,” *Eng. Struct.*, vol. 256, p. 113983, Apr. 2022, doi: 10.1016/J.ENGSTRUCT.2022.113983.
- [131] G. H. Mahmud, A. M. T. Hassan, S. W. Jones, and G. K. Schleyer, “Experimental and numerical studies of ultra high performance fibre reinforced concrete (UHPFRC) two-way slabs,” *Structures*, vol. 29, pp. 1763–1778, Feb. 2021, doi: 10.1016/J.ISTRUC.2020.12.053.

- [132]A. International and files indexed by mero, “Standard Test Method for Total Evaporable Moisture Content of Aggregate by Drying 1,” Accessed: Sep. 16, 2023. [Online]. Available: www.astm.org.
- [133]ASTM, “ASTM C 127-08: Standard Test Method for Density, Relative Density (Specific Gravity), and Absorption of Fine Aggregate,” pp. 1–7, 2008.
- [134]B. Statements and T. Size, “Standard Test Method for Sieve Analysis of Fine and Coarse Aggregates,” *Annu. B. ASTM Stand.*, vol. 04, no. 571, pp. 5–9, 2011.
- [135]A. C33, “Standard specification for concrete aggregates, ASTM C 33-86,” *Annu. B. ASTM Stand.*, vol. i, 2AD.
- [136]Astm C39/C39M, “Astm C39/C39M,” *Stand. Test Method Compressive Strength Cylind. Concr. Specimens*, vol. 04, no. March, pp. 1–5, 2001.
- [137]Anonim, “ASTM C 469 Standart Test Method For Static Modulus of Elastitisitas and paission’ Ratio of Concrete in Compression.,” vol. i, 2006.
- [138] *Design of concrete structures*. 2021.
- [139]“Liam PhD Thesis.pdf.” .
- [140] fib CEB-FIP, “fib Bulletin No. 65: Model Code for Concrete Structures 2010,” 2012, Accessed: Dec. 08, 2023. [Online]. Available: <https://www.fib-international.org/publications/fib-bulletins/model-code-2010-final-draft,-volume-1-detail.html>.
- [141]R. K. Choubey, S. Kumar, and M. Chakradhara Rao, “Modeling of fracture parameters for crack propagation in recycled aggregate concrete,” *Constr. Build. Mater.*, vol. 106, pp. 168–178, Mar. 2016, doi: 10.1016/J.CONBUILDMAT.2015.12.101.
- [142]B. E, “Sectional analysis of reinforced concrete members- Appendix A: program manuals,” *Ph.D Thesis*, pp. 1–86, 2000.
- [143]F. J. Vecchio and M. De Lorenzi, “Mechanics of Reinforced Concrete Course Notes,” 2009.
- [144] ASTM C171-07, “Standard Specification for Sheet Materials for Curing

Concrete 1,” *ASTM Int.*, pp. 1–2, 2007.

Appendix A: Calculation Sheets

A1 Slab Design

S/No.	Calculation	Values Obtained
1.	<p>Selection of Depth</p> $h_s = 120mm \geq h_s = \frac{l_n(0.6 + \frac{f_y}{1000})}{30}$	120mm - Condition Satisfied
2.	<p>Slab Dimensions</p> <p>Length of long span l_x = 1200 mm</p> <p>length of the short span l_y = 1200 mm</p> <p>Selected thickness of the slab = 1200mm</p> <p>l_y/l_x = 1</p>	Slab is two-way → $l_y/l_x=1$
3.	<p>Characteristics & Materials</p> <p>Live load = 1.9kN/m²</p> <p>Dead load = 0.5kN/m²</p> <p>Concrete Strength = 30MPa</p> <p>Steel Strength = 475N/mm²</p> <p>Unit Weight of Concrete = 24kN/m³</p> <p>Diameter of Rebar = 11.3mm</p> <p>Specified Concrete Cover = 20mm</p>	Use 20mm Cover based on table requirements above
4.	<p>Computation of Loading & Analysis of the Slab</p> <p>Self-weight of the Slab = $0.12 \times 24 = 2.88$ kN/m³</p> <p>Combined Dead Load = $0.5 + 2.88 = 3.38$ kN/m²</p> <p>$W_f = 1.25(\text{Dead Load}) + 1.5(\text{Live load}) = 7.05$ kN/m²</p> <p>$M_f = W_f \times l^2/8 = 1.27$ kN/m²</p> <p>$M_{\text{positive}} = 0.036 \times W_f \times l^2 = 0.036 \times 7.075 \times 1.2 = 0.366$ kNm</p> <p>Factored Moment: $M_o = q_u l_{2a} l_n^2/8 = 7.075 \times 1.2 \times 0.9^2/8 = 0.859$ kNm</p>	

5.	<p>Reinforcement</p> <p>$d = h - \text{cover} - 0.5\phi_{\text{rebar}} = 120 - 20 - 11.2/2 = 94.4\text{mm}$</p> <p>Area of 1 10Mbar = 100mm^2</p> <p>Reinforcement ratio $\rho = \frac{A_s}{bd} = \frac{8 \times 100}{1200 \times 94.4} =$ 0.0071 or 0.71%</p>	0.71% for both directions
6.	<p>Shear Reinforcement & Requirement</p> <p>Not required since 2-way slabs are generally not subjected to shear, In addition, the slab is not subjected to torsion.</p> <p>Therefore, the governing equation is $V_c = \phi_c \lambda \beta \sqrt{f'_c} b_w d_v$ $= 1 \times 1 \times 0.21 \times \sqrt{30} \times 1200 \times 94 = 129\text{kN}$</p>	Not required
7.	<p>Deflection Requirements</p> <p>Actual Span/Depth Ratio < limiting Value</p> <p>$1200/94 = 12.8 < l_n/20$</p>	Condition Satisfied

A2 Yield Line Calculations

$$M_r = \phi_s A_s f_y \left(d - \frac{a}{2}\right) / 10^6$$

$$M_r = 1 * 333 * 400 \frac{94.4 - \frac{0.25}{2}}{10^6} = \mathbf{12.56kNm}$$

The estimation of the load at failure is then calculated using the equation as below:

$$P = \frac{8 * M_p * L}{L - a}$$

$$= \mathbf{133.97kN}$$

To obtain Collapse for the different RC slabs, we use the stress block parameters:

$$M_r = \phi_s A_s f_y \left(d - \frac{a}{2}\right) / 10^6$$

By solving for a and substituting the actual value of f'_c for the different low carbon concrete into the above, we obtain:

$$P_{NC} = 112.54kN$$

$$P_{LC-C} = 112.59kN$$

$$P_{LC-CF} = 112.57kN$$

$$P_{LC-CFS} = 112.57kN$$

A3 Response-2000 Calculations

By substituting the moment obtained from the sectional analysis into the equation below:

$$P = \frac{8 * M_p * L}{L - a}$$

The M_r was found to be 19.5kNm, 19.7kNm, 19.8kNm and 19.8kNm. Therefore:

$$P = \frac{8 * M_p * L}{L - a} = \mathbf{208.00kN}$$

$$P = \frac{8 * M_p * L}{L - a} = \mathbf{210.13kN}$$

$$P = \frac{8 * M_p * L}{L - a} = \mathbf{211.20kN}$$

$$P = \frac{8 * M_p * L}{L - a} = \mathbf{211.20kN}$$

Therefore:

$$P_{NC} = \mathbf{208.00kN}$$

$$P_{LC-C} = \mathbf{210.13kN}$$

$$P_{LC-CF} = \mathbf{211.20kN}$$

$$P_{LC-CFS} = \mathbf{211.20kN}$$

Appendix B: Experimental Testing of Two-Way LCC Slab-Completed Works

B1 Fabrication of the Formwork

The quality of the formwork used for the slabs is important for giving it a smooth finishing surface and important in ensuring structural integrity of the slabs being made. The aim of the slab formwork was to provide a temporary structure for the mixed concrete until the slab perfectly assumes the shape of the formwork and to give it an enclosed space to prevent loss of water by evaporation during the early days of the initial curing.

To achieve this, first the formwork was designed and built using the CSA A23.1[96], AutoCAD, to aid visualization of the formwork before the construction. The form materials and the braces were obtained from IHL, Canada. Therefore, the formwork was constructed with temporary openings which were symmetric joints at the base for the forms to conform with CSA A23.1[96]. The form ply was cut with use of a panel saw in the Wood-work room of the High-Bay Lab. Four sizes of 1200mm ply boards were first cut, for the 4 different slabs and labelled accordingly. Then another 8 ply boards of 1500mm-by-750mm comprising of two per set for each slab was cut and labelled also. Then 8 pairs of ply board measuring 1500mm-by-120mm and another 1200mm-by-120mm was also sawed using the panel saw; and for both 8 pairs 2 each was mandated to be used for each slab. The plane saw as machine as the ability to make horizontal cuts by pushing the play wood along the line or axis where the cut is requires; and has the ability to make vertical cuts by moving the sawing toolbox in the vertical-upward direction and in the vertical-downward direction.

Then the coupling of the form ply was the next task at hand. Since the form was constructed to be temporary according to the standards used, the use of permanent glues was avoided; but screws of at least four in numbers were rather introduced at the ends of the slabs to fasten the cut pieces together and in that regards. The 1200mm-by-1200mm boards were fasted to the 1500mm-by-1500mm boards using 12 screws of 1.5inches using a drill bit. The side boards were then coupled to the end-to-end corners and to the base of the 1200mm-by-1200mm boards which were just one layer in top of the 1500mm-by-1500mm boards.

To provide more restraint and support. Additional 2-by-2 lumber was cut into 1500mm(8Nos.) and 1200(8Nos.) to provide horizontal support and to resist expansive forces due to tear at the base of

the form. These braes were fasted with 2inches screw both vertically and horizontally along the x-axis and y-axis of the erected formwork.

In addition, diagonal braces were provided on the four sides of the each of the slabs prior to the casting and was fastened to the 1500mm-by-1500mm base and to the top of the side forms. Three diagonal braces on the sides (x and y axis) of the forms were provided to further strengthen the forms.

As a final resolute to close of void, and irregularities along any sides of the form planes, a while sealant otherwise referred to as construction adhesive was used to seal off all edges inside the slabs and areas of joints formed in the slab area. This was also to prevent leakage of the concrete slurry, and to provide an idea area to lock in all the contents of the concrete thereby providing a well-defined edge for the slabs that were casted. To then give it a smooth finish surface, the formworks were treated with grease through the internal dimensions of the slab formwork.

Figure B.1, B.2, B.3, and B.4 shows the ideal area formwork design using AutoCAD, the modelling of the formwork using SketchUp, the plane saw cutting machine and the formwork as built in the laboratory.

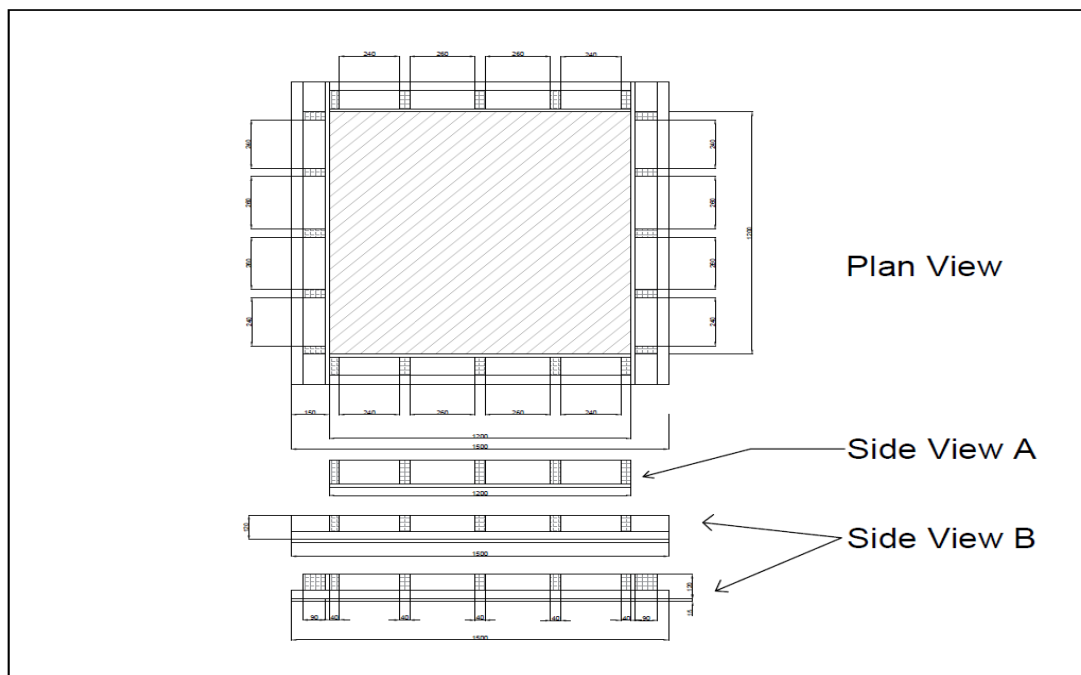


Figure B.1-AutoCAD Formwork Draft

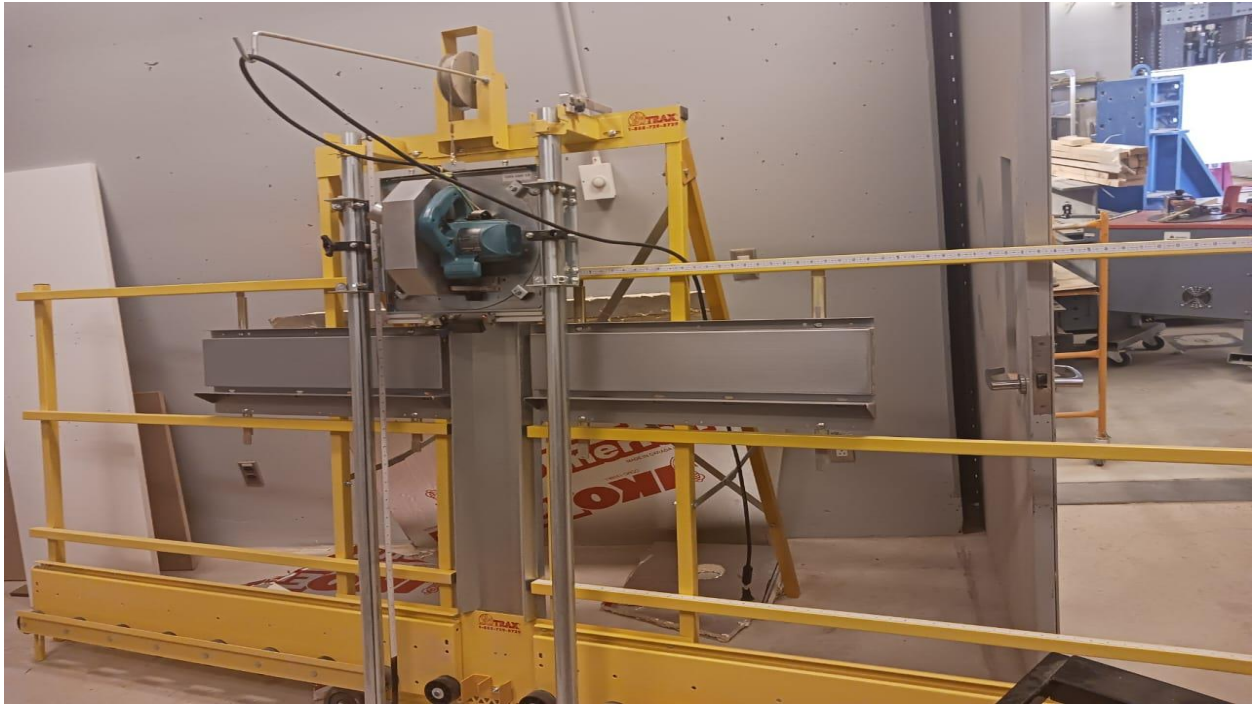


Figure B.2-The Panel Saw



Figure B.3-Clamping of the Form ply during Cutting



Figure B.4-The Erected Slab Formwork/As-built & Application of Sealant

B2 The Reinforcement Work

B2.1 Cutting of the Reinforcement, Anchorage & Bending of the Reinforcement

The use of reinforcement for structural concrete is a very common practice in civil engineering, and therefore proper cutting as regards to lengths, anchorage and bending must be done properly in order not to jeopardize the structural integrity of the reinforced concrete.

In this research, 10M bars were used for the slabs and to begin cutting, the use of personal protective equipment was prioritized (PPE), this included helmet, safety glasses, safety cutting gloves as well as N95 face masks.

To first proceed, the diameter of the reinforcing bars was confirmed to be 100mm² approximately and the diameter was 10mm. Upon confirmation, the tools for the cutting such as the measuring tape, a black colour permanent marker, the tool kit for adjusting the cutting and bending angles. The pedals, cutting ring and the bending ring were tested to be working with a dummy rebar of same dimensions to the experimental material.

Secondly, the cutting length use were measured to be 1320mm and marked out using the black permanent marker. The Rebar Cutting machine known as the FASTCUT Model FRH-850 Bender with cutter head option was used for the cutting and the bending. Therefore 32 number of 1320mm

10M bars were cut by using one and to hold the rebar on the left and using the right hand to hold the sample wated after cutting while at the same time placing the right leg on the pedal to initiate and stop the cutting process respectively. The same number of bars were bent at an angle 90° on both the left- and right-hand side of the rebar to give the anchorage pattern according to the detailing; this was curved to provide the needed lateral support and to improve the shear resistance of the slab. While the cutting box was on the back side of the pedal, the bending was achieved by adjusting the respective programmable bend angle control on the side-side control box of the machine (capable of holding up to 6 angles in memory and increasing accuracy). Upon completion of the cutting and bending the machine was disconnected form the power source and cleaned with a wire brush to remove residual matter and prevent any form of injury to users.

As a precautionary measure during the cutting and pending operation, loose clothing was avoided and the hands and skin and not in contact with the cutting areas or bending region of the machinery and the cutting manual was read in detail to be able to understand the cutting and the bending operations of the machine.



Figure B.5- The FASTCUT Model FRH-850 Bender with Cutter

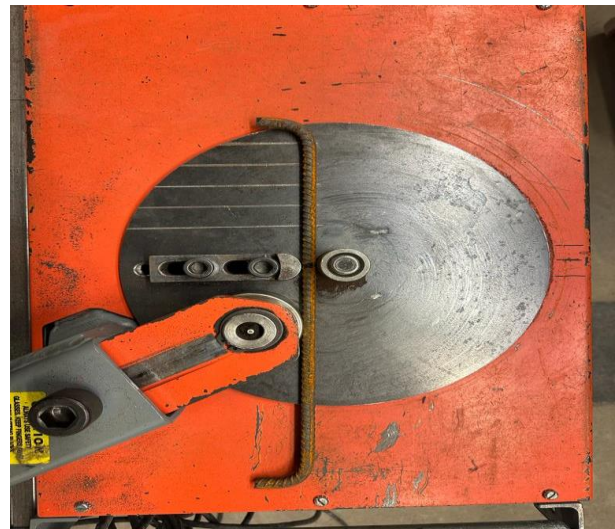


Figure B.6--Sample Test Bending in Progress

B2.2 Placement of the Reinforcement & Spacing

After the cutting and the bending of the rebar had been achieved with respect to the requirements based on the design, the bend up bars were placed in the formwork and the reinforcement were

connected in both directions by the use of rebar ties made up of a wire mesh. The purpose of this was to be able to secure the rebar at its exact position and at the same time to be able to create a stable grid for the application of the distributed fiber optic sensors (DFOS).

The cover dimensions of 20mm were also adhered to; which is the distance between the formwork and the reinforcement placed. This was simply achieved by the use of 3D printed chairs made of filament material and designed as a u-shape with a flat base to be of height of the same height as the concrete cover required. The purpose of these chairs was to provide the reinforcement the needed support due to the concrete weight during the placement and at the same time to secure its current position and alignment as indicated in the design detailed drawing in subsequent section of this thesis. Figure B.7 and B.8 shows the 3D-printed chair and temporary rebar placement respectively.

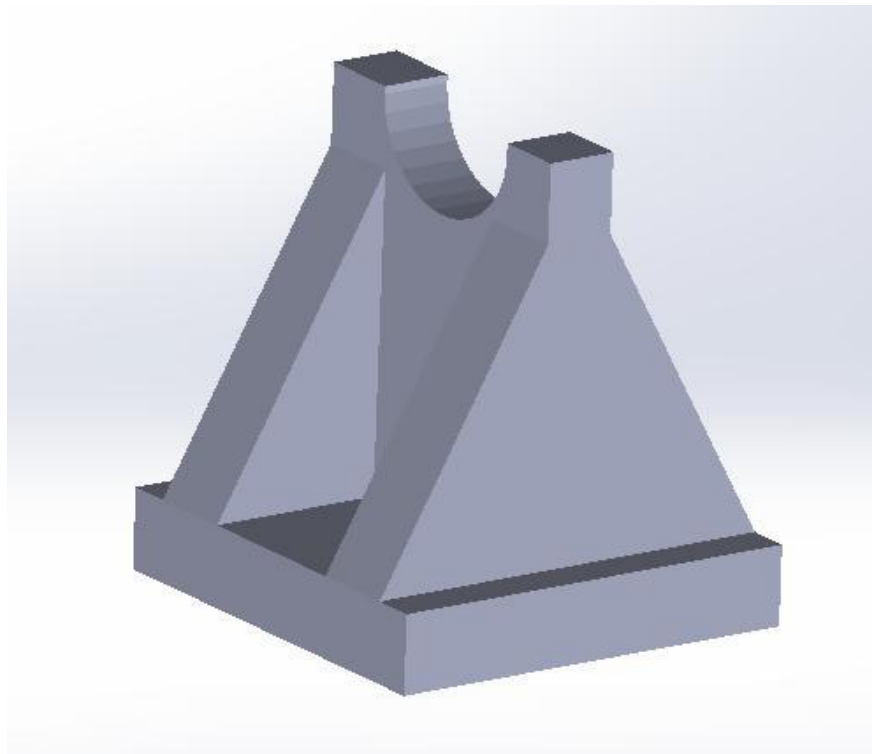


Figure B.7-The 3D Printed Filament Rebar Chair used as Concrete Cover

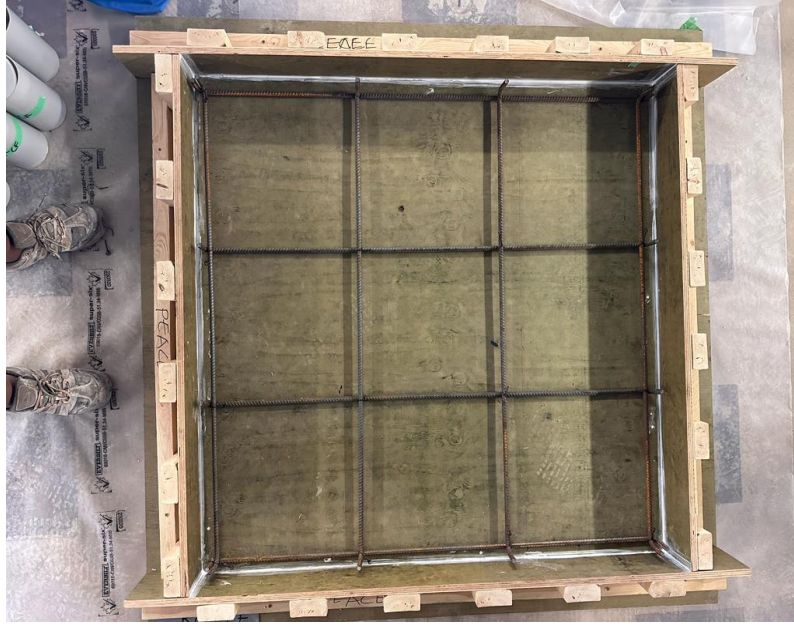


Figure B.8-Temporary Rebar Placement

B3 Concrete Testing Standards

Canada as a country in North America follows a set of provincial and national codes for her testing and standards in construction related projects or for quality control. However, for the purpose of this research, the certain standards have been assessed and have been used in conjunction with other existing Canadian standards and for the investigation of the properties of the fresh and the hardened concrete. While some of them have been mentioned in the previous section of this thesis and report. Other sections under 4.6 of this thesis makes reference to the standards used; and some of them include: ASTM International Standards, and the CSA A23.1/A23.2, popularly referred to as the “Concrete materials and methods of Concrete Construction/Test methods and Standard Practices for Concrete”. While the CSA Standards are known to be jointly published by CSA-Canadian Standards Association, the ASTM is mostly regulated and applicable in America. However, across the world the American set of standards have been adopted for laboratory and field testing in accordance with other nationally used codes in different jurisdiction.

Further discussions on the placement, and testing methodology adopted for the fresh and hardened concrete for this research along side with the pictorial representation are detailed in the sections below.

B3.1 Strain Guage FOS & Instrumentation Design

B3.2 Strain Guage Instrumentation Design

The strain gage instrumentation design plan was carried out utilizing AutoCAD 2-D. In the design, two strain gages were placed at opposite directions corresponding to two adjacent corners of the loading plate by 93mm in the bottom and the top of the concrete by the use special techniques presented in the section below.

The first two strain named SG1 and SG2 were placed at the 407mm from the side surface of the concrete and the third and the fourth strain gages were also placed at distance 407mm for the right hand side of the slab ensuring centredness and alignment with the deformed reinforcing steel bars in embedded into the concrete and these lines were also marked on the top surface of the concrete to capture these approximate points and to be also to obtain the strain on the top layer of the concrete by the use of similar installation approach which is detailed below.

Figure B.9 below shows the configuration.

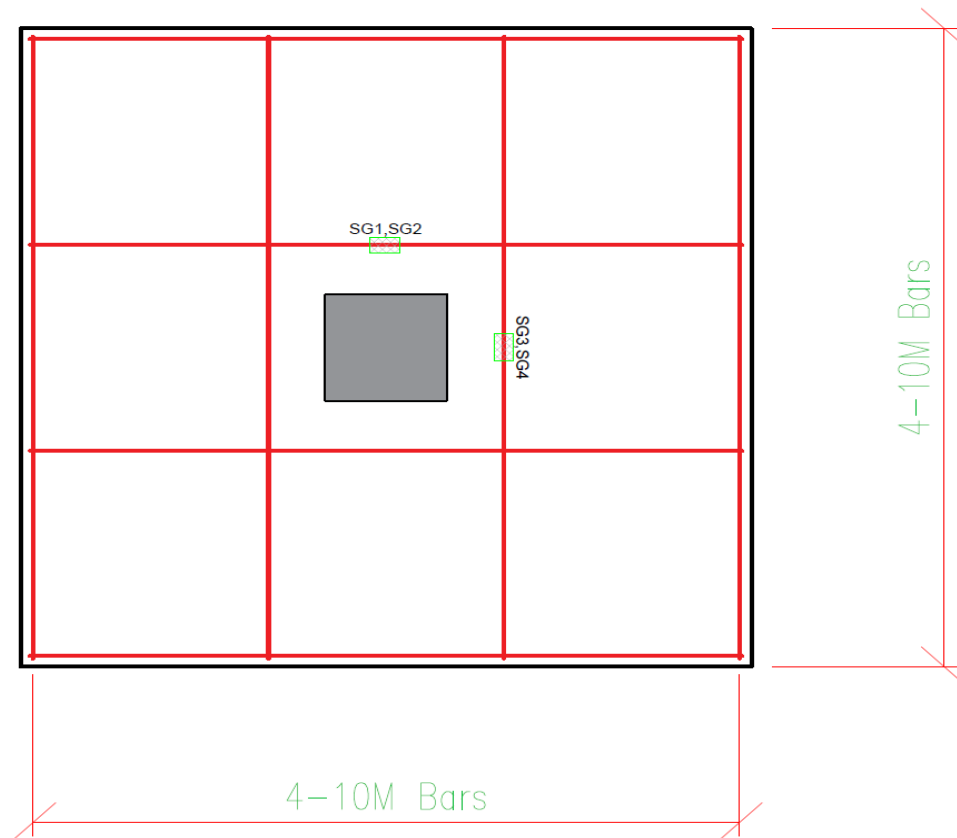


Figure B.9 Rebar & Strain Gage Plan

B3.3 Strain Gauge Application

Strain gages are known to be used to monitor stress and deformation in structural members as applicable to civil engineering. The appropriate materials for the strain gage application were gathered together such as the soldering kit, Kapton tape, Teflon tape, lead wires and multimeter as a calibration device to verify and confirm the accuracy of the strain gage.

Foil strain gages obtained were produced by Showa Measuring Instruments Co., Limited and specification was type N11-FA-5-120-11 with a gauge length of 5mm and a resistance of $120 \pm 0.3\%$ and a gage factor of $2.11 \pm 1\%$ with a thermal output of ± 2 and lot number of 0060-021.

To begin, the rebar was filled up to 10mm and was cleaned with Isopropanol to disinfect and clean contact areas with strain gage. The red, black, and green strain gauge wires were cut opened using a wire cuter. The next process was to obtain the opened ends and twist while ensuring that the soldering kit was being heated up. The strain gauge was exposed carefully and was welded to the black and the white wires. The third wire were trimmed off by the use of a small scissors. Another thing that was done was a 5mm Kapton tape was placed on the area of application to prevent direct contact with the gages, and the gauges extension were protected using a rubber cloves and the strain gages was applied using a gorilla superglue, and a generous amount of liquid rubber compound was placed on the strain gages, and as a final step, Teflon tape was placed and a generous amount of the gorilla epoxy glue was applied suing a cotton bud and was tested to be working by the use of a multimeter. Then zip ties were used to hold the strain gage firmly in position. The strain gages were left to air dry for 48 hours before movement.

Figure B.10 and B.11 shows the specification of the strain gage and the applied strain gages for the rebar in consideration. While other related figures are shown in figure B.12 and figure B.13 respectively.



Figure B.10-Sample Strain Gage Specification



Figure B.11-Applied Strain Gage

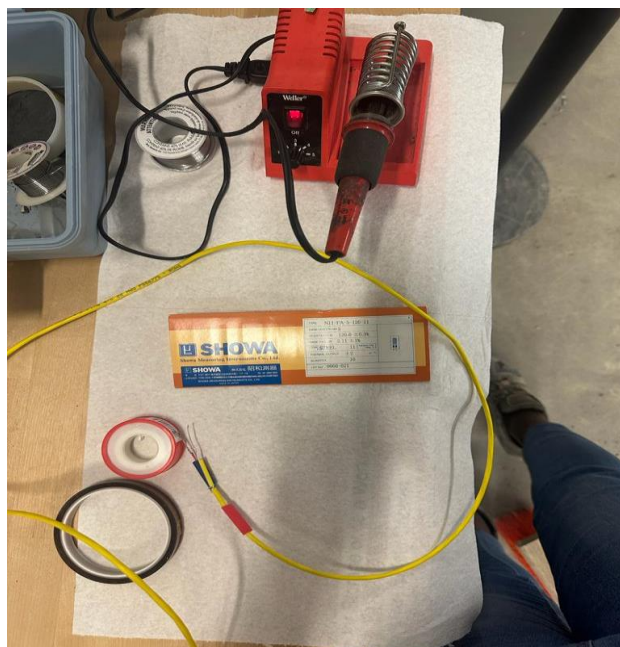


Figure B.12a-Strain Gage Installation Kit

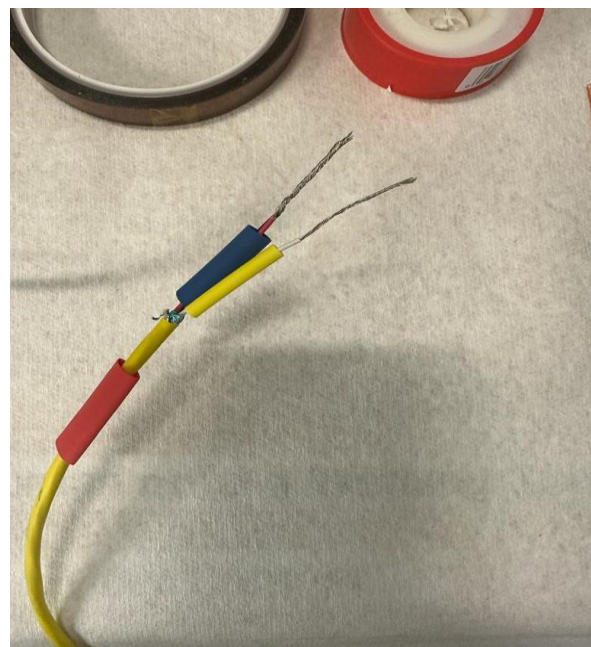


Figure B.12b-Exposure of the strain Gage Wires

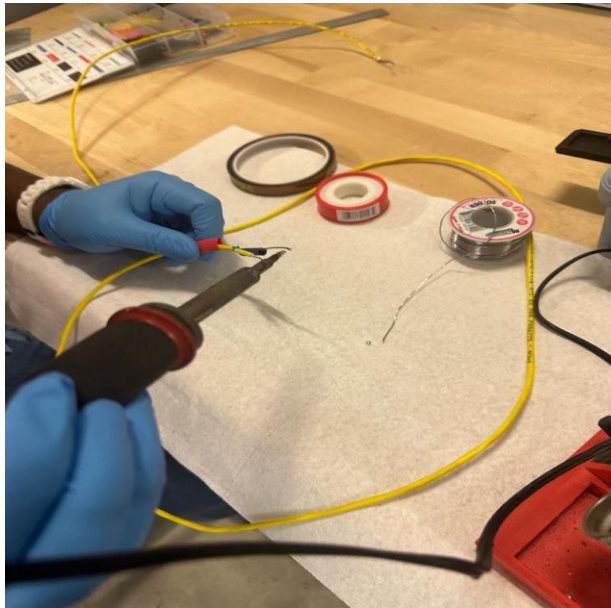


Figure B.12c-Soldering of the Exposed Wires

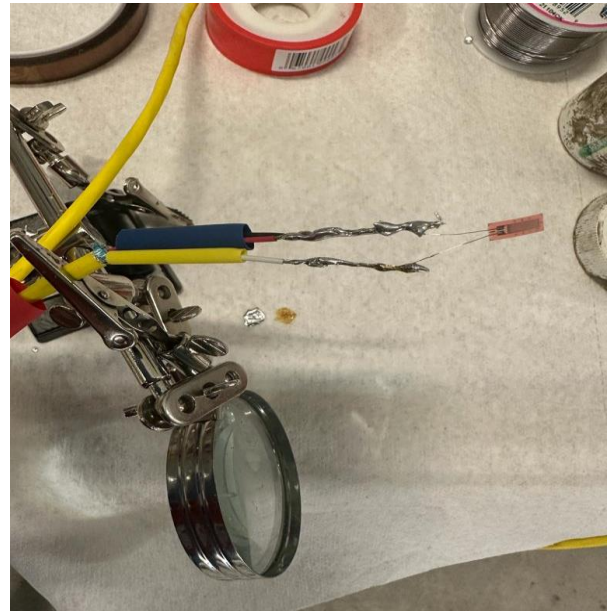


Figure B.12d-Soldering the Strain Gage with Lead wires



Figure 5.13a-Gorilla Two-Part Epoxy



Figure B.13b-Gorilla Superglue



Figure B.13c-Kapton Tape

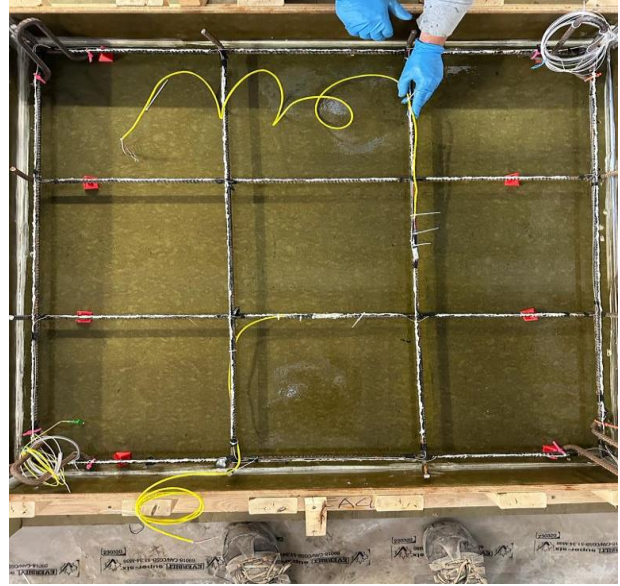


Figure B.13d-Applied Strain Gauges with Wires

B3.3.1 Precautions in Applying Strain Gauge

As a precautionary measure during the application of the strain gauges, liquid contents were kept far as much as possible to prevent any form of short-circuiting and destruction to the strain gauges. Care was taken not to allow the strain gauge wires to be in contact with the rebar using a Kapton tape to secure the connection points and the ends. Figure B.14 shows details.



Figure B.14-Strain Gage Application

B3.4 DFOS Instrumentation & Concreting

DFOS is an acronym for Distributed Fibre Optic Sensing. This involves the instrumentation of the steel bars with the use of fibre optic sensing wires for the purpose of transmitting signals, measuring strain and for structural health monitoring applications. The FOS wires were gently exposed by the use of special DFOS splicing scissors and the exposed fibers were cleaned with isopropanol to prevent dust and contamination of contact points during the when joining with the yellow DFOS patch connectors. A while tube was placed into the white DFOS wire to secure the connecting ends which were subjected to heat after the joining. The DFOS wire and the yellow patch connecting wires were place in the splicing machine after cutting their tips and removing the layers of the fibers on them and were joined together by the use of a heating tube to finish the slicing successfully.

The DFOS sensing wires were measured using a steel table in the High Bay Lab. The wire was attached to the sides of the rebars to capture the yielding strains along the sensing length of the rebars. Firstly, . While the bars were grooved otherwise referred to as deformed, an electrical tape was first used to hold the sensing lengths along the rebar after cleaning adequately with isopropanol. The fibre was then placed along the outline straight line of the rebars by the use of a cotton applicator and a gorilla 2 part epoxy glue. The DFOS was labelled as DFOS T₁, FOS B₁ and FOS T₂ and FOS B₂. The DFOS wires were taken out of the slab using a transparent tube through corners that were less prone to strains when load was being applied and were kept in a transparent polyethene bags to preserve their structure and original condition form moisture and damage due to movement and handling.

The DFOS was allowed to dry, and it was keyed in the LUNA Odisi. Upon the solid formation of the DFOS to the reinforcing bars. A white silicon was applied through out the sensing length of the DFOS wires. The main goal of using the DFOS was to be able to obtain the strain and changes as well as the crack widths that was being formed as a result of the application of loads. Figure B.15 to B.21 shows details of the figures.

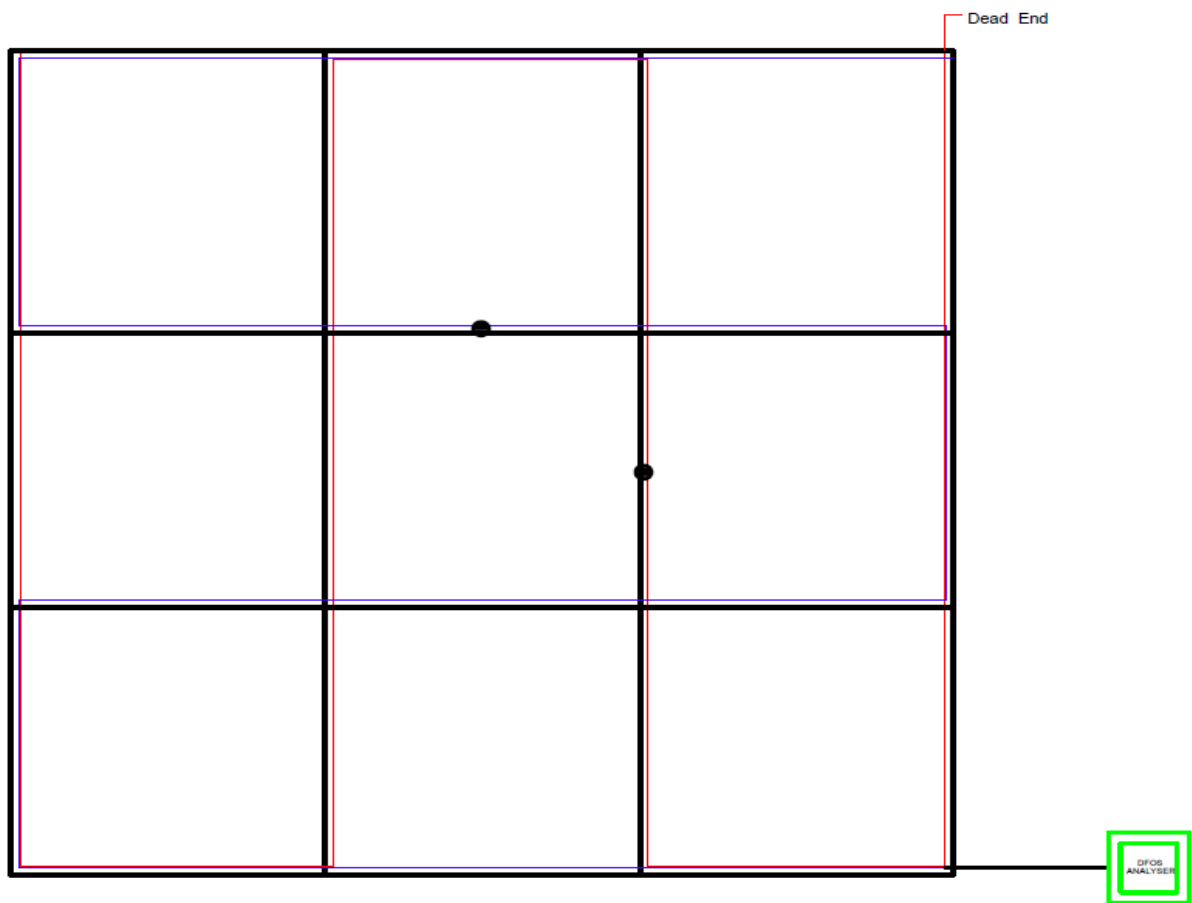


Figure B.15-DFOS Analyser



Figure B.16-DFOS Instrumentation in Progress

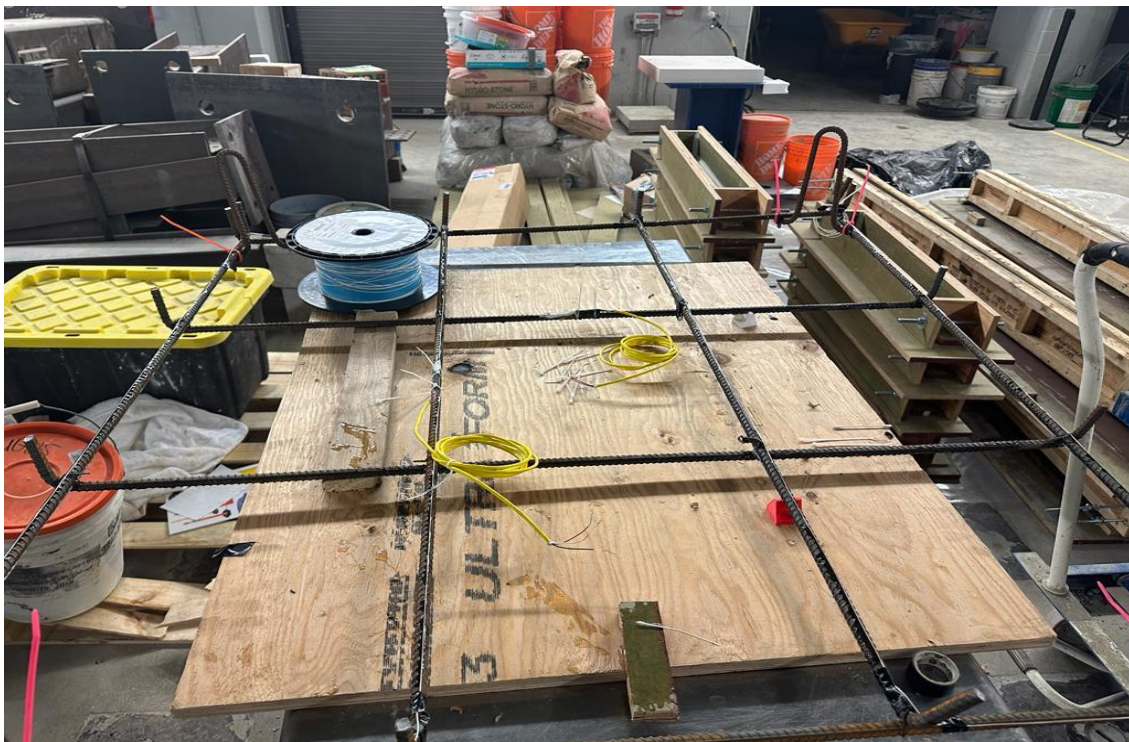


Figure B.17-DFOS After Instrumentation



Figure B.18-DFOS After Silicon Glazing



Figure B.19-DFOS and Strain Gage Wrapped into Polythene Bags

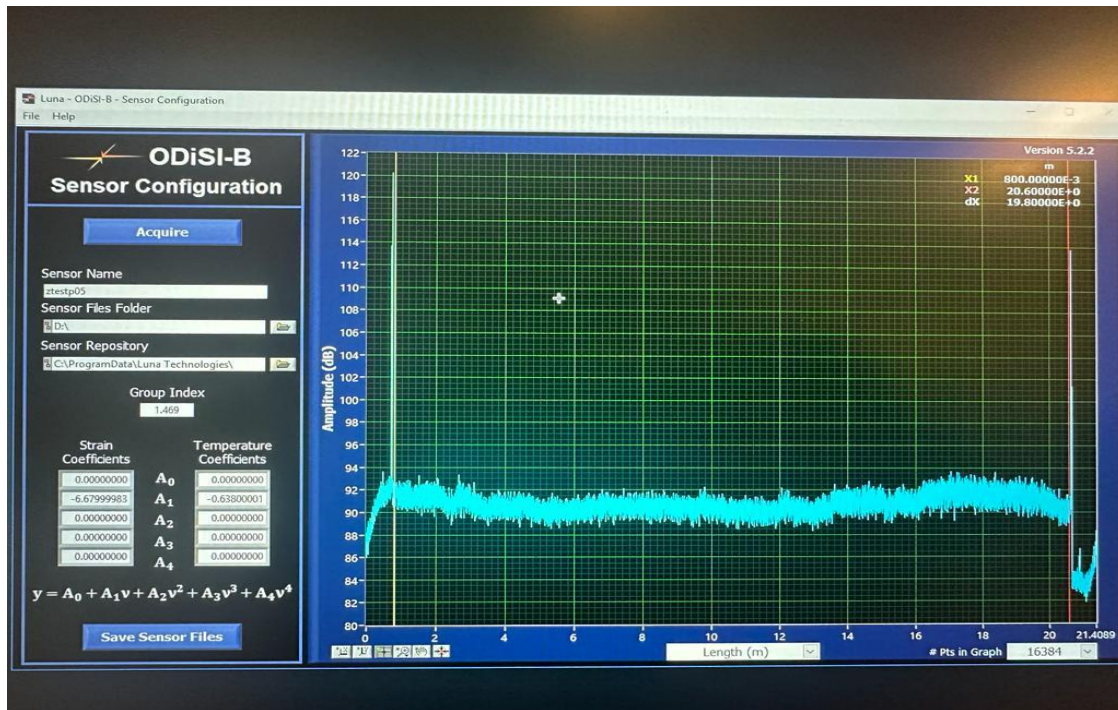


Figure B.20-Acquired Sensor Configuration

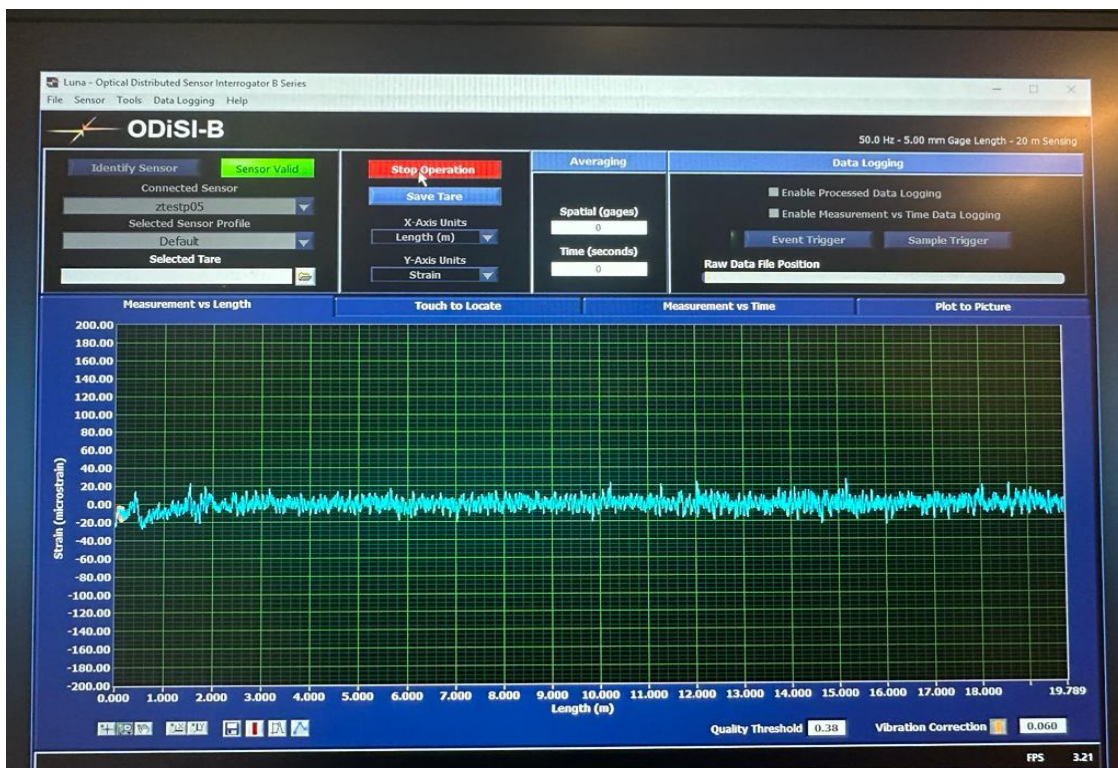


Figure B.21-Acquired Sensor Signal for the LUNA ODiSI-B

B3.4.1 Loops Over Sensing Lengths to Sensing Lengths

The design sensing length were at 1 meter each of both ways of the slab, l_y and l_x to be precise. This also translates from edge of support to edge of support of the slab which was sufficiently able to pick up the distributed strain measurement in the embedded reinforcing bars. This 1m defined the full sensing length of each rebar and for the reinforcement in the longitudinal direction, a total sensing length of 4m and for the transverse reinforcement also a total sensing length of 4m each was also provided. The top of the concrete was further provided with sensing lengths of 2 m each in the x and in the y direction at the middle strips of the slab.

B3.4.2 Intermediary Non-sensing Lengths and Dead Loop

During the fixation of the FOS wires to the rebar, loops were created at intermediary change in directions to sufficiently carry out the signals and pick up the strain measurement distinctively. While gently placing them at corners on the formwork away from sharp edges. Each loop measured approximately 500mm to the next direction of entry with DFOS sensing wire.

B3.4.3 Dead Ends

The dead ends of each sensing wires of the slab were formed but the use of a 1inch slice of pencil encapsulated with an electrical tape to sufficiently close-up the sensing areas and properly lopped during the casting of the slabs.

B3.4.4 Application of Two Part-Epoxy

Gorilla Two-Part epoxy was used for the application of strain gages and for the application of the DFOS to the steel bars. The application of the glue as a powerful agent was seen within few hours of use. It consisted of a resin and a hardener. While the resin provided the adhesive properties, the hardener served as the catalyst which initiated the chemical reaction that transformed the glue from a liquid state to a solid state. Apart from it providing rigidity to the FOS, it also provided a protective covering by linearly bonding it to the sides of the rebars.

B3.4.5 The Pouring of the Fresh Concrete

Prior to the pouring of the concrete in the different slabs, the surfaces of the forms were well prepared by treating it lightly with grease, to serve as a lubricant, to prevent bonding permanently with the forms, and for easy shuttering and striking.

The concrete was conveyed from the large pan mixer into a wheelbarrow and the content were gradually deposited using a scoop and a shovel into the forms and care was taken to prevent concrete from disturbing or hitting the DFOS wires. Further care was also take to prevent segregation of the constituent materials and without adversely affecting the specified qualities of the concrete as specified in CSA A23.1-09[96].

In like manner the concrete cylinders were prepared according to the standards and were given a blow of 25 per layer for 3 layers and the surface was lightly rodded off to give it a smooth appearance and the cylinder was tapped slightly on the sides.

Therefore, in accordance with Section 7.2.4.2, all concrete placed were in horizontal layers and as such permitted proper bonding of subsequent layers. Figure B.22 and B.23 are shown below.



Figure B.22-Preparation for Concrete Placement into Formwork



Figure B.23-Placement of the Concrete

B3.4.6 Vibration Requirement

Based on the requirements specified in the code, mechanical vibrator referred to as a poker vibrator was used to densify the concrete by lightly vibrating the voids in-between the rebar and the top of the concrete, taking into consideration the size of the reinforcement as well as the spaces between the reinforcements. This also aided proper compaction of the concrete and giving it a smooth finishing surface for architectural purposes. It was properly done to prevent honeycombing, segregation, and any defective surface.

B3.4.7 Finishing of the Concrete Surface

Upon reaching the desired volume equivalent to the slab thickness of 120mm, a first trowel was used to screed off excess concrete from the surface and to close out the appearing surface pores to produce a finished surface. After which a Marshalltown 16 inch beveled end magnesium hand float was used to give the concrete a finish. In addition, all diagonal braces were removed and unscrewed from the side walls of the slab formwork. Finally, to give it a flat appearance, a 2-by-2 lumber board was slightly used to light tap the surface of the finished concrete. Figure B.24 shows the finished concrete surface.



Figure B.24: Concrete Finishing

B3.4.8 The Curing Regime of the Fresh Concrete

Since rapid moisture loss in concrete can cause cracks within and outside to develop in the concrete, the curing regime was such that it allows to conceal the moisture at the top by provision of a vapor barrier polyethylene sheeting between the finish operation according to section 7.4.1.2 of CSA A23.1-09 and ASTM C171-07[144]. This was also aimed at eliminating plastic shrinkage cracks that may arise in the hardened concrete.

In addition to this initial process of concealing the moisture, the concrete was allowed to undergo basic air-cure for 3 days before the complete formwork was removed. The slabs were wrapped and water-cured in a damp burlap that was also wrapped with a polythene sheet to prevent leaks or spill and extended wet cured for 30 days each, which was the same benchmark standards used for the cylinders.



Figure B.25-Transportation of the Slab to the Curing Location



Figure B.26-Wrapping and Curing of the Slabs in Progress

Figure B.25 and B.26 shows the hoisting with a crane and the curing of the slabs, while table B.1 shows the allowable curing regimes and as per CSA A23.1-09 which were adopted in this study.

Table B.1-Curing Regimes Based on CSA A23.1-09[96]

Curing Type	Name	Description
1	Basic Curing	3 days to attain 40% of the specified strength
2	Additional Curing	7 days to attain 70% of specified Strength
3	Extended Wet Curing	A wet curing of 7 days

B3.4.9 Shuttering & Formwork Removal & Temporary Storage

The shuttering of the form was achieved by unscrewing the countersunk nails with the use of appropriately sized drilling bit. Also, all diagonal connected hoists were attached to a crane to use to lift up the slabs and detached them, from the base of the formwork. Figure B.27 shows details of the shuttered formwork after 3 days of initial curing.



Figure B.27-Shuttering of the Slabs at 3days of Initial Curing

Appendix C: Experimental Testing of Two-Way LCC Slabs-Future Work

C1 The Set-Up &, DFOS Acquisition & Slab Flexural Response

Four equal sized square slabs measuring 1200mm x 1200mm x 120mm were constructed and were prepared for flexural testing. One slab was produced using conventional concrete and served as the control specimen and the remaining three slabs were produced with three different LCC mixtures of varying recycled/secondary materials content.

The slabs were tested under one point loading and were simply supported on all four sides. To determine the effect that increasing amounts of recycled and secondary materials have on the flexural (moment) capacity, load-deflection response, and crack patterns, LCC slab specimens were compared to the control specimen. The experimental results were then compared to current CSA A23.3-19 code predictions for flexural capacity and maximum deflection to assess the implications for design of two-way slabs produced with LCC.

The Distributed Strain Behaviour of the Two-Way Slabs will be collected in the High Bay Lab of York University **using** the Luna Odisi and the flexural behaviour as well as the capacity of the slab will be compared to the data obtained from the ATENAGid model, **codes**, and the sectional analysis **using** Response 2000. Distributed Fibre Optic Sensing(DFOS) Technology will be used to acquire the distributed strain data of the three low carbon concrete reinforced slabs and as well as the normal concrete slabs as they undergo two-way bending. The data and results obtained will enhance understanding of the impact of these materials on the structural performance of reinforced slabs.

C2 Testing Methodology of the Two-Way Slabs

The testing methodology of the two-way slabs present the steps involved in the experimental testing the procedure for the data collection of the

C2.1 Slab Testing Set-up & Design

Since the two-way slab has already been designed to resist bending by two-way action, the testing methodology will follow suit by taking cognisance of the load applied and the boundary conditions. Four symmetric slabs are expected to be mounted on the steel test frame in the High-Bay Lab of York University. The supports had a total clear span of 900mm on the four sides and each direction had a roller support and a pinned support. The rollers and the pinned supports were

welded to a plate of 100mm thick. The supports centreline was at 100mm from the edge of the slab on the four sides.

Given the boundary conditions, the slabs would be then loaded in flexure with a force of $P(kN)$, while the reactions would be at $P/2$ on the left hand and the right-hand sides of the slabs. To prevent localized failure, they were supported on box steel section and intermediary I-beams spanning between the supports on the x-axis.

The actuator has a known capacity of 250kN and a loading plate of 200mm by 200mm was placed underneath the base of the actuator. To measure the displacement at any given point in time, subject to the application of the load, a series of potentiometer (LPs) was used to obtain the vertical deflections during the tests and the distributed fiber optic strain was measured by using a distributed fiber optic system which is based on the Rayleigh Backscattering Principle. The Slab will then be made to undergo flexural failure and the data obtained will be used to make some conclusions and recommendation about what needs to be done.

As the test proceed, photographs will be obtained that measure the strain and the plates of the bottom steel and top concrete strain will be plotted and the relevant solutions will be made also.

Below are the sketches that show the plan of the tests frame as well as the experimental set-up for the flexural testing.

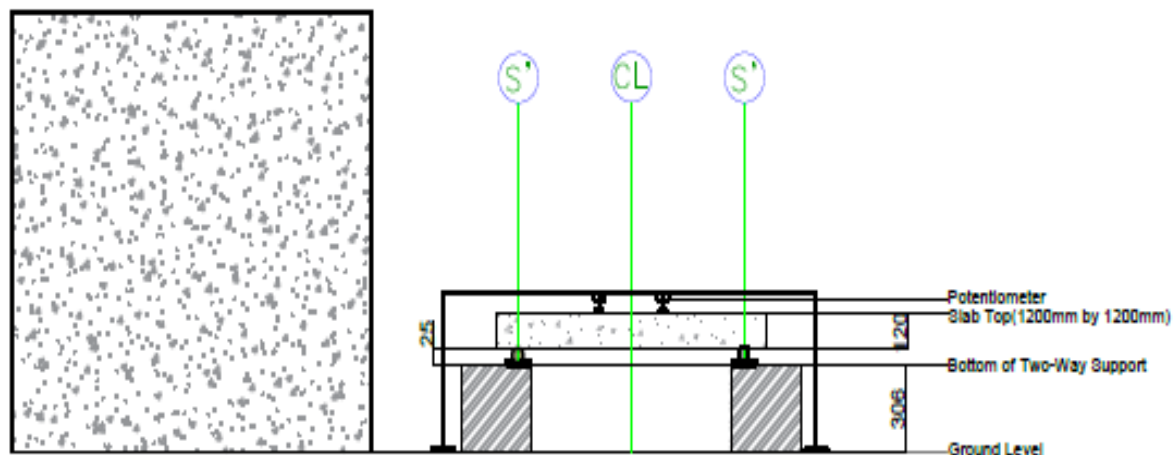


Figure C.1-The Test Frame Set-Up Front View

Appendix D: Material Certificates



Slag Cement
Revision date: September 25, 2020

SAFETY DATA SHEET

8.3 Individual Protection Measures:

Eye/Face Protection: Wear approved tight-fitting chemical safety goggles. Wear a face-shield or full-face respirator when needed to prevent exposure to airborne dusts. Contact lenses should not be worn.

Skin Protection: Wear waterproof, snug-fitting alkali-resistant gloves, boots, knee and elbow pads to prevent skin exposure. Wear protective clothing with long-sleeves and long pants. Protective clothing can be taped inside gloves and boots. Evaluate resistance under conditions of use and maintain protective clothing carefully. Contact safety supplier for specifications. Follow proper procedures for removing gloves.

Respiratory Protection: When dust concentrations in air exceed the occupational exposure guidelines, always wear an approved respirator. Wear an approved air-purifying respirator with an appropriate cartridge, N95 rating or higher. Consult with respirator manufacturer to determine respirator selection, use and limitations.

A respiratory protection program that meets the regulatory requirement, such as OSHA's 29 CFR 1910.134, ANSI Z88.2 or Canadian Standards Association (CSA) Standard Z94.4, must be followed whenever workplace conditions warrant a respirator's use.

Other Protection: Have adequate washing facilities and eyewash fountain readily available in the work area for immediate emergency use.

Every attempt should be made to avoid skin and eye contact with Slag cement. Do not get powder inside boots, shoes or gloves. Do not allow wet, saturated clothing to remain against the skin. Promptly remove clothing and shoes that are dusty or wet with Slag cement mixtures. Wash clothing and shoes thoroughly before reuse.

Do not eat, drink or smoke where this material is handled, stored and processed.

Wash hands thoroughly before eating, drinking and smoking.

Remove contaminated clothing and protective equipment before entering eating areas.

Section 9: Physical and Chemical Properties

9.1 Information on basic physical and chemical properties:	
Appearance:	Solid; grey or white powder
Odour:	Odourless
Odour threshold:	Not applicable
pH:	>8 - 10
Melting point/freezing point:	Not applicable
Initial boiling point and boiling range:	Not applicable
Flash point:	Not applicable
Evaporation rate:	Not applicable
Flammability:	Not flammable or combustible
Upper/lower flammability or explosive limits:	Not applicable
Vapour pressure:	Not applicable
Vapour density:	Not applicable
Relative density:	3.1 – 3.2 (water = 1)
Solubility (ies):	Slightly soluble in water (0.1 – 1%)
Partition coefficient (n-octanol/water):	Not applicable
Auto-ignition temperature:	Not available
Decomposition temperature:	Not available
Viscosity:	Not applicable

Section 10: Stability and Reactivity

10.1 Reactivity:

Reacts slowly with water forming hydrated compounds, releasing heat and an alkaline solution.

10.2 Chemical Stability:

Stable at normal ambient and anticipated storage and handling conditions.

10.3 Possibility of Hazardous Reactions:

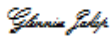
Aqueous solutions are highly alkaline and may corrode aluminum.

10.4 Conditions to Avoid:

Avoid unintentional contact with water / moisture and with strong acids and other incompatible materials.



CERTIFICATE OF ANALYSIS: MISSISSAUGA PLANT
CSA: GROUND GRANULATED BLAST FURNACE "DURA SLAG CEMENT" (TYPE S)

		ANALYSIS OF: May-2022	
	CSA-A3001-18 REQUIREMENTS	LIMITS	RESULTS
PHYSICAL	Fineness 45 µm Sieve (%) Retained	≤ 20	1
	Autoclave % Expansion	≤ 0.5	0.01
	Blaine (m ² /kg)		640
	Air Content (%)		8
	Slag Test Cube Compressive Strength at 7-days (MPa / PSI)		24.2 / 3512
	Control Cement Compressive Strength at 7-days (MPa / PSI)		32.4 / 4701
	Slag Activity Index at 7-day (%)		75
	Slag Test Cube Compressive Strength at 28-days (MPa / PSI) *		41.5 / 6024
	Control Cement Compressive Strength at 28-days (MPa / PSI) *		39.8 / 5772
	Slag Activity Index at 28-day (%) *		104
CHEMICAL	Sulphide Sulphur (%)	≤ 2.5	1.2
	Sulphate Reported as SO ₃ (%)	≤ 4.0	2.9
COMMENTS:			
Parameters with no limit listed are included for information purposes only, and are not requirements of the standards. The reference portland cement used for slag activity testing meets the requirements stated in CSA A3004-C7 clause 4.3(c). * Indicates result from previous month.			
This certifies compliance with CSA-A3001-18 Type S Ground Granulated Blast-Furnace Slag. The data is typical of product shipped by Ash Grove, a Division of CRH Canada Group Inc.. Individual shipments may vary.			
REPORT PREPARED BY:		PRINT DATE:	
 Glennise Jakop, Quality Manager		June 16, 2022	

Ash Grove Cement Company (a CRH Company), Mississauga Cement Plant, 2391 Lakeshore Road West, Mississauga ON, L5J 1K1



Basic Quality Statistical Summary Report

Plant 3N65-FBA DixieYard #2
Product 8941-RC,20-0MM AGGNEO PRO
Specification OPSS Granular A
Period 10/15/2021 - 11/15/2021

Sieve/Test	Tests	Average	Target	Specification
1.06" (26.5mm)	9	100.0		100-100
3/4" (19mm)	9	92.1		85-100
0.530" (13.2mm)	9	75.3		65-90
3/8" (9.5mm)	9	62.7		50-73
#4 (4.75mm)	9	42.5		35-55
#8 (2.36mm)	9	33.3		
#16 (1.18mm)	9	24.5		15-40
#30 (.6mm)	9	16.2		
#50 (.3mm)	9	9.1		5-22
#100 (.15mm)	9	4.6		
#200 (75µm)	9	2.3		2-8
Pan	9	0.0		

Query Query Selections
 Date Created 11/15/2021
 Date Range 10/15/2021 - 11/15/2021
 Plant Cawthra Depot
 Sample Type Shipping



May 5, 2021

Lafarge Canada Inc.

Re: Proctor Values of Aggregate products from: FBA Cawthra Depot

The products listed below are manufactured to meet the OPSS 1010 requirements and tested at source, unless otherwise stated. Although it is not a requirement of OPSS 1010, proctor values are tested internally by Lafarge from time-to-time to determine and track historical data and trends. These values may or may not be representative of the material currently being shipped from source.

Time Period: 2019-2021			
Product Description	Product Code	Max Dry Density (Proctor-Std) (kg/m ³)	Optimum Moisture (Proctor-Std) (%)
RC,20-0MM AGGNEO PRO	8941	1889	13.6
RC,50-0MM AGGNEO PRO	8943	1914	12.9

This data shall only be used for estimating or comparison purposes. Lafarge strongly recommends that the customer utilize an accredited 3rd Party consulting firm to test the aggregate for updated proctor values. Lafarge is pleased to assist in collecting and providing samples for third party testing, at no cost to Lafarge.

If you have any questions or concerns, please feel free to contact me at 905 538-0641.

Yours truly,

Chris Thomas

Chris Thomas
Quality Control Supervisor
WGTA Aggregates

LAFARGE CANADA INC.
6509 Airport Road, Mississauga ON, L4V 1S7
Phone: (905) 738 - 7070
www.buildingbettercities.ca | www.lafarge-na.com

 A member of
LafargeHolcim

SAFETY DATA SHEET

Revision date: August 1, 2023

Section 1: Identification

1.1 Product identifier:

St Marys Portland Cement
 St Marys Portland-Limestone Cement (ENVIROCEM™, Contempra™)

Alternate names:

- CSA A3000 Types GU, MS, MH, HE, LH, HS, GUL, HEL, MHL, LHL
- ASTM C150/AASHTO M85 Types I, IA, II, II-MH, I-II, III, IV, V
- ASTM C595/AASHTO M240 Types IL

1.2 Relevant identified uses of the substance or mixture and uses advised against:

Identified uses:

Industrial uses in manufacture of concrete, mortars and grouts for building materials and pavement.

Uses advised against:

Keep out of reach of children.

1.3 Details of the supplier of the Safety Data Sheet:

St. Marys Cement
 55 Industrial Street
 Toronto, ON
 M4G 3W9

Information Telephone Numbers

In Canada: 1-800-268-6148

In USA: 1-800-462-9157 ext. 537

1.4 Emergency telephone number:

In Canada: 1-813-996-8666 CANUTEC (Call Collect or *666 Cellular)

In USA: 1-800-462-9157

Section 2: Hazards Identification

2.1 Classification of the substance or mixture:

Skin Irritation Cat. 2; H315

Eye Damage Cat. 1; H318

Specific Target Organ Toxicity, Single Exposure, Cat. 3; H335

Carcinogenicity Cat. 1; H350 (inhalation)

Specific Target Organ Toxicity, Repeated Exposure, Cat. 1; H372 (inhalation)

2.2 Label elements:



Danger.

H315: Causes skin irritation.

H318: Causes serious eye damage.

H335: May cause respiratory irritation.

H350: May cause cancer by inhalation.

H372: Causes damage to lungs through prolonged or repeated exposure by inhalation.

Prevention

P201: Obtain special instructions before use.

P202: Do not handle until all safety precautions have been read and understood.

P260: Do not breathe dusts.

P264: Wash hands and exposed skin thoroughly after handling.

P270: Do not eat, drink or smoke when using this product.

P271: Use only outdoors or in a well-ventilated area.

P280: Wear protective gloves/ protective clothing and eye protection/face protection.

Response

P302+ P352: IF ON SKIN: Wash with plenty of water.

P321: Specific treatment: Caustic burns must be treated promptly by a doctor.

SAFETY DATA SHEET

Revision date: August 1, 2023

Section 2: Hazards Identification

2.2 Label elements: (continued)

P301+P330+P331: IF SWALLOWED: Rinse mouth. Do NOT induce vomiting.
P332+P315: If skin irritation occurs: Get medical advice/attention.
P362+P364: Take off contaminated clothing and wash it before reuse.
P305+P351+P338: IF IN EYES: Rinse cautiously with water for several minutes. Remove contact lenses, if present and easy to do. Continue rinsing.
P310: Immediately call a POISON CENTER or doctor.
P314: Get medical advice/attention if you feel unwell.
P304+P340: IF INHALED: Remove person to fresh air and keep comfortable for breathing. P308+P313: If exposed or concerned: Get medical advice/attention.

Storage

P405: Store locked up.
P403+P233: Store in well-ventilated place. Keep container tightly closed.

Disposal

P501: Recycle and or dispose of contents/containers in accordance with local/regional/national/ international regulations.

2.3 Other hazards:

Dusts from this product, when combined with water or sweat, produce a corrosive alkaline solution. The potential exists for static build-up and static discharge when moving cement powders through a plastic, nonconductive, or non-grounded pneumatic conveyance system. Static discharge may result in damage to equipment and injury to workers.

Section 3: Composition/Information on Ingredients

Chemical Name	CAS No.	Wt. %	GHS Classification
Portland Cement	65997-15-1	90 - 100	Skin Irrit. 2; H315 Eye Dam. 1; H318 Skin Sens. 1, H317. STOT SE 3, H335
Calcium oxide	1305-78-8	0.3 – 3.0	Skin Irrit. 2; H315 Eye Dam. 1; H318
Crystalline silica	14808-80-7	0.1 – 1.5	Carc. 1; H350 STOT RE1; H372
Chromate compounds	Not available	<0.1	Not available
Nickel compounds	Not available	<0.1	Not available

Section 4: First Aid Measures

4.1 Description of first aid measures:

Precautions: First aid providers should avoid direct contact with this chemical. Wear chemical protective gloves, if necessary. Take precautions to ensure your own safety before attempting rescue, (e.g. wear appropriate protective equipment).

Inhalation: If breathing is difficult, remove victim to fresh air and keep at rest in a position comfortable for breathing. Seek medical help if coughing or other symptoms persist. Inhalation of large amounts of Portland cement requires immediate medical attention. Call a poison center or doctor. If the individual is not breathing, if breathing is irregular or if respiratory arrest occurs, provide artificial respiration or oxygen by trained personnel. It may be dangerous to the person providing aid to give mouth-to-mouth resuscitation. If unconscious, place in recovery position and get medical attention immediately.
Maintain an open airway.

SAFETY DATA SHEET

Revision date: August 1, 2023

Section 2: Hazards Identification

2.2 Label elements: (continued)

P301+P330+P331: IF SWALLOWED: Rinse mouth. Do NOT induce vomiting.
P332+P315: If skin irritation occurs: Get medical advice/attention.
P362+P364: Take off contaminated clothing and wash it before reuse.
P305+P351+P338: IF IN EYES: Rinse cautiously with water for several minutes. Remove contact lenses, if present and easy to do. Continue rinsing.
P310: Immediately call a POISON CENTER or doctor.
P314: Get medical advice/attention if you feel unwell.
P304+P340: IF INHALED: Remove person to fresh air and keep comfortable for breathing. P308+P313: If exposed or concerned: Get medical advice/attention.

Storage

P405: Store locked up.
P403+P233: Store in well-ventilated place. Keep container tightly closed.

Disposal

P501: Recycle and or dispose of contents/containers in accordance with local/regional/national/ international regulations.

2.3 Other hazards:

Dusts from this product, when combined with water or sweat, produce a corrosive alkaline solution. The potential exists for static build-up and static discharge when moving cement powders through a plastic, nonconductive, or non-grounded pneumatic conveyance system. Static discharge may result in damage to equipment and injury to workers.

Section 3: Composition/Information on Ingredients

Chemical Name	CAS No.	Wt. %	GHS Classification
Portland Cement	65997-15-1	90 - 100	Skin Irrit. 2; H315 Eye Dam. 1; H318 Skin Sens. 1, H317. STOT SE 3, H335
Calcium oxide	1305-78-8	0.3 – 3.0	Skin Irrit. 2; H315 Eye Dam. 1; H318
Crystalline silica	14808-60-7	0.1 – 1.5	Carc. 1; H350 STOT RE1; H372
Chromate compounds	Not available	<0.1	Not available
Nickel compounds	Not available	<0.1	Not available

Section 4: First Aid Measures

4.1 Description of first aid measures:

Precautions: First aid providers should avoid direct contact with this chemical. Wear chemical protective gloves, if necessary. Take precautions to ensure your own safety before attempting rescue. (e.g. wear appropriate protective equipment).

Inhalation: If breathing is difficult, remove victim to fresh air and keep at rest in a position comfortable for breathing. Seek medical help if coughing or other symptoms persist. Inhalation of large amounts of Portland cement requires immediate medical attention. Call a poison center or doctor. If the individual is not breathing, if breathing is irregular or if respiratory arrest occurs, provide artificial respiration or oxygen by trained personnel. It may be dangerous to the person providing aid to give mouth-to-mouth resuscitation. If unconscious, place in recovery position and get medical attention immediately.
Maintain an open airway.